UNIVERSITAT DE BARCELONA
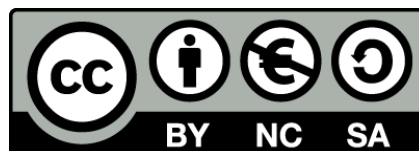
Identification of snow avalanche release areas and flow characterization based on seismic data studies

Pere Roig Lafon

Identification of snow avalanche release areas and flow characterization based on seismic data studies

Pere Roig Lafon

PhD Thesis

2021

UNIVERSITAT DE BARCELONA

RISKNAT – Natural Hazards Research Group
Geomodels Research Institute
Department of Earth and Ocean Dynamics
Faculty of Earth Sciences
University of Barcelona

Identification of snow avalanche release areas and flow characterization based on seismic data studies

Dissertation presented by Pere Roig Lafon to apply for the
degree of Doctor for the University of Barcelona. This thesis
is made under the Doctorate programme of Earth Sciences
(HDK09) of the University of Barcelona and supervised by
Dr. Emma Suriñach Cornet

April 2021

Per vosaltres Anna, Jaume, Martí i Adrià.

Per tu, Maite.

AGRAÏMENTS

Ha estat un treball llarg, amb alts i baixos, però finalment he acabat la redacció d'aquesta tesi. Res hauria estat possible sense l'acompanyament de totes les persones que han cregut en mi i m'han donat el suport necessari en cada moment.

Per començar, voldria donar el més profund agraïment a la Dra. Emma Suriñach, directora d'aquesta tesi. Des del treball final de carrera, en què em va brindar l'oportunitat de començar a treballar en l'estudi de les allaus de neu, ha estat sempre un suport clar i ferm en l'elaboració de tots els projectes que han anat sortint. La gran experiència en la redacció de projectes, el tractament de senyal sísmic i un punt de vista sempre revelador, m'han portat a la culminació d'aquest projecte de tesi doctoral. Vull agrair-li , a més a més, el gran esforç en el dilatat procés de redacció: no ha estat fàcil i la crisi de la Covid19 encara ho ha complicat més. Gràcies, també, per donar-me l'oportunitat d'iniciar-me en el món de la recerca i introduir-me en l'aprenentatge de la sismologia.

Voldria tenir un agraïment especial per a la Dra. Mar Tapia. La seva experiència en la gestió de dades sísmiques, la instal·lació d'estacions sísmiques i les inestimables consultes per perfilar els mètodes de processat del senyal sísmic han estat crucials en l'elaboració d'aquesta tesi. També li he d'agrair la desinteressada dedicació en la resolució de dubtes. Crec que ens ho hem passat molt bé treballant junts, tant en les instal·lacions de sensors sísmics a Vallée de la Sionne (VDLS, Suïssa), com en les visites de manteniment als diferents sensors de la xarxa del LEGEF (Laboratori d'Estudis Geofísics Eduard Fontserè, Institut d'Estudis Catalans IEC). Estic també molt agraït a la Dra. Cristina Pérez Guillén, per passar-me el testimoni en la gestió de la instal·lació sísmica de VDLS, per totes les explicacions durant les múltiples vegades que hi hem anat a fer manteniment i pels innombrables consells, plens d'experiència, per aplicar l'ús del senyal sísmic en l'estudi de les allaus de neu.

El treball amb senyal sísmic per a la caracterització de les allaus de neu perd sentit si es desconnecten les interpretacions del fenomen que s'estudia. En aquest sentit voldria agrair a la Dra. Glòria Furdada les detallades explicacions centrades a entendre el desencadenament de les allaus de neu i en concret l'anàlisi de les fotografies de zones de sortida d'allaus a VDLS. A més a més, la seva experiència en els primers anys d'estudis de registres sísmics d'allaus de neu m'ha aportat informació molt valuosa per a l'elaboració de la tesi. Faig extensiu l'agraïment a tota la resta de membres del grup de recerca RISKNAT, i en especial al Dr. Joan Manuel Vilaplana, per les detallades explicacions sobre gestió del risc i la perillositat, i al Dr. Giorgi Khazaradze, per les seves idees en gestió de sèries temporals i grans bases de dades. També voldria agrair a la Dra. Maria Ortuño l'oportunitat de formar equip en la redacció d'un article periodístic sobre l'allau de Rigopiano (Itàlia) i l'allau d'Arinsal (Andorra), una forma diferent de conèixer el fenomen i de divulgar la ciència traslladant la gestió de riscos geològics al públic general.

Igual d'importants han estat els companys/es en els estudis de Doctorat –Robert, Ane, Octavi i Xabi–, per les penes i alegries que hem passat junts al despatx, als dinars i al camp. Tot aprenentatge és bo i sempre és millor ben acompanyat. Sempre era una alegria compartir el cafè de mig-matí, els dinars i les xerrades d'actualitat amb l'Ane i l'Octavi. Gràcies, Robert, per les divertides sortides de camp durant el Màster i l'intens sentit de l'humor que sempre ens fa agafar perspectiva de tot (sempre necessari!). I gràcies, Xabi, per estar sempre disposat a venir al camp –un viatge a Suïssa mai fa mal–, pel treball mà a mà en la redacció d'articles de premsa, i pels debats sobre ciència, política, fotografia i sobre la vida en general. I a tots, gràcies per les bones estones passades al despatx, al camp i als congressos. No vull deixar de mencionar els companys de la carrera –Gerard, Sandra, Frede, Eli, Héctor, Alba i Laura, entre d'altres–, ja que trobo que és un bonic tresor poder seguir compartint la vida amb vosaltres; encara que passin els anys, quan ens trobem sempre és un goig. M'agradaria també donar un especial agraïment al Dr. Pablo Valenzuela. Ens vam conèixer en un dels primers congressos que vaig assistir com a doctorand i des de llavors han estat molts els consells sobre la tesi i les bones estones.

Durant l'elaboració de la tesi he tingut l'oportunitat de fer estades de recerca a Davos (Suïssa) i a París (França). Ambdues han estat molt bones experiències a nivell personal i crucials per a l'elaboració de la tesi.

De l'Institute for Snow and Avalanche Research (SLF, Davos, Suïssa), m'agradaria donar les gràcies a la Dra. Betty Sovilla per acollir-me al seu grup de recerca, per l'interès mostrat en la feina feta i per la quantitat d'hores invertides en la descripció de les allaus de neu i en detallar el seu comportament per establir comparacions amb les dades sísmiques. També he d'agrair al Dr. Anselm Köhler totes les explicacions sobre la interpretació de dades de GEODAR i les idees per a la interpretació del comportament de les allaus de neu. Cal agrair també les gestions del Dr. Pierre Huguenin, Martin Hiller, Michael Hohl i en François Dufour per fer que la instal·lació de Vallée de la Sionne funcionés correctament, brindant-nos tota l'ajuda possible per a solucionar qualsevol mal funcionament en el sistema d'adquisició de dades sísmiques. A més a més, li he de donar les gràcies a Pierre Huguenin per les valuoses fotografies de les zones de sortida d'allaus de neu (presents en aquesta tesi). Així mateix, cal agrair la dedicació del Dr. Perry Bartelt, que va invertir nombroses hores a introduir-me en el funcionament del programa de modelització RAMMS quan tots just estava començant el doctorat. També vull fer extensiu l'agraïment a tots els companys que em van acollir a Davos, que van fer que l'estada fos una experiència molt gratificant –Louis Quéno, Michael Kyburz, Camille Ligneau, Gregor Ortner i Natalie Brozova.

Pel que fa a l'estada a l'Institute de Physique du Globe de Paris (IPGP), voldria agrair a la Dra. Anne Mangeney les explicacions i el treball en detall sobre el programa de modelització SHALTOP, així com a la Dra. Clara Levy i a la Dra. Virginie Durand l'atenció rebuda i tota l'ajuda en l'ús del programa de modelització SHALTOP. També vull agrair-li al Dr. Julian Kühnert la bona acollida i les bones estones a París i Alemanya.

Passant a agraïments més personals, no pot faltar una menció especial al meus pares, Anna i Jaume. Res en aquesta tesi hauria estat possible sense el vostre suport incondicional. Gràcies per haver-me ensenyat des de petit el valor de l'esforç, el compromís i la solidaritat.

Als meus germans, Martí i Adrià, també us vull donar les gràcies per ser on cal, quan cal. La vida és més fàcil quan entre els tres fem pinya. I com a referents de vida, gràcies a la Quimeta, l'Antonio, la Maria i el Fernando. M'agrada pensar que tot aquest esforç en part és també vostre i, per tant, l'èxit també és compartit. Gràcies per tot.

Als meus amics i amigues, Mireia, Quim, Laura, Pau, Irene, Joan, Enoc, Eric, Raimon i molts altres. Per totes les estones de desconnexió, d'excursions, cims, hores d'esport, de natura i de música. És important saber desconnectar per tornar a connectar amb més força i, en això, la vostra presència ha estat vital. Gràcies per la visita a Davos i pels últims consells d'estil per perfilar la portada i les correccions en les primeres pàgines de la tesi. En especial, gràcies al futur doctor Enoc Martínez per les llargues converses sobre ciència i tecnologia. Gràcies també a l'Eloi (també futur doctor) i a la Marina. Han estat força anys compartint pis i donant-nos suport mútuament en els bons i mals moments. També he de donar les gràcies a l'Anna i al Toni, a la Montserrat i al José Luis. Gràcies també, Maria, pels consells finals en el disseny de la portada.

I tancant la llista i, per això, la menció més important: gràcies, Maite. Com bé saps, acabar aquesta tesi no hauria estat possible sense tu. Ets qui més m'ha patit i m'ha ajudat quan anava faltat de forces, qui m'ha animat a seguir quan més costava. Cada punt i cada pàgina d'aquesta tesi també els has escrit tu. Espero que junts escriguem moltes pàgines més.

ACKNOWLEDGEMENTS

Equally important have been the colleagues in the PhD studies -Robert, Ane, Octavi and Xabi-, for the pains and joys that we have spent together in the office, in the meals and into the field. Every learning process is always better in good company. It was always a pleasure the morning coffee, the lunch breaks and the news talks with Ane and Octavi. Thank you Robert for the fun field trips during the Master and the intense sense of humour that lets us to take perspective of everything (always necessary!). And thank you Xabi for always being ready to come to the field trips for the maintenance of the seismic stations -a trip to Switzerland is always welcome-, for hand-in-hand work in press articles writing process and the intense debates on science, politics, photography and life in general. And to all, thank you for the good times spent in the office, in the field and at the congresses. I do not want to forget to mention my fellow students -Gerard, Sandra, Frede, Eli, Héctor, Alba and Laura, among others-, I find it a beautiful treasure to continue sharing the life with all of you; although the years go by, it is a pleasure whenever we meet. I would also like to give a special thanks to Dr. Pablo Valenzuela. We met at one of the first congresses that I attended as a doctoral student and since then there have been many good times talking about the thesis and life.

During the PhD studies I had the opportunity to perform research stays in Davos (Switzerland) and in Paris (France), both very good experiences on a personal level and crucial for the preparation of the thesis.

Regarding the stay at the Institute for Snow and Avalanche Research (SLF, Davos) I would like to thank Dr. Betty Sovilla for letting me join her research group, for the interest shown in the work I am carrying on and for the lots of hours invested in the description of the snow avalanches and in detailing their behaviour for its comparison with the seismic data. Also, thanks to Dr. Anselm Köhler for all explanations on the interpretation of the GEODAR data and the tips for the interpretation of the behaviour of snow avalanches. I would also like to thank to Dr. Pierre Huguenin, Martin Hiller, Michael Hohl and François Dufour their efforts to ensure that the Valle de la Sionne installation is always working properly, giving us all possible help to solve any failure in the seismic data acquisition system. Also, thank you Pierre Huguenin for the valuable photographs of the snow avalanche release areas (shown in this thesis). I would also like to thank Dr. Perry Barlet for the dedication when I was just starting my PhD studies, spending many hours introducing me to the RAMMS snow avalanche modelling program. I also want to extend my thanks to all the colleagues in Davos, making the stay a very rewarding experience -Louis Quena, Michael Kyburz, Camille Ligneau, Gregor Ortner and Natalie Brozova-.

Regarding the stay at the Institute de Physique du Globe de Paris (IPGP), I would like to thank Dr. Anne Mangeney for the explanations and detailed work on the SHALTOP modelling program, as well as Dr. Clara Levy and Dr. Virginie Durand for the attention received and all the help in using the SALTOP modelling program. Also thank you to Dr. Julian Kühnert for the good times in Paris and Germany.

About more personal acknowledgments, I would like to give a very special thanks to my parents, Anna and Jaume. Nothing in this thesis would have been possible without your unconditional support and teaching me since I was a kid the value of effort, commitment

and solidarity. To my brothers, Martí and Adrià, I also want to thank you for always being there when you are necessary. Life is easier with both of you as a team. And as life referents, I would like to thank to Quimeta, Antonio, María and Fernando. I like to think that all this effort is also partly yours and therefore, success is also shared. Thanks for everything.

To my friends Mireia, Quim, Laura, Pau, Irene, Joan, Enoc, Eric, Raimon and many others. For all the disconnecting moments, excursions, summits, hours of sports, nature and music. It is important to know how to disconnect in order to reconnect with more energy, and in that your presence has been vital. Thank you for the visit in Davos and for the latest style tips for outlining the cover and first pages of this thesis. Special thanks to (coming Dr.) Enoc Martínez for the long conversations about science and technology. Thanks to Eloi (also coming Dr.) and to Marina. There have been many years sharing a flat and supporting each other in good and bad times. Also, thanks to Anna and Toni, Montserrat and Jose Luís. Thanks also Maria, for the final tips in the design of the cover.

And closing the list and therefore the most important mention, thank you Maite. As you well know, finishing this thesis would not have been possible without you. You are the one who has suffered me the most, the one who helped me when I was lacking strength and who has encouraged me to continue when it was the most difficult project to accomplish. Each point of the thesis has also been written by you. I hope that we will write many more pages together.

CONTENTS

LIST OF FIGURES

LIST OF TABLES

SYMBOLS AND ACRONYMS

- **m.a.s.l.**   Metres above sea level

- **s.p.s.**   Samples per second

- **PSD**   Power Spectral Density

- *At(t)*   Total envelope of the seismic signal (3 comp)

- **STA/LTA**   Short Term Average / Long Term Average

- *t0*   Activation of the VDLS data acquisition triggering system ($t0 = 0$ s)

- *sp*   Seismic data sampling rate

- *Fn*   Nyquist frequency ($Fn = sp/2$)

- **VDLS**   Vallée de la Sionne experimental site

- **PR1**
- **PR2**
- **CB1**
- **CB2**

Main snow avalanche release areas at VDLS

- **A**
- **B**
- **C**
- **D (Bunker)**

Caverns at the VDLS experimental site, where the seismic stations and other instrumentations are deployed.

Conceptual model ADSR

- **A**   Attack in sound synthesis envelope generators
- **D**   Decay in sound synthesis envelope generators
- **S**   Sustain in sound synthesis envelope generators
- **R**   Release in sound synthesis envelope generators

Snow avalanche description

- **WSA**   Wet Snow Avalanche
- **PSA**   Powder Snow Avalanche
- **POW**   Powder snow layer (aerosol) in snow avalanches
- **DENSE**   Dense snow layer in snow avalanches

Snow avalanche regions

- **FRONT**   Snow avalanche frontal region
- **E/T**   Snow avalanche energetic and turbulent region
- **TAIL**   Snow avalanche tail region

Seismic signal sections

- **SON**   Signal Onset
- **SBO/SOV**   Signal Body / Signal Over the Sensor
- **STA**   Signal Tail
- **SEN**   Signal End

Frequency content information

- **DF** — Dominant Frequency (for Q and L components)
- **C** — Spectral Centroid (for Q and L components)
- **Cmean** — Mean spectral centroid values of Q and L components
- **Cmean median** — *Cmean* values smoothed using a 5-sample moving median for the whole SOV section

Seismic signal rotation

- **ZNE** — Geographic coordinate system
- **QLT** — Local coordinate system at VDLS site for snow avalanche seismic data studies
- **inc** — Incidence angle on 3D seismic data rotation (*inc = slope*+90º)
- **baz** — Back-azimuth angle on 3D seismic data rotation

Seismic particle polarization

- **V-J method** — Method for the study of the seismic signal polarization from Vidale (1986) and Jurkevics (1988)
- **in** — Seismic wave incidence angle obtained from the seismic particle motion
- **ba** — Back-azimuth angle obtained from the seismic particle motion
- **R** — Linearity value obtained from the seismic particle motion polarization study

- **BAZ** — Back-azimuth angle obtained from the seismic particle motion of the SON section, after combining the information of all time windows. Used for the snow avalanche release area identification.
- **GRD** — Combinate value, product of the incidence and linearity values of the SOV section, for every time window n (*GRD*(n) = *in*(n)·*R*(n)). Used for the snow avalanche flow characterization.
- **GRD median** — *GRD* values smoothed using a 5-sample moving median for the whole SOV section

ABSTRACT

Snow avalanches are gravitational mass movements produced in mountain areas, when part of the snow cover is released and descends downhill. Due to the increase in the practice of mountain winter sports and population growth in the mountain areas (with the increase in infrastructure), monitoring snow avalanches and assessing the affect they can cause becomes essential. Physical measurements for snow avalanche flow characterization and monitoring are commonly used to understand phenomena better (e.g., Sovilla et al., 2008; Köhler et al., 2016; Geopraevent [www.geopraevent.ch]), among which are the seismic vibrations generated by snow avalanches, the study of which started within the framework of the UB Avalanche Research Group (currently UB-RISKNAT Avalanche Research Group) in the early 1990s (Sabot et al., 1998).

The main objectives of this PhD thesis are the identification of the snow avalanche release areas and the snow avalanche flow regime characterization with the use of seismic data. We aim to search for new methods for conducting detailed studies of the seismic signal generated by snow avalanches, considered as a moving seismic source. Moreover, the intention is that all such methods should able to be automated in order to make them suitable to form part of warning systems and/or first response data.

One of the main bases for achieving these objectives is to use widely tested seismological methods designed for the study of single seismic sources (e.g., earthquakes, explosions). In order to adapt them to a record of a moving source generating seismic vibrations (snow avalanches), we decided to apply windowing methods to the seismic signal so that the seismic signal could be processed in small portions, and then extract the information to perform more detailed studies. Over each time window of the seismic signal, we perform the study of ground particle motion polarization (3D) and obtain the frequency content information (Power Spectral Density).

In order to translate the expertise of the UB-RISKNAT Avalanche Research Group on the interpretation of seismic signals from snow avalanches, we decided to search for a criterion to identify the seismic signal sections based on their amplitude. The evolution of the total envelope of the seismic signal ($At(t)$), including the amplitude of the 3 components, allows us to establish a criterion for the identification of the different sections of the seismic signal produced by a snow avalanche.

These seismic signal sections are linked to the relative position of the snow avalanche front with respect to the position of the seismic sensor. For each of the sections of the seismic signal, we apply a different methodology to obtain different information about the snow avalanche flow in each avalanche part. We seek to identify the snow avalanche release area by analysing the signal produced at the beginning of the snow avalanche mass movement (Signal Onset - SON). The study of the polarization of the ground particle motion (3D, ZNE coordinate system) makes it possible to identify the area where the first vibrations are generated, and by extension link it to the start of the snow avalanche mass movement. By analysing the seismic signal section corresponding to when the snow avalanche mass is

flowing over the seismic sensor (Signal Over the sensor - SOV), we characterize the snow avalanche flow and identify the different regions in the snow avalanche. The seismic signal is rotated to the QLT coordinate system in order to better link the information of the seismic signal to the flow progression direction. The use of time windows is crucial for obtaining an evolution of the ground particle motion and the frequency content throughout the SOV section.

Furthermore, we are able to identify the moment when the snow avalanche mass starts to move (first vibrations generated by the snow avalanche) using an appropriate configuration of the STA/LTA algorithm. It is a common method in seismology for the automatic detection of earthquakes and other low amplitude vibrations, over the background seismic noise, and has been adapted for our purposes.

Work on this PhD thesis has also enabled us to establish a homogenization of the seismic data processing steps for studying snow avalanches, based on the UB-RISKNAT Avalanche Research Group expertise. We automated these processes for all the data acquired in the Vallée de la Sionne test site between winter seasons 2013 and 2020, thereby creating a database consisting of more than 420 seismic events (source: automatic data acquisition system activation managed by the SLF). From all these events we managed to identify the snow avalanches from their seismic signatures and to test both of the methods designed in this thesis: the release area identification and the flow characterization.

Although the designed methods are subject to some limitations, we consider that the contribution to novel approaches for the study of the seismic signal produced by moving sources is proved. The release area identification has a very good success rate (78%) in a supervised application. The automated execution could be improved with a better isolation process for the seismic signal at the start of the snow avalanche (SON section). The method for the flow characterization provides new information regarding the interaction of the flow with the ground and with the snow cover. We consider that future studies in this direction may yield information about the snow avalanche basal friction as an indirect measurement.

This thesis demonstrates the high utility of short-period seismic sensors (3D) placed in the snow avalanche paths in order to identify and describe the snow avalanche behaviour. We also demonstrate the opportunities created by placing a short-period seismic sensor (3D) close to the release areas in order to monitor the start of snow avalanches. As main advantages, the seismic data can be processed in real time and the seismic stations are easy to deploy with low maintenance (important features for monitoring difficult access mountain regions). The snow avalanche release identification method could provide the basis for more robust warning systems, both as first intervention data and/or for a statistical study of the occurrence of snow avalanches on a given mountain slope.

RESUM

Les allaus de neu són moviments de massa produïts a les zones de muntanya quan s'allibera part del mantell de neu i baixa muntanya avall. Com a conseqüència de l'augment de la pràctica dels esports de muntanya hivernals i el creixement de la població i de les infrastructures a les zones de muntanya, esdevé essencial controlar les allaus i avaluar l'afectació que poden provocar. És habitual l'ús de mesures de variables físiques per a la seva detecció i caracterització (e., Sovilla et al., 2008; Köhler et al., 2016; GEOpraevent [www.geopraevent.ch]). Entre elles, el registre de les vibracions sísmiques generades per les allaus, l'estudi de les quals es va iniciar en el Grup d'Allaus de la Universitat de Barcelona (actualment UB-RISKNAT Grup d'Allaus) a l'inici dels anys 1990 (Sabot et al. 1998).

En aquesta tesi els objectius principals són la identificació de les zones d'alliberament d'allaus de neu i la caracterització del seu tipus de flux a partir de l'ús de dades sísmiques. Perseguim la recerca de noves maneres de realitzar una caracterització detallada del senyal sísmic generat per allaus de neu, considerades fonts sísmiques en moviment. A més, busquem que tots els mètodes puguin ser automatitzats, de manera que siguin adequats per formar part de sistemes d'alerta i/o com a dades de primera resposta.

Una de les principals bases per perseguir els objectius esmentats és l'ús de mètodes sismològics àmpliament provats per a l'estudi de fonts sísmiques puntuals (e., terratrèmols, explosions). Per tal de poder aplicar-los a un registre sísmic d'una font en moviment (allaus de neu), decidim implementar mètodes de tractament del senyal en finestres de temps, per tal de poder treballar-hi en petites porcions i extreure'n la informació necessària per realitzar uns estudis més detallats. En cada finestra del senyal sísmic, realitzem l'estudi de la polarització del moviment de la partícula sísmica (3D) i obtenim la informació del contingut en freqüències (Densitat Espectral).

Amb l'objectiu d'aprofitar l'experiència del grup de recerca UB-RISKNAT (Grup d'Allaus), vam decidir buscar un criteri per a la identificació de les seccions del senyal sísmic basat en la seva amplitud. L'evolució de l'evolvent total del senyal sísmic ($At(t)$), que inclou l'amplitud dels 3 components, ens permet establir un criteri per a la identificació de les diferents seccions del senyal sísmic produïdes per una allau de neu.

Aquestes seccions del senyal sísmic estan relacionades amb la posició relativa del front de l'allau respecte a la posició del sensor sísmic. En cadascuna de les seccions del senyal sísmic hi apliquem una metodologia diferent per tal d'obtenir informació específica sobre l'allau. Analitzant el senyal sísmic produït per l'inici del moviment de l'allau de neu (secció SON), perseguim identificar la zona des d'on s'ha alliberat. Amb l'estudi de la polarització del moviment de la partícula sísmica (sistema de coordenades ZNE, 3D), és possible identificar l'àrea des d'on es generen les primeres vibracions i que, per extensió, es relaciona amb l'inici del moviment de l'allau de neu. Analitzant el senyal sísmic corresponent al pas de l'allau per sobre el sensor sísmic (secció SOV), caracteritzem el tipus de flux i identifiquem les diferents regions en el cos de l'allau de neu. Per relacionar millor la informació extreta del senyal sísmic amb la direcció en què progressa l'allau muntanya avall, fem la rotació del senyal

cap al sistema de coordenades QLT. L'ús del tractament del senyal sísmic en finestres de temps és crucial per obtenir l'evolució del moviment de la partícula sísmica i l'evolució del contingut en freqüències al llarg de tota la secció SOV.

Així mateix, també podem identificar l'instant en què s'inicia el moviment de l'allau (primeres vibracions que genera), mitjançant una configuració adequada de l'algorisme STA/LTA. Aquest és un mètode comú en sismologia per a la detecció de terratrèmols i altres vibracions de baixa amplitud sobre el soroll sísmic de fons. Hem adaptat aquest algorisme al nostre propòsit, obtenint resultats molt satisfactoris.

L'elaboració d'aquesta tesi també ens ha portat a establir una homogeneïtzació dels passos en el processament de dades sísmiques per al seu estudi en els treballs sobre allaus, basat en l'experiència del Grup d'Allaus de UB-RISKNAT. Hem automatitzat aquests processos per a totes les dades adquirides al lloc experimental de Vallée de la Sionne entre el 2013 i el 2020, de manera que hem aconseguit crear una base de dades amb més de 420 esdeveniments sísmics (font: activacions del sistema d'adquisició de dades, SLF). De tots aquests esdeveniments hem aconseguit identificar les allaus de neu a partir de la seva signatura sísmica i posar a prova els mètodes dissenyats en aquesta tesi.

Tot i que hi trobem algunes limitacions, considerem que queda demostrada la contribució en nous enfocaments per a l'estudi del senyal sísmic produït per fonts sísmiques en moviment. La identificació de l'àrea de sortida de les allaus té una taxa d'èxit molt bona (78%) en una aplicació supervisada. L'execució automàtica es podria millorar perfilant el procés d'aïllament del senyal sísmic corresponent a l'inici de l'allau de neu (secció SON). El mètode per a la caracterització del tipus de flux proporciona nova informació relacionada amb la interacció de l'allau amb el terreny i amb el mantell nival. Considerem que futurs estudis en aquesta direcció podrien conduir a obtenir informació sobre la fricció de l'allau.

Aquesta tesi demostra la gran utilitat dels sensors sísmics de curt període (3D) col·locats a les zones de trànsit de les allaus de neu per identificar-les i descriure'n el comportament. A més a més, queden també demostrades les oportunitats que brinda situar un sensor sísmic de curt període (3D), proper a les zones d'alliberament d'allaus de neu, per a monitoritzar el seu desencadenament espontani. Com a principals avantatges, les dades sísmiques es poden processar en temps real i les estacions sísmiques són fàcils de desplegar amb poc manteniment (característiques interessants per monitoritzar regions de muntanya de difícil accés). El mètode d'identificació de zones d'alliberament d'allaus de neu pot ser la base d'un sistema d'alerta més robust, que aporti informació de context per a una primera intervenció (en cas que l'allau produeixi danys). També pot ser utilitzat per a l'estudi estadístic de l'ocurrència d'allaus de neu en determinades zones de muntanya ja prèviament identificades, mitjançant l'adquisició de dades durant tota la temporada hivernal i el processament a posteriori.

Chapter 1

Introduction

Snow avalanches are gravitational mass movements that occur in snowy mountain regions when part of the snow cover is mobilized downslope. Four main factors are needed for the occurrence of a snow avalanche: snow accumulation, slope inclination, a weak layer on the snow cover and a trigger that starts the mass movement. It is not easy to prevent a snow avalanche once it has already started and becomes an extreme hazard for populations in mountain areas. Therefore, the mapping of the areas where they are usually triggered and a good knowledge of snow avalanche behaviour, are essential for their prevention and risk reduction.

The use of seismic data for snow avalanche monitoring is not new, and multiple approaches to it already exist: from only detection (regional or local scale) to flow characterization. In this thesis, I focus on snow avalanche location and flow description using seismic stations placed in the snow avalanche path. Proximity to the seismic source is a key factor for our approach to the snow avalanche description.

As an introduction to the main purposes of this thesis, the presentation of snow avalanche classification, a brief description of the state-of-the-art use of seismic data for snow avalanches monitoring, and a short presentation of snow avalanches numerical modelling are all necessary. After this, the motivation and main goals are presented, bearing in mind all the expertise presented.

1.a. Snow avalanche classification

Snow avalanches are not always the same. All snow avalanches are released from hills with slopes between 25° and 55°, the most common being between 30°-45° (McClung et al., 1993). The snow accumulation and the different snow layers depend on the mountain topography (slope and orientation) and on the meteorology, also conditioning the amount of snow that can be mobilized. The snow avalanche behaviour on its way downhill depends on this amount, as well as the type of snow and its evolution along the snow avalanche path.

From the type of release area, snow avalanches can be loose snow (non-cohesive) or slab snow avalanches. Loose snow avalanches start from a certain point on the slope and increases in size with the snow incorporated by the erosion of the snow cover on the way down. Slab snow avalanches are released due to the existence of a weak layer in the snow cover, and all the initial volume of snow is mobilized together. Normally, slab snow avalanches are the biggest and most dangerous for their size and energy.

Classification for the size of snow avalanches is a matter of the volume of snow mobilized and the maximum runout distance achieved for the snow avalanche front. In different mountain regions, the snow avalanche size classification may differ. We use the same classification system as the WSL Institute for Snow and Avalanche Research SLF, defined by the European Avalanche Warning Service (EAWS) and based on the Canadian classification (McClung et al., 1993). It is a practical size snow avalanche classification defined by the Canadian civil protection, focused on the destructive effects of snow avalanches and relating them to their maximum runout distance (in relation to the position on the mountain slope), the path length and its volume (Table 1.1).

Regarding snow avalanche zonation, there are three main areas: release area, track area and runout area. The release area for a snow avalanche could be multiple or single. It is affected by the climatic conditions (wind, temperature and altitude) and by the topographic conditions conducive to snow accumulation. Normally, the release areas of snow avalanches are known thanks to the visual identification of scars on the snow cover, at the top of the snow avalanche tracks. The track zone is normally marked by the absence of vegetation. Slopes with a common snow avalanche occurrence did not have trees. The track zones could be open slope or channelled, each of which affects the snow avalanche trajectory and behaviour (erosion, dispersion, etc.). The slope at the track zone tends to be constant and equal to or less than that in the release area. At the runout area the slope is lower. The snow avalanche flow tends to slow down until it stops due to the increase of friction; related to more mass on the snow avalanche body and a decrease in the slope.

———

Table 1.1 - The snow avalanche size classification according to its potential damage, maximum runout distance related to the mountain slope, and its dimensions (path length and snow volume). This classification is used by the SLF, defined by the EAWS and based on the Canadian classification. Adapted from: www.slf.ch.

Size	Potential damage	Max runout distance	Dimensions	
			Path length	Volume
Small (sluff)	Unlikely to bury a person. In extreme terrain is a danger of falling	Stops on release area (steep slope)	< 50 m	100 m³
Medium	Can bury, injure or kill people	Stops on track zone, at the end of the steep slope	50 – 200 m	1000 m³
Large	Can bury and destroy cars, small buildings and trees	Stops on runout area (run on slope below 30° over less than 50 m)	< 1000 m	10000 m³
Very Large	Can destroy buildings and small forests	Stops on runout area (run on slope below 30° over more than 50 m)	> 2000 m	100000 m³
Extremely large	Catastrophic destructive potential	Reaches the floor of the valley	> 2000 m	> 100000 m³

The snow avalanche behaviour depends on the snow density, related to the different layers present in the snow flow and its evolution along the snow avalanche down-hill (Köhler & McElwaine et al., 2018; Sovilla et al., 2015; Sovilla et al., 2018). On a large scale, snow avalanches can be differentiated from Powder Snow Avalanches (PSA), Wet Snow Avalanches (WSA) and Transitional Snow Avalanches (starting as a PSA and reaching the runout area as a WSA). The density and cohesion of the snow are key factors for snow avalanche flow identification and classification, which is strongly related to the temperature and the water content in the snow avalanche flow (McClung et al., 1993). The low-density snow is related to aerosol powder layers on top of the snow avalanche, which are colder and have lower water content in comparison to the denser layers. The high-density snow is related to basal dense layers, which are much warmer and have a higher water content than low density layers. The presence of these different layers defines the classification of the types of snow avalanche and their flow structure, as follows:

PSA: The Powder Snow Avalanches flow structure can be reduced to two main layers: an upper aerosol (powder) layer and a dense core in a basal position. The aerosol layer has low density and is the fastest moving layer of the snow avalanche. The dense core has a higher density, is still dry and is slower than the aerosol layer. The interaction of the snow avalanche with the snow cover and its position on the snow avalanche body allows us to define 3 other snow avalanche parts: the front, the intermittency region and the tail. The PSA develops a dilute front before the main front of the snow avalanche, both characterized by low

density (ρ<100 kg/m3) and high velocity (v>40 m/s) (#1 in Figure 1.1). The intermittency region is identified by large energy fluctuations generated by dense flow collisions with the snow cover (ρ≈200 kg/m3), with high velocity in all layers of the snow avalanche flow (v>40 m/s). It generates snow entrainment and is identified as one of the factors responsible for the powder cloud generator (#2 in Figure 1.1). The tail of the snow avalanche is characterized by a dense flow (ρ>200 kg/m3) with more basal friction (#3 in Figure 1.1). It has lower velocity values in the basal layers (v<20 m/s) than in the upper powder layers (v≈40 m/s) (#4 in Figure 1.1) and tends to decrease in velocity until the flow stops (Sovilla et al., 2015; Sovilla et al., 2018). All the velocity values are point values and are parallel to the flow direction.

WSA: The Wet Snow Avalanche flow structure is characterized by having only a dense layer, with higher humidity and more cohesive than in PSAs. According to the position on the body of the snow avalanche, two parts are defined: front and tail. The frontal velocity (v≈30 m/s) can be faster than the tail velocity (v<20 m/s) and is more constant than in a PSA (Sovilla et al., 2016). The entrainment is at the front of the snow avalanche and can generate deposition on the sides of the flow, parallel to the direction of flow (as levees in granular flows).

Transitional: Snow avalanches cannot always maintain the same rheology along the whole path. In full PSAs and full WSAs, the snow avalanche structure is constant along the path, with minor changes in the flow rheology. However, changes in the snow water content (humidity) produces changes in the snow avalanche behaviour and flow regimes. The snow avalanche body incorporates more water content at a lower altitude (runout areas) due to warmer air temperatures and/or more water content in the snow cover (rain or melting snow). This increase in the water content of the flow produces an increase in the density and cohesion of the snow flow, changing its behaviour from a PSA to a WSA (Köhler & Fischer et al., 2018). Transitional snow avalanches are large in size and must be released from a location with weather conditions different from those in the runout area. The flow behaviour is different depending on the position of the snow avalanche path.
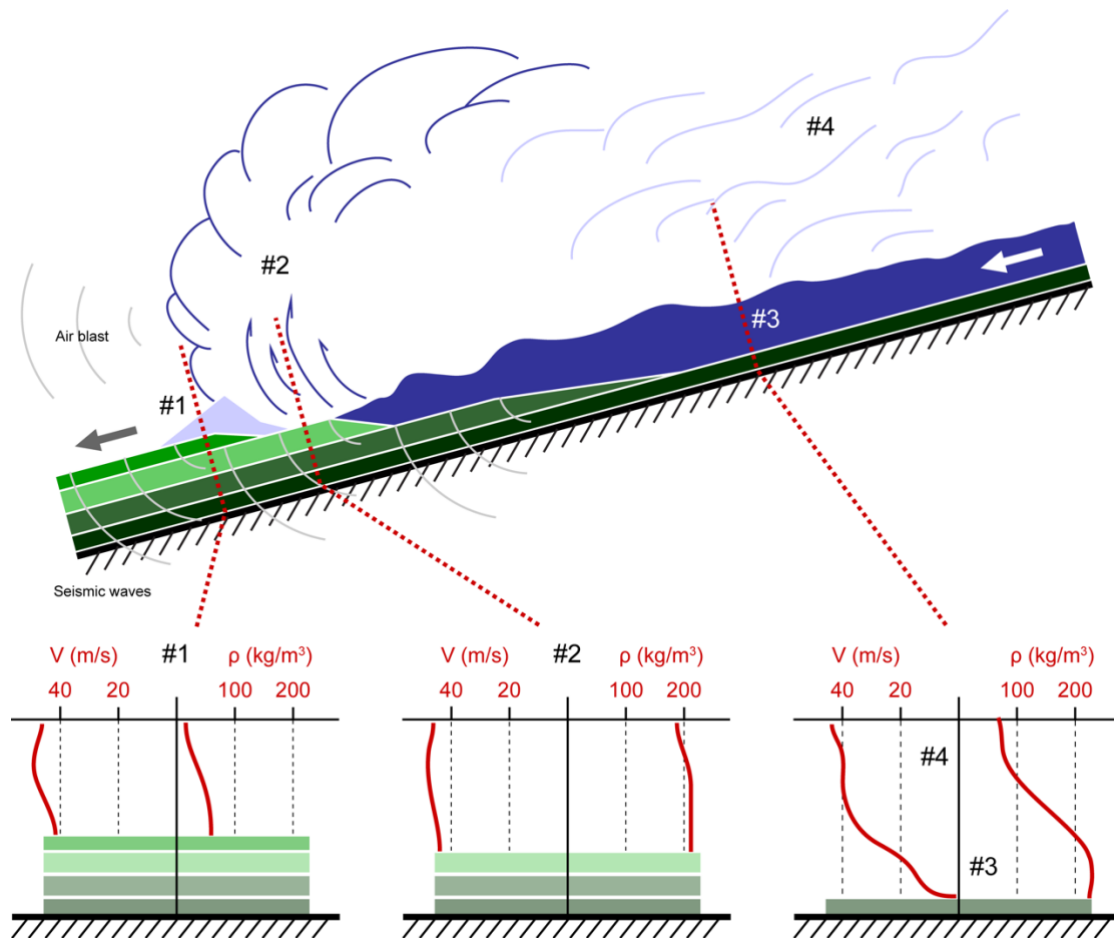
Figure 1.1 - Diagram of the structure of a PSA with its different parts. The layers of the snow cover are shown in green. The frontal region (#1), the intermittency region (#2), the dense core as a basal layer (#3) and the powder cloud (#4) are indicated. The positions of the vertical profiles are indicated in red, showing the velocity (m/s) and density (kg/m3) values that define each part. The sources of the seismic waves and acoustic waves are also indicated. Figure adapted and modified after Kogelnig et al. (2011) and Sovilla et al. (2015 and 2018).

From the seismic data analysis point of view, the rheology and the flow description of the avalanche constitute some of the most relevant information. The seismic source is not the same in a PSA and in a WSA, and neither is it in an aerosol region (most likely to produce infrasound vibration) or the dense basal layer (in closer contact with the ground and more responsible for the generation of the seismic ground vibrations) (Kogelnig et al., 2011).

Snow avalanche descriptions are currently made by studying the snow avalanche deposit and with pictures or videos of the snow avalanche obtained by automatic recording systems. In the development of snow avalanche identification using remote sensing technologies, the use of RADAR systems is proving to be more popular in commercial solutions (e.g., Geopraevent AVYX® Avalanche radar [www.geopraevent.ch]; Wyssen avalanche LARA® Long Range Avalanche Radar [www.wyssenavalanche.com]) and for snow avalanche research on detection and characterization. The use of RADAR systems enables frontal velocity descriptions of the snow avalanche to be made, being complementary with seismic techniques and infrasound instrumentation.

The use of RADAR systems designed for the detection of gravitational mass-movements (GEODAR) and the representation of RADAR data in Moving Target Identification plots (MTI) becomes one of the non-invasive tools with more potential on the snow avalanche flow description (Köhler et al., 2016; McElwaine & Köhler et al., 2017; Köhler & Fischer et al., 2018) (find a complete presentation of the GEODAR system in Chapter 2 and Chapter 5). A low-resolution and portable GEODAR system (called mGEODAR) was recently presented as a solution for early warning systems and land management (Köhler et al., 2020). Using the GEODAR data MTI plots, part of the flow regimes can be identified. This information is used in this thesis as a reference for the seismic data analysis.

1.b. Snow avalanche seismic monitoring and numerical modelling

1.b.i. Seismic monitoring of snow avalanches

The uses of seismic data for the study of snow avalanches started in the early 90's and has been improved in recent years with the technical evolution of computing power and seismic stations. The first reference to snow avalanche seismic data is from Russia (Firstov et al., 1992). In 1994, the UB-RISKNAT Avalanche Research Group started the first experiments for the acquisition of snow avalanche seismic recordings conducted in the Catalan Pyrenees (Spain). The first identification of the seismic vibrations produced by snow avalanches was carried out by the UB Avalanche Team, currently RISKAT-UB avalanches, to establish the basis for the identification of snow avalanches in terms of the evolution of the frequency content, and the duration and amplitude of the avalanche signals in the seismic recordings (Sabot et al., 1998). Taking advantage of the 3D seismic data (seismic stations with three components) the ground particle motion of these seismic vibrations was studied.

At that time, the snow avalanche seismic signal was identified as a non-invasive method for snow avalanche monitoring purposes. However, some limitations were identified, such as the distance variation of the seismic stations position from the source (snow avalanche body) and the difficulty involved in recording the start of the snow avalanches. The link between the seismic signal amplitude and the volume of the snow avalanche was identified, as well as the possibility of enhancing the seismic data capabilities in order to study snow avalanche dynamics rather than using it solely for detection purposes.

Since 1999, snow avalanche seismic signal studies using 3D seismic stations have improved thanks to a more detailed recognition of the time-frequency evolution. The identification of the snow avalanche position relative to the seismic station enabled a relative location of the avalanche along the path to be carried out. The high frequency content was linked to dense snow avalanche flow and the low frequency content to powder snow avalanches (Biescas et al., 2003). More dense snow avalanches produce longer seismic signals than less dense snow avalanches (powder). Moreover, the use of spectrograms representations and the treatment of a huge amount of seismic data recorded from different

types of snow avalanches enabled a criterion to be established, as well as the creation of a catalogue and the definition of a visual reference for identifying snow avalanches from the seismic signal (Biescas, 2003; Suriñach et al., 2005).

Assuming that most of the seismic signal is produced by the erosion of the snow avalanche front on the snow cover (Vilajosana et al., 2007a; Gauer & Issler, 2004), the use of cross-correlation between the seismic signal produced by the same snow avalanche recorded in two separate seismic stations allowed the propagation of the snow avalanche front along the path to be obtained as well as the deduction of the snow avalanche front speed (Vilajosana et al., 2007a). Assuming a cylindrical model from the ground seismic wave propagation, and considering the wave attenuation, the energy dissipated by snow avalanches was calculated, likewise from the recordings at two separate seismic stations (Vilajosana et al., 2007b).

At this point, the seismological methods classically used with single seismic sources achieve good results in the study of snow avalanches (moving sources). The use of sonic wave recordings (infrasound) rather than seismic waves allowed different vibrations sources from the same snow avalanche to be identified. The main sources of the seismic vibrations produced by snow avalanches come from the basal friction of the snow avalanche - a dense basal layer flowing over the snow cover or over the ground (Kogelnig et al., 2011). The infrasonic vibrations are generated by the suspension layer on top of the snow avalanche body (Kogelnig et al., 2011). The initial stages of the snow avalanches are easier to detect in the infrasound data. On the other hand, the stopping phases -related to the abrupt mass stop, already identified in the first snow avalanche seismic data acquisition experiments (Suriñach et al., 2000)- are recorded only in the seismic data and never in the infrasound data. The effects of the different flow regimes on the generated seismic data and infrasound records have been tested, with the conclusion that they are complementary techniques for snow avalanche monitoring and characterization purposes. From the cross-correlation between seismic data and infrasound data produced by the same snow avalanche, it can be identified that part of the seismic vibrations is produced by the infrasound coupling to the ground (Suriñach et al., 2016). The infrasound data are more sensitive to the start of the snow avalanches and are capable of detecting more distant sources, being deployed across entire mountain regions for snow avalanche detection purposes and used as part of snow avalanche early warning systems (e.g., Marchetti et al., 2015; Wyssen avalanche IDA® Infrasound Detection System [www.wyssenavalanche.com]).

More detailed analyses of the time-frequency evolution of the seismic signal produced by snow avalanche enabled more detailed descriptions of the snow avalanche flow to be made, linking the different sections of the seismic signal to different parts of the snow avalanche: frontal region, turbulent region and dense tail (Pérez-Guillén et al., 2016). The energy distribution along the seismic signal produced by the snow avalanche serves as a tool for identifying the general flow regime of the avalanche and classify it according to Powder, Wet and Transitional avalanches (Pérez-Guillén et al., 2016).

The use of the different sections of the seismic signal recognized from the spectrogram representations plays an important role in the analysis of the seismic signal generated from

snow avalanches. The relative position avalanche-seismic station is a key factor to establish the link source-signal. Using the frequency content evolution recorded during the approach of the snow avalanche to the seismic station and processing the spectrograms as images for the application of a Hough Transform, the snow avalanche front speed (Suriñach et al., 2020) could be deduced.

The acquisition of the seismic signal generated by snow avalanches allows information to be obtained on other sources that can also be studied. It is interesting how the application of seismology enabled the identification of a spontaneous avalanche triggered by an earthquake, as a demonstration that this type of spontaneous avalanche triggering is possible with specific snow conditions and a sufficiently strong earthquake (Pérez-Guillén et al., 2014). Moreover, the study of the snow avalanche artificial release methods (Gazex®) from the wave field generated showed the importance of the use of a complete 3D wavefield information in the snow avalanches studies (Suriñach et al., 2011).

Recent studies in Japan have showed the ability to identify snow avalanches with the use of a permanent seismic network (short-period 1 Hz, 3D seismic stations) deployed to monitor volcanic activity. The snow avalanches can be identified from the seismic signal and tracked along the downhill path with the use of an amplitude source location method (ASL) (Pérez-Guillén et al., 2019), and validated the use of numerical models performed with Titan2d software [http://www.gmfg.buffalo.edu/].

Furthermore, the snow avalanche of Rigopiano (a deadly snow avalanche which affected a resort hotel in Italy in January 2017), was recorded and studied with the use of the seismic station network managed by the Italian Geophysical Institute (Instituto Nazionale di Geofisica e Vulcanologia, INGV). Only the snow avalanche seismic signal at the seismic station closest to the snow avalanche location (17 km), a 3D broad band station could be identified. The seismic data was used for the validation of the snow avalanche model calculated with RAMMS [https://ramms.slf.ch/ramms/], and the model helped to understand the seismic data (Braun et al., 2020).

In another direction, snow avalanche forecasting and detection studies exist that are less related to what the avalanche is like and more to determining where and when the snow avalanche is released. To that end, the use of seismic arrays in the mountain valleys using beamforming techniques enabled spontaneous snow avalanche releases (Herwijnen et al., 2016; Heck et al., 2017) to be identified. It also served to train Hidden Markov Models (HMM) for the identification of snow avalanche seismic signals in continuous seismic data stream mode, and to perform a classification for regional snow avalanche statistics of snow avalanche occurrence (Heck et al., 2018). The seismic stations used for the automatic location of snow avalanches have only uniaxial geophones in a vertical position (14 Hz eigenfrequency), in a single position or in 7 geophones array. These seismic station configurations are designed by focusing on objectives other than the configuration used by the UB-RISKNAT for the study of snow avalanches - 3D seismometers, short-period (2 Hz or 1 Hz eigenfrequency) and broadband (0.5 Hz eigenfrequency). See Chapter 2 for further details.

_____

1.b.ii. Numerical modelling of snow avalanche flow

Snow avalanche studies conducted with seismic data use as a validation for the identification of the source all possible measurements from other instrumentation and even pictures. Since the very beginning of seismic data, studies of snow avalanche comparisons with numerical modelling of the snow avalanches studied (Sabot et al., 1998) have been performed. In the UB-RISKNAT research group, we have recently used two modelling programs: RAMMS and SHATOP.

The RAMMS software (Rapid Mass Movements Simulation), developed by the SLF (Christen et al., 2010), is one of the most advanced modelling software for 3D numerical modelling of snow avalanches, debris flows and rockfalls. It is based on the Voellmy-fluid friction model, widely used in mass movement numerical modelling, updated as the Voellmy–Salm model in Switzerland for snow avalanche runout calculation (Salm, 1993). The Voellmy-fluid friction model divides the friction as dependent on two parameters: Coulomb (μ), related to normal stress, and a drag coefficient (ξ). The SHALTOP modelling software has been developed by the Institut de Physique du Globe de Paris (IPGP) (Bouchut et al., 2003; Mangeney-Castelnau et al., 2005), based on the Saint Venant and Savage–Hutter models, specializing in the numerical modelling of shallow water mass movements and self-channelling granular flows (Mangeney et al., 2007, Lucas et al., 2014). The SHALTOP model is designed to calculate the trajectory and deposit of landslides, also validated with comparisons with seismic records of landslides (Levy et al., 2015). In collaboration with the IPGP, we carried out some tests in an attempt to model snow avalanches using SHALTOP and identify any link to snow avalanche behaviour. We found that it was possible to model snow avalanches with a full dense behaviour, which are more similar to granular flows, using SHALTOP software with some adjustments to the Coulomb friction angle (Roig-Lafon et al., 2018).

As a result of the tests performed with RAMMS::AVALANCHE module v1.6.2 and SHALTOP v2016, both mass movement modelling programs only can model the dense part of snow avalanches. One of the main output values from both modelling programs are the friction values throughout the snow avalanche body flowing downslope. The evolution of the friction forces along the snow avalanche body flowing over the seismic sensors position could be linked to seismic signal amplitude. These values can be linked to the snow avalanche outputs in a qualitative way, serving as a validation criterion for the snow avalanche models (Roig-Lafon et al., 2017; Roig-Lafon et al., 2018). The seismic data also serve as a criterion for the identification of the mean front velocity (time arrival to the seismic sensors positions), thereby identifying whether the snow avalanche path is well represented by the snow avalanche models. This information allowed us to identify which model is the most suitable for different kinds of snow avalanches when considering their flow regimes. The Voellmy-Salm model provides a better fit with the denser part of PSA (RAMMS), while the Saint Venant & Savage–Hutter models gives a better representation of the dense behaviour of WSA (SHALTOP).

Once the snow avalanche flow regime is identified, with the use of field information or geophysical measurements like a seismic signal, it is possible to choose the most suitable

friction model for the snow avalanche (e.g., Voellmy-Salm or Saint Venant). Furthermore, geophysical measurements help to set the friction coefficient on the modelling calculations (Coulomb friction μ), which is always a free parameter difficult to decide and with huge affects on the model final result.

By extension, it determines the selection of a numerical modelling software that may provide a better representation of the flow; a choice between RAMMS, SHALTOP or other modelling software based on other friction models (e.g., Titnan2D).

1.c. Motivation

When working with snow avalanche numerical modelling and comparisons with the seismic signal produced by snow avalanches, the most notable limitations concern the correct identification of the snow avalanche release area, the snow avalanche mass determination, and the identification of the snow avalanche flow regime, required for the election of the friction model, as mentioned above.

All this information is generally well defined in snow avalanches artificially triggered in full-scale experiments for scientific studies based on videos, photogrammetry, RADAR data and field measurements. However, in spontaneous snow avalanches, the release area is usually not so well defined, and the snow mass and flow regime involved can only be deduced from the snow avalanche deposits (field information or pictures, should weather conditions allow). In these cases, in the absence of this initial information, too many assumptions are needed to run a numerical model of a snow avalanche, and too many uncertainties are also involved. Consequently, the snow avalanche model becomes less feasible and less reliable.

In these situations, the non-invasive geophysical methods for measuring snow avalanche parameters are effective and very powerful for snow avalanche detection, identification and classification. It is widely proved that the generated seismic signal is one of the best measurements for use in snow avalanche studies and yield excellent results in detection and snow avalanche description. Seismic stations can be deployed to record the seismic vibrations produced by snow avalanches, or data from seismic stations of the institutional seismology services network can also be used for different objectives in snow avalanche monitoring. Seismic stations and sensors arrays could be placed outside the snow avalanche occurrence sites for a regional monitoring and detection purposes. Seismic stations could also be deployed in positions close to snow avalanche sites or buried in snow avalanche paths for a near-field snow avalanche monitoring and description purposes. In all cases, and in comparison to other geophysical instrumentation, seismic stations are easy to deploy, are non-invasive to the snow avalanche flow, and cause no interference on the measurements.

The UB-RISKNAT Avalanche Research Group seismic signal data base of snow avalanches is large enough (see Section 2.b) to find a method for locating snow avalanche release areas in the near field. Furthermore, the large number of avalanche types and sizes allows us to contribute to the seismic description of the snow avalanche flow type.

On the other hand, avalanches have traditionally been studied from a frontal, external or internal position, with sensors installed on obstacles (e.g., Sovilla et al., 2008; Kyburz et al., 2020). It is known that the interaction of the avalanche with the ground and/or with the snow cover is one of the main causes of energy loss from the snow avalanche (e.g., erosion, entrainment, collisions) (e.g., Biescas et al., 2003; Vilajosana et al., 2007b; Pérez-Guillén et al., 2016). However, this interaction has not yet been detailed or studied in depth.

The scientific community devoted to the study of snow avalanches needs a more accurate description of the avalanche. I have examined the already known seismological methods in order to adapt them for application to moving seismic sources. These methods provide unequivocal criteria for the identification of snow avalanche release areas and for a more precise description of the snow avalanche flow regime based on their seismic record.

1.c.i. Main Goals

The seismic signal constitutes our main tool. For the study of the seismic signal produced by moving sources, I trust in the adoption of methods widely tested in the study of seismic signal single sources (Power Spectral Density, ground particle motion, amplitude envelope, etc.), adapted to the study of moving sources such as snow avalanches. Furthermore, the seismic signal is one of the less machine-consuming data flows that can be processed in real-time, which is an important advantage for field measurements in early warning systems. The creation of a sufficiently robust method would be a good starting point for the creation of automatic tools capable of being implemented in mountain areas with a smaller infrastructure deployment.

As a main goal, my intention is to obtain a complete description of snow avalanches with the use of seismic data, with the aim of exporting the expertise of the UB-RISKNAT group regarding snow avalanche seismic data interpretation -seismograms and spectrograms- to unequivocal values; in other words, to quantify the expertise. From this point of view, I seek to determine the release areas of snow avalanches and to identify the flow regime with a time resolution comparable to other qualitative classifications.

When working with such a big data base of seismic signal, which is necessary for my goal, I first need to define a standard criterion for data transformation and representation. Moreover, in order to process all the data and make them available for further studies, this process must be automatic.

Regarding the seismic signal processing for snow avalanche studies, I trust in the use of short-period 3D seismic sensors. The ability to record ground vibrations in all directions will enable us to acquire better interpretations and link better the vibrations observed at their source.

To this end, I define the following objectives:

1. Structure and homogenize seismic signal processing for snow avalanche studies, with the aim of constructing the most complete database possible.

2. Identify the start of the seismic signal produced by first moves of the snow avalanche and define a criterion for the identification of the seismic signal sections related to snow avalanche flow, based on seismic signal amplitude.

3. Define a criterion based on ground particle motion (3D seismic data) for the identification of snow avalanche release areas.

4. Define a criterion based on the combination of ground particle motion and frequency content evolution to apply the expertise on snow avalanche seismic signal identification to flow regime characterization.

5. Automate all possible steps in the seismic signal processing to test its ability for application to real-time data.

To achieve all these goals, I have used common techniques of signal processing (e.g., windowing, PSD) and habitual techniques on seismology for single sources (e.g., ground particle motion polarization, STA/LTA ratio). Wherever possible, all the data and results obtained have been compared with RADAR information (GEODAR MTI plots), pictures of the site and field information.

After Chapter 1, which constitutes this introduction, Chapter 2 presents all the instrumentation and the experimental site where all the snow avalanches under study were recorded. The seismic data homogenization process and the creation of the seismic database are also presented here. Chapter 3 presents all the seismic data processing methods used in this thesis, and the novel methodologies designed for the snow avalanche release identification and the classification of flow regime. The results achieved for the snow avalanche release identification are shown in Chapter 4, where a well-identified case study from pictures is first presented and used to test and to set out the method, below which are five case-problems for the snow avalanche release location. Chapter 5 presents the results achieved for the flow regime identification based on the seismic data information. Three different cases are exposed with different snow avalanche behaviour and different data available to validate the results. Both methods for snow avalanche release and flow regime identifications have points in common, detailed and analysed in the Discussion (Chapter 6). Finally, the Conclusion of this PhD thesis (Chapter 7) is given with the goals achieved, limitations, outcomes, and ideas for future work.

Chapter 2

Characteristics of the experimental site and snow avalanche seismic database

The quality of the results and interpretations we can obtain from the seismic data is strongly linked to their acquisition. For a better understanding of the data and results, this section is devoted to presenting the experimental site where this PhD thesis is developed, the seismic sensors spatial distribution and their configuration.

The vibrations produced by snow avalanches can be recorded at different places and with different sensor configurations; regional or local scale, seismic sensor and geophones arrays or 3D sensor systems, for example-. The UB-RISKNAT Avalanche Research Group started to record snow avalanches using 3D seismometers in 1994 with methods similar to those used in classical seismology for earthquake studies, earth monitoring and earth seismic exploration. The seismic sensors were deployed close to the snow avalanche path, at some protected areas. The proximity between the seismic sensors and the mass movement - ground vibrations generator - is considered crucial for obtaining the most available information, seeking to minimize the attenuation effect due to the distance between the source and the sensor. In consequence, the quality of the seismic data for the studies we aim to perform in this PhD thesis is better the closer the sensors are to the snow avalanche. As we will see in Chapter 5, for the flow regime characterization using seismic data, we need recordings from when the snow avalanches are flowing straight over the seismic sensor. The seismic sensor placement is not always possible because of the destructive power of the

avalanche. However, in our case, special concrete shelters on the site allow us to bury the 3D sensors in the snow avalanche path.

We aim to use the seismic data as a tool for a better understanding of snow avalanches, their internal behaviour and energy distribution inside the flow, and also to be able to develop a tool useful for snow avalanche risk assessment. The research conducted on an experimental site allows us to obtain context information and other complementary data for analysing and extract information of the seismic records. However, it is important not to lose the ability to extrapolate these results in order to apply seismic data characterization methods to other sites - experimental or not - and other mountain regions.

2.a. Characteristics of the experimental site

2.a.i. Vallée de la Sionne (VDLS) experimental site description

All the data used in this PhD thesis were recorded at the Vallée de la Sionne experimental site (VDLS) in Switzerland (Figure 2.1). This full-scale experimental site was created by the WSL Swiss Federal Institute for Snow and Avalanche Research SLF in 1997, for the purpose of obtaining the necessary experimental data to improve snow avalanche models, and to gain a better understanding of avalanche dynamics (Ammann, 1999; Jóhannesson et al., 2006). Until now, the site has been a location for deploying new technologies (GEODAR, FMCW radar) and improving physical sensors for snow avalanche recordings (Sovilla et al., 2013; Köhler et al., 2016; Sovilla et al., 2018). Has become the perfect experimental site for snow avalanche activity monitoring systems testing. The experimental site is open to different research institutes around Europe including the UB-RISKNAT Avalanche Research Group. This group has been installing seismometers along the snow avalanche path since 1997 (Sabot et al., 1998; Suriñach et al., 2000), improving the seismometer spatial distribution, improving the configuration and updating the equipment until the present time, in close collaboration with the SLF (see Section 2.b).

The experimental site is at Valais Canton (Switzerland), 7 km to the north of the city of Sion and close to the Anzère Ski Resort. It is in the western Swiss Alps area, known as Bernese Alps (les Alpes Bernoises), north of the Rhône river. The highest point of the site is at 2700 m.a.s.l. and the lowest point at 1300 m.a.s.l., with a total path length of 2500 m and a vertical drop of 1400 m facing to the East. Alongside the slope there are two main channels, the southernmost called Channel 1 and northernmost called Channel 2 (Figure 2.2a). Different concrete shelters are built along the avalanche path for the installation of the measuring instrumentation, all with continuous electrical power and network communications between them (Ammann, 1999). These shelters are known as Caverns, three of which are used for the installation of the UB-RISKNAT seismometers: Caverns A, B and C placed respectively at the release area, the track zone and the runout area of the main snow avalanche path (Figure 2.2a and Figure 2.2b).
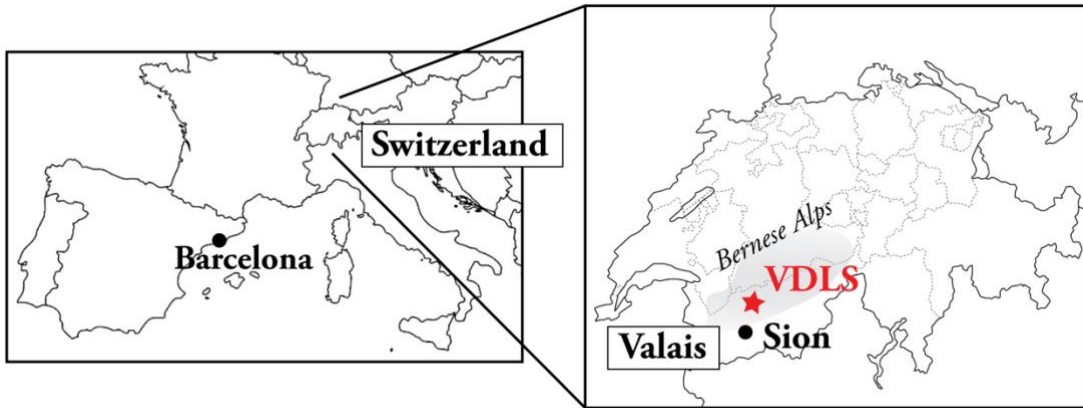
Figure 2.1 - Location of the VDLS experimental site at the Valais Canton near Sion. It is in the south-west of Switzerland, close to the French and Italian borders, in a region of the Alps known as the Bernese Alps.
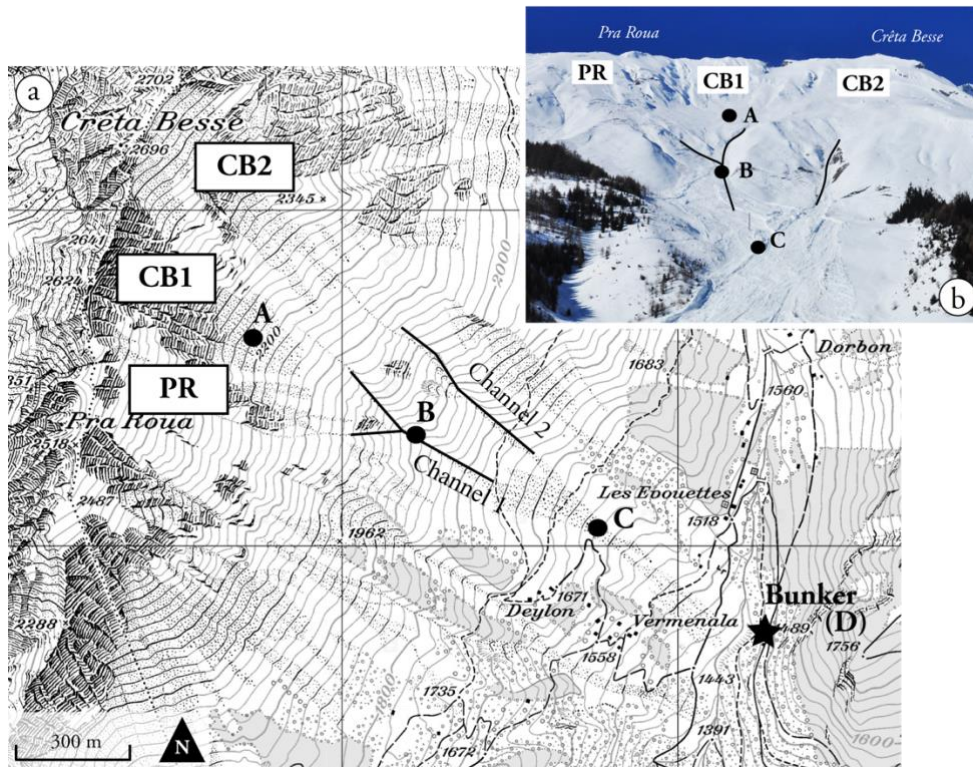
Figure 2.2 - a) Topographic map of the VDLS experimental site. b) Picture of the VDLS slope from the Bunker position. Both with the naming and the position of the instrumented channels, the main avalanche release areas and the position of the caverns where the measuring instrumentation are placed (see Section 2.b). Topographic base map from the Swiss Federal Office of Topography (Swisstopo - map.geo.admin.ch). Picture by Pierre Huguenin (SLF-Sion).

This site was chosen because the return period of small, medium and large snow avalanches is sufficient to obtain enough data recordings during every winter season (Veitinger & Sovilla, 2016). The effect of the winds from the west increases the snow accumulation over the slopes and at the top of the release areas close to the mountain ridge. At the site, major snowfalls occur during the apex of the winter seasons in the northern hemisphere (November-March). Snow avalanches during wintertime are dry-snow avalanches, typically developing a dilute powder cloud sometimes separated from the dense part. Depending on the avalanche size, this dilute powder cloud rises up the opposite slope. After the first major snowfall (November-December), wet-snow avalanches mainly occur, as in springtime (Sovilla et al., 2013). Moreover, access to the site is quite easy for maintenance work.

As defined by the SLF, three main release areas are recognized at the site named like the summits on the mountain ridge. From south to north, the release areas are Pra Proua (PR), Crêta Besse 1 (CB1) and Crêta Besse 2 (CB2). The mean slope values are 42.4° for CB1, 36.2° for CB2 and 37.7° for PR. The CB1 area is the steepest with the greatest roughness and is separated from CB2 by a rock ridge. The CB2 and PR areas have a more homogenous terrain surface, smoother and more continuous (Veitinger & Sovilla, 2016). Avalanches released at PR normally descend by Channel 1 (where Cavern B is placed, facing to the Mast and Cavern C) and by the Deylon stream channel (not instrumented and out of the measurements rang)-. Avalanches released at CB1 descend mainly by Channel 1, while avalanches released at CB2 descend mainly via Channel 2 (Figure 2.2a).

With regard to the geomorphology, the site is channelled with the narrowest part situated close to 2000 m.a.s.l. at Channel 1 and Channel 2, between the release areas and the runout zone (Figure 2.2b). The mean slope at the release area is close to 40°, while at the runout area it is close to 20°. Some parts in between may have higher slopes because of the erosion of the channels. The position of the caverns along the slope may affect the seismic data recorded there. For this reason, we need to consider the places where the seismic sensors are to be located in order to obtain the best possible data interpretations.

From the geological point of view, the region is characterized by the presence of limestone rocks and marls from the Upper and Lower Cretaceous (Maastrictian and Urgonian) over schists basement from the Jurassic (Callovian-Oxfordian). Rock formations are very layered and folded due to the alpine orogenic compressing and faulting processes (Cenozoic). (Geological Atlas of Switzerland - GA25). That carbonate rocks can only be observed at the ridge and the higher parts of the site. The main coverage consists of glaciological sediments of the last glacial period (Pleistocene), lateral moraines made of the same rocks (carbonates) and clay matrix (Figure 2.3).
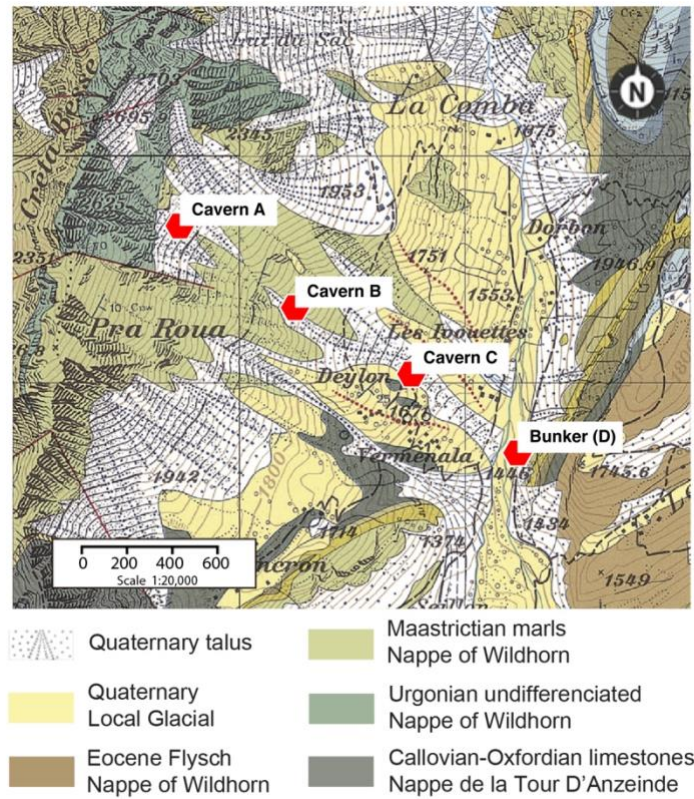
Figure 2.3 - Geological map of the VDLS with detailed information of the upper layers and surface deposits.
Cavern locations (A, B, C and Bunker D) in red hexagons (Section 2.b). Base map and geological information
from the Geological Atlas of Switzerland (GA25), Saint- Léonard, no. 35; http://map.geo.admin.ch/. After
Biescas (2003) and Pérez-Guillén (2016).

2.a.ii. Description of the recording locations and instrumentation installed

As mentioned above, the VDLS experimental site was built with the purpose of
recording as much information as possible of snow avalanches behaviour. The UB-
RISKNAT Avalanche Research Group took advantage of this situation and has been
installing seismometers at the VDLS since the site became operative in 1999. Avalanche
studies using seismic signals by the UB Avalanche Team started some years before (1995) in
the Catalan Pyrenees (Vall de Núria and Vall de Boí) and in a prototype of installation (1996)
at the VDLS (Sabot et al., 1998; Suriñach et al., 2000; Suriñach et al., 2001). However, the
avalanche seismic records at the VDLS obtained between 1999 and 2003 constitute a big
step forward for snow avalanche seismic recognition and the beginning of the techniques
developed and used nowadays (Suriñach et al., 2000; Suriñach et al., 2001; Biescas, 2003).
From 2004 to 2007, seismometers of the UB-RISKNAT Avalanche Research Group were
installed at the Ryggfonn experimental site (Norway) (Vilajosana et al., 2007a; Vilajosana et
al., 2007b; Vilajosana, 2008), where the acquisition systems for the study of the snow
avalanche seismic signal were notably improved. In 2008, the seismic installation returned to
VDLS, applying the knowledge acquired at the Ryggfonn site installation and adding the
deployment of an infrasound sensor, thereby developing new technologies (Kogelnig et al.,
2011; Kogelnig et al., 2014). From 2008 until 2016, the installation was improved with

sensors placed at all the available caverns along the snow avalanche path (Pérez-Guillén et al., 2014; Pérez-Guillén et al., 2016; Pérez-Guillén, 2016).

The initial concrete structures were built in 1999, buried into the ground (caverns) and wired with power and internet connection, then improved and increased in number over the following years until the present cavern distribution and configuration (Figure 2.4). From top to bottom, we present the different Caverns. Closer to the top of the experimental site is Cavern A (2250 m.a.s.l.) (Figure 2.4b). Cavern B (1894 m.a.s.l.) is placed at Channel 1, considered as the track area (Figure 2.4c). It is at Cavern C (1620 m.a.s.l.), located at the runout area, where most of the sensors are installed. Cavern C consists of two main concrete caverns: C2, where the Mast managed by the SLF is installed (main obstacle), and C1, 60 m downslope from the Mast (C2) where the seismic installation of UB is placed (Figure 2.4d and Figure 2.5e). Hereinafter we mention Cavern C1 as Cavern C, where the seismic station is located. See Table 2.1 for the detailed coordinates of the cavern positions.

The main control centre at VDLS is called Bunker (sometimes Cavern D) and is placed at the counter slope, facing north-east. It is in a safe place, where only the powder cloud of large avalanches can reach that position, and is constructed to protect all the installation inside against avalanche impacts (

Figure 2.4f). The construction is bigger than the caverns on the slope. The power supply and the network for all the instrumentation at Caverns A, B and C are managed from there. The Bunker network is also accessible from outside via VPN (Virtual Private Network) and is capable of managing the instrumentation and download data throughout the winter season without being physically inside the Bunker, which is normally not possible due to the snow accumulation. Moreover, the Bunker location is suitable for certain instruments such as radars and video cameras, because the view of the avalanche path from that point enables an external recording of the avalanches facing the avalanche front. The installation is improved every season, thereby providing a considerable amount of snow avalanche data.

Table 2.1 - Coordinates of the VDLS Cavern positions in Swiss Datum (CH1903) used by the SLF and in the World Geodetic coordinate System (WGS84).

	CH1903 LV03-M	WGS84	Height (m.a.s.l.)
Cavern A	N: 593741 E: 127707	Lat: N46º 18' 2.67" Long: E07º 21' 26.67"	2250
Cavern B	N: 594225 E: 127335	Lat: N46º 17' 50.64" Long: E07º 21' 49.30"	1894
Cavern C (C1)	N: 594762 E: 127040	Lat: N46º 17' 41.10" Long: E07º 22' 14.40"	1620
Bunker (Seismic sensor)	N: 595244 E: 126693	Lat: N46º 17' 29.88" Long: E07º 22' 36.94"	1482
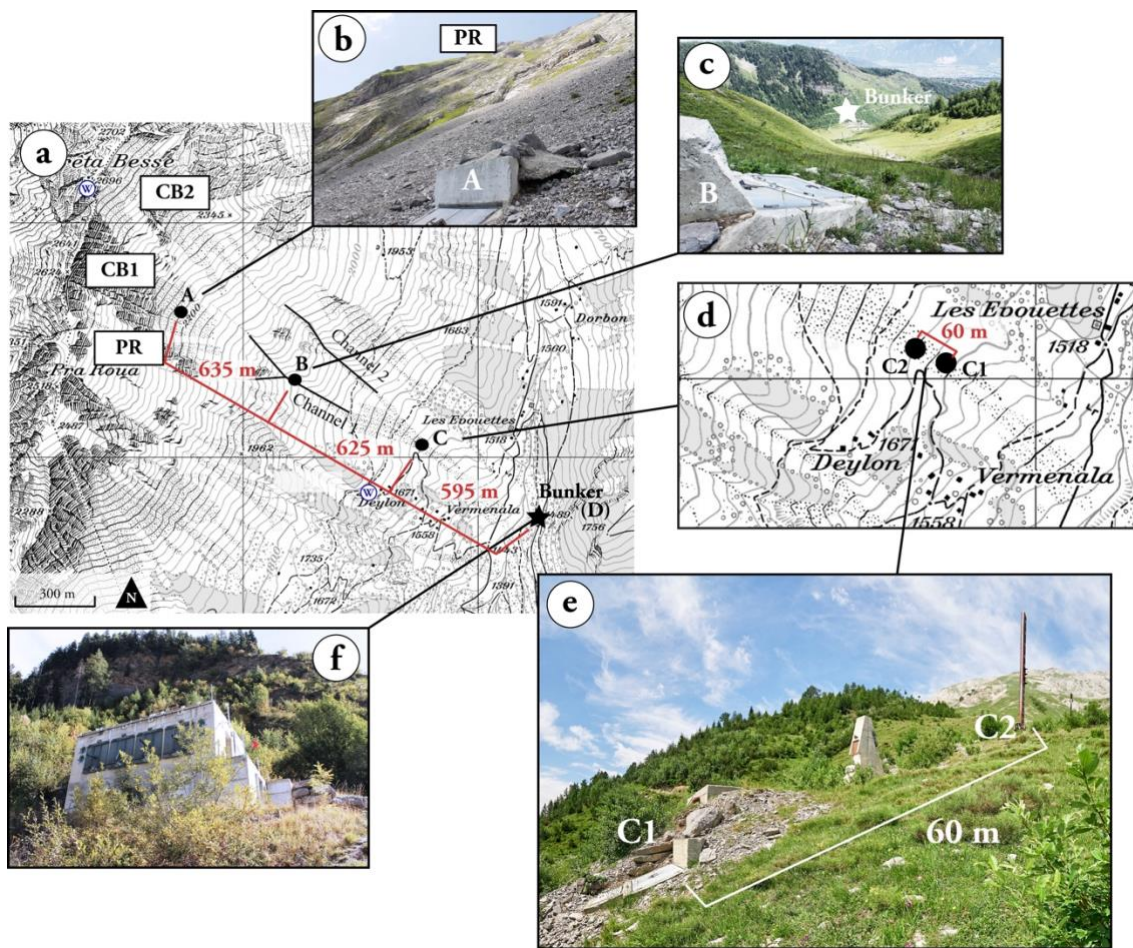
Figure 2.4 - Pictures of Cavern positions. a) Map of VDLS indicating the cavern positions, the release areas, the weather station positions (w in blue) and the distances between caverns in red, measured over the digital elevation model, following the slope direction. b) Picture from Cavern A in the south-west direction facing the Pra Roua release area. Cavern A in the foreground. c) Picture from Cavern B facing the avalanche path and Bunker position. Cavern B in the foreground. d) Detailed map of Cavern C position indicating the distance between the seismometer (C1) and the Mast obstacle (C2) locations e) Picture of Cavern C area with the distance between the Mast (C2) and the seismic station (C1) locations f) Picture of the Bunker frontal wall facing the VDLS main slope taken from the *La Sionne* river in the north-east direction.

Two weather stations are located outside the cavern positions and far from the snow
avalanche path, in secure places. One is placed at 1695 m.a.s.l. between Cavern C and the
Deylon stream path, and the second one at the top of the experimental site, close to the
Crêta Besse summit (Figure 2.4a).

The SLF Avalanche Dynamics team manages the main technical installation at VDLS.
Frequency Modulated Continuous Wave radars (FMCW) are installed at Caverns A, B and
C providing local measurements of vertical velocity profiles and used to estimate the flow
depth and the mass deposition, as well as to determine erosion (Sovilla & Bartelt, 2002;
Marshall et al., 2007; Ash et al., 2010; Pérez-Guillén et al., 2016; Sovilla et al., 2018). The
Mast at Cavern C is 20 m high and equipped with velocity, pressure and temperature sensors,
and a high-speed camera (Sovilla et al., 2016; Kyburz, et al., 2018). With this information,
the SLF Avalanche Dynamics team studies the dynamics of the avalanche at the runout zone
when the snow avalanche is fully developed. (Sovilla et al., 2008; Sovilla et al., 2018).

The SLF Avalanche Dynamics team, in collaboration with Durham University (UK),
the University of Cambridge (UK), the University of Sheffield (UK), the University of Leeds
(UK) and University College London (UK), developed a Frequency Modulated Continuous
Wave Phased Array radar named GEODAR (GEOphysical flow dynamics using pulsed
Doppler radAR) (Brennan et al., 2009; Vriend et al., 2013; Ash et al., 2014). The GEODAR
has been installed at the Bunker position since 2010. This equipment enables different
avalanche fronts to be tracked along the whole slope, giving information about the position,
velocity and the avalanche size. Using the Moving Target Identification (MTI), a relationship
between the GEODAR data signatures and different flow regimes along the avalanche path
was plotted, and different stopping mechanisms were defined (Köhler et al., 2016; Köhler et
al., 2018). The snow avalanche data representation and interpretations from GEODAR and
Mast sensor data (flow height, pressure and velocity sensors) are very useful for the
calibration of the seismic methodologies and are complementary to the seismic
interpretations.

The underground location of the caverns at the VDLS site allows us to install the
seismometers on the avalanche path without any risk of damage to the sensors (Figure 2.5).
The seismic data obtained from these positions relative to the source of the seismic
vibrations provides a clue for the seismic interpretation and the processing methodologies
developed by the UB-RISKNAT Avalanche Research Group and for this PhD thesis.
Seismology is a non-invasive method that detects the interaction of the different parts of the
avalanche with the snow cover and terrain (erosion, impacts on the ground and changes of
air pressure), and is sensitive enough to infer different flow regimes, types of snow and
avalanche dimensions (Suriñach et al., 2000; Suriñach et al., 2001; Biescas et al., 2003;
Vilajosana et al., 2007a; Vilajosana et al., 2007b; Kogelnig et al., 2011; Pérez-Guillén et al.,
2016; Pérez-Guillén, 2016).

The seismic equipment installed at VDLS has undergone minor changes in recent
years; basically, the update of the data recording systems, the increase in the number of
seismometers and changes in some locations. At the outset, in1999, only one seismometer
was placed in Cavern D (Bunker) (Figure 2.5a), although its number has increased until today,

when there is a total of 5 seismometers deployed in all available caverns (two in Cavern C) and one infrasound sensor in the Bunker position. A detailed relation of the different installations from 1999 until 2016 can be found in Pérez-Guillén (2016). The instrumentation deployment between season 2012-2013 and season 2019-2020 has not been altered, including one Broad-band seismometer at Cavern C (Figure 2.5e). The broadband seismic sensor was installed at Cavern C in 2012 with the aim of detecting any possible low frequency deformation of the ground due to the avalanche load to the ground, and also for recording low frequencies in the seismic generation processes. The lowest frequency signal (<1Hz) was recognized as resulting from the interaction of the snow avalanche with the obstacles on the experimental site (Mast, at Cavern C position).

The seismic station deployment for the data used in this PhD thesis is carried out with only two data acquisition systems (DAS), where the seismic sensors are plugged and manage the data acquisition process: 1) REFTEK 130-01 from REF-TEK systems Inc., hereinafter mentioned as REFTEK (Figure 2.5f), and 2) Spider nano Remote Unit from Worldsensing Co., hereinafter mentioned as Spider (Figure 2.5c).

The last update of the VDLS seismic sensor installation was conducted in season 2013-2014. A new seismic station was installed at Cavern A to search for seismic information from the release area of the snow avalanche (Figure 2.5c). The data from this seismic station placed at Cavern A are treated in this PhD thesis for the first time and constitute an important factor for snow avalanche remote detection and description.

Two geophones managed by the SLF team are installed at Cavern A and B. They are part of the automatic triggering system installed at VDLS, for starting the data acquisition of all the instrumentation installed at VDLS when a spontaneous snow avalanche is released. The triggering system is configured as follows: when one of the geophones exceeds an amplitude threshold (Cavern A or B), it sends an electric impulse to all the instrumentation and computers installed at the VDLS site to start the recording systems. Only one geophone exceeding the amplitude threshold is needed to activate the system trigger. The automatic triggering system is normally configured at a peak amplitude of 0.098 mm/s and is tested and supervised by the SLF managing team of VDLS.

The data acquisition systems (DAS/dataloggers) of our seismic stations at VDLS record in continuous mode, acquiring data throughout the whole season (data stream [a]). This continuous data includes background noise and earthquake data recordings, which are very useful for time synchronization and sensor calibration. The automatic triggering system impulse is also received by REFTEK data acquisition systems (DAS) installed at Caverns B, C and Bunker (D). The RETEK DAS are configured to generate a secondary data file with higher sample rate when the trigger system is activated (data stream [b]). These files are time-synchronized with the other VDLS instrumentation and are very useful for data comparison.
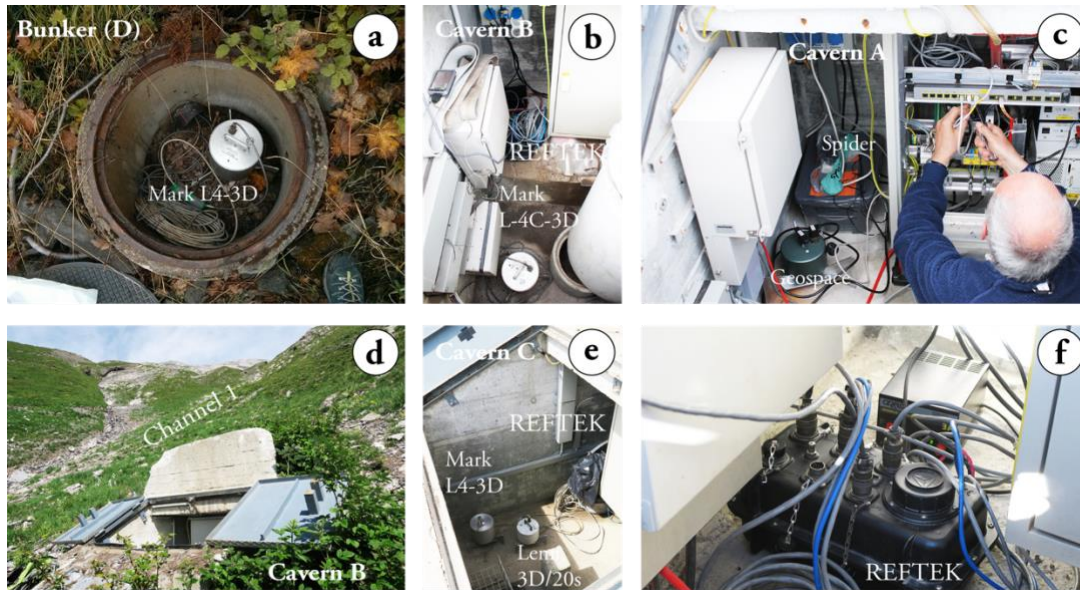
Figure 2.5 - Pictures of the installation process and instrumentation at VDLS. a) Mark L4-3D seismometer placed at Bunker position (view from above). b) Inside Cavern B with the Mark L-4C-3D seismometer in the lower part of the image, and the REFTEK datalogger (black) plugged to the power at the upper part. c) Inside Cavern A with the Geospace seismometer on the left and Martin Hiller (responsible for VDLS installation) managing the network switches. d) Cavern B with the doors open. e) Inside Cavern C1 with the Mark L4-3D and Lennartz 3D/20s seismometers on the left and the REFTEK datalogger on the right. f) Detail of a REFTEK datalogger with all cables plugged and the power supply on the back. Pictures taken by Pere Roig in different years during maintenance at the VDLS installation between 2012-2020,.

Below we describe the seismic instrumentation placed in each cavern.

- **Cavern A**

Cavern A, located between the Pra Roua and Crêta Besse 1 release areas, is the measuring cavern closest to the avalanche release areas. A small 3-component seismometer called Mini-seismonitor from Geospace Technologies (2Hz eigenfrequency, 500/6 Vs/m sensitivity) is installed at this position. Although the sensitivity of this sensor at low frequencies is limited to 2Hz, we consider it is enough for a good seismic recording of avalanches close to the release area, with a short distance between the emitter -snow avalanche- and the seismic sensor. The seismometer is plugged to a Spider Nano data acquisition system (Worldsensing Co.) recording the seismic components continuously on 3 different channels with a 100 Hz sampling rate (samples per second = s.p.s.). All data are recorded and kept in continuous mode (data stream [a] config. at Table 2.2). Since no continuous GPS for time-fitting is possible, the time is fixed at the beginning of the season and adjusted over the season with the help of earthquake seismic signals. The triggering system impulse from the VDLS main installation cannot be received by the Spider Nano, therefore only records in the continuous mode (no data stream [b] in Cavern A).

- **Cavern B**

This cavern is placed at Channel 1, inside the gully part. A 3-component seismometer Mark L-4C-3D (1Hz eigenfrequency, 280 Vs/m sensitivity) is placed inside. This is a short period seismometer used in classical local earthquake monitoring and crustal structure studies. It is plugged to a 6-channel datalogger REFTEK DAS-130-01 and configured to obtain two main information data streams: [a] recording the 3 components with a sampling rate of 100 s.p.s. in continuous mode; [b] recording a 700 s long file with 200 s.p.s. sampling rate when the VDLS trigger system is activated (Table 2.2). The data stream [b] is configured to include a 60 s of data prior to the trigger activation (pre-trigger data). This pre-trigger data option allows us to record and save information from before the VDLS trigger system is activated (ring buffer).

- **Cavern C**

At Cavern C, located in the runout area, two seismometers are deployed: one 3-component short-period Mark L4-3D (1Hz eigenfrequency, 275 Vs/m sensitivity) and one 3-component Lennartz 3D/20s broadband seismometer (0.05Hz eigenfrequency, 1000 Vs/m sensitivity). Both sensors are plugged into the same REFTEK DAS-130-01, 3 channels per sensor. The data stream [a] includes all six channels recording in continuous mode at a 100 s.p.s. sampling rate. The data stream [b] activated by the VDLS trigger system only includes data from the Lennartz broadband sensor at a 200 s.p.s. sampling rate, and 60 s pre-trigger (Table 2.2).

- **Cavern D (Bunker)**

The Bunker is located on the counter slope in front of the VDLS main avalanche path. This was the first location where a seismic sensor was installed. We maintained this location because the position provides an external view of the avalanche. The UB installation at the Bunker position includes one seismic sensor and one infrasound sensor. Both are placed outside the main building to avoid noise and electronic interferences. Currently, the seismometer is a 3-component short-period Mark L4-3D (1Hz eigenfrequency, 275 Vs/m sensitivity) and the infrasound sensor (barometer) is a Chaparral Model 24 (0.1 Hz eigenfrequency, 2V/Pa sensitivity) with a pipe structure installation for a proper recording of the infrasonic waves (Kogelnig et al., 2011; Kogelnig et al., 2014). Both sensors are plugged into a REFTEK DAS-130-01, three channels for the seismometer and one channel for the infrasound sensor. The data stream [a] includes all data from both sensors recorded at a 100 s.p.s. sampling rate, the same configuration as the REFTEKs at Caverns B and C. The data stream [b] is activated by the VDLS trigger system and includes all four channels for 700 s, including the 60s pre-trigger data, at 100 s.p.s. (Table 2.2). In this case, since [a] and [b] have the same sampling rate, the [b] stream data files are only useful for the time synchronization with other instrumentations, being activated at the

same time by the VDLS trigger impulse. The sampling rate for the trigger data stream [b] is 100 s.p.s. due to disk memory limitations. Because these sensors are placed outside the snow avalanche path, we considered that a 100 s.p.s. sampling rate is high enough to prevent information loss due the distance and ground attenuation (1-50 Hz frequency range); and datafiles are small enough to prevent data loss due to memory disk overwriting.

Thanks to this dual recording system ([a] and [b] data streams) we are able to obtain a continuous recording of the whole season at a 100 s.p.s. sampling rate and specific files for each VDLS trigger system activation. The trigger files have twice higher sampling rate, data prior to the trigger activation and data files time synchronised.

It is possible to save data from before the trigger system activation thanks to a ring buffer function working on REFTEK DAS. A ring buffer consist of a disk memory loop with the length of the pre-trigger duration (60 s in this case), which is continuously overwritten with [b] data stream configuration. The ring buffer data is only saved when the trigger is activated, included on trigger data file and prior to the trigger activation.

All installations at the caverns are wired to the local network and connected to a main seismic data server located in the Bunker. Using the REFTEK software RNC2, the download of the triggered files from all the REFTEK dataloggers to the main seismic data server is automatic (named VDLS-Allaus-Server). Data from Cavern A are only downloaded to the server if the VDLS trigger system is activated. Data are transferred on request from the VDLS-Allaus-Server to the data server at the UB-RISKNAT Avalanche Research Group office in Barcelona (Spain), known as the UB-Allaus-Server, where data are classified and saved in different backups. Access to the VDLS instrumentation is conducted via the VPN managed by the SLF.

The trigger system activations are notified through the SLF. During the winter season, data from the trigger activations of all the caverns are pre-processed and the time series plotted after convertion to ground motion scale (m/s) for the entire trigger data file (700 s), and also the corresponding spectrograms. This is a fast mode of observing the data and recognizing what is happening in near-real time at VDLS. At the end of the season, all the continuous data are downloaded from the dataloggers of all caverns and saved to the VDLS-Allaus-Server and in the UB-Allaus-Server in different backups, accessible and ready to be used. For a detailed description of the data processing for near-real time seismic data evaluation and organized archive, see Section 2.d, where the method created for this purpose is described.

Table 2.2 - Summary of the VDLS seismic stations installation with sensors, data acquisition systems (DAS) and configuration used in recent winter seasons (since 2012).

Position	Sensor	DAS	Configuration
Cavern A	Short-period geophone Mini-seismonitor (2Hz) Geospace Technologies	3-channel Spider Worldsensing	3-component recording [Z N-S E-W] [a] Continuous: 100 s.p.s. [b] No trigger configuration
Cavern B	Short-period seismometer Mark L-4C-3D (1Hz)	6 channels DAS-130-01 REFTEK	3-component recording [Z N-S E-W] [a] Continuous: 100 s.p.s. [b] Trigger file: 200 s.p.s., 700 s length including 60 s pre-trigger
Cavern C	Short-period seismometer Mark L4-3D (1Hz)	6 channels DAS-130-01 REFTEK	6-component recording [Z N-S E-W] both sensors [a] Continuous: 100 s.p.s., both sensors [b] Trigger file: 200 s.p.s., 700 s length including 60 s pre-trigger only broadband seismometer
	Broadband seismometer Lennartz 3D/20s		
Bunker (Cavern D)	Short-period seismometer Mark L4-3D (1Hz)	6 channels DAS-130-01 REFTEK	4-component recording ([Z N-S E-W] + I) [a] Continuous: 100 s.p.s. [b] Trigger file: 100 s.p.s., 700 s length including 60 s pre-trigger
	Infrasound sensor Chaparral Model 24		

2.a.iii. Seismic characterization of the VDLS experimental site

The acquisition process of seismic vibrations includes the transmission of the seismic waves from the source to the seismic sensor position and the recording process, which may affect the final available data, differing from the original generation of the seismic vibration. Although we can control the registration process when installing and configuring the seismic stations, the transmission of the seismic waves from the source to the seismic sensor is not under our control.

In order to work with the data recorded at the VDLS seismic stations, we need to know the conditions for a validation of the results and for having more confidence in the data. A detailed characterization of the local site effects and background noise allows us to identify if some frequencies are attenuated or amplified due to the position of the seismic sensor, and if any significant differences in the frequency content and amplitude exist between the components of the same seismic station [ZNE].

- **Local site effects and seismic wave attenuation**

The geological context of the site, including the basement rocks, the sediment depositions and the geomorphological conditions of the slope, are the main terrain characteristics that may affect the seismic waves. These factors may contribute to changes in the amplitude and frequency content of the signal, as well as between the 3 components of the same seismometer (see Suriñach et al., 2000). All seismic sensors at VDLS are placed

over quaternary glacial sediments. This sediment cover can cause signal attenuation or amplification due to the response of the materials to the seismic vibrations affecting the recorded seismic signal, such as a low-pass filter experiencing less amplitude and attenuation on the higher frequencies, or a high-pass filter having the opposite result.

Large field campaigns and reference recordings are needed for a proper seismic characterization,. Pérez-Guillén (2016) showed that the recorded amplitudes at the Cavern A seismic station are higher than those recorded at the other caverns, and that the amplitude values at the Cavern B seismic station are the lowest in comparison to those of all VDLS seismic stations. The quantification of the ground motion was obtained using PGA (Peak Ground Acceleration, obtained from the maximum acceleration value) and PSA (Pseudo-Spectral Acceleration, maximum relative displacement spectrum values) analysis. This quantification was carried out using data from eight different local earthquakes recorded in all the seismic stations located at the VDLS site. These values are related to the soil where the seismometers are placed and to the topographical effect (flat top of the mountain at Cavern A versus gully part at Cavern B). None of our seismic stations are installed directly in bedrock or on non-inclined slopes. Hence, it is not possible to obtain the real amplification factors because of the lack of a reference station.

The geology context and the topography may affect the seismic records of earthquakes and events farther from the experimental site. In these cases, the seismic wave fronts always come from different source positions. The basal rocks, sediments layer and topography around the seismic sensors position have special relevance for the recording of the seismic waves. For snow avalanche seismic data recordings, the source is always over the ground surface and transmits the vibrations to the same sediment layer where the seismic sensors are placed. In consequence, we may assume that the influence of the site effects on the seismic signal are not relevant when comparing between the different snow avalanche data recorded at the same site.

On the other hand, snow avalanches normally do not slide directly over the ground (soil). They often slide over the snow cover formed by different snow layers with different physical properties and different thicknesses. Seismic vibrations generated by snow avalanches first propagate over the snow cover before reaching the boundary snow-soil to transmit the vibrations into the ground. Pérez-Guillén (2016) found that the attenuation of the first compressional wave is lower in dense snow, with the maximum attenuation for frequencies over 100 Hz, while for light snow the attenuation is higher with the maximum over 10 Hz. Assuming that the light snow is usually entrained, and that the attenuation due to a dense snow base layer only affects frequencies over 100 Hz (not recorded with the used seismic stations configuration, we work with frequencies lower than 100 Hz), we consider that the snow cover does not attenuate the seismic signal.

- **Background noise**

Background noise studies carried out at Caverns B, C and D (Bunker) on records of spontaneous triggered avalanches show that the background noise level before the avalanche release is between the typical ranges of the noise models of Aki and Richards (1980) and

Peterson (1993) (Pérez-Guillén, 2016). This means that the seismic signal generated by the avalanche is not overlapped by signals of other seismic sources. For avalanches triggered artificially, however, the background noise level is higher, affecting the typical frequency ranges of the avalanche seismic signals (f > 10 Hz) (Pérez-Guillén, 2016). This noise must be taken into account for an accurate interpretation of the avalanche seismograms.

Up to now, the background noise levels of Cavern A had not been previously characterized. For the characterization of the background noise of this location, we use the same methodology applied in Pérez-Guillén (2016) to the data of the other stations at VDLS for the sake of a correct comparison. We consider 15 minutes of seismic background noise and perform the calculation of the Power Spectral Density (PSD) on 1.5 s time intervals throughout the whole 15 minutes of seismic signal for each component of the seismometer. The noise spectrum mean values are computed using all the PSDs for each component. The noise spectrum is plotted together with the noisy and quiet models of Aki and Richards (1980), and the new low (NLNM) and high (NHNM) noise models of Peterson (1993). The noise study was performed for all the stations in all caverns for validation and control purposes. The results obtained in Caverns B, C and D are in agreement with the conclusions in Pérez-Guillén (2016), and the results obtained in Cavern A are coherent with the results of the other seismometers. Figure 2.6 shows 15 minutes of seismic signals of the background noise, by components, of all the seismometers installed at VDLS, obtained simultaneously. These data are used to perform the background noise plots of the locations shown in Figure 2.7. The seismic background signal recorded in the broadband seismic sensor (Cl in Figure 2.6), looks different due to the capacity to record lower frequency content than the other seismic sensors. This low frequency content in the broadband seismic sensor (Cavern C, Lennartz seismometer [Cl]), is more noticeable in the PSD representations, being more noisy than other VDLS seismometers in frequencies under 1 Hz (f<1 Hz), but still within the noise model limits (Cl plots in Figure 2.7).

The background noise levels at Cavern A are within the noise model values (Figure 2.7). In frequencies around 10 Hz, the noise levels at Cavern A are higher than the background noise recorded in seismic stations placed at Cavern B and C, probably due to the effect of the topography because the seismometer is located at the highest topographic position. The Cavern A seismometer eigenfrequency is higher (2 Hz) than that of the other seismic sensors, cutting off the lower frequencies (Table 2.2). Despite all these observations, the PSD noise values in Cavern A are still within the noise model boundaries previously mentioned. The Cavern D noise levels are higher in frequencies over 10 Hz due to the proximity to urbanized areas (higher and closer anthropic noise).
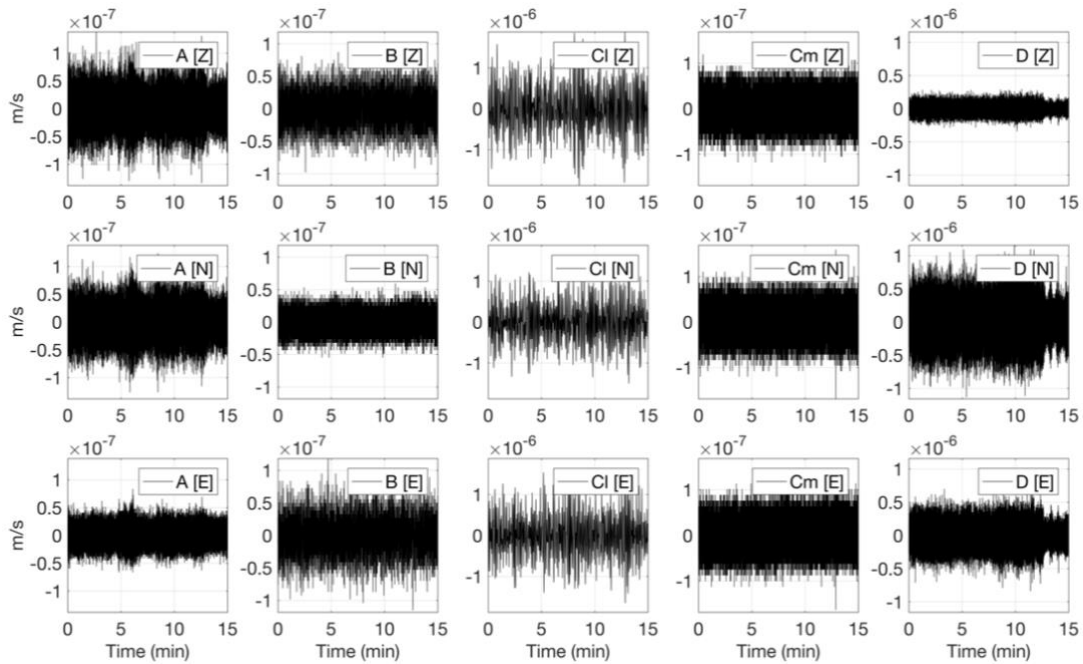
Figure 2.6 - Noise signals (15 minutes) recorded in all the seismometers installed at VDLS. From left to right, Cavern A, Cavern B, Cavern C Lennartz (broad-band), Cavern C Mark (short-period) and Cavern D. From top to bottom components vertical (Z) and the two horizontals (N-S[N+], E-W[E+]).
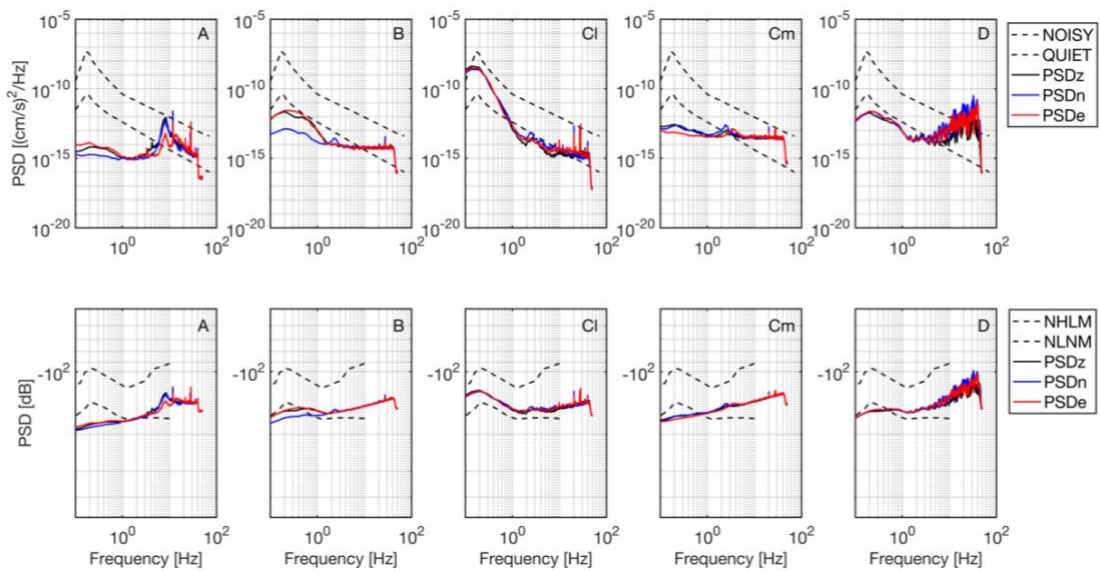
Figure 2.7 - Background noise plots. Power Spectrum Density (PSD) for data of all VDLS seismometers and components. From left to right, Cavern A, B, C Lennartz (Broad-band), C Mark (short-period) and Bunker (D). PSDz (Z), PSDn(N-S) and PSDe (E-W) curves plot plotted on top with the NOISY (higher) and QUIET (lower) model curves from Aki & Richards (1980) and on bottom the NHLM (higher) and NLNM (lower) model curves from Peterson (1993).

This background noise study is performed using the same methodology as in Pérez-Guillén (2016), for an easy comparison between installations. Note that the background noise results for Cavern A and for the broad-band seismic sensor in Cavern C, conducted for the first time in this PhD thesis, are similar to that of the other locations.

The PSD background noise values of all the seismometer's locations are admissible and coherent. Consequently, the Cavern A seismic station is valid for snow avalanche studies. However, it is important to take into account that the seismometer is the closest to the release area and also very close to the detonation point of the explosions in the artificially triggered avalanches. The signal of these explosions and the anthropogenic noise generated must be considered, filtered or deleted for interpretation. For these reasons, we prefer to use spontaneous avalanches (no explosion) when working with Cavern A seismic data.

2.b. Snow avalanche seismic data

Although data since 1999 until the present are at our disposition, only data between 2012 and 2020 are used in this PhD thesis. Since the 2012-2013 winter season until 2019-2020 winter season, the seismic station configuration was very similar, making it easier to establish comparisons between the data of the winter seasons. This period (2012/2013 - 2019/2020) also coincides with my participation in the field installation of the seismic stations at VDLS and its maintenance. The broadband seismic sensor (Lennartz) was installed at Cavern C in the winter season 2012-2013 and has been in operation until the present day, while the seismic station at Cavern A was deployed for season 2013-2014. Both are an important addition to the seismic installation at VDLS. It is the first time that data recorded in the seismometer located at Cavern A have been analysed and used for snow avalanche studies.

The configuration of the seismic stations at VDLS is unique and enables us to obtain data from different parts of the avalanche path (release, track, runout area and outer avalanche path view). Data from all the seismic stations together provide us with the opportunity to arrive at a general interpretation of the snow avalanche. Moreover, I would like to point out that not all data and sensors configuration are useful for all the studies.

Seismic data from different caverns were used for different purposes. Data recorded at Cavern A were useful for the determination of the location of the avalanche release area, because its location is the closer to release area (see Chapter 4). Data from Cavern B and C were mainly used for the characterization of the snow avalanche flow regime. Cavern B is located inside Channel 1, in the running part of the track. At this location, the big avalanches are not yet fully developed. The situation of Cavern C, in the runout area, allows us to record the avalanche vibrations when it is fully developed. The data of the sensors placed at the Bunker were not considered in this PhD thesis. The Bunker sensors data are included in the homogenous data representations and data packages of the database, with the aim of acquiring a complete overview of the entire avalanche and all data classified and available in a complete data set structure (see Section 2.b). The outer position of these sensors (infrasonic

and seismic) is very useful qualitatively, thereby helping in the interpretations and complementing the understanding of the phenomena.

Usually, once a year, if weather conditions are good enough, the SLF organizes an experiment for triggering snow avalanches artificially by explosives from a helicopter. Generally, experiments were only performed after a significant snowfall (>0.8 m) where large avalanches can be expected (Veitinger & Sovilla, 2016). The largest avalanches are normally recoded during the experimental days, thus the data from these days tend to be the most interesting. However, more avalanches are recorded on non-experimental days (naturally released) providing a more complete and more variable database. From the seismic data point of view, the explosives detonation is recorded by the seismic stations and constitutes an unwanted seismic noise for the snow avalanche seismic data studies. On the other hand, the seismic vibrations produced by the detonations is of interest for time synchronization between the seismic stations data (Pérez-Guillén, 2016) and for testing new methodologies (see Subsection 3.d.i).

Between the 2012-2013 and the 2019-2020 winter seasons at VDLS, there were a total of 534 triggered activations (considering all activations due to different seismic sources, not only snow avalanches). Different seismic sources like earthquakes, anthropic noise, explosions, animals, rock-falls, other mass movement and snow avalanches (those we are interested in) can activate the trigger system. Moreover, during the experiment days the trigger system is activated manually by the SLF team. Because of all these reasons, not all trigger activations recorded at VDLS correspond to snow avalanche data, and the fact that trigger is activated by a snow avalanche does not necessarily mean that the data are valid or that the snow avalanche is large enough to be studied. As result, from all the trigger activations, 357 correspond to snow avalanches of all sizes (mainly small) confirmed by the SLF, and 60 trigger activations correspond to earthquakes. The remaining activations are due anthropic noise (airplanes, detonations from the Anzère ski resort, etc.) or other seismic vibration generators (like animals, wind, storms, etc.), with no interest for the snow avalanche research. When trigger activations are caused by a snow avalanche, the snow avalanche adopts the same name as the trigger activation code for its study, matching the SLF naming code for all the VDLS data.

In this PhD thesis, the smaller avalanches were used for the release area identification and large avalanches were used for the study of the flow regime. Not all the avalanches can be recorded at all seismic stations due to technical issues of the instrument installation or to the data-saving processes. For this reason, we perform a recognition of all the available trigger activation data for each avalanche that we are interested in analysing. Between the 2012-2013 and the 2019-2020 winter seasons, it was possible to study 26 large avalanches with enough data from all the sensors. However, in this PhD thesis more data from smaller avalanche are used. It is crucial for us to have a large amount of available seismic data ready to be processed in order to test the newly developed methods. Each results section details the snow avalanche seismic data used to develop and test the different methods, corresponding to the release area identification (Chapter 4) and the snow avalanche flow regime seismic classification (Chapter 5).

2.b.i. Data archive structure and protocol for a database creation

Like every sensor or informatic installation, the seismic station installations at VDLS require regular maintenance. Moreover, the amount of data generated season by season needs to be classified and managed in order for it to be saved correctly, thereby ensuring easy access for working with it. As previously mentioned, the recording systems installed at VDLS are mainly REFTEK dataloggers connected to a computer placed in Bunker, the VDLS-Allaus-Server, managed by the UB-RISKNAT Avalanche Research Group. All the connections to the seismic stations at VDLS for data management and downloading are centralized in this server.

The data download from REFTEK dataloggers to VDLS-Allaus-Server is automatic, using the RTPD network protocol running on the RNC2 software (REFTEK Co.). The incorporation of the seismometer at Cavern A plugged to a Spider data acquisition system (Worldsensing Co.), outside the REFTEK environment, was one more addition to the data downloading process and data archive continuity. The equipment uses different network protocols and has no automatic data downloading system to the main server, and up to now the data from Cavern A have been downloaded manually to the VDLS-Allaus-Server. Although the data download process involves basic network management and data files copying process, I consider it important to highlight that the maintenance of all the seismic stations and data structure requires special attention throughout the entire season, to check that all the stations are connected to the VDLS-Allaus-Server and all the data are transferred correctly.

In the interests of coherence and the ability to localize data on all servers, the data structure is the same as that created by the REFTEK software, including manually the data from Cavern A. The data archive structure includes different folder levels generated according to the day, sensor and data stream (continuous or trigger). For every new day a new folder is created with the Julian day number code (YYYYDDD ex. 2019360 being December 26th, 2019). Inside every day-folder, one folder is created for each seismic station. Inside every station folder, three different sequentially numbered folders are generated. Folder \0 contains health files of the stations, folder \1 contains the continuous data files (data stream [a]) and folder \2 contains the trigger seismic data files (data stream [b]). All data files are automatically named by the dataloggers using a numerical code that includes the UTC time and the date. Figure 2.8 presents a diagram of all the data flow from recordings in the data acquisition systems (Figure 2.8a) to data archive (Figure 2.8b and Figure 2.8c) and database (Figure 2.8h and Figure 2.8i). The data structure generated is replicated on all the data archive copies and back-ups (Figure 2.8j).

The VDLS seismic data archive grows during the winter season. When there is a trigger system activation, the new data recorded are transferred to the UB-Allaus-Server (server computer located at the UB office, Barcelona) and processed in order to determine whether or not the trigger activation corresponds to an avalanche. To date, this process has been performed manually, which makes the data evaluation more time-consuming, less efficient, and more likely to have errors in the processing steps. In order to process the data of the ongoing winter-season as well as all the data from past seasons, I have created a protocol

that can be automatized and is very helpful for the management of the VDLS seismic data archive (Figure 2.8e, Figure 2.8f, Figure 2.8g and Figure 2.8h). All data are managed and processed using MATLAB® R2018a (MathWorks Co.). However, it is possible to implement all the steps with any other numerical computing software capable of managing seismic data (Python, for example). The automated protocol is designed to work with trigger data files, but the protocol steps are the same for applying it to continuous data.

The protocol consists of five different steps.

1. Conversion of the downloaded data files to a usable file format. A general characteristic of the data acquisition systems is that each one has its own data file format and conversion software. All the seismic data files are converted using the software provided by REF-TEK Inc. and by Worldsensing Co., to the mSEED format (MiniSEED, Standard for the Exchange of Earthquake Data (SEED) with no headers) and the SAC format (Seismic Analysis Code software file format). Both are standard seismic data formats including only the waveform data in counts units. The complementary information (sampling rate, duration, time, transfer function) of the acquired data is not included in the datafiles headers due to the configuration of the dataloggers. The date and time information are contained in the name of the seismic data file when created and can be extracted from there in the data processing. The stations do not have a permanently installed GPS antenna, which is only connected during the installation prior to each winter season. For this reason, the time is not updated during the season experiencing some time drift between stations. Seismic data time normally needs to be corrected using the time-fitting between the instruments. The location is fixed by the GPS.

2. Conversion of the raw time series values into a ground motion unit system. This conversion is essential from the perspective of the physical process. The seismic stations record the data as the electrical potential difference of the internal mass moving within a coil, in Volts; one coil for each component of the three axial sensors. These values need to be converted to ground motion velocity, in m/s. The conversion factors are different for every sensor and datalogger, and they are provided by the manufacturer of the instrumentation (poles and zeros; instrument responses; transfer functions). Because we are only working with the frequency response on the flattened part of the transfer function (frequency/amplitude) for every seismic sensor, we only consider the sensitivity of each seismic sensor and datalogger for the seismic data convolution, the result being the seismic signal in velocity (m/s) of the ground vibrations. For easy access, the conversion factors are saved in plain text files capable of being read by coding programs for automatization purposes, emulating the response files headers included in seismic data files (e.g.: SAC, SEED), but adapted to the VDLS seismic installation.

3. Time series offset and detrend corrections. These corrections are necessary to avoid undesirable effects in the spectrum calculations. Both corrections are a typical seismic data routine. Data are not filtered at this point so as to maintain all the information for further studies. The filtering routines are detailed in each data processing steps searching for snow avalanche information (see Subsection 3.a.iv).

4. Time synchronization. Having all the data of one event with the same base of time is a requirement for facilitating processing and comparison of the snow avalanche data. The VDLS trigger system activates the recordings at Caverns B, C and D at the same time, so the time is synchronized between these caverns (data stream [b]). However, because the dataloggers had no access to an external clock for this synchronization, and because their internal clock had some drift during the season, a time synchronization is necessary in cases where the trigger system is not activated. This is the case of the seismic data belonging to the continuous data stream. To find and correct the time offset between them, reference points are necessary. The vibration produced by local earthquakes recorded at the seismic stations is used to fit the time between the stations. Using the P-wave arrival time at the position of the different stations, the offset time is corrected, considering the P-wave time travelling from the earthquake epicentral position to the VDLS sensors position and between them (e.g., Pérez-Guillén, 2016). The offset time for each station is calculated manually and is established at the beginning of the winter season (with an accuracy of ± 0.1s). The offset time of every station may undergo some variation throughout the winter season recording, for which reason the time synchronization needs to be updated. For the database creation, the time synchronization between seismic stations could incur some error due to the time drift of the DAS internal clocks at each seismic station. Should a large avalanche or some other interesting event occur, a new synchronization is usually carried out with data from a recent large teleseism. The more recent the teleseism the greater the precision of the time synchronization, and thus part of the time drift on the dataloggers may be discarded. When working with seismic data for specific studies where the time synchronization between seismic stations is mandatory, some manual adjustments could be required on time synchronization from seismic data on the trigger files database.

5. Creation of trigger files database. All data files are saved in mat files (file format from MATLAB® software, widely used by UB-RISKNAT Avalanche Research Group). These mat files include information on the conversion factors and time synchronization corrections. This information contained in the same file is important for contextualization and for the availability of information regarding the process steps applied to the data. These files are included in the database for processed trigger files data, using

a folder structure that allows us to find and use the data programmatically in order to work with it. These are clearly separated from the raw data archive. In the trigger files database, the directory structure levels are made to separate each season and each trigger activation. The triggers are numbered by the SLF team and the same file naming is maintained to make the data comparison easier. The names of the folders for the trigger data files start with the capital letters AV and include the date of occurrence in the format YYYYMMDD followed by the trigger number (example: AV20171230_3026, the trigger number 3026, recorded on December30th, 2017). The earthquake data downloaded and processed for the time fitting process are saved in a folder with the capital letters EQ, followed by the date of occurrence and a trigger number exceeding 9,000 (not SLF code). Inside every trigger activation folder, three more folders are created, named: "/MAT", including the mat files, "/PLOTS" to save representations of the seismic data and "/SAC" to include the data in SAC format. All processed data are ready to be read in MATLAB® software using mat files or in other software (with no conversions) using sac files.

Summarizing, all data are saved in two different data structures. The data archive (Figure 2.8b and Figure 2.8c) includes the raw data files from all seismic stations, in the same original folder structure created at the VDLS-Allaus-Server. It is replicated at the UB-Allaus-Server (Figure 2.8d) and to all the backups (Figure 2.8j). It includes both the continuous data files (data stream [a]) and the trigger data files (data stream [b]). The database (Figure 2.8h and Figure 2.8i) includes the resulting files after processing the data from trigger activations (data stream [b]) in a more usable data format (Figure 2.8e and Figure 2.8f). The database also includes the plots of all the data from all sensors (Figure 2.8g), being an easy system for recognizing the information of every trigger activation.
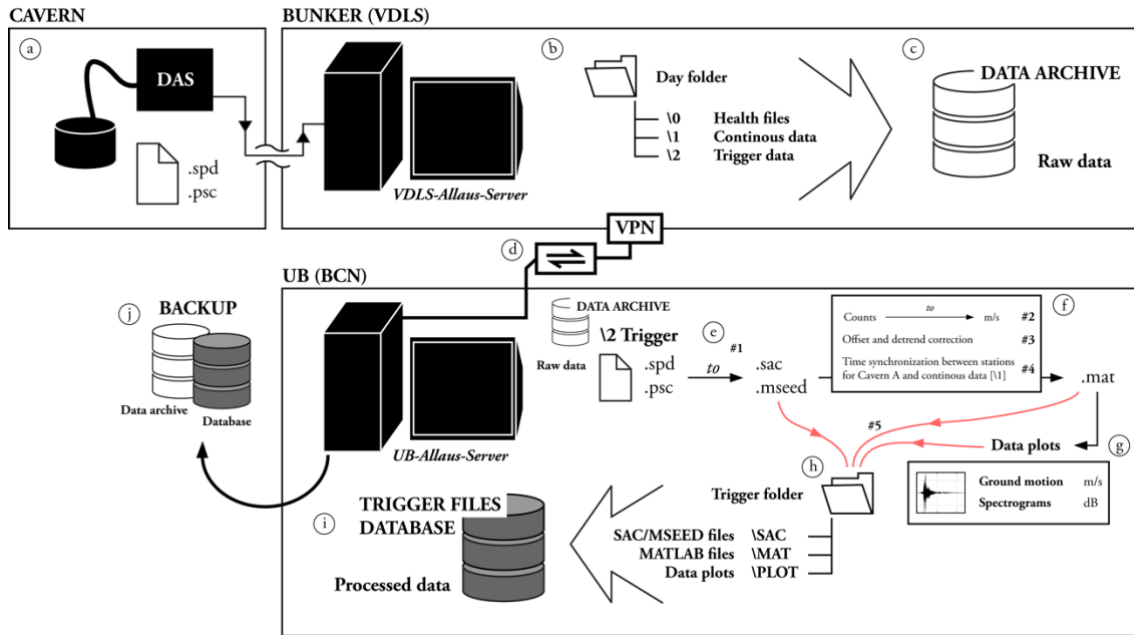
Figure 2.8 - Diagram of the entire data flow from the recording at the data acquisition systems (DAS) (a) to
the Data Archive (c) and to the Trigger files Database (i). The data archive is created at the VDLS-Allaus-
Server (b) and replicated at the UB-Allaus-Server (d). The seismic data is processed (e) and saved in sac and
mat files (f). The data are represented in seismograms and spectrograms (g) included in the trigger files
database folders (h). The Data Archive and Tigger file Database are replicated in different backups (j).

2.b.ii. Homogenous data representation

The processed data of the trigger system activations treated above (trigger files
database) are displayed in two different representations (seismograms and spectrograms),
providing a solution to check the seismic information on the trigger activations visually and
then proceed to preliminary interpretations (Figure 2.8g). In these first data plots, we
maintain the same representation parameters (axes limits and time length) for all data,
including all seismic stations and for all trigger system activations. The use of common plot
parameters constitutes the basis for a homogenous representation of the data, which is one
of the key points for correct data comparison and interpretation.

The data are represented in two different seismogram combinations: a) each of the
three components for every sensor separately (not shown); b) the vertical component (Z) of
every seismic station corresponding to the different caverns, including the infrasound sensor
data (pressure values in Pascals, Pa) (Figure 2.9). The length of all plots is the duration of the
trigger file (normally 700 s), and the time zero (0 seconds) corresponds to the moment of
activation of the VDLS triggering system ($t0$). The seismic stations are configured with a pre-
trigger time record, saving the data before the activation of the VDLS triggering system. The
pre-trigger time is normally 60 s, thus the seismic data representations start at -60 s from the
trigger system activation ($t0 = 0$ s) and the maximum time is 640 s. The total length of the
seismic signal for the trigger data stream considering the pre-trigger time is 700 s.
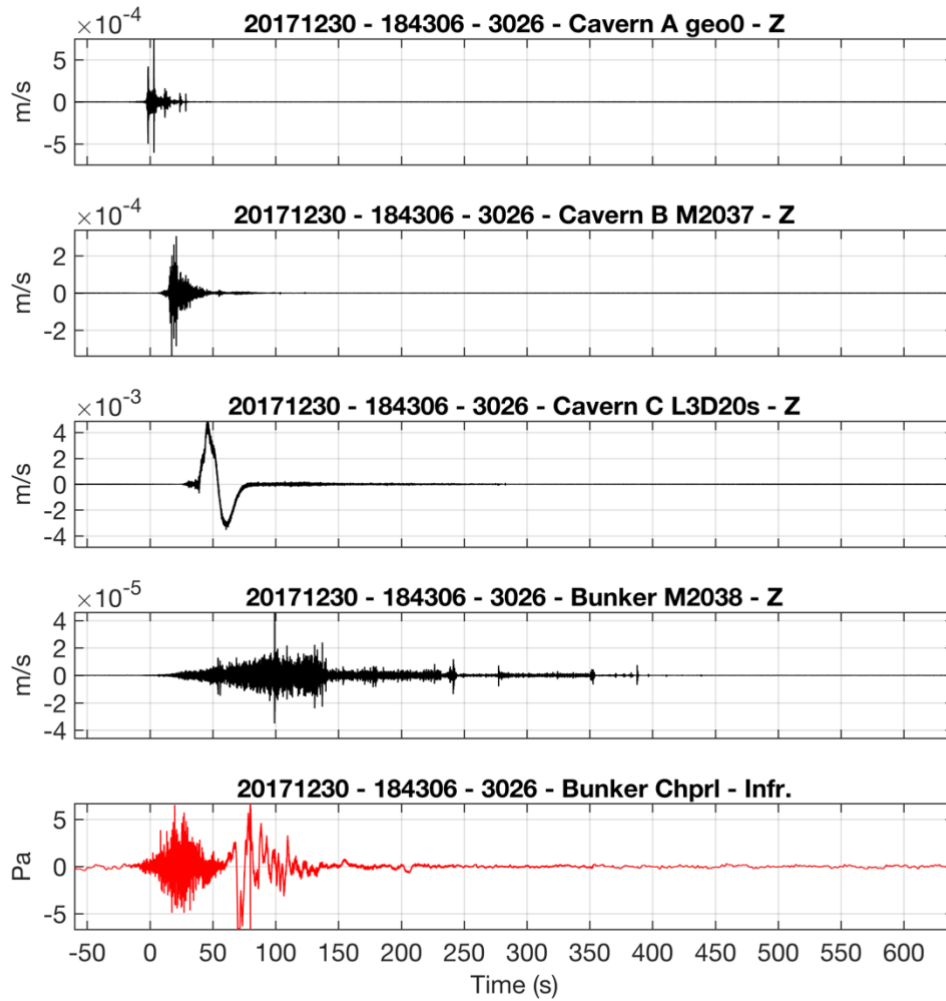
Figure 2.9 - Example of the plots created for every trigger file for seasons from 2012 until the present time. In black: Seismograms (m/s) of the vertical component (Z) recorded in each cavern seismometer. The numerical codes between short dash typo correspond to the date (YYYYMMDD), the trigger activation time in UTC and the trigger activation number code, respectively, followed by the names of the cavern and sensor and component. From top to bottom: Cavern A (seismometer geo0), Cavern B (seismometer M2037), Cavern C (seismometer L3D20s, broadband), Bunker (seismometer M2038). In red: infrasound signal (Pa) (Chaparral sensor) with a similar code. The Infr indicates the infrasound measurement. All plots include the data of the entire trigger files from -60 s to 640 s (700 s in total with 60 s pre-trigger). Time zero corresponds to the instant of the trigger activation.

In the representation b) (Figure 2.9), the amplitude axis scale (m/s) for the [Z] component is adjusted for every sensor to visualize all data regardless of the amplitude. However, it is important to consider the vertical axis values when comparing data plots between sensors (Figure 2.9) and between data different trigger files.

Spectrograms constitute the other representation used to check the triggers and make preliminary interpretations. The data are represented in two different spectrogram combinations, like the seismograms: a) each of the three components for every sensor separately (not shown); b) the vertical component (Z) of every sensor corresponding to the different caverns, including the infrasound sensor data (Figure 2.10). Spectrograms are a

widely known representation in the field of mass movement seismology and the main representation used by the UB-RISKNAT Avalanche Research Group to identify snow avalanche seismic signals and recognizing their evolution (e.g., Biescas et al., 2003). The spectrograms are computed by performing the PSD (Power Spectral Density) (e.g., Brigham, 1974) in time windows of the seismic signal, using Hanning windows of a given duration and a certain time overlapping. It is a 3-dimensional representation with a colour scale. The vertical axis is for the frequency bands, the horizontal axis for the time and colour scale for the amplitude of every frequency band in each particular time window. After trying different Hanning window durations, for the automatic representations of the spectrograms I selected 1 s of duration and a 50% of overlap. In the UB-RISKNAT Avalanche Research Group, we tend to use other windowing configurations with different time window lengths (e.g.: 0.61 s length and 50% overlap in Suriñach et al., 2020; 1.28 s length and 50% overlapping in Vilajosana et al., 2007b, and in Pérez-Guillén et al., 2016) according to the length of the signal represented and the desired low-frequency resolution. The chosen configuration here is regarded as the standard one for the created database and allows us to represent frequencies from 1 Hz to 50 or 100 Hz, depending on the sampling rate of 100 or 200 s.p.s. (Shannon-Nyquist theorem, see Section 3.a for a detailed explanation on the time-frequency resolution relationship).

The Power Spectral Density (PSD) is performed for each 1s time window. For a better representation, the amplitude scale for every frequency band (A [(m/s)2/Hz]) is represented in dB (dB = 10·log10(A)). In the representation, the values are shown in JET colour map scale, which is widely used in seismic data representation. In this colour map, the highest amplitude values are in red and the lowest amplitude in blue, grading between them to yellowish and to greenish tones.

In order to compare data between sensors, stations and between avalanches, I decided to lock the colour scale limits between -210 dB (blue tones) and -90 dB (red tones) for all the seismic signal spectrogram representations. The colour scale for infrasound data is locked between -100 dB and 0 dB (Figure 2.10). These colour scale boundaries are the result of the calibration of a huge quantity of avalanches at the VDLS experimental site (since 2012 until 2019). With this representation, the recognition of characteristics of interest in the first visual approach becomes faster. Stronger seismic signals have reddish colours and can be linked with larger avalanches (or with an avalanche passing straight over the sensor). The duration of the avalanche or the general flow regime can be also inferred from the first visual approach. Using this representation with the same colour scale, it is easier to find the large avalanches and interesting trigger activations data such as earthquakes or explosions.
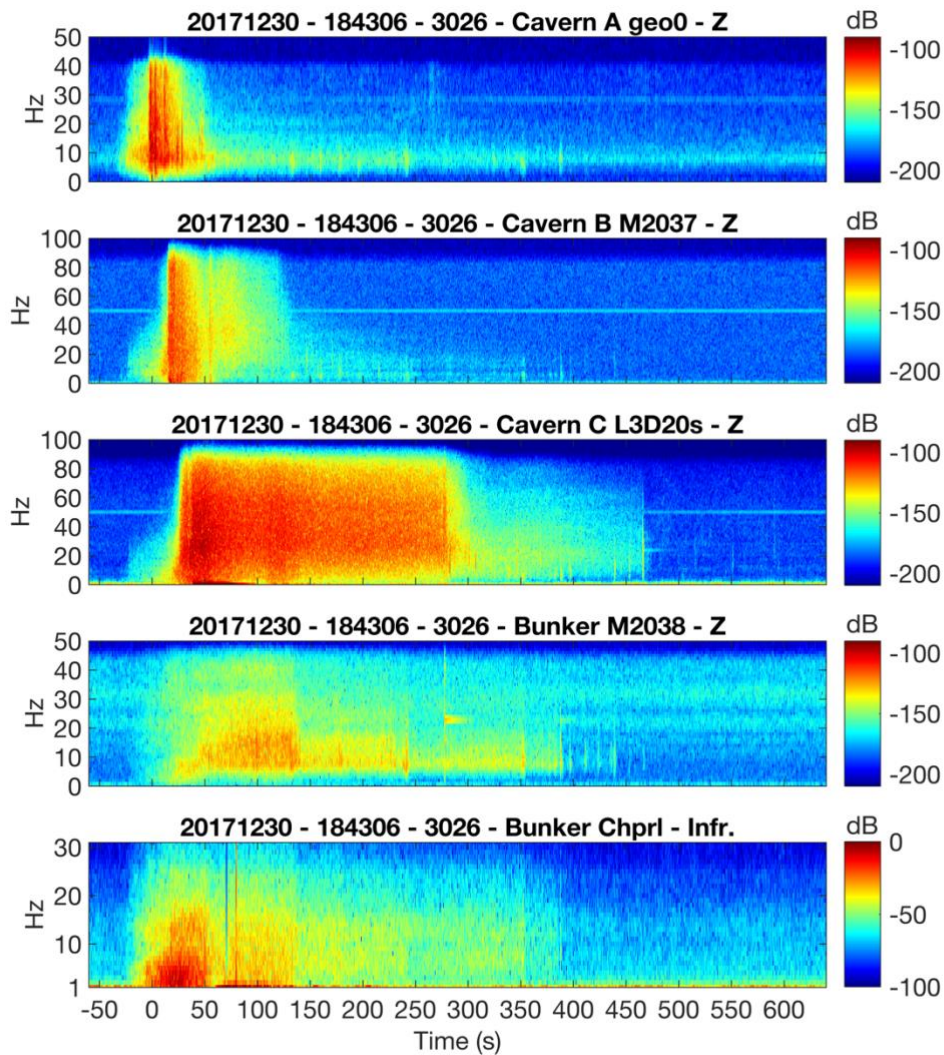
Figure 2.10 - Example of the plots created for every trigger file for seasons from 2012 until the present time. Spectrogram representations of the seismic data trigger files are shown in Figure 2.9 with the same numerical codes and order representation. Note the different vertical scales according to the sampling rate. Colour scale in dB, limits of the seismic data [-210dB -90dB] and limits of the infrasound data (bottom) [-100dB 0dB]. Time zero corresponds to the instant of the trigger activation.

All the protocol steps of data processing, representations of the data and database managing actions, are joined in a unique code written in MATLAB® R2018a (MathWorks Co.). It was created to provide easy access to all the data belonging to the research group, because of: 1) the necessity for processing and comparing a large amount of trigger activations data at VDLS; 2) the requirement for a standardized way of processing the data, and 3) the capability of evaluating trigger activations seismic data in the shortest time possible in each ongoing winter season data at VDLS. Until the present, the UB-RISKNAT Avalanche Research Group processed the data of every trigger activation data file manually. After this processing procedure, the seismic data are ready and available for more detailed processing procedures searching for release areas (see Chapter 4) and for flow regime identification (see Chapter 5).

Having the data ready for use as fast as possible during the ongoing winter season data acquisition provides us with a near real-time tool for the evaluation of trigger system activations at VDLS. In addition, the availability of a homogeneous protocol for the seismic data classification and representation for past winter seasons at VDLS allows us to guarantee easy access to all data and to establish a common base for conducting comparisons and studies throughout different winter seasons data.

Chapter 3

Seismological procedures used for snow avalanche classification and data representation

The seismological definition of snow avalanches and their representation has been known for many years. Based on seismic waveforms and frequency content identification, the avalanche flow regime and a qualitative description of the snow avalanche behaviour along the avalanche path can be performed (Sabot et al., 1998; Suriñach et al., 2001; Biescas et al., 2003; Vilajosana et al., 2007a & 2007b; Pérez-Guillén et al., 2016). The evolution of signal processing techniques and more powerful computing machines and routines allow us to go deeper into the signal processing workflows to extract more detailed information and to increase the resolution of the information contained in the seismic signals.

Signal processing can be confusing and sometimes the seismic signal processing tools are used in different ways to look for different outputs and interpretations. This chapter is focused on showing all seismological signal processing tools used in this dissertation and on the new methods proposed. The different types of representation, naming and parametrization for clarifying and setting a common background are also presented.

3.a. Signal processing tools

3.a.i. 3D seismic data rotation

The seismic sensors at the VDLS test site are 3D, with the components oriented as follows: two horizontal components in the north-south and east-west directions, and the vertical component normal to them. In the data acquisition systems (DAS), Channel (Ch) 1 is for vertical component (Z) positive values in the zenith direction, Ch 2 for north-south component (N) with positive values facing north, and Ch 3 for the east-west component (E) with positive values facing east. This is the usual channel configuration and geophone orientation used for seismic stations of all seismic networks as an agreement for easier use and interpretation of the data. Hereinafter, this configuration will be referred to as [ZNE].

The seismic stations placed at VDLS have one clear objective: to record seismic data of snow avalanches for their subsequent study. At VDLS, the avalanches only can descend from one direction, being released close to the mountain ridge and moving down the slope to the Sion river. Consequently, although the geophones are placed on the flat and oriented toward ZNE, the seismic components were rotated in order to link the seismic data better to the snow avalanche direction. The rotation of the 3D seismic signal at VDLS was previously used by Pérez-Guillén (2016). We add the data of one more seismic sensor (Cavern A), required to update and adapt the rotation method to the data available and to the information on which we focus. With this rotation, and using a data processing routine, the new coordinate system for the seismic signals at VDLS is the [QLT], being the component normal to the ground surface, L the component parallel to the major slope facing the main avalanche flow direction, and T the component normal to the other two and parallel to the ground surface. The terminology is the same as that used in seismology (see IRIS Web service rotation methods as an example [service.iris.edu/irisws/]), but with a different meaning focusing on the slope direction. The seismic data needs to be rotated from the ZNE coordinate system to QLT. Both coordinate systems are related by two angles, necessary to perform the rotation of the seismic components: *baz* and slope (Figure 3.1). These angles are fixed and defined by the topography and location of the sensor. The *baz* angle, on the NE plane, corresponds to the back-azimuth from the sensor position pointing to the release areas in the main slope direction (from north in a clockwise direction). The *slope* angle, in the plane Q-L, is formed by the ground surface in the main slope direction and the horizontal plane at the sensor position. These angles relate the ZNE and QLT coordinate systems and are used to rotate the seismic signals recorded in the ZNE coordinates to the QLT coordinates. The rotation method used is adapted from the rotation of the 3D seismic data method used by IRIS (Incorporated Research Institutions for Seismology), based on Plešinger et al., (1986).

The method was originally designed for rotating the seismic signal in order to align the components to the seismic wave field. In our case, the method was adapted to match with the VDLS slope morphology. For this reason, the incidence angle defined in the IRIS method (*inc*) is adapted to the *slope* angle, being over the horizontal (*inc* = *slope*+90°) (Figure 3.1).
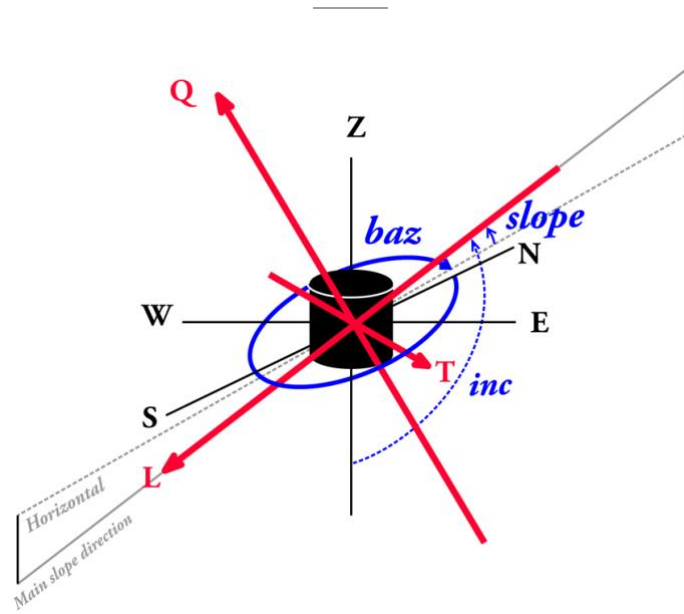
Figure 3.1 - Coordinate systems in a sensor. In black, the geographic coordinate system [ZNE], orientation of the seismometer (black cylinder). The grey line indicates the main slope direction and grey dashed line its projection on the horizontal plane (N-E, orthogonal to Z). In red the QLT coordinate system. L coincident with the main slope direction. In blue, the back-azimuth angle (*baz*), the incidence angle (*inc*) and the *slope* angle, relating both coordinate systems and used in the data rotation.

The rotation matrix M3D (**3.1**) is built using *baz* and *inc* angles to relate both coordinate systems (ZNE and QLT) using the matrix transformation equation (**3.2**).

$$M_{3D} = \begin{bmatrix} \cos inc & \cos inc \cos baz & \cos inc \sin baz \\ \sin inc & -\sin inc \cos baz & -\sin inc \sin baz \\ 0 & \sin baz & -\cos baz \end{bmatrix} \qquad 3.1$$

$$\begin{bmatrix} Q \\ L \\ T \end{bmatrix} = M_{3D} \begin{bmatrix} Z \\ N \\ E \end{bmatrix} \qquad 3.2$$

To keep the same arrangement used in the ZNE coordinate system and to adapt the rotation method to the snow avalanche seismic data studies, the components are arranged as follows: the component normal to the ground surface direction in the first position (Q), the component in the flow direction in the second position (L), and the component parallel to the ground surface but perpendicular to the flow direction in the third position (T).

For VDLS, the *baz* angle is considered to be 299° for all seismic sensors, being the main slope direction and average avalanche propagation direction (Figure 3.2). This direction does not cover all the avalanche directions, although it is advisable to have all seismic sensors aligned. The *slope* angle is different for every sensor, because the topography is not the same along all the avalanche path. The slope values are 35° at Cavern A, 20° at Cavern B (after the gully part where the sensor is placed), and 19° at Cavern C (the mean slope at the runout area) (Figure 3.2). These values are obtained from the VDLS site Digital Elevation Models

and field measurements. The bunker (Cavern D) seismic data are not rotated. These data are used as a reference, although they are not used for calculations in this PhD thesis.
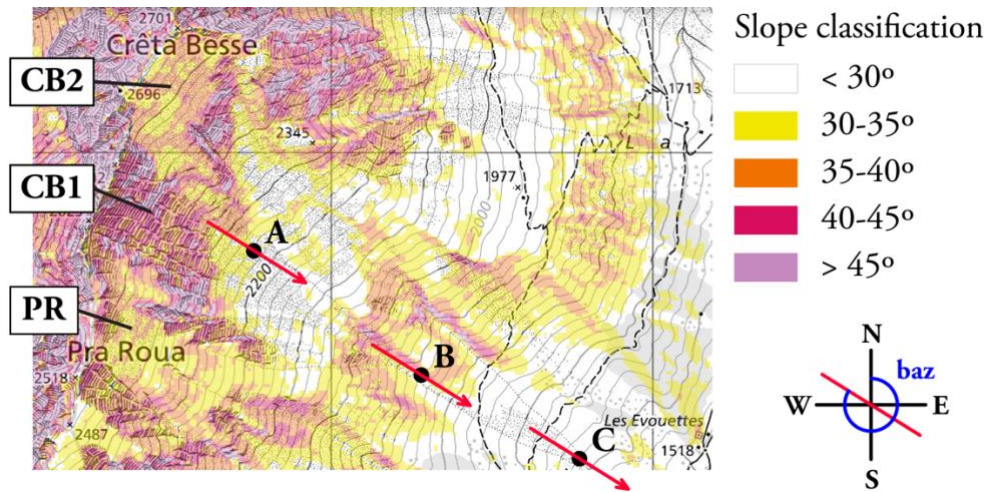
Figure 3.2 - Map of the VDLS experimental site with the slope classification (>30º) made by Swiss Topographic Services using swissALTI3D digital elevation model with 10 m resolution [online: map.geo.admin.ch]. Red arrows pointing to the main slope direction of propagation of the snow avalanches and L component of the QLT coordinate system. Back-azimuth angle (*baz*) calculated from north to the main slope direction pointing to the release area from the sensors position, in a clockwise direction, according to the IRIS Web Services data rotation schema, [online: service.iris.edu/irisws/rotation/docs/1/help/] and Plešinger et al., (1986).

3.a.ii. Envelope

The envelope of an oscillating signal is a function curve outlining the extremes of these oscillation amplitudes in a time series representation. The envelope can be the upper or the lower envelope depending on whether it is outlining the upper part of the oscillation or the lower one. In order to include all the oscillations in the positive upper part, we calculate the envelope using the Hilbert transformation of the absolute positive values of the seismic signal (*y*QLT,*t*), for every component [QLT] and every sampling time (t) (3.3) (Earle & Shearer, 1994). Thereafter, using (3.4) the component envelopes are joined together for every single time step *At(t)*.

$$A_{QLT}(t) = \sqrt[2]{|y_{QLT,t}|^2 + h(|y_{QLT,t}|)^2} \qquad\qquad 3.3$$

$$At\ (t) = \sqrt[2]{A_Q^2 + A_L^2 + A_T^2} \qquad\qquad 3.4$$

The Total Envelope (*At*) is a common data representation widely used by the UB-RISKNAT Avalanche Research Group. The *At* is normally smoothed using a moving average method each 0.5 s and, sometimes, is normalized between [0 1]. The *At* values have the ability to show the amplitude of the whole seismic signal and are very useful for comparing time series of other snow avalanche data (Vilajosana et al., 2007a; Vilajosana et al., 2007b; Vilajosana et al., 2008; Pérez-Guillén et al., 2014; Pérez-Guillén et al., 2016).

The spectrogram representations with the amplitude values in logarithmic scales are widely used, and most of the seismic data interpretations linked to snow avalanches are made using these data representations (see Subsection 2.b.i). To compare the time series with the spectrograms, it is useful to have the amplitude values of the time series in a logarithmic scale. To this end, we convert the Total Envelope (*At* [m/s], not smoothed) to decibels (dB) (3.5).

$$A_{t\ [dB]} = 10 \cdot \log_{10}\left(A_{t\ [m/s]}\right) \qquad\qquad 3.5$$

After this, the data are smoothed using the *smoothdata* function of MATLAB® software (introduced in MATLAB® R2017a) (Figure 3.3) using the gaussian method and a 4second moving time window. In the following data envelope plots, and for all the methodology described later in this chapter, we use the Total Envelope (*At*) (including all three components seismic data) in a logarithmic scale and smoothed as described (Figure 3.3d).
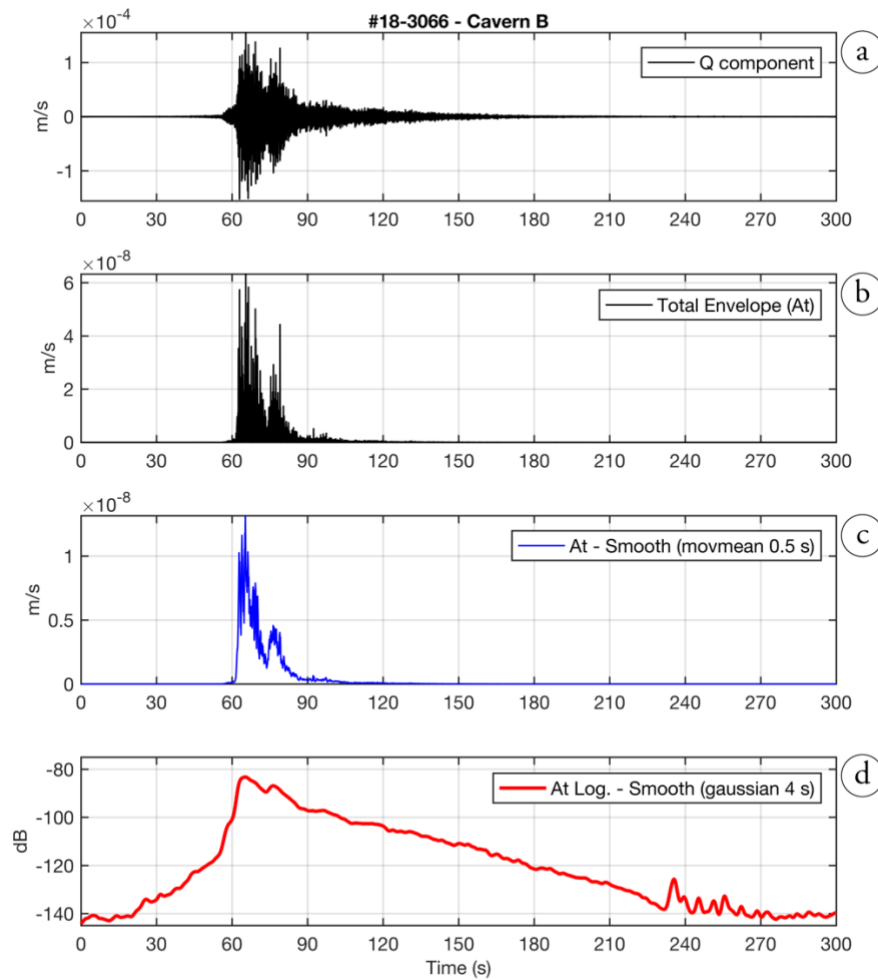
Figure 3.3 - Seismic data recorded in Cavern B at VDLS, during the snow avalanche #18-3066. From top to bottom: a) Q component seismic signal ground motion (m/s). b) Total envelope (At). c) Total envelope (At) smoothed, using a moving average every 0.5 s. d) Total envelope (At) in logarithmic scale smoothed, using the gaussian method in 4 s window. Note that the logarithmic scale allows us to obtain more visual information in the intervals before the maximum values (0-60 s) and in the last parts of the seismic signal (150-300 s).

3.a.iii. STA/LTA algorithm

The STA/LTA, short term average (STA) over long term average (LTA), is a trigger algorithm widely used in weak-motion seismology. Many other triggering systems exist but the STA/LTA algorithm seems to be one of the most sensible and configurable for different purposes (Withers et al., 1998) still used in digital data records and seismic data processing software. This method is very useful for seismic noise isolation, since it is able to detect trigger and de-trigger times for micro-seismic events, and also for noise calculation because it considers only the noise level seismic signal (Trnkoczy & Bormann, 2012).

The method consists in calculating the average of the absolute amplitude values ($|y_k|$) in two consecutive moving-time windows of different lengths (N_S and N_L). This average can be calculated for any of the 3 components (k = [1 2 3] or [Q L T] or [Z N E]). The short time window (N_S) gives us the short-term amplitude average value (STA) (3.6) and is sensitive to the seismic events by changing its value for seismic amplitude peaks. The large time window (N_L) gives us the long-term amplitude average value (LTA) (3.7) and also provides the seismic noise level information. The STA/LTA ratio is calculated continuously for every Ns time window and compared to threshold levels.

$$STA = \frac{1}{N_S} \sum_{n=N_L}^{N_S+N_L} |y_{k,n}| \qquad 3.6$$

$$LTA = \frac{1}{N_L} \sum_{n=1}^{N_L} |y_{k,n}| \qquad 3.7$$

The threshold levels must be defined for every site or every kind of event one wishes to record or identify, as well as for defining the duration of the time windows for STA and LTA. The accuracy and trustworthiness of the method depend on the configuration of the STA/LTA algorithm triggering parameters. A common configuration takes into account the seismic data between the moment when the ratio STA/LTA exceeds a certain threshold value (Activation) and when the ratio STA/LTA falls below a certain threshold value (detrigger time, Deactivation) (Figure 3.4). The isolated portion of the data may be regarded as the seismic event detected by the STL/LTA method and saved for its analysis (e.g.: earthquake location of energy calculation).

The time average durations and trigger thresholds can be appropriately configured to detect the part of the data to be isolated. In the example given In Figure 3.4, the duration of the average windows is adjusted for the detection of the earthquake data. For snow avalanche data detection, the average and threshold values used are different. See Subsection 3.b.ii for a detailed configuration of the STLA/LTA algorithm for snow avalanche detection used in this PhD.

The STA/LTA algorithm is available in some data-loggers for processing seismic data in real time. The automatic triggering system at VDLS (managed by the SLF) does not use this algorithm (only an amplitude threshold criterion), and consequently the trigger time does not allow the data of the first snow avalanche steps we are interested in to be recorded. Moreover, these first vibrations did not activate the VDLS triggering system. We use this STA/LTA algorithm in the seismic data of snow avalanches in the continuous stream at Cavern A to recognize the start of the mass movement (not in real-time). The detection of

the start of the mass movement is crucial for isolating the first seismic signal produced by
the snow avalanche.
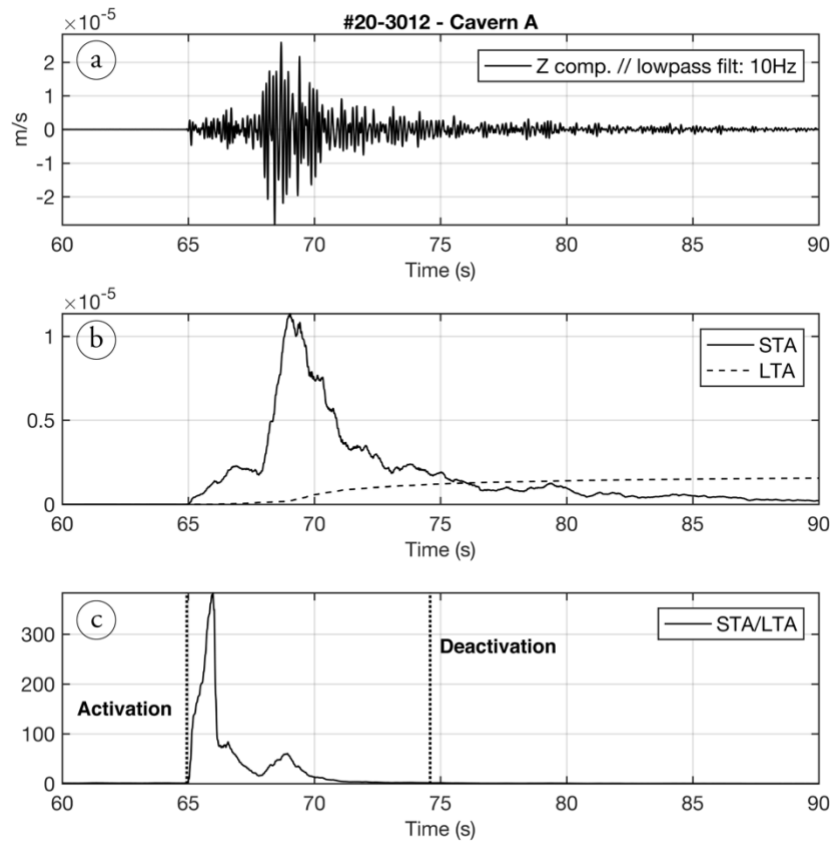
Figure 3.4 - Seismic data recorded at Cavern A at VDLS of an earthquake M2.9 close to VDLS, (#20-3012
VDLS trigger activation: 2019-11-30 02:14:45 UTC). From top to bottom: a) seismic signal ground motion
(m/s) vertical component Z (earthquake data, not rotated), b) STA (1 s) and LTA (30 s) values in moving
time windows and c) STA/LTA ratio. The black dotted line indicates the trigger activation time (threshold
STA/LTA>2, t=65s) and the deactivation time (threshold STA/LTA<1.5, t=74.5s).

3.a.iv. Filtering

The recording of seismic data for avalanche studies in this PhD thesis is performed by
using short-period sensors (except at Cavern C, where one broad-band sensor is installed),
all of which are triaxial seismometers. Because of the type of seismic sensors and the
sampling frequency used (Chapter 2), the seismic raw data frequency range is between $1 -
100$ Hz, falling to 0.05 Hz at Cavern C when using the broadband sensor. This is the range
we are able to achieve, although as observed by the UB-RISKNAT Avalanche Research
Group, most of the seismic energy transferred by the avalanche to the ground does not
exceed 100 Hz and is mostly between $1 - 50$ Hz.

Filtering is an important procedure throughout the data process and must be
conducted properly to exclude the assumption of filtering errors and boundary artifacts as
valid results. The seismic data are filtered at different steps during all the data processing in

order to isolate the most interesting frequency bands of the recorded data. All data were filtered with a 4th order Butterworth filter, widely used and tested in seismic signal data processing. This is the most common filter used by the UB-RISKNAT Avalanche Research Group (Biescas et al., 2003; Vilajosana et al., 2007b; Pérez-Guillén et al., 2016). Generally, we use a bandpass filter to isolate the frequency bands where most of the seismic energy is concentrated, or to isolate the frequency bands that we wish to focus on in further data process steps. In case of considering only low frequency bands (close to 1 Hz), we use a low-pass Butterworth filter of the same 4th order to avoid boundary artifacts during the filtering process.

For the filtering we use the MATLAB® filter design function (*butter.m*) and the *filtfilt* filtering function for a zero-phase digital filtering, thereby avoiding phase changes observed using other filtering functions (Matlab Help Center, [on-line]). Widely tested, we consider this the less intrusive filtering method for our data.

3.a.v. Windowing

In signal processing, the windowing process consists of isolating part of the signal (window time length) using a windowing function. This allows us to perform the processing steps and calculations needed only on that part of the signal. The window function is applied recurrently to every time window with a certain chosen overlap.

One of the easiest windowing processes is the use of a square-shaped windowing function, isolating the time window and considering the rest of the signal as a zero value (Brigham, 1974; Smith, 2011). Due to the abrupt transition from signal to zero, the application of square-shaped windowing functions can produce unwanted artifacts (like ripple and ringing) and may lead to some false values in the spectral analysis of the signal. After some tests, we chose the Hanning window (cosine-sum) (Brigham, 1974), which provides the best relationship between signal-noise and does not induce noise in the frequency content. The Hanning windowing function is widely used and tested in snow avalanche seismic data processing by the UB-RISKNAT Avalanche Research Group for the calculation of spectrograms.

The window length must be chosen appropriately to prevent loss of part of the information or to avoid a wrong information from the data. As presented in Chapter 2, the data acquisition sampling rate is generally 200 s.p.s. in the trigger data stream and 100 s.p.s. in the continuous data stream on the DAS. According to Nyquist-Shannon Theorem (Nyquist, 1928; Shannon & Weaver, 1964; Brigham, 1974), the frequency range of a signal is exactly half of the sampling rate. Consequently, in data sampled at 200 s.p.s. we are able to obtain information up to 100Hz following eq. **3.8** where *Fn* is the Nyquist frequency and n the number of samples per second (s.p.s.). *Fn* is the top limit for the signal frequency content interpretation.

$$Fn = \frac{n}{2} \qquad\qquad 3.8$$

The length of the time window determinates the range resolution we can achieve in the frequency domain. The resolution in the frequency domain defines the available frequency range of the lowest frequency bands. The time window needs to be at least the same length as the largest period required for enabling work with (Period=Hz-1), the lowest frequency band range. To estimate the frequency domain resolution (ΔF) (3.9) and by extension the lowest frequency content range achieved from the window length, we need to consider the time window length (Δt), according to the Nyquist-Shannon theorem.

$$\Delta F = \frac{n}{(\Delta t \cdot n)} \qquad\qquad 3.9$$

As an example, the frequency resolution achieved for a one-second duration time window ($\Delta t = 1s$) of a seismic signal recorded at 200 s.p.s. (n = 200), is 1 Hz. The minimum instrumental frequency of Mark geophones (Cavern B, C and Bunker) is 1 Hz, the minimum instrumental frequency of the Mini-seismonitor from Geospace installed at Cavern A is 2 Hz, and the minimum instrumental frequency of the Lennart broadband seismometer installed at Cavern C is 0.05 Hz (the lowest in VDLS). Bearing this in mind, we consider that with a one-second time windows ($\Delta t = 1$ s) we achieve enough resolution in the frequency domain for a low frequency range close to the instrumental limits. The window length and the overlapping can be adjusted according to the resolution and range we are interested in. One-second length windows are narrow enough to perform spectral analysis with a sufficiently good time-evolution ratio to appreciate the seismic signal evolution and to obtain an adequate low frequency range. The overlapping between windows is adjusted for each use, as follows: 50% in spectrogram representations (see Subsection 2.b.ii), 10% in frequency content evolution studies (see Section 3.c) and 50% for particle motion studies (see Section 3.d).

3.a.vi. Ground particle motion analysis

Particle motion studies are used for the determination of the type of seismic wave recorded. Since P waves are longitudinal (compressional waves), the direction of the seismic particle motion can be used to pinpoint the origin of the arriving wave front. The polarization of the ground particle motion used for the calculation of the back-azimuth direction between the seismic source and the seismic sensor was defined by Vidale (1986) and improved by Jurkevics (1988). Our team applied this technique to the location of a rockfall on two occasions with good results using one or two triaxial sensors (Vilajosana et al., 2008; Guinau et al., 2019; Tapia et al., 2020). This technique was also applied to the location of one avalanche front from the Cavern B sensor at the VDLS test site (Pérez-Guillén, 2016).

Hereinafter, the seismic signal polarization method from Vidale (1986) and Jurkevics (1988) will be referred to as the V-J method. The study of the polarization following the V-J method consists in the definition of the covariance matrix (C_{ij}) for the 3D seismic data (3.10) and in solving the eigenproblem (3.11),

$$C_{ij} = \frac{1}{N} \sum_{s=1}^{N} u_i(s)u_j(s) \qquad\qquad 3.10$$

$$(C - \Lambda)\, P = 0 \qquad\qquad 3.11$$

where N is the duration of the time series in samples, s the sample and u_i (i=1,3) the seismic signal components (ZNE or QLT). Resulting from the eigenproblem are the eigenvectors P = [p1 p2 p3], which are the projection of the dominant directions defining the covariance matrix (around the particle motion), and the eigenvalues Λ = [λ1 λ2 λ3] related to the length of the eigenvectors (factor which scales the eigenvector). Ordered from the largest to the shortest, we are able to determine the main orientation of the polarization of the 3D seismic data inferred from the orientation of the eigenvectors [p1 p2 p3] (3.12), being the eigenvector corresponding to the largest eigenvalue [λ1] (3.13). Each eigenvector is defined by its component decomposition in the coordinate system axis (ZNE or QLT) and the related orientation angles. The orientation of the vectors from the reference axis is obtained trigonometrically (3.14). Considering the [QLT] coordinate system, the back-azimuth (*ba*) angle indicates the direction of the seismic station pointing to the seismic source in the [L-T] plane, measured from 0 to 360° in a clockwise direction from +L, and the incidence (*in*) indicates the direction from where the incoming wave front arrives at the [Q-L] plane, measured from 0 to 180° from -Q direction.

$$P = \begin{bmatrix} p1 \\ p2 \\ p3 \end{bmatrix} = \begin{bmatrix} p1_Q & p1_L & p1_T \\ p2_Q & p2_L & p2_T \\ p3_Q & p3_L & p3_T \end{bmatrix} \qquad \textit{Eigenvectors } 3.12$$

$$\Lambda = \begin{bmatrix} \lambda1 & 0 & 0 \\ 0 & \lambda2 & 0 \\ 0 & 0 & \lambda3 \end{bmatrix} \qquad \textit{Eigenvalues } 3.13$$

$$in = \tan^{-1}\left(\frac{p1_Q}{p1_L}\right) \qquad ba = \tan^{-1}\left(\frac{p1_T}{p1_L}\right) \qquad 3.14$$

A further output from this methodology is the linearity of the seismic signal polarization (R), which is very useful as a quality criterion for the polarization results. Linearity is calculated using the eigenvalues [$\lambda1\ \lambda2\ \lambda3$]. The resultant values are dimensionless between 0 and 1. The R values (**3.15**) are related to the amount of polarization of the seismic wave.

$$R = 1 - \left({(\lambda_2 + \lambda_3)}\middle/{2\lambda_1}\right) \qquad 3.15$$

When linearity values (R) are lower (close to 0), the seismic wave particle motion is more round-shaped, and the eigenvalues are more similar between them [$\lambda1 \approx \lambda2 \approx \lambda3$]. In this case, the polarization incidence and the back-azimuth angles (*in*, *ba*) of the seismic wave are less evident. Orientation angles with low linearity values should not be used because they could be arbitrary. Therefore, when linearity values are high enough (over 0.5 or 0.8 under criteria), the ground particle motion acquires a more ellipsoid shaped (polarized with one evident dominant orientation). At least one of the eigenvalues ($\lambda1$) is larger than the others [$\lambda1 >> \lambda2 > \lambda3$] (Figure 3.5). In these cases, the incidence and back-azimuth angle calculations are better linked to the ground particle motion and polarization is more representative. In theoretically perfect body waves (P, S), the degree of linearity is 1 and there is only one nonzero eigenvalue ($\lambda1$) (Jurkevics, 1988).
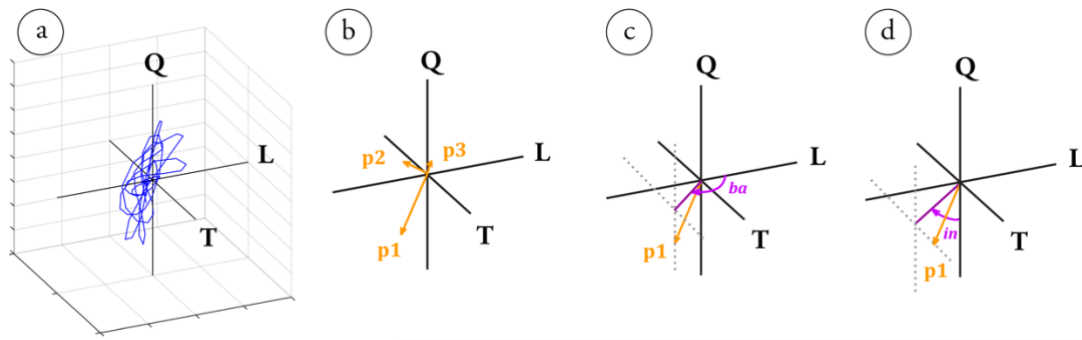
Figure 3.5 - Example of the particle motion study and the extraction of the polarization information. a) Seismic data particle motion (blue) in QLT coordinate system. b) Eigenvectors (orange) related to particle motion 3D shape. c) Eigenvector with the largest eigenvalue (p1) and the back-azimuth angle (*ba*) in the L-T plane) (purple). d) Eigenvector with the largest eigenvalue (p1) and the incidence angle (*in*) in the Q-L plane (purple).

This methodology is applied in the different sections defined in the avalanche seismic signal when looking for different information related to the snow avalanche mass position and the interaction of the snow mass with the ground (see Section 3.d). For these reasons, some parts of this V-J method are adapted by focusing on every purpose, always considering the basis of the method and its limitations.

3.b. Avalanche seismic signal sections

In earthquake seismology, the connection between the seismic signal hypocentre and the position of the seismic sensor is crucial for understanding the resulting recorded seismic signals and for making an accurate interpretation. At the scales involved in earthquake seismology, the generation of the seismic waves can be considered as single sources, all vibrations coming from the same origin (the earthquake hypocentre). From the hypocentre to the seismic sensor position, the different seismic waves may be fully developed and can be studied in the seismic data record.

In the study of the seismic waves generated by mass movements -snow avalanches in this case- these assumptions are not valid, and the seismic signals must be interpreted in a different way. Although the position and conditions of the seismic stations are known, the source of the ground vibration, which is multiple and no single, moves over the ground surface generating multiple wavefronts with different arrival times at the sensor.

For the interpretation and for further calculations, it is very important to define the relative position between the sensor and the avalanche front for each section of the seismic signal, and always take these observations into account when analysing the seismic signal.

3.b.i. Definition of seismic signal sections (SON, SOV/SBO, STA, SEN)

For a better understanding of the recorded seismic signal from snow avalanches, the UB-RISKNAT Avalanche Research Group described a criterion to define different sections on the snow avalanche seismic signal. The first description was made from data recorded at the Ryggfonn Experimental site (Vilajosana, 2008), based on the frequency content and amplitude evolution of the seismic signal. Three main sections were defined: Signal Onset, Signal Body and Signal Tail (Vilajosana, 2008). The seismic section definition changed to: Signal Onset, Signal Over sensor and Signal End (Pérez-Guillen, 2016). This classification is always relative to the sensor position on the snow avalanche path and is made qualitatively using the seismic signal amplitude and frequency content evolution, evaluated from the spectrogram plots (see Subsection 2.b.ii for a detailed description of the spectrograms calculation and description). Using the JET colour map, the reddish colours correspond to the largest amplitude seismic signal and the bluish colours to the lowest amplitude seismic signal, on the amplitude scale considered ([-210 -90 dB on a logarithmic scale). The vertical axis is related to the frequency bands and the horizontal axis corresponds to the time scale.

The first section of the seismic signal considered starts when the signal amplitude exceeds the background noise and ends when the seismic signal reaches the maximum amplitude and a full range of frequency content. This section is referred to as the Signal Onset (SON). At the beginning of the SON section, low frequencies are predominant and increase progressively to the full frequency range. The seismic signal amplitude also increases until reaches its maximum. A frequency content evolution can be observed in the spectrograms and has recently been used to estimate the velocity of the front of the avalanche and infer the rheology of the flow (Suriñach et al., 2020). This SON section is linked to the first steps of the mass movement of the snow avalanche, including the seismic record from the start of the mass movement until the front of the avalanche reaches the seismic sensor position or relative elevation close to the sensor (same altitude and in the same VDLS area, but not straight over the sensor). The maximum frequency shifting and the amplitude increasing are related to the decreasing distance between the avalanche front (source of the seismic signal) and the seismic sensor position. The amplitude and high frequency attenuations due to the ground effect become less effective the closer the avalanche is to the sensor. This is a consequence of the seismic wave propagation properties (Aki & Richards, 1980).

For the second and third sections, various approaches have been proposed. In the second section of the seismic signal, called the Signal Body (SBO) in Vilajosana (2008), the amplitude of the seismic signal remains high and the frequency content is in its full range (Figure 3.6), being linked to the avalanche front passing over the sensor. The SBO is followed by the third section called the Signal Tail (STA) in Vilajosana (2008), where the energy content of higher frequencies gradually decreases, linked to the snow avalanche tail passing over the seismic sensor (Figure 3.6). Pérez-Guillén (2016) proposed a new division of the second and third signal sections, considering the SBO and STA as one, and referred to as the Signal Over sensor (SOV) (Figure 3.6). The SOV section duration is larger than the SBO section and takes into account all that part of the avalanche flowing over the sensor. The

third section in the Pérez-Guillén (2016) classification is called the Signal End (SEN). Part
of the seismic signal was not included in the Vilajosana (2008) classification. The SEN
section corresponds to the ending of the seismic signal where the amplitude and frequency
content are much lower than in the other sections (Figure 3.6). This is linked to the seismic
vibrations originated by the snow avalanche flowing downslope from the seismic sensor
position. The SEN section includes the stopping phases, a characteristic seismic signature
with high amplitude originating in the slowing down processes of the snow avalanche flow
(Suriñach et al., 2000).
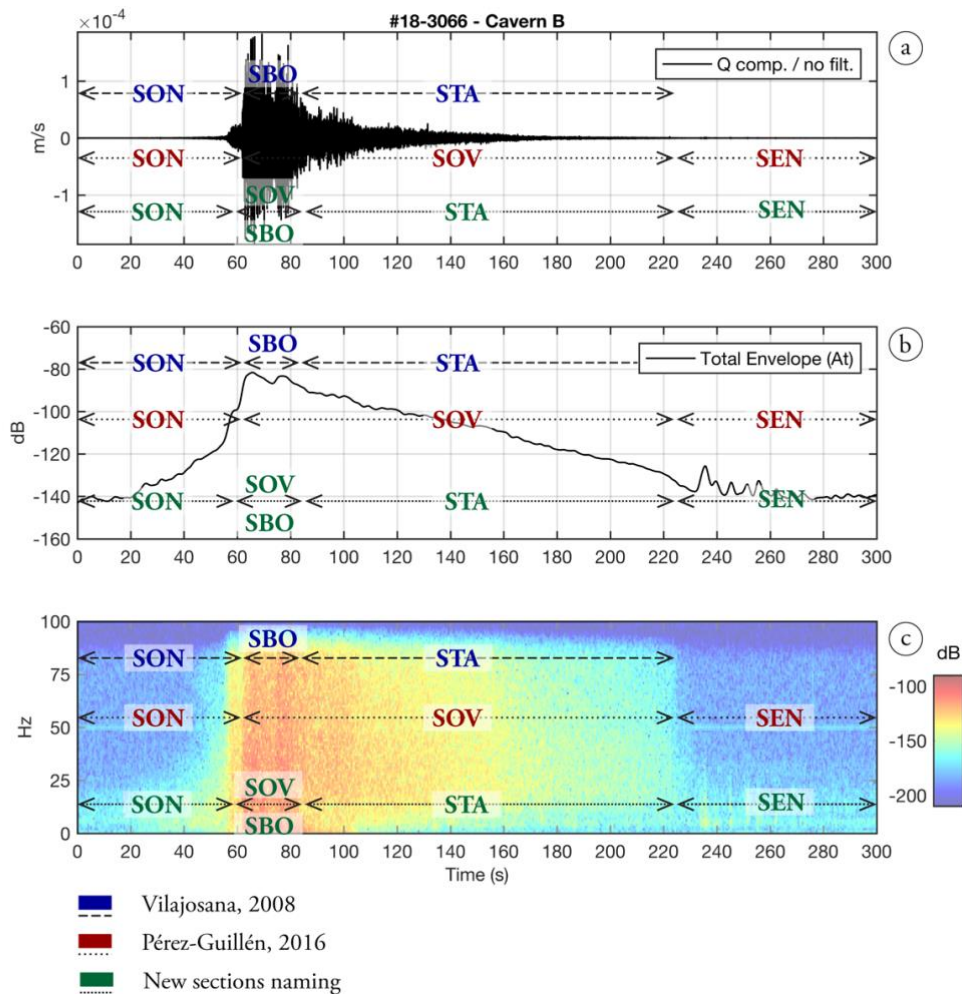
Figure 3.6 - Seismic data recorded at Cavern B at VDLS during the snow avalanche #18-3066. From top to
bottom: a) seismic signal of the Q component ground motion (m/s) (not filtered). b) Total Envelope At (in
dB). c) spectrogram representation in dB colour scale. In the tree plots are indicated the names of the
different seismic sections according to Vilajosana, 2008 (blue), Pérez-Guillén, 2016 (red) and the current
proposal for the seismic sections used in Roig et al. (2018) and Suriñach et al., (2020) (green).

The main differences between the Vilajosana (2008) and Pérez-Guillén (2016) sections
are linked to a different consideration of the relative position of the avalanche front. Here,
we seek to clarify and merge both seismic signal section classifications. As a first
approximation, Roig et al. (2018) and Suriñach et al. (2020) proposed the inclusion of the
Vilajosana (2008) Signal Body (SBO) and Signal Tail (STA) as sections of the Signal Over

sensor (SOV) in Pérez-Guillén (2016). However, going further in the interpretations of the seismic sections, I decided to merge the SOV and SBO sections into one (SBO/SOV section), with the only difference of taking into account whether the snow avalanche mass flows over the sensor (SOV) or not (SBO), evaluated from seismic amplitude criterion (see next Subsection 3.b.ii) (see Figure 3.6). At this SBO/SOV section, the seismic signal has the highest amplitude, and the frequency content range is complete. In the new classification, the SON section is shorter and the SBO/SOV starts earlier than in the older classification. To this end, I consider that part of the seismic signal before the maximum amplitude values is of interest for the flow regime classifications, above all in large Powder Snow Avalanches (see Figure 3.6).

The STA section corresponds to the seismic signal generated when the tail of the avalanche is flowing over the sensor, or close enough at the same topographic altitude. In this signal section the amplitude decreases, and the frequency content changes slightly towards lower frequencies than in the SBO/SOV section, although it remains close to the full range.

In comparison, the Signal End (SEN) section has a lower frequency content and lower amplitudes than STA (due the ground attenuation) and includes the stopping phases. The stopping phases can be recognized by high amplitude peaks at the final section of the seismic signal (Sabot et al., 1998; Suriñach et al., 2001). These are probably related to stopping mechanisms, friction overcoming the snow avalanche running force and freezing temperature effects. Stopping phases are normally if the avalanche mass stops close enough to the sensor (front or tail) and can be recorded by all the sensors if the snow avalanche is big enough (large amount of snow).

We propose a redefinition of the meaning of the sections to fit the Total Envelope observations of the snow avalanches in relation to the sensor position, as follows.

SON: Signal Onset. This corresponds to the section of the seismic signal linked to the approximation of the avalanche front to the sensor (when the approaching section is SOV) or close to the sensor at the same topographic altitude (when the approaching section is SBO). The seismic signal amplitude increases and the frequency shifts from low frequency to its full range.

SBO (Signal Body) and SOV (Signal Over sensor): The first corresponds to the section of the seismic signal related to the passing of the snow avalanche front for the same sensor altitude, but not over it. The second corresponds to when the avalanche front passes straight over the sensor. Both display the maximum amplitude and full range frequency content.

STA: Signal Tail. This corresponds to the section of the seismic signal related to the passing of the avalanche tail (dense) over the sensor or for the same altitude (not over). The full-range or high frequency content (>10Hz) is present and amplitude attenuation appears.

SEN: Signal End. This corresponds to the last section of the seismic signal of snow avalanches. It is related to the seismic vibrations generated by the snow avalanche flowing down-slope from the seismic sensor position. Low amplitude and low frequency content due to the ground effect attenuation are observed. It can include the stopping phases.

Spectrogram representations are widely used and provide us with all the necessary information that also contains consistent clues for the snow avalanche seismic signal section interpretation. However, a numerically unambiguous method for the seismic section classification has yet to be defined. In the search for a parametrization and a method to determine the duration of the different sections of snow avalanche seismic signal, Pérez-Guillén et al. (2016) proposed a methodology using the seismic Cumulative Energy (*CE%*) to establish the limits between the seismic signal sections. This method has a strong relationship with the start of the mass movement and requires a perfect time fitting. Furthermore, the recognition of whether the snow avalanche front passed over the sensor or close to it still needs to be made with the visual interpretations of the spectrogram representations, for which the *CE%* do not become a criterion.

I preferred to adopt an alternative approach by quantifying the qualitative observations of spectrograms in a logarithmic scale. As presented in Subsection 2.b.i, the amplitude in the spectrograms can be represented in a linear or logarithmic scale, but in this case the logarithmic scale is more suitable for achieving a better visualization at low amplitude values. The logarithmic scale is expressed in decibels (dB = $10 \cdot \log 10(A)$). As defined in this study, the limits of the colour scale of the spectrograms are always the same for all avalanche data and all sensors [-210 -90] dB. This definition allows us to compare the data representations (see Subsection 2.b.i). From the expertise acquired by the UB-RISKNAT Avalanche Research Group, we are able to identify qualitatively the boundaries between the seismic signal sections and thereby evaluate if a snow avalanche is flowing over the sensor or not. Looking for a criterion that can enable us to identify the same information numerically, I decided to use the Total Envelope in a logarithmic scale (see Subsection 3.a.ii), having all three component vibrations [QLT] in the same envelope (*At*). As defined in this study, the limits for the representation of the *At* values are [-160 -60] dB, and always the same for all avalanche data and all sensors.

3.b.ii. Parametrization of the seismic signal sections

A parallelism can be established between the Total Envelope (*At*) of the seismic signal and the sound synthesis envelope generators, known as ADSR from the initial letters of its sections: Attack, Decay, Sustain and Release (Moog, 1964; Vail, 2014). This parallelism is helpful for understanding the interpretation of the Total Envelope of the seismic signal and was an inspiration to analyse the signals. Sounds in sound synthesizers are defined by four stages related to the sound level and the duration of the sound when it is activated in the synthesiser (Figure 3.7).

Attack (A): time between the sound activation until it reaches the maximum sound volume.

Decay (D): time between the maximum volume (attack level) and the subsequent sustain level, lower or equal to the maximum attack volume.

Sustain (S): volume level at which the sound is reproduced until the activation stops, from the start of the sound activation at the start of the Attack section.

Release (R): time running between sustain volume level until the volume falls to zero, when the sound activation is released (deactivation) after the Sustain section and at the beginning of the Release section.

In Figure 3.7, the capital letters A, D, S, and R correspond conceptually to the SON, SBO/SOV, STA and SEN sections. Unlike in the ADSR sections, the limit between SON and SBO/SOV is not at the maximum amplitude of the envelope, as we will see later in this chapter. Note in Figure 3.7 how the background seismic noise level becomes value of amplitude 0 for the ADSR plot, and unlike in the ADSR plot the sustain (S) section does not maintain the amplitude. Conceptually, the activation (the start of the A section) will be the start of the seismic signal generated by the snow avalanche, and the deactivation time (between S and R sections) corresponds to the time when the snow avalanche stops flowing over the sensor (STA-SEN boundary).

When comparing the snow avalanche seismic signal Total Envelope (*At*) with the conceptual ADSR sound synthesis model, the Attack-Decay-Sustain-Release sections can be recognized and linked to the snow avalanche seismic sections. The SON section has the same definition as the Attack, an increase in signal amplitude/volume (dB). The SBO/SOV section can be compared with the Decay section, just after the amplitude reaches its maximum value (in the SBO/SOV we consider it starts slightly before, see Table 3.1), and the amplitude decreases until reaching the Sustain section (S). In the snow avalanche seismic signals, the amplitude also decreases in the STA section, when the avalanche tail flows over the sensor (or close to it). The SEN section corresponds to when no avalanche mass is flowing over the sensor (seismic vibration produced downslope from the sensor position) and is comparable to the Release section (R), until the amplitude/volume reaches the background noise level.
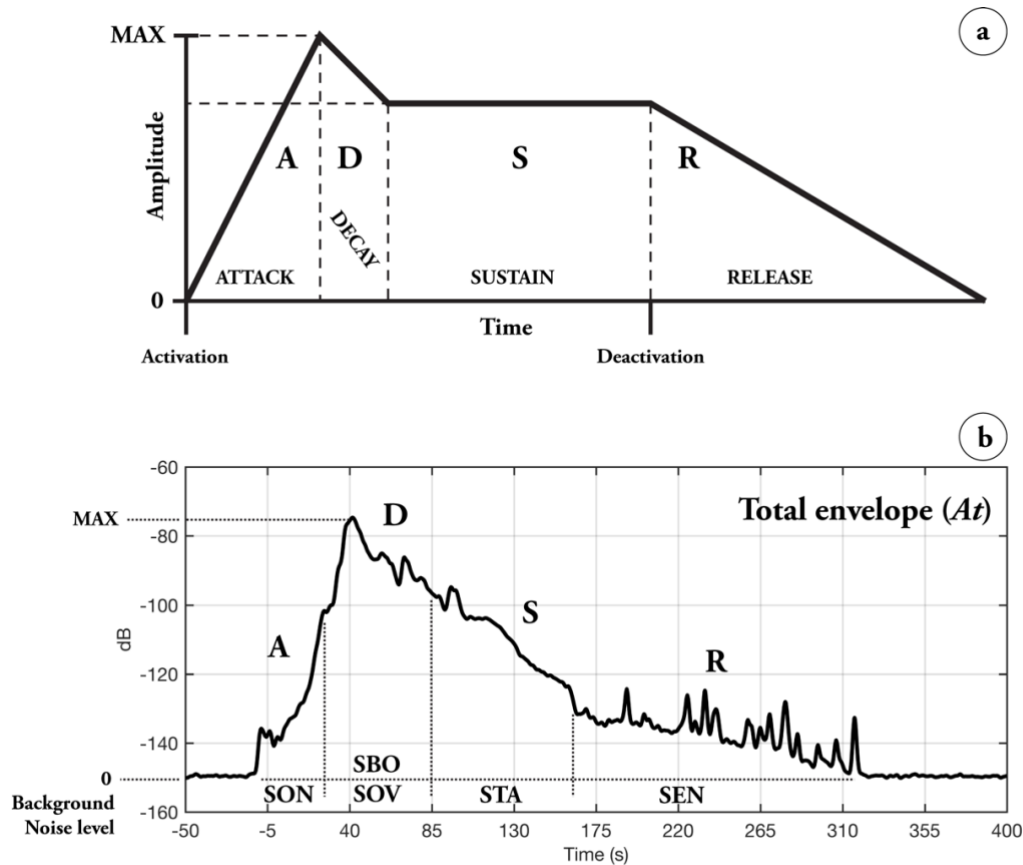
Figure 3.7 - a) Conceptual representation of the ADSR envelopes (adapted from Vail, 2014). Amplitude versus time with indicators of the separation between the different sections. b) Total envelope (At) of the seismic data recorded during avalanche#18-3041 at Cavern B, only as an example. Note the comparison between the ADSR envelope sections and the Total Envelope sections of seismic data.

In brief, the SON section is conceptually related to the Attack stage of the ADSR envelopes; the SBO/SOV are conceptually related to the Decay stage of the ADSR envelopes; the STA is conceptually related to the Sustain stage of the ADSR envelopes, and SEN is conceptually related to the Release stage of the ADSR envelopes.

This parallelism of interpretation helps us to obtain a schematic idea of what the Total Envelope (At) of the avalanche seismic signal looks like when it is over the sensor. If we find the amplitude values for the limits between the different sections, we will be able automatically to split the signal in order to work with it separately. Moreover, as in sound synthesis, the duration of each section can be null, skipping directly to the next one. This will provide us with clarity and accuracy when identifying the snow avalanche sections according to the criterion of whether or not the snow avalanche is flowing over the sensor.

The Total Envelope values (At) of all the avalanches between 2012 and 2020 at the VDLS test site were calculated and analysed. We found that, for all the snow avalanches and between seasons and sensors, the snow avalanche seismic signal Total Envelope (At) for the different seismic sections are similar. These At values can be linked to the snow avalanche mass position relative to the seismic sensor. It is important to recognize the limits between

sections of the snow avalanche seismic signals in order to determine whether the snow avalanche front passed over the sensor or not.

Ranges of At values were obtained from a calibration using data from the VDLS test site between 2012 and 2020 (Table 3.1) to define the limits between the seismic signal sections. These ranges can be used to infer whether an avalanche front passed over the sensor or not. Should the At values fail to reach or exceed -81 dB, then the snow avalanche front did not pass over the seismic sensor. The limit between the SON and SBO/SOV sections is located at -102 dB and the limit between SBO/SOV and STA is for values less than -89 dB. Values below -128 dB delimit the STA and SEN sections. Figure 3.8a shows a nice example of the At of snow avalanche seismic data recorded at Cavern B, where the different section limits of the seismic signal can be identified using the At threshold criteria. The maximum value is higher than -81 dB, indicating that the avalanche front passes over the seismic sensor (SOV section). The red line defines the limit between SON-SOV sections (-102 dB threshold), the blue line defines the limit between SOV-STA sections (-89 dB threshold) and the green line the limit between STA-SEN sections (-128 dB).

In an ideal snow avalanche with only one front, all these seismic sections will appear one after the other in the seismogram, enabling detection of the limits between sections from the At thresholds. This can be done mainly at Cavern B, where the avalanche has normally only one front (Figure 3.8a). However, many other avalanches have different fronts, passing over or near the sensor at different times (Figure 3.8b). In these cases, classification of the sections can also be done using the Total Envelope amplitude criterion, although the sections are more difficult to define because of the overlap of different seismic waves coming from the different fronts, and the changes in the At values are not clear enough.

Table 3.1 - Sections SON, SBO, SOV, STA and SEN of the snow avalanche seismic signal and the classification criteria based on the At values in dB.

Figure 3.8 - Examples of Avalanche Total envelopes. a) At of the seismic signal recorded at Cavern B during snow avalanche #18-3026 at VDLS. Only one avalanche front flowing over the sensor (max At > -81dB in the SOV section). In red, the limit between the SON and SOV sections. In blue, the limit between the SOV and STA sections, and in green the limit between the STA and SEN sections. b) At of seismic signal recorded at Cavern A during snow avalanche #18-3041 at the VDLS. Two consecutive avalanche fronts: the first one not flowing over the sensor (SBO1) and the second one flowing over the sensor (SOV2). In red, the limit between the SON and SBO1 sections. The dotted line indicates the limit between both fronts data (SBO1 and SOV2). In blue, the limit between the SOV2 and STA section, and in green the limit between the STA and SEN sections. Note the difference between 1) and 2) whether the front pass over the sensor or not.

One difference between the ADSR envelopes and the snow avalanche Total Envelope classification is that the limit between the SON (conceptually, Attack) and the SBO/SOV (conceptually, Decay) sections is not selected at the maximum At. As an example, in an schema of a Powder Snow Avalanche (PSA) flowing over a seismic sensor at VDLS (Figure 3.9), the arrival of the powder front (t1 and POW in Figure 3.9), corresponds to the end of the SON section and to the start of the SBO/SOV section (light-blue colour in Figure 3.9). The largest At value (in red) corresponds to the arrival of the dense part of the avalanche (dark-blue and DENSE in Figure 3.9), a few seconds later than t1, and included in the SBO/SOV section. The maximum peak of the At values is related to the passage over the sensor of the most energetic part the avalanche, which arrives at the seismic sensor position after the powder front due to the different front velocity (powder fronts are much faster) (red line in Figure 3.9).

For these reasons, unlike in ADSR envelopes, the *At* threshold for detecting the limit between SON and SOV/SBO is not at the maximum *At* value. In other type of snow avalanches (e.g., without a fully developed powder front), the *At* threshold at -102 dB (Table 3.1) also works well, since it is close enough in time to the arrival of the main snow avalanche front (the front velocity of all snow avalanche parts are more similar).
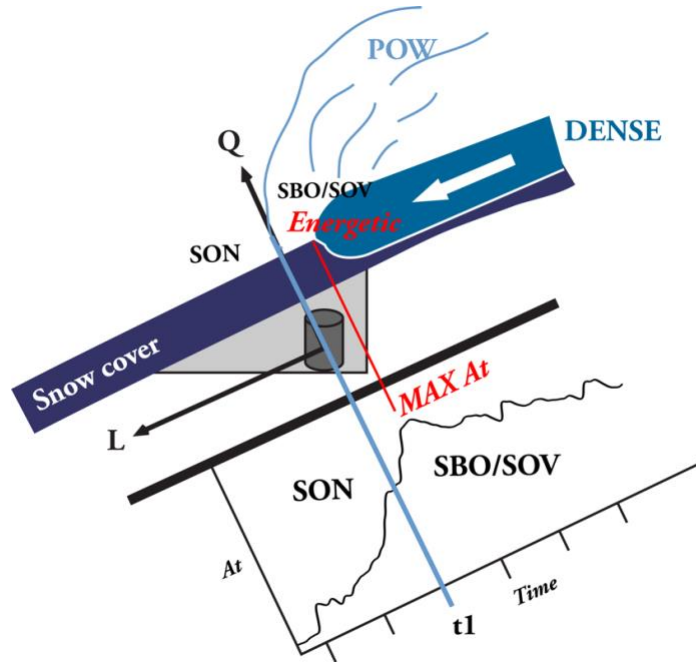
Figure 3.9 - Diagram showing the position of a seismometer in a cavern at VDLS (A, B or C), with the Q and L axis and an ideal PSA avalanche flowing over the sensor, and the *At(t)* values of the seismic signal recorded in the sensor. The SON - SBO/SOV boundary at time t1 when the powder part (POW) reaches the sensor is indicated. The maximum *At* value (red) corresponds to the arrival of the most energetic part of the avalanche, followed by the dense layer.

All the seismic signal sections defined are used in the analysis of the seismic signals in the later chapters: the SON section in snow avalanche release identification, the SOV section (no SBO) and STA section in the snow avalanche flow regime classification, and the SEN section in the snow avalanche stopping phases. Determination of the start of the mass movement (time zero) is performed with other criteria and not the *At* values. When working with the SON section data, we need to know the exact time at which the seismic vibrations generated at the start of the snow avalanche mass movement exceed the background noise level. This is neither possible nor unambiguous when using the *At* values. For the detection of the first seismic vibrations arising from the start of the snow avalanche, the STA/LTA ratio becomes a better option (see Subsection 3.a.iii). This method is widely used for weak-ground motion events detection, becoming really effective on low amplitude changes like the one we are looking for. To recognize the start of the mass movement from the data of the seismic station at Cavern A, we set the STA length up to 2 s and the LTA length up to 10 s. The seismic data files are delimited in time by the VDLS trigger activation and pre-trigger duration. The time zero (t=0 s) corresponds to the VDLS trigger activation, and the running averages start at the beginning of the data file (pre-trigger time, normally -60 s from the VDLS trigger activation). Using these time lengths for the moving amplitude averages, we consider that the snow avalanche starts when the STA/LTA ratio exceeds 2.5, and

consequently when the SON section starts. This corresponds conceptually to the activation time in ADSR envelopes.

Figure 3.10 shows the seismic signal recorded at Cavern A during avalanche #18-3013 at the VDLS test site, as an example for the identification of the start of the SON section (Figure 3.10a). The dashed line indicates the time t=0 s that corresponds to the VDLS trigger activation time (*t0*). The STA/LTA ratio values (Figure 3.10b) indicate the start of the snow avalanche when STA/LTA > 2.5 at -24.5 s (red line), before the VDLS trigger activation time. The spectrogram (Figure 3.10c) and the *At* values (Figure 3.10d) also show the difference between the background noise level and the seismic signal coming from the snow avalanche at this time. In other snow avalanches (not in the avalanche shown), the transition from the background noise to the seismic data generated by the first movements of the snow avalanche is smoother and more difficult to identify. With the STA/LTA ratio we can detect this difference clearly and unequivocally. Here, we use the vertical component (Z) of the seismic data directly, because when working on the SON section seismic data the rotation to the QLT coordinate system is not necessary (see Subsection 3.d.i in this chapter).
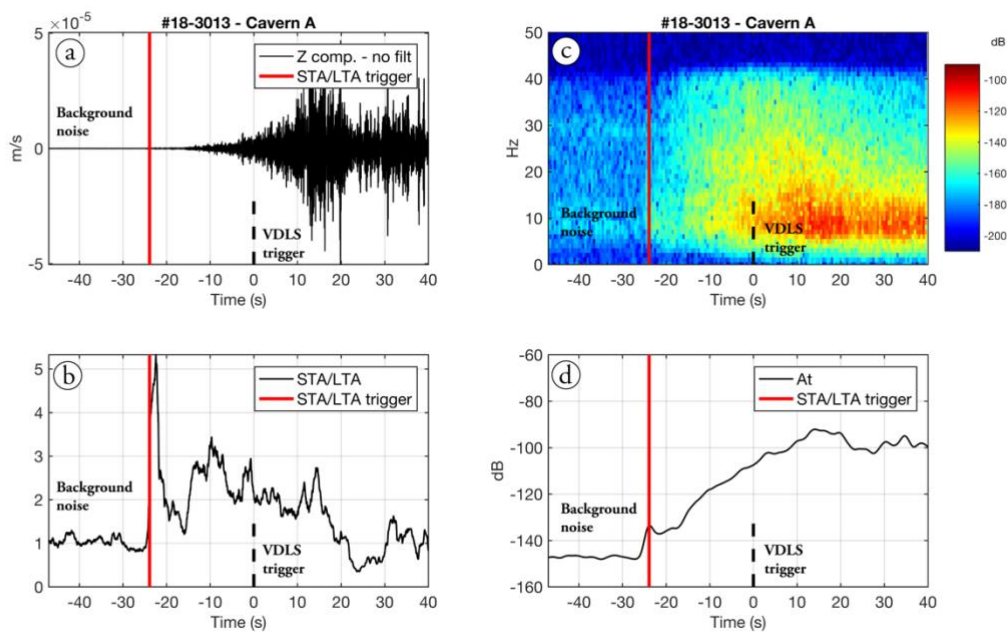
Figure 3.10 - Example of STA/LTA triggering procedure using the seismic data recorded at Cavern A during avalanche #18-3013 at the VDLS test site. a) ground motion (m/s) vertical component (Z). b) STA/LTA ratio. c) Spectrogram of the same data (vertical component). d) *At* data (3 components). In all plots t = 0 s corresponds to the activation time of the VDLS trigger system (black dashed line). Note that the avalanche starting time obtained from STA/LTA threshold (red) is earlier than VDLS trigger activation, at -24.5 s.

3.c. Avalanche seismic frequency content evolution

The frequency content of the snow avalanche seismic signals is related to the different parts of the avalanche flow (Pérez-Guillén, 2016). Low frequencies (f<10Hz) are related to the more energetic turbulent region and higher frequencies (f>10Hz) to the dense/tail parts

(Pérez-Guillén et al., 2016; Pérez-Guillén, 2016). Usually, the limits of this range of frequencies are not strict and the limits between the different avalanche parts can be mixed or imprecise. Moreover, the frequency content can be linked to the flow regime of the avalanche. Pérez-Guillén (2016) recognized that the Powder Snow Avalanches (PSA) mainly generate low frequency content (f<10Hz) and Wet Snow Avalanches (WSA) mainly generate a higher frequency content than PSA (f>10Hz).

Looking for more detailed information on the snow avalanche frequency content, I decided to use a new representation based on the calculation of the frequency content of the seismic signal in short windows of the time series. For this, I use time windowed data analysis to extract numerically the evolution of the frequency content and frequency dominances. The study and representations are performed for every component [QLT].

The time windowing process is conducted using a 1 s Hanning window and a 10% of overlap - note the difference with the "classical" spectrogram windowing parameters that use 50% of overlap for 1 s window. Considering the configuration of the seismic stations at VDLS, this windowing time length is selected to have enough resolution in the low frequency content range. With 1 s length windows, the resolution achieved in frequency content is 1 Hz, which is regarded as enough for the interpretation of the snow avalanche flow regime evolution. A frequency content lower than 1 Hz cannot be studied (see Subsection 3.a.v). We perform the calculation of the Power Spectral Density (PSD) for every time window. The results in linear scale are normalized between 0 and 1, considering the lowest and largest PSD values in the time window.

From the PSD values, y(f), for every time window we obtain the Dominant Frequency (*DF*, frequency with the maximum presence) (**3.16**) and the Spectral Centroid (*C*, the weighted centre of the frequency distribution) (**3.17**), used for mass movement studies in Saló et al. (2018), Guinau et al. (2019) and Tapia et al. (2020). *DF* is the most relevant frequency in the time window seismic signal considered, and *C* is related to a concept of clarity of the signal.

$$DF = \max_{0 \leq f \leq \text{Fn}} \left(y(f)_{QLT} \right) \qquad\qquad 3.16$$

$$C = \frac{\sum_{f=0}^{Fn-1} f \cdot y(f)_{QLT}}{\sum_{f=0}^{Fn-1} y(f)_{QLT}} \qquad\qquad 3.17$$

In these equations, f corresponds to the 1 Hz wide frequency bands, *Fn* is the Nyquist frequency (*Fn* = 1/*sp*) with *sp* the sampling rate, and *y(f)* corresponds to the PSD values for each frequency band. Both *DF* and *C* values are computed for all three components [QLT] and their evolution will be used as a flow regime identification criterion (Chapter 5). To obtain a complete frequency time evolution of an avalanche seismic signal, the PSD for every consecutive time window and the *DF* and *C* values for every time window are represented. As an example, Figure 3.11 shows this representation for avalanche #18-3066 recorded at

VDLS. The presence of the different frequency bands (1 Hz wide) for every time window seismic signal is represented in weighted dots for the normalized PSD values in the plots (Figure 3.11). The biggest dot corresponds to the frequency band with more presence (*DF* value), decreasing its size until reaching the minimum presence at the PSD.
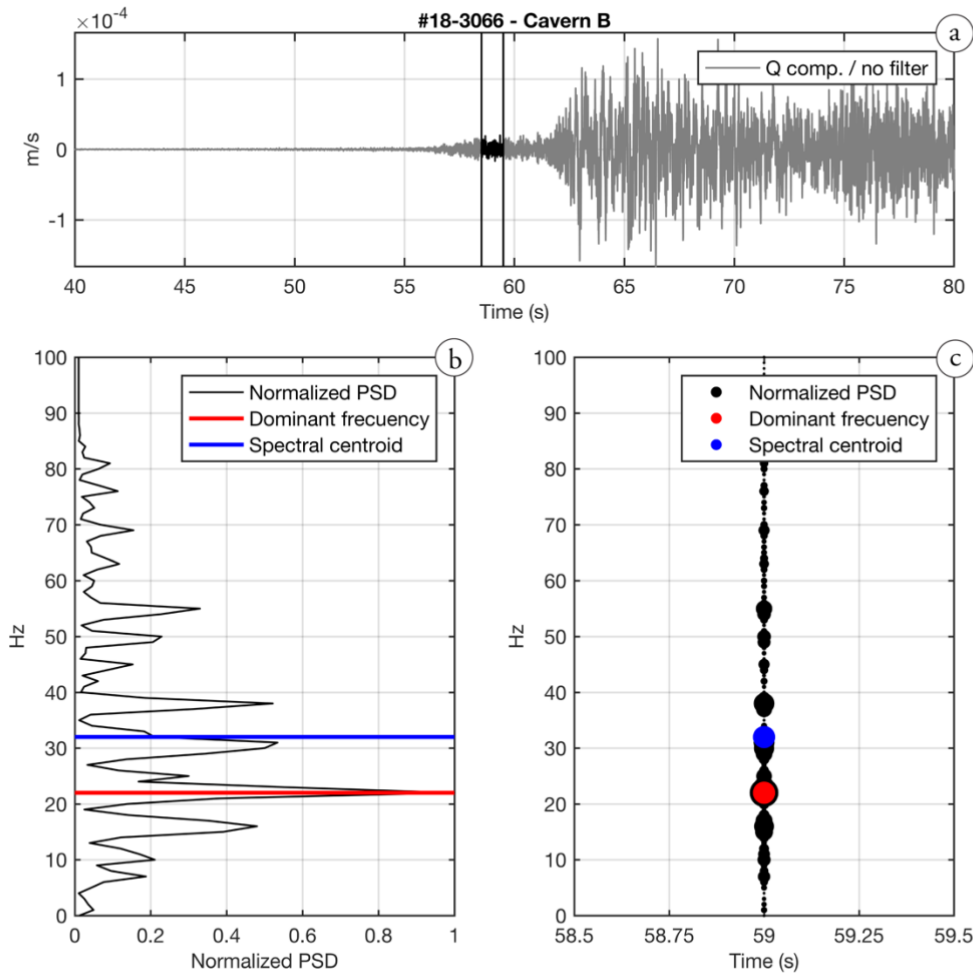
Figure 3.11 - Normalized PSD of a 1s time window a) Seismic signal recorded at Cavern B during snow avalanche #18-3066 at VDLS. In black, the 1 s (between 58.5 s and 59.5 s) time window studied. b) Frequency content distribution with PSD normalized [0 1]. c) PSD in dots, located at the centre of the time window (59s), weight sized according to their PSD representation for the 1 Hz frequency bands. In both plots: Dominant Frequency (*DF* = 22 Hz) in red, and Spectral Centroid (*C* = 32 Hz) in blue.

The frequency content evolution is observed from the plot of all the PSD of the time windows represented in weighted dots in terms of time. We seek to determine the frequency content evolution without any link to the seismic signal amplitude normalizing the values for every time window. Figure 3.12 displays the frequency analysis plots of avalanche #18-3066, for the seismic signal between -20 to 120 seconds. Figure 3.12a shows the spectrogram of the Q component, Figure 3.12b shows the dot plot for the PSD in time widows for the whole seismic signal, and Figure 3.12c the *DF* (red) and *C* (blue) values extracted from time windows PSD for the whole seismic signal. Note that between 55 s and 59 s the full frequency

content range is not relevant in the spectrogram plot (low amplitude in comparison to the signal after 60 s, in yellow), but it is very noticeable in the frequency time evolution plot (big black dots), only frequency content information and not considering amplitude information in comparison to the rest of the seismic signal (grey lines in Figure 3.12).
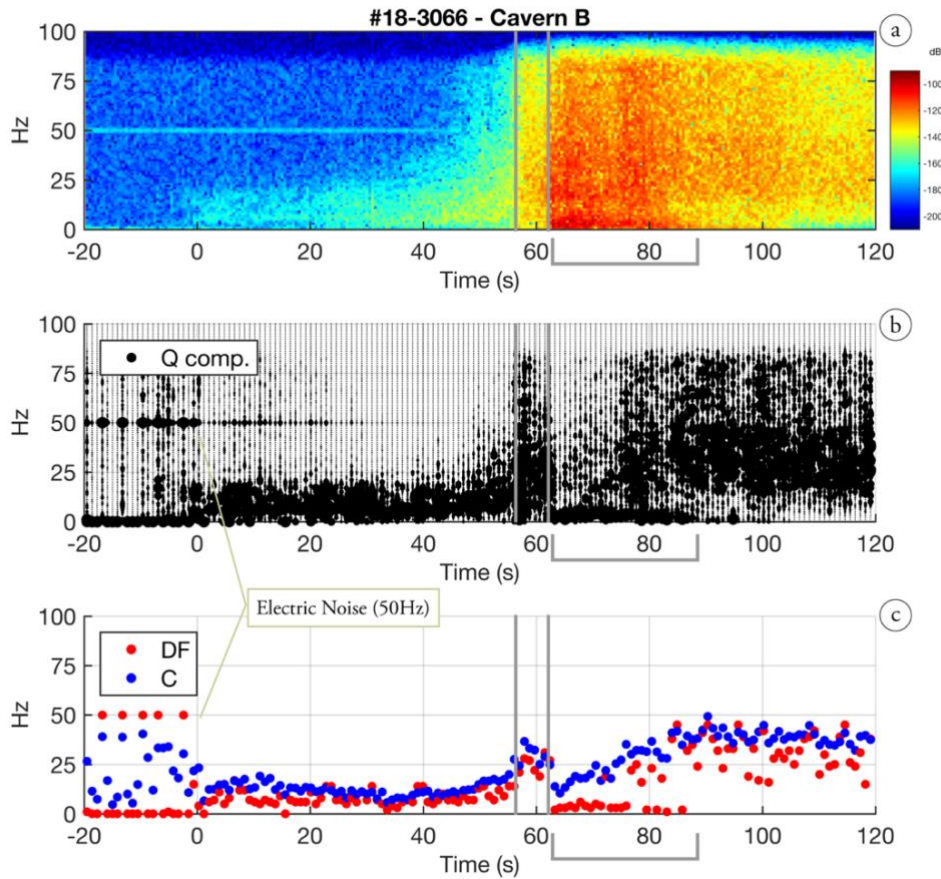
Figure 3.12 - Frequency analysis of the Q component seismic signal recorded at Cavern B during snow avalanche #18-3066 at VDLS (natural trigger). a) spectrogram computed as specified in Ch. 2 (1 s window, 50% overlap). b) PSD normalized Scatter plot computed in 1 s time windows and 10% overlap. c) Dominant Frequency (*DF*) (red) and spectral Centroid (*C*) (blue) extracted from the PSD calculated in time windows. Note in all plots the 50 Hz electrical noise between -20s and 20s. Time section isolated manually between -20 s to 120 s. The t= 0 s corresponds to the VDLS trigger activation and the negative time values correspond to the pre-trigger seismic data.

We consider this interval to be the initial arrival of the powder cloud front, and consequently the end of the SON section. Moreover, note between 60 s and 85 s a clear dominance of the lowest frequencies (1 Hz), which is also observable in the spectrogram (in red in low frequency bands), but without the same clarity and precision at the start and at the end (see *DF* values in Figure 3.12c). Further interpretations using the evolution of the *DF* and *C* values (Figure 3.12c) allow us to link this frequency content evolution interpretations to a different rheology of the snow avalanche parts. It is important to be aware of the limitations in the resolution and range of the seismic signal and the methodology used (due filtering and windowing) to avoid drawing incorrect conclusions. This data representation

allows us to examine the snow avalanche seismic signal from another point of view in all the seismic signal sections.

3.d. Polarization analysis

This section is devoted to presenting the application of the particle motion analysis to the different sections of the seismic signal generated by snow avalanches and the different information obtained from the different sections. Recognition of the seismic signal sections is made using the *At* threshold values criteria and the STA/LTA ratio to detect the start of the snow avalanche seismic signal (SON section) (see Section 3.b).

The particle motion polarization parameters (*ba*, *in*, *R*) can be linked to different processes and observations, depending on whether we consider that the movement of the ground particles comes from seismic wave fronts generated far from the sensor (plane wave) or if they are generated directly above it. Therefore, the data must be interpreted accordingly.

3.d.i. Applied to snow avalanche release area identification

For the avalanche release area identification, we use the seismic data recorded at Cavern A corresponding to the first steps of the snow avalanche release. The Cavern A seismic sensor is the one located closer to the main release areas of the VDLS experimental site, recognized by the SLF after years of observations (Chapter 2). Due to its proximity to the release areas, the seismic data recorded at Cavern A from the release of the snow avalanches suffer less ground attenuation (amplitude, frequency) than other seismic stations because it is closer to the seismic source (snow avalanche first movements), including the largest amount of information available.

The back-azimuth information extracted from the seismic wave field gives us information about the release area, relating this back-azimuth information to the seismic source position and, by extension, to the snow avalanche mass release. The main release areas of VDLS can be defined using back-azimuth ranges from Cavern A position, deduced geographically (Pra Roua and Crêta Besse areas, see Chapter 2). For a better understanding of the results, we decided to split the Pra Roua release area into two. The back-azimuth ranges for the release areas are: 175°-215° for PR2 (green in Figure 3.13), 215°-260° for PR1 (yellow in Figure 3.13), 260°-315° for CB1 (red in Figure 3.13) and 315°-5° for CB2 (blue in Figure 3.13). These limits for the release areas are used as a reference. The back-azimuth values obtained from the seismic data which are close to these limits should be considered carefully.
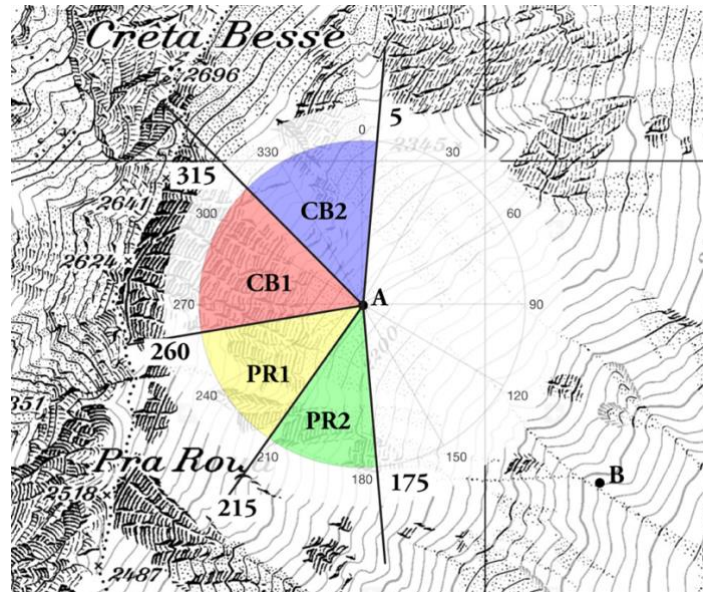
Figure 3.13 - Detail of the topographic map of the VDLS test site (base map from Swiss topographic service 1:25000 [geo.admin.ch]). Over the map, the projection of the back-azimuth range directions and the release areas identified from Cavern A. In green Pra Roua 2 (PR2), in yellow Pra Roua 1 (PR1), in red Crêta Besse 1 (CB1) and in blue Crêta Besse 2 (CB2).

Since we are interested in the release areas, the back-azimuth calculations and representations must be applied only to seismic data coming from the beginning of the snow avalanche movement. The first steps of the snow avalanche mass release correspond to the Signal Onset section (SON) of the seismic signal, delimited from the STA/LTA ratio threshold and the At (Total Envelope) threshold. See Section 3.b of this chapter for a detailed explanation of the criterion used for the seismic section isolation.

As an example, of the data processing workflow on snow avalanche release identification, we use seismic data from snow avalanche #18-3041. This was a large powder snow avalanche naturally released at 08:55 UTC on January 17th, 2018, from the CB2 area (Figure 3.14). The Cavern A seismic data corresponding to the SON section were filtered using a Butterworth low-pass filter at 10 Hz, to avoid the high frequency seismic noise (filtering routine at Subsection 3.a.iv). The seismic data are not rotated, in this case maintaining the components orientation to ZNE. After tests performed with a rotated seismic signal to the QLT coordinate system, we considered that the seismic data rotation was not necessary. The back-azimuth directions are related to the orientation from the north (back-azimuth) and the seismic data are already recorded in this coordinate system. Therefore, it is not necessary to rotate the seismic data components to relate them.

The seismic signal of the SON section is processed in time windows, the seismic wave polarization calculations being made for each time window seismic signal. (see Subsection 3.a.v for a detailed explanation of the windowing process) (Figure 3.14a). The length of the time windows is 1 s with a 50% overlap using the Hanning window. For every time window we obtain the back-azimuth values (*ba*) and the linearity (*R*) (Figure 3.14b). The back-azimuth values (*ba*) obtained are represented in planar polar coordinates with reference to the geographic coordinates: y axis for N-S direction and x axis for the W-E direction (Figure

3.14c). The ba values origin is in the north direction (0°) increasing clockwise for the whole 360°. The radial axis of the polar plot varies according to time (s) in time windows corresponding to the SON section, starting from outside the polar plot (start of the SON) until reaching the centre (the end of the SON section). The polar coordinate representation gives us an image of the approach of the source of the ground vibrations to the sensor (Figure 3.14d).

The back-azimuth value dots (*ba*) are weighted using the linearity values of each time window seismic signal (*R*) (Subsection 3.a.vi). The ba values are represented with bigger dots as high is the *R* value. With the use of linearity to weight the back-azimuth values, we aim to reinforce and better represent the more polarized seismic waves while giving less importance to the less polarized waves (Figure 3.14d). The seismic signal time windows whose seismic particle motion has lower linearity values are less important for the final evaluation of the release area identification. Low linearity back-azimuth values correspond to a rounder shaped particle motion, and the relevance and reliability of these back-azimuth values must be considered with caution.

With all the back-azimuth values weighted, we compute a histogram with the accumulation of back-azimuth values in bands of 5° (called 'bins' in histogram calculations), weighted using the linearity values (*R*) corresponding to each ba value. From the histogram we extract the back-azimuth band with the greatest accumulation of ba values. We regard the centre of the histogram band as the mean back-azimuth value for the whole seismic SON section named *BAZ* (Figure 3.14e). The histogram allows us to deduce the mean direction of the approaching front and the evolution trend (Figure 3.14e). The deduced mean back-azimuth value (*BAZ*) has a minimum standard deviation of ±2.5° corresponding to the width of the histogram band (5°) from its centre and may have larger deviation values according to the dispersion of the ba values from all the time window seismic signal. The standard deviation is detailed for every *BAZ* value and represented on the planar polar plot (Figure 3.14e). With the *BAZ* value we can numerically evaluate the orientation range from the source of the seismic signal, and in consequence the approximate position of the seismic source during the SON section seismic signal, which is related to the release area of the snow avalanche.
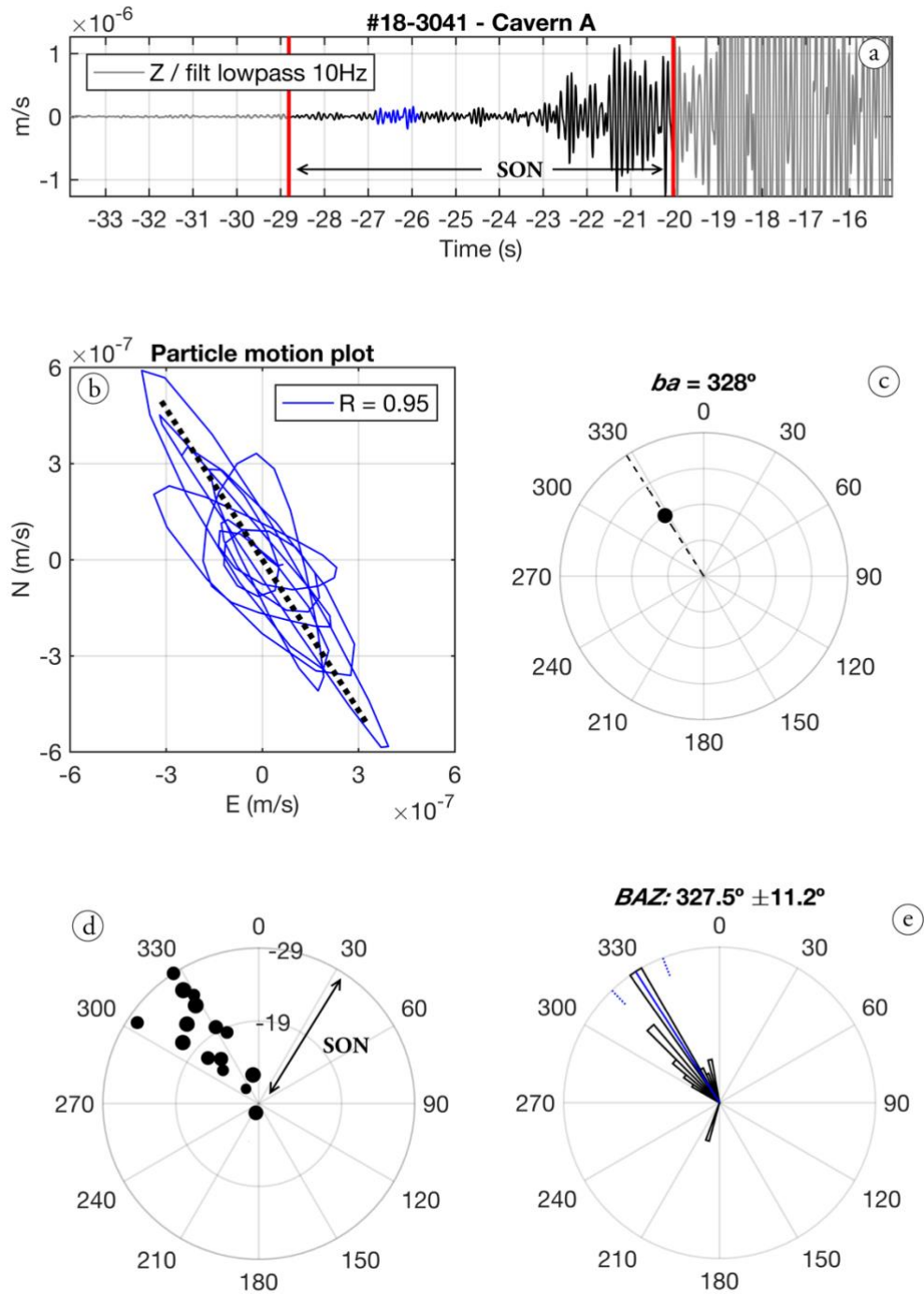
Figure 3.14 - Localization procedure from a seismic signal recorded at Cavern A during snow avalanche #18-3041 at VDLS. a) Vertical component (Z) filtered with a 10Hz low pass filter. Signal before the activation of the VDLS trigger system (t=0s). In red, the limits of the SON section. In blue, the 1 s time window studied. b) Particle motion plot on the N-E plane of the seismic signal time window considered (blue in a)), with a high linearity (R=0.95). c) Planar coordinate system plot with the black dot and dashed line indicating the back-azimuth direction (ba = 302º) calculated from the time window selected. d) Planar polar plot of the ba values from the SON section in time windows. The point size is related to R for each window. e) Histogram of the ba values and the *BAZ* direction (327.5º) with a standard deviation of ±11.2º (both in blue).

The presented procedure works better in naturally triggered snow avalanches. In artificially triggered avalanches, the seismic vibrations generated by the explosive detonations cause false triggering using the STA/LTA ratio threshold and Total Envelope values (At), giving false time values to isolate the SON seismic part. However, these seismic data become very useful in the calibration process and for testing the method, given that the explosions and release areas are located very accurately.

As an example, we present the application of the method to the data of snow avalanche #17-3033 recorded in an experiment at the VDLS test site on March 8th, 2017 (Figure 3.15). This avalanche was triggered using explosives at the CB1 release area. The seismic vibrations produced by the explosion recorded at Cavern A are found in Figure 3.15a. Using the particle motion method, from the Cavern A position we were able to locate the detonation at a back-azimuth direction of 292.5º ±2.5º in the CB1 direction (Figure 3.15d). The STA/LTA ratio and Total Envelope (At) exceed the thresholds values for the SON isolation in the detonation seismic signal (blue in Figure 3.15). For this reason, the SON section isolation method did not work for the snow avalanche release due to the interference of the seismic noise coming from the explosion. By manually isolating the SON section of the seismic signal between 13 s and 23 s (blue in Figure 3.15a, b and c), which corresponds to the first movements of this avalanche, we are able to apply the release location method to this seismic signal (red in Figure 3.15a). The results show a BAZ direction of 272.5º ±9.54º, which corresponds to the CB1 release area (Figure 3.15e). The back-azimuth (ba) values are not as clear as desired because of the noise coming from the detonation, but the result is valid.

Figure 3.15 shows the back-azimuth calculations using the detonation and the SON section seismic signals of an artificially triggered avalanche. In blue (a), the first seismic waves correspond to the detonation. The blue lines in the STA/LTA ratio and At plots (b and c) mark its limits. The red seismic signal in (a) corresponds to the SON section of the snow avalanche and the red lines in (b) and (c) its limits. Figure 3.15(d) shows the BAZ value of the detonation seismic data (only a 1 s time window) and (e) corresponds to the representation of the ba values (black dots), its associated histogram (white) and the resulting BAZ value (in red) of the SON section. In both plots (d and e), the standard deviation of each BAZ value obtained is indicated by dashed lines. Note that both BAZ values of the detonation and SON section are in the CB1 release area.
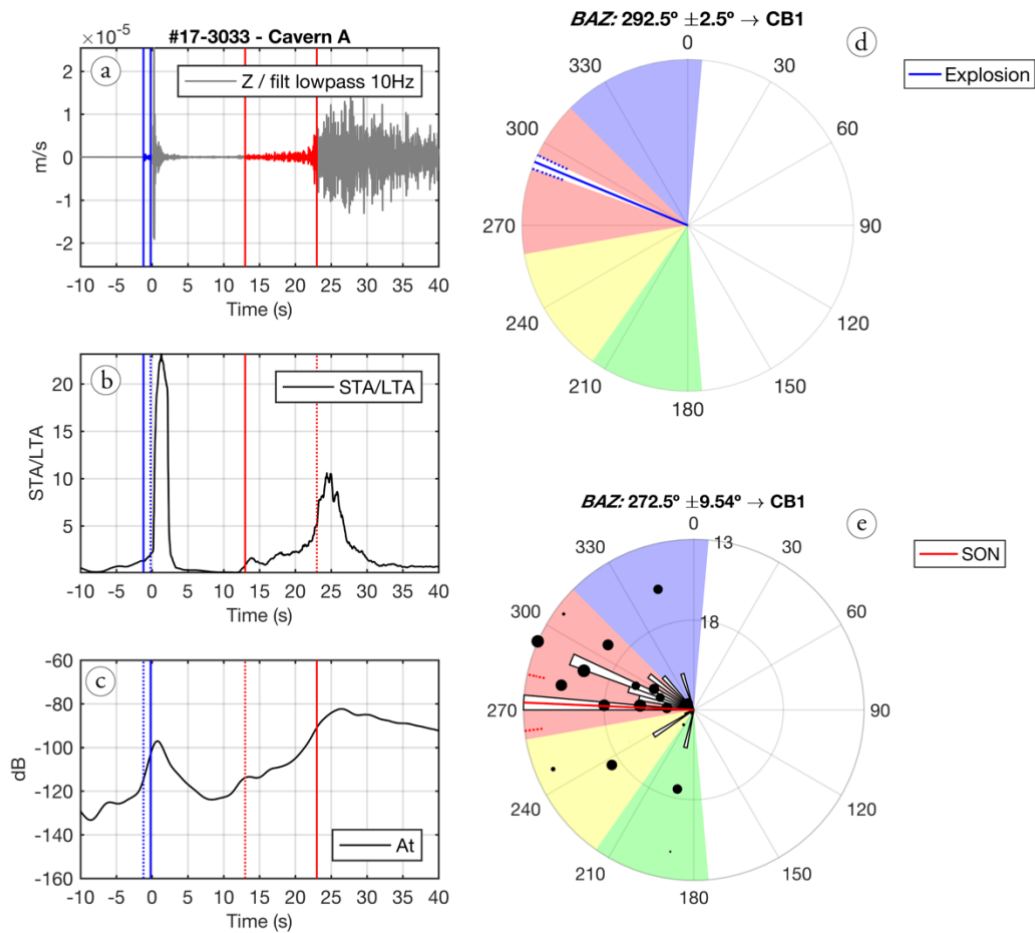
Figure 3.15 - Localization procedure from the seismic signal recorded at Cavern A during snow avalanche #17-3033 triggered using explosives, recorded in an experiment day at VDLS. This avalanche was triggered using explosives from CB1. a) Seismic signal from Cavern A, vertical component (Z), filtered with a lowpass Butterworth at 10Hz. Detonation time at 0 s. b) STA/LTA ratio values. c) Total envelope (*At*) values. d) Planar polar plot of the *BAZ* calculated from the detonation seismic signal (blue seismic signal and lines in a, b and c). e) Planar polar plot of the ba values, histogram and *BAZ* calculated from the SON seismic signal (red seismic signal and lines in a, b and c).

3.d.ii. Applied to snow avalanche flow regime characterization

From the point of view of the seismic characterization of the snow avalanche flow, we already know that the frequency content of the seismic signal is linked to the flow regime at large time scales (Powder or Wet snow avalanches) (Pérez-Guillén, 2016). The amplitude of the seismic signal can also provide us with information about the relative position of the avalanche front and which section of the seismic signal we are considering (section 3.b). One of the results in Sabot et al. (1998) was that the vibrations recorded at the seismic stations are generated by the interaction of the avalanche snow mass with the ground, changes in the slope and/or between the snow avalanche layers. The particle motion of parts of the snow avalanche had already been performed in order to study the characteristics of snow avalanche seismic signals in Suriñach et al. (2000).

For further in-depth knowledge of the generation of the avalanche seismic signals, we decided to seek information regarding snow avalanche rheology and behaviour by treating the seismic signal in time windows. The application of the particle motion analysis and the frequency content studies in time windows gives us information on the particle motion and frequency content evolution along the seismic signal, as well as enabling us to detect any changes therein. Our aim in this regard is to determine the relationship of these changes with snow avalanche behaviour, based on observations of our previous seismic characterizations. To this end, we consider only the seismic signals coming from the snow avalanche mass flowing over the sensor (SOV and STA sections), in order to obtain: a) the incidence angle of the collision, and b) a direct link with the frequency content in every time window seismic signal. In this analysis we study the first body waves generated in every collision of the snow avalanche, which allows us to link the particle motion polarization to the snow avalanche interaction with the ground and/or the snow layers, when flowing over the seismic sensor.

The use of the SON and/or SEN sections is not appropriate because they correspond to waves generated far from the seismic sensor. This method is designed for seismic signals generated when the snow avalanche flows over the seismic sensor (SOV section), otherwise the results could not be linked to the behaviour of flow.

Due to the distribution of the seismic stations along the path, the snow avalanches only pass over the Cavern B and Cavern C seismic sensors. Only the snow avalanches released from the CB1 area pass over Cavern A. Moreover, the seismic sensor position at Cavern A is too close to the release area and the snow avalanche flow is not yet fully developed. The Cavern D (Bunker) position is outside the VDLS track and the runout area; therefore, snow avalanches never pass over this position, only the deposition of the largest snow avalanches recorded at the VDLS site-.

Most of the ground vibrations generated by snow avalanches are considered to be between 1-50 Hz, given that there is no relevant information in higher and lower frequencies: bandpass filtered between 2-40 Hz (2nd order) in Suriñach et al. (2001); 1-50 Hz (4th order) in Biescas et al. (2003); 1-40 Hz (8th order) in Vilajosana et al. (2007a); and 1-45 Hz (4th order) in Pérez-Guillén et al. (2016). Due to technical limitations, there are no records for vibrations of a longer period (only the broad-band data at Cavern C), and no higher frequency content because of the sampling rate of the seismic stations (maximum 200 s.p.s.). We observed only resonances and harmonics higher than 65Hz. Sometimes harmonics at Cavern B can be dominant and more present than the fundamental frequency, generated by the snow avalanche flow, between 1-50 Hz. Furthermore, the broadband data from sensor at Cavern C (Lennartz) is able to record frequencies lower than 1 Hz, where we found some ground deformations related to the snow avalanche collision with the Mast. It is of interest to consider the high frequency resonances and/or long-period ground deformations. However, these frequency bands are not useful for the flow regime characterization method described in this PhD thesis. For these reasons, all data from Cavern B and Cavern C sensors are filtered using a Butterworth band-pass filter (4th order) to preserve frequencies between 1-50 Hz.

To illustrate the characterization procedure, we use the seismic signal recorded at Cavern B during snow avalanche #13-3019, released from the CB1 area on February 1st, 2013, at 16:15 UTC (Figure 3.16). It was a fully transitional snow avalanche, described and studied in depth in Subsection 5.b.iii. The seismic signal is rotated to QLT components (Figure 3.16a) and frequency content evolution is studied using the time window PSDs (Figure 3.16b). In this example, the signal was recorded at the Cavern B seismic station, although it could have been from Cavern C.

To isolate the SOV section of the seismic signal, and to ensure that the snow avalanche was flowing over the sensor, we use the Total Envelope threshold criterion (*At*) (see Section 3.b). The SOV section is recognized between 21.4 s and 85.8 s using the *At* threshold criterion (Section 3.b) (black dashed lines in Figure 3.16c). A detailed inspection allows us to recognize two avalanche fronts, one around 25 s and the other around 35 s (Figure 3.16a, Figure 3.16b and Figure 3.16c) (described in detail in Subsection 5.b.i). In this example, both snow avalanche fronts are considered as only one SOV section. All three components of the seismic signal are necessary to determine the SOV section using the *At* threshold method and to perform the particle motion polarization.

The seismic data of the SOV section are processed in time windows of 1 s duration with a 10% of overlap, as in the frequency content studies (see Section 3.c). We obtain for every time window (n) the Dominant Frequency (*DF*) and Spectral Centroid (*C*) values to recognize the frequency content evolution in the Q and L components (Figure 3.16d and Figure 3.16e). We also obtain the mean *C* value from *C-Q* and *C-L*, smoothed in 5 sample windows (*Cmean median*) (Figure 3.16e). We only consider the frequency content information of the Q component, which is more closely linked to vertical dynamics on the flow, and of the L component, which is more linked to horizontal evolution of the flow.

To emphasize the changes in the frequency content of the Q component (normal to the slope), and only taking the most energetic frequencies of the particle motion into account, we apply a 10 Hz width filter on the seismic signal of all three components close to the *DF-Q* value of every time window (n). In the case where the *DF-Q* is lower than 10Hz, a lowpass Butterworth filter (4th order) at 10 Hz is applied to emphasize the lowest frequencies of the seismic signal. In the case where the *DF-Q* is higher than 10 Hz, we apply a 10 Hz width bandpass Butterworth filter (4th order) centred at the *DF-Q* value. As an example, the *DF-Q* value of the n window in Figure 3.16 (between yellow lines) is *DF-Q* = 34 Hz. The seismic signal of the time window n is filtered to preserve only the frequencies between 29 Hz ([*DF-Q*] -5 Hz) and 35 Hz ([*DF-Q*] +5 Hz) (Figure 3.16d). All three components are filtered using the same frequency window defined using the *DF-Q* value. We consider that the Q component is most likely to undergo changes in the frequency content related to the changes in the ground interaction of the snow avalanche front or snow avalanche body.

We then apply the study of the particle motion to the time window n seismic signal (1 s long, filtered around *DF-Q* value), using the 3-component [QLT] to acquire polarization information (Figure 3.16f). The particle motion of the time window seismic signal in the Q-L plane is represented in black (Figure 3.16f). The green line indicates the polarization direction calculated using the V-J method. The L axis direction (horizontal) is reversed to fit

the interpretation of the seismic data with the flow direction downslope (see Figure 3.16f, x axis with the positive on the left-hand side). Figure 3.16g shows a schema of the p1 vector (main polarization direction) and the incidence angle measured from the L component direction (*in*, in red), and its link with the snow avalanche path slope.

From the definition of the p1 eigenvector, we only take the *in* angle, since we are looking for changes in the interaction of the snow avalanche with the slope in the Q-L plane. Note the difference between this *in* angle and the incidence angle defined in the V-J method (described in Subsection 3.a.vi). In this case, the *in* angle is measured from the +L component direction in order to relate these values to the flow direction. The *in* values in the L direction are zero when the particle motion and p1 directions are parallel to the ground/slope surface facing down-slope (L+ component) (Figure 3.16g). The *in* values of the Q component direction are $\pi/2$ or $-\pi/2$ when facing up (+Q) or down (-Q), respectively, related to a particle motion normal (out or into) to the ground surface (Figure 3.16g). The intermediate *in* values yield information about the snow avalanche motion in the Q-L plane in the down-slope direction. The *in* value is calculated for every time window (n) in the SOV section (Figure 3.16g, h, i and j). The linearity (R) values (V-J method) for each window give us a quality criterion for the interpretation of the polarization results (see Subsection 3.a.iv). Those time windows with greater polarized particle motion provide more valuable information and can be better linked to the snow avalanche behaviour.

To highlight the *in* values of a more polarized particle motion corresponding to a certain time window (*n*), for the *N* time windows covering all the SOV section, we decided to multiply the angle *in*(*n*) (radians) by the corresponding *R*(*n*) [0-1] value. The resultant value is referred to as *GRD*(*n*) and is expressed in radians (**3.18**).

$$GRD(n) = in(n) \cdot R(n) \qquad n = 1, N \qquad\qquad 3.18$$

The *GRD* values interpretation could be conducted in the same way as for the in values. The evolution of the *GRD* values (Figure 3.16j) and the *GRD median* (smoothed curve using 5 samples moving median), give us an important criterion for identifying the different snow avalanche flow regimes.
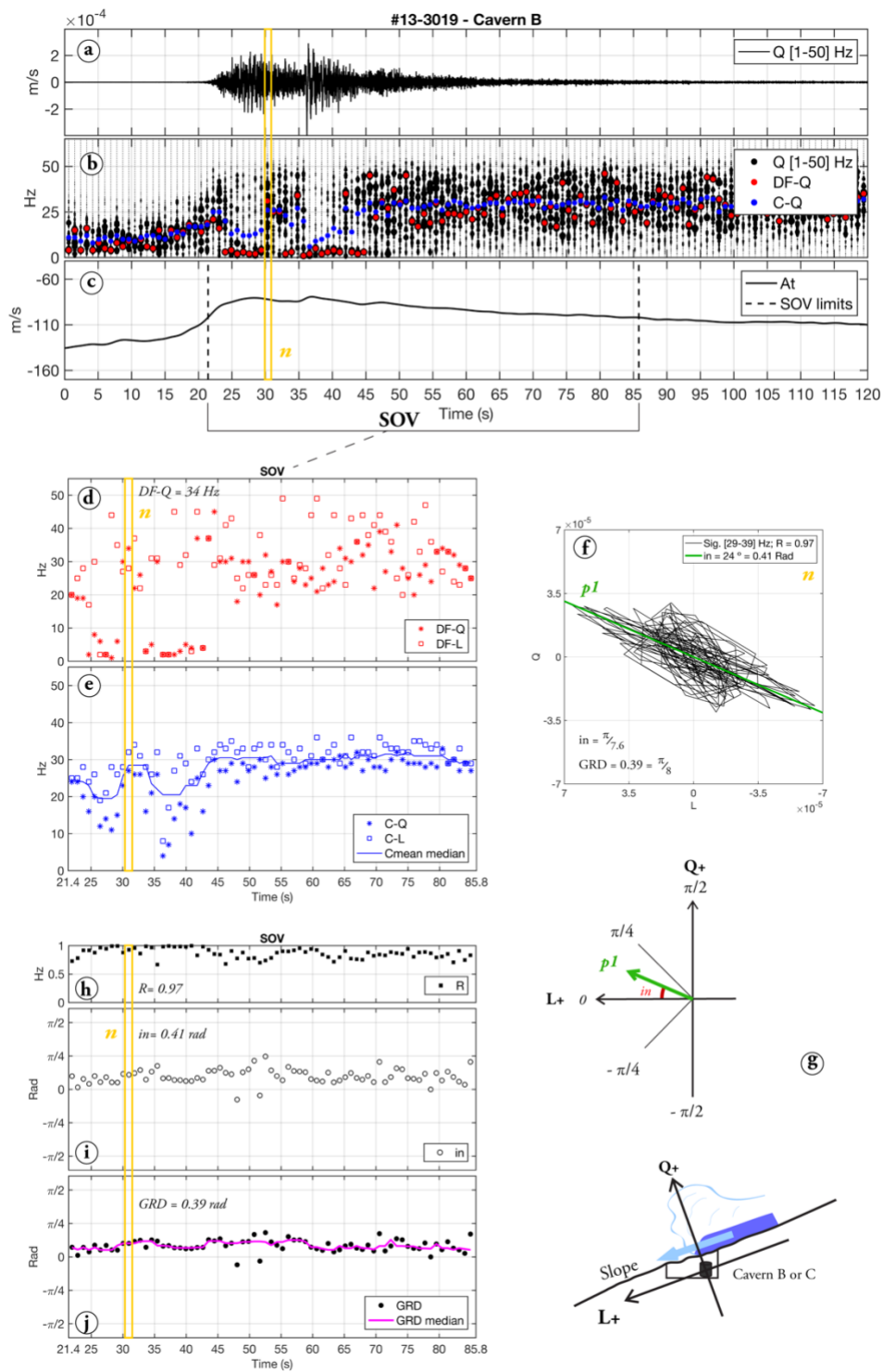
Figure 3.16 - Snow avalanche flow regime characterization procedure from seismic signal of snow avalanche #13-3019 recorded at Cavern B. a) Q (m/s) seismogram filt. 1-50 Hz. In yellow, a selected window n. b) Q PSD normalized scatter plot in 1 s time windows and 10% overlap (black dots), *DF-Q* (red dots) and *C-Q* (blue dots). c) Total envelope (*At*) and selected SOV section (dashed line). d) *DF-Q* and *DF-L* values of the SOV section. e) *C-Q*, *C-L* and *Cmean median* of the SOV section. f) Particle motion plot of the n selected window seismic signal [Q-L plane] with the resulting values. In green, the p1 vector (V-J method). g) Schema with the p1 vector on the Q-L coordinates, the *in* angle (red) and below the link with the snow avalanche flow over the sensor. h) The SOV section R values from the particle motion polarization, i) *in* values for every time window and j) *GRD* values (black dots) with the smoothed median (magenta line).

We consider only the particle motion information in the Q-L plane, given that it is the information most closely linked to the snow avalanche flow evolution, vertical changes, breaking process, and other flow interaction between layers and with the topography (Figure 3.16h).

The combination of the frequency content evolution (*DF*, *C*) and the *GRD* values related to the polarization of the particle motion computed for every time window (n), constitute a tool that enables us to study the behaviour of the snow avalanche mass over the seismic sensor. We link the *GRD* values (and by extension the angle of incidence (in)) with the generation of the seismic vibrations produced by the mass interaction with the slope surface. The application of this method is presented in Chapter 5.

———

Chapter 4

Snow avalanche release identification

To identify the snow avalanche release area, we decided to focus on the ground vibrations produced by the initial steps of the snow avalanche. If we are able to locate the generation point of these first seismic vibrations, we will be able to determine the area from where those vibrations are coming, and by extension the area from where the snow avalanche was released. The situation of the sensor in Cavern A is ideal for this purpose, since it is close enough to the release areas of the avalanches to record them properly and is located on an open slope without topographic effects.

For the back-azimuth calculations using the particle motion polarization studies, we decided to consider the same coordinate system as that employed where the seismic sensors are installed [ZNE]: the vertical component with the positive facing up (Channel 1, Z), the north-south component with the positive facing north (Channel 2, N) and the east-west component with the positive facing east (Channel 3, E). The seismic signal is not rotated in this case.

In Section 4.b we present examples to illustrate the usability of the method and the reliability of the results. The release area identification method was developed and tested using all the snow avalanche data available recorded at the Cavern A seismic station (between season 2015-2016 and season 2019-2020), as presented in Section 4.c.

4.a. Cavern A orientation calibration

The orientation of the Cavern A seismic sensor was checked every season with the records of seismic data of one identified earthquake (time, epicentre position, and magnitude). Because the direction of the P-wave front is known (epicentre position from seismological services), the back-azimuth calculated using the particle motion should fit with the direction of the sensor position to the epicentre (V-J method). In case of major problems in the orientation of the seismic sensor, the data were rotated to the correct position of the sensor and better fit with the ZNE directions.

The earthquake information was extracted from the European-Mediterranean Seismological Centre (EMSC - www.emsc-csem.org) and Swiss Seismological Service (SED - www.seismo.ethz.ch). We use the largest earthquake possible, closer enough to the VDLS experimental site that activated the automatic triggering system. Frequencies higher than 2 Hz were only considered because of the limitations of the geophone eigenfrequency of the Cavern A seismometer (see Chapter 2).

As an example, we used the M4.6 earthquake with epicentre in Switzerland (Canton of Uri) that occurred on March 6th, 2017, at 20:12.07 UTC and at a distance of 138km from VDLS. The seismic waves of the earthquake activated the automatic triggering system of VDLS (trigger code #17-3031). The back-azimuth direction of the Cavern A position to the epicentre, measured from cartography information and epicentre location from EMSC and SED, is 60.14° (Figure 4.1a).

The particle motion polarization method (V-J method) applied to the first P-waves recorded (Figure 4.1b) gave us a back-azimuth direction of 61.15° (Figure 4.1c). While a difference of one degree (1°) could make a huge difference if an epicentre were positioned far from the seismic sensor, we nevertheless considered that a difference of one degree (1°) would be an acceptable margin of error when working with seismic data generated from a snow avalanche close to the seismic sensor position and in movement.
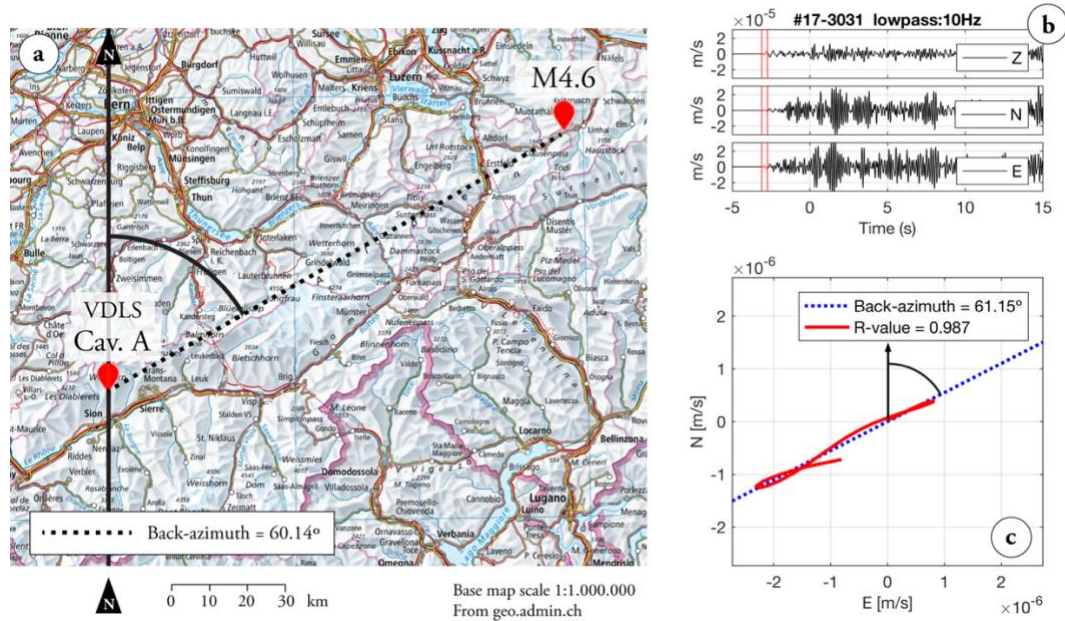
Figure 4.1 - Example of calculation of the back-azimuth direction of an earthquake epicentre using the polarization of the P-wave particle motion (V-J method). Data from trigger #17-3031, corresponding to a M4.6 earthquake occurring in Switzerland (138km from VDLS). a) Map of Switzerland with the position of the seismic station (VDLS – Cavern A) and the earthquake epicentre in red. The back-azimuth direction denoted by a black dotted line (60.14°). b) Seismogram of the earthquake data recorded at Cavern A, components ZNE (10Hz lowpass filtered). The red lines delimit the time window of the signal used in the particle motion analysis (c). c) Particle motion of the horizontal components [N-E] (in red) and the back-azimuth denoted by a blue dotted line (61.15°).

4.b. Snow avalanche release area identification

The snow avalanches selected were the ones with less seismic background noise and with a detailed identification obtained from pictures and an SLF data report. Initially, we used spontaneous snow avalanches and snow avalanches triggered using explosives, but the spontaneous avalanches seismic signals are better because of the lower presence of seismic noise (produced by the detonation). Consequently, we focus more on spontaneous snow avalanches because the data quality is better and the variety of avalanches higher. The method used and proposed is described in Subsection 3.d.i. In this chapter we present the main results as well as tests carried out for the snow the avalanche release area identification. First, in Subsection 4.b.i we present the tests of the method applied on a well described avalanche with two fronts and a well-defined release area (using pictures of the VDLS site). Then, in Subsection 4.b.ii, we use the method on the seismic data generated by five different avalanches with no previously identified release area in order to test the ability to deduce from where they are released.

4.b.i. Snow avalanche #18-3066

On February 16th, 2018, a spontaneous snow avalanche was released, activating the VDLS experimental site recording system at 05:08 UTC. This trigger activation is known as #18-3066, using the SLF trigger identification code. At the time of the avalanche there was no visual information of the release area or of how it descended. Thanks to the SLF-Sion team, we were able to obtain pictures of the VDLS site two weeks before and 3 days after the snow avalanche occurred (30/01/2018 – 19/02/2018). The comparison of both pictures allowed us to identify some scars at the release area, which could correspond to the snow avalanche. Between January 30th and February 19th there were 6 trigger activations at VDLS, all of which were snow avalanches released over Cavern A (triggers from #18-3061 to #18-3066, see Subsection 4.b.ii). The trigger #18-3066 corresponds to the biggest avalanche released and the only one that reached Caverns B and C. The association of the top scars and avalanche deposits with the snow avalanche was easier in case #18-3066. The pictures were taken two days after the avalanche occurred and the runout area identification was clearly visible.

The identification of the snow avalanche was performed using a combined interpretation of the GEODAR data and the seismic data interpretation (Köhler et al., 2018; Roig et al., 2018), merged with the SLF-Sion team field observations and pictures from the VDLS release area, taken after the trigger #18-3066 activation. This avalanche was classified as a large transitional one, based on the flow regime classification presented in Köhler, McElwaine, & Sovilla (2018), and released from two different areas with a time lapse of 30 s (approx.). The first release was detached from CB1 (close to CB2) from a scar identified on the snow cover close to the Crêta Besse ridge (I), and descent Channel 1 (I at Figure 4.2a and Figure 4.2b). The second release was detached from CB2 and descent Channel 2. At CB2, two main scars are identified on the snow cover: one closer to the Crêta Besse ridge (II-a) and one in a more "advanced" position (II-b), involving more snow and eventually becoming the main snow avalanche release (II-a and II-b at Figure 4.2a and Figure 4.2b). From the interpretation of the GEODAR MTI plot, it can be deduced that the main release area of the snow avalanche was on the maximum range of the GEODAR pulse (2700 m range), which corresponds to the Crêta Besse summit (Figure 4.2a and Figure 4.2c). In Figure 4.2c the reddish colours correspond to snow avalanche mass movement on the range (vertical axis) and time position (horizontal axis) used for identifying the snow avalanche flow along the VDLS slope (fronts related to the release areas identified are denoted by black arrows). Before the VDLS trigger activation, the snow avalanche had already been released from another area (Figure 4.2c). This release previous to the trigger system activation can be studied from the seismic data thanks to the continuous data stream and pre-trigger seismic data (see more details on the seismic data in Figure 4.3).
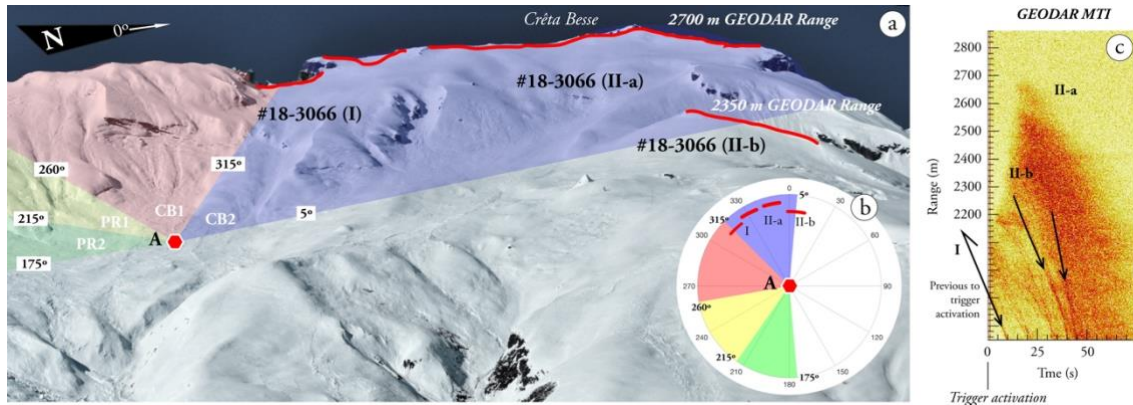
Figure 4.2 - a) Picture of the Crêta Besse area of the VDLS site, taken on February 19th, 2018, three days after the snow avalanche of trigger #18-3066. The colour shades (green, yellow, red and blue) indicate the back-azimuth ranges of the main release areas (PR2, PR1, CB1 and CB2) from Cavern A (red hexagon). Numbers indicate the back-azimuth direction limits between the main release areas in degrees (see Subsection 3.d.i. for a detailed explanation of the back-azimuth data plot representation). b) The same in polar coordinates plot. In a) and b) the red lines delimit the snow avalanche release scars identified on the snow cover, related to release areas of trigger #18-3066 snow avalanche: I is for the first release and II for the two second releases (II-a and II-b). c) Part of the GEODAR MTI plot from Kohler et al. (2018) and Roig et al. (2018), indicating the range where the main release (II-a and II-b) can be identified, and the first release previous to the VDLS trigger activation (I). Black arrows indicate the fronts identified in the GEODAR MTI plot (arrow I indicates the projection of front I, released before the GEODAR data *t0*). Picture by Dr. P. Huguenin from SLF-Sion.

This snow avalanche is well described and becomes very useful for testing and reinforcing the release identification method using seismic data. This is one of the largest natural avalanches recorded in the Cavern A seismic station and provides very good quality data for analysis.

The results of the analysis are presented in Figure 4.3. Note that t = 0 s is the time of the VDLS triggering system activation, considered as a reference time for all data synchronization. Both snow avalanche fronts can be clearly recognized in the time series of the seismic data recorded at Cavern A at -30 s and 9 s, respectively (Figure 4.3a, Figure 4.3b and Figure 4.3f). The maximum Total Envelope (*At*) value (-87.8 dB) corresponds to the second front (*At*-II), suggesting that this front is larger than the first one, *At*-I < *At*-II (Figure 4.3c and Figure 4.3g). The *At* of both fronts exceed the -102 dB threshold, enabling detection of the boundaries between the SON-SBO/SOV sections. However, the *At* values do not reach the threshold of -81 dB, indicating that the snow avalanche main fronts did not pass directly over the sensor (SBO-I and SBO-II in Figure 4.3c and Figure 4.3g). As regards the STA/LTA ratio values (10s/2s configuration), the seismic vibrations of the first avalanche front (I) exceed the 2.5 threshold (Figure 4.3d), being a valid criterion for the SON-I section isolation. However, the STA/LTA ratio values for the second front (II) did not reach the 2.5 threshold until the front passed over the seismic sensor because of the mixing of seismic signals coming from the first front and the second one, and thus are not usable for the SON-II section isolation (Figure 4.3h).

Using the *At* values and the STA/LTA algorithm, the automatic isolation system delimits the SON-I section of snow avalanche #18-3066 between -38 s and -30.6 s. This time interval corresponds to the snow avalanche first front (I) (in red in Figure 4.3a, Figure 4.3b,

Figure 4.3c and Figure 4.3d). The SON-I section seismic signal is used for the mean back-azimuth (*BAZ*) calculation. The *BAZ* for the SON-I section is 312.5º ±10.0º (Figure 4.3e). This direction corresponds to CB1, although it is in the boundary with the CB2 area. It fits with the release area scar detected in the VDLS picture, indicated as I in Figure 4.2.

Figure 4.3e shows the polar coordinates with the results of the release area identification calculated using the SON-I section seismic signal. The black dots denoted the back-azimuth values, size-weighed using the linearity values (*R*), the black line indicates the *BAZ* direction (mean back-azimuth), and the dotted lines indicate the standard error of dispersion. The white histogram in Figure 4.3e corresponds to the accumulation of the back-azimuth values considering its weight (*R* values). In all polar coordinate plots, the solid background colours correspond to back-azimuth range values indicating the main release areas, previously defined and shown in Figure 4.2: green for PR2, yellow for PR1, red for CB1 and blue for CB2.

For the second front (II), the STA/LTA ratio is not useful for identifying the start of the mass movement due to the mixing of seismic vibrations coming from the first front (I) (Figure 4.3h). Although the STA/LTA ratio plot can be used for a visual identification, we decided to use the Total Envelope (*At*) values of the seismic data to identify the SON-II section (start and end) (Figure 4.3g). Note that when using the *At* values as a criterion to define the SON-II, we must take into account that there is a part of the seismic signal coming from the first front (both mixed), and consequently the data amplitude may be larger.

After the first front (SBO-I section, Figure 4.3g) the *At* values tend to decrease (STA-I) until they start to increase again. We assume that this change in tendency of the *At* values is due to the approximation of the second front, and therefore this is the limit between the STA-I and the start of the SON-II. The *At* values start to increase until they reach the -102 dB threshold, which corresponds to the second front arrival to the sensor (start of the SBO-II) (Figure 4.3g). The limit between the STA-I and the SON-II is at -9 s and the end of the SON-II is at 9 s. The *BAZ* direction obtained from the SON-II section is 327.5º ±13.8º (Figure 4.3i), corresponding to CB2 release area. The construction and description of the plot in Figure 4.3i is the same as for Figure 4.3e for the SON-I seismic section data. Although the result for the SON-II is not as clear as for the SON-I, the *BAZ* value is consistent and sufficiently valid.
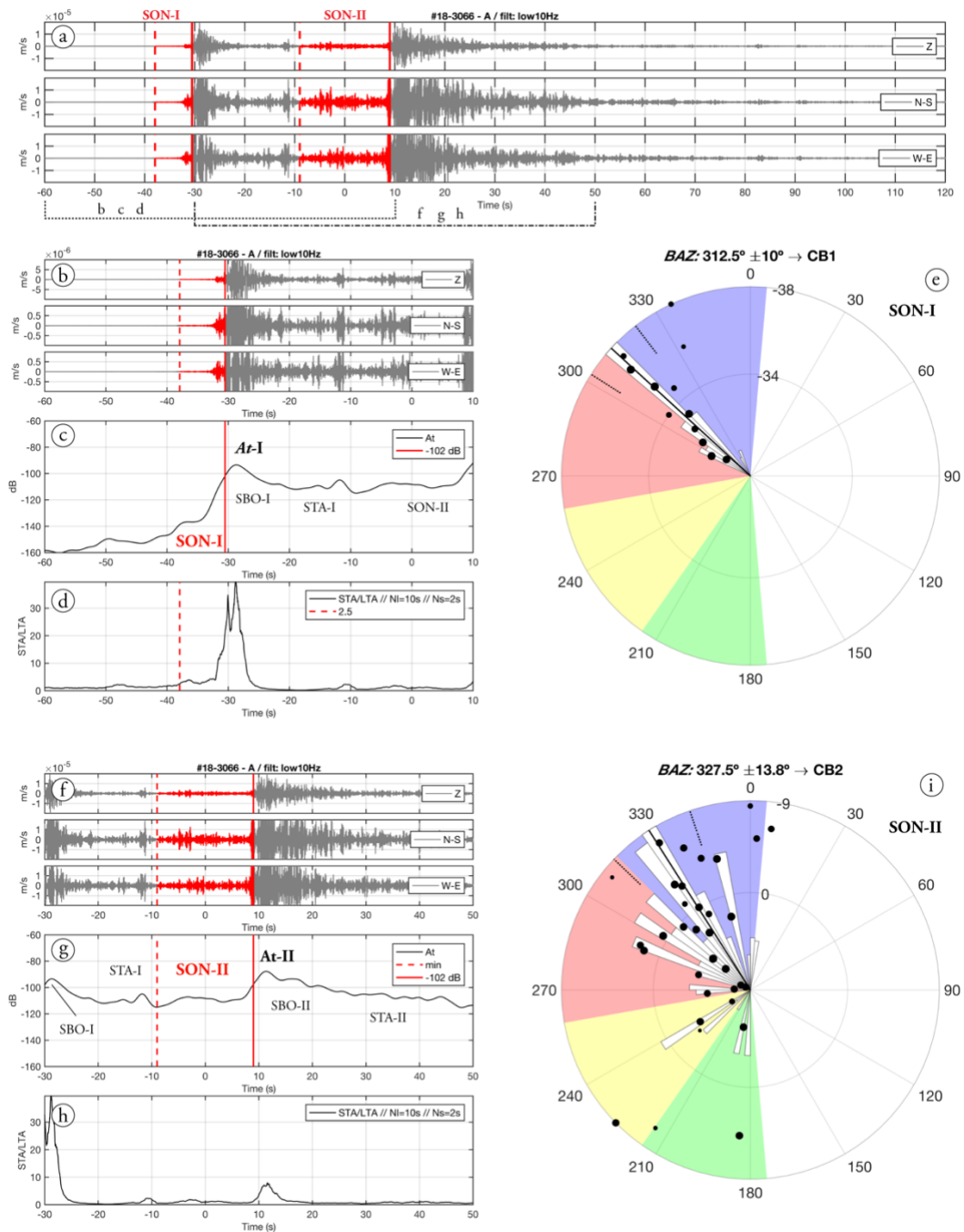
Figure 4.3 - Release area identification for snow avalanche #18-3066. Analysis of the seismic data recorded at Cavern A. a) Time series of the three components [ZNE] of the seismic ground motion (m/s), 10 Hz lowpass filtered, highlighting the SON-I and SON-II sections in red. The b) and f) are a detail of a) for the first and second fronts. The c) and g) are the Total Envelopes of the b) and f) seismic signals (At [dB]) indicating the maximum At for both fronts (At-I and At-II) and the delimitation of the end of the SON-I and SON-II sections (red lines). In g) the red dashed line delimits the start of the SON-II section. The d) and h) are the STA/LTA ratio plots for b) and f) used to delimit the start of the SON-I section (not used in SON-II section). The e) and i) are the polar coordinates plots with the BAZ (black line), standard deviation (short black dashed lines) of the back-azimuth values (black dots), and histogram of the back-azimuth values accumulation (white). The radius values in the circles correspond to the time scale. The background colours correspond to the different snow avalanche release regions at VDLS (see Subsection 3.d.i for a detailed explanation of the back-azimuth data plot representation).

A detailed Interpretation of the back-azimuth values obtained from the SON-II section allows us to make interpretations in order to understand the snow avalanche path downslope. The back-azimuth values represented in polar coordinates for SON-II are not in perfect alignment, as in SON-I. The back-azimuth values tend to be aligned from the release area II-a to the Channel 2 direction, following the topography (blue arrows in Figure 4.4). Only three back-azimuth values correspond to release area II-b. This observation fits with the fact that this release area is much smaller than release area II-a. As a consequence, the ground vibrations generated in release II-b, with less mass involved, are smaller than the ones generated by release area II-a, and in consequence with fewer detections. We consider that the back-azimuth values at the Pra Roua direction (Figure 4.4) are more closely related to the first avalanche front, which between -9 s and 9 s is in a downslope position, as a result of the mix of the seismic ground vibrations coming from both snow avalanches. These back-azimuth values can be considered as "noise" for the BAZ direction calculation, due to the presence of multiple wave fronts coming from different sources (both fronts) and/or related to a front in a downslope position far from the seismic station. The linearity values (R) are lower than the ones on CB2 area, having less weight in the calculation of the BAZ direction (dot sizes are smaller). This "noise" in the back-azimuth values have less relevance in the BAZ direction calculation, and do not affect the obtained BAZ direction, achieving a good result in the identification of the release areas.
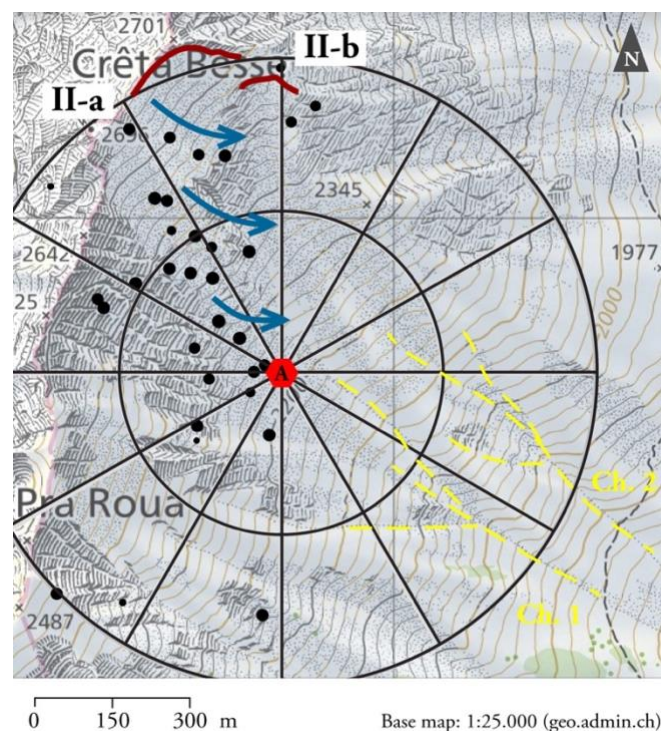
Figure 4.4 - Polar coordinates plot with the back-azimuth values of the SON-II section of the snow avalanche of trigger #18-3066 over the VDLS topographic map [base map 1:25000 from Swisstopo - geo.admin.ch]. The release areas II-a and II-b identified from pictures in red. Channels 1 and 2 are indicated by dashed yellow lines. The back-azimuth trends following the topography and facing to channel 2 are denoted by blue arrows.

The BAZ directions obtained from SON-I and SON-II are in agreement with the back-azimuth values of release areas (I, II-a and II-b) obtained from the GEODAR MTI

plot (Köhler et al., 2018; Roig et al., 2018) and from the pictures taken three days after the snow avalanche occurred.

4.b.ii. Deducing the release areas of snow avalanches #18-3061 to #18-3065

Prior to the snow avalanche #18-3066, five triggers were recorded at VDLS. All of them were related to spontaneous snow avalanches triggered in two days (from 30th, 2018, to February 19th, 2018 (Table 4.1). The comparison of the pictures obtained before and after this period allowed us to identify some possible release areas of the snow avalanches detected by the automatic triggering system.

The VDLS automatic triggering system was activated three times on January 31st: at 02:12 UTC (#18-3061), 19:02 UTC (#18-3062) and at 22:36 UTC (#18-3063) (Table 4.1). It is not possible to link each snow avalanche to a specific release area. The seismic data of these trigger activations recorded at Cavern A were processed using the methodology described in order to resolve this situation.

As presented in Chapter 2, the VDLS experimental site has an automatic triggering system based on two geophones managed by the SLF team: one in Cavern A and the other in Cavern B. Depending on the seismic vibrations and from where the snow avalanche comes, the trigger is activated from Cavern A or Cavern B. This only affects the position of the time zero ($t0 = 0$ s) in our seismic data time series. When the trigger system is activated from Cavern A, the $t0$ is normally closer in time to the start of the mass movement (start of the SON section). If the trigger system is activated from Cavern B, the time lapse between the start of the mass movement and the $t0$ is longer (sometimes more than the 60 s pre-trigger data). This is not a significant issue because the Cavern A seismic station is recording in continuous data stream mode, but it is important to take it into account when analysing the data. For these reasons, the SON section in Cavern A data always before $t0$, and often the entire SON section is before the $t0$.

Table 4.1 - List of the analysed spontaneous snow avalanches at VDLS between the 30/01/2018 and 19/02/2018. Trigger code: name of the avalanches, Date and Time: date and time of avalanche occurrence. The dates when the pictures of the VDLS were taken are also indicated.

Trigger code	Date	Time	
	30th of January of 2018		Pictures of VDLS
#18-3061	31st of January of 2018	02:12 UTC	
#18-3062	31st of January of 2018	19:02 UTC	
#18-3063	31st of January of 2018	22:36 UTC	
#18-3064	12th of February of 2018	07:01 UTC	
#18-3065	12th of February of 2018	12:01 UTC	
#18-3066	16th of February of 2018	05:08 UTC	
	19th of February of 2018		Pictures of VDLS

- **#18-3061**

The automatic triggering system was activated from Cavern B at 02:12 UTC on 31/01/2018. The seismic data recorded at Cavern A shows a markedly smaller amplitude than other snow avalanches recorded at this cavern (note the 10^{-7} factor in the amplitude

seismogram axis, Figure 4.5a). The maximum value of the Total Envelope At is -124 dB. Since it is lower than -102 dB (criterion for SON section isolation) it suggests either that it is a small avalanche or is far from the seismic sensor position. In this case, since we cannot use the SON isolation criterion already defined, we consider that the instant when the Total Envelope reaches its maximum value is a good approximation to define the limit between the SON-SBO sections (Figure 4.5b). On the other hand, the STA/LTA algorithm allows us to identify the instant when the seismic signal of the snow avalanche front exceeds the background noise level (STA/LTA >2.5) (Figure 4.5c). Taking into account the criterion presented, we obtained that the seismic signal time window between -62.10 s and -59.87 s corresponds to the SON section. Taking advantage of the continuous data stream of Cavern A, we retrieve the seismic signal before the trigger activation. Because of the short length of the SON section (2.24 s), only two time-windows were performed for the back-azimuth calculation (1 s length with 50% overlap). This is not an ideal situation, although it is enough to calculate the BAZ direction and evaluate the back-azimuth values, given the available data. The BAZ is 177.5° ±54.9°, pointing to the PR2 region (Figure 4.5d).
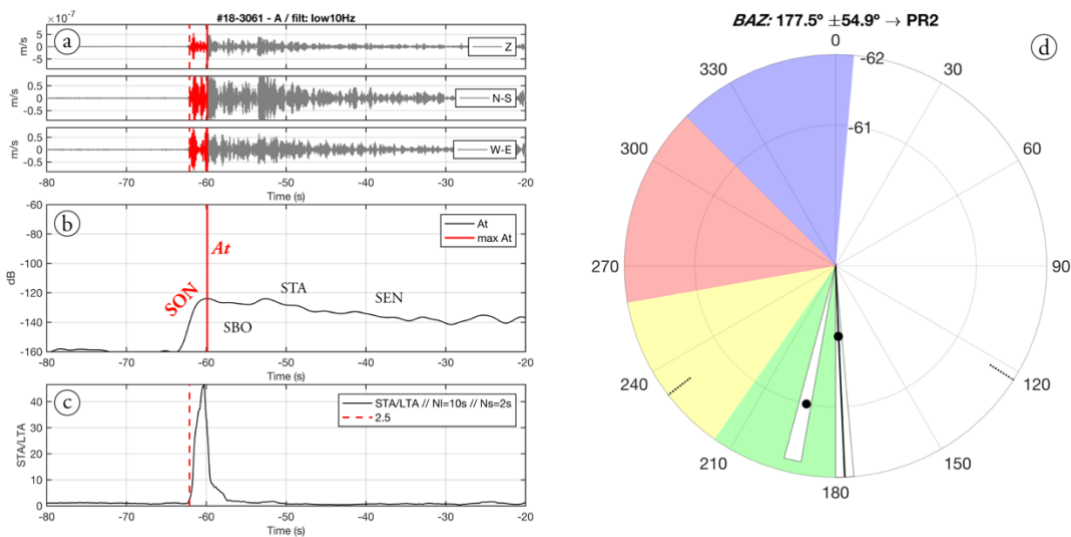
Figure 4.5 - Release area identification for snow avalanche #18-3061. Analysis of the seismic data recorded at Cavern A. a) Time series of the three components [ZNE] of the seismic ground motion (m/s), 10 Hz lowpass filtered, highlighting the SON section in red. b) Total Envelope of the seismic signal (At [dB]) indicating the end of the SON section at the maximum At values -due to the low amplitude seismic signal- (red line) and followed by the SBO, STA and SEN sections. c) The STA/LTA ratio plot used to delimit the start of the SON section (red dashed line). d) Polar coordinates plot with the BAZ (black line), standard deviation (short black dashed lines) of the back-azimuth values (black dots) and histogram of the back-azimuth values accumulation (white). The radius values in the circles correspond to the time scale. The background colours correspond to the different snow avalanche release regions at VDLS (see Subsection 3.d.i for detailed explanation of the back-azimuth data plot representation).

Considering the two back-azimuth values and the low amplitude of the seismic signal, we deduce that the release area of the avalanche is far from Cavern A to the south, and the avalanche did not descend along the VDLS main channels. The back-azimuth and amplitude values obtained are in agreement with a release area observed in the pictures at a lower position in the Pra Roua region (Figure 4.6a). From there, snow avalanche traces descending along Deylon channel are observed, which is in accordance with the results obtained. This

area is located at the southern part of VDLS and is outside the main experimental channels (1 and 2) (Figure 4.6b).
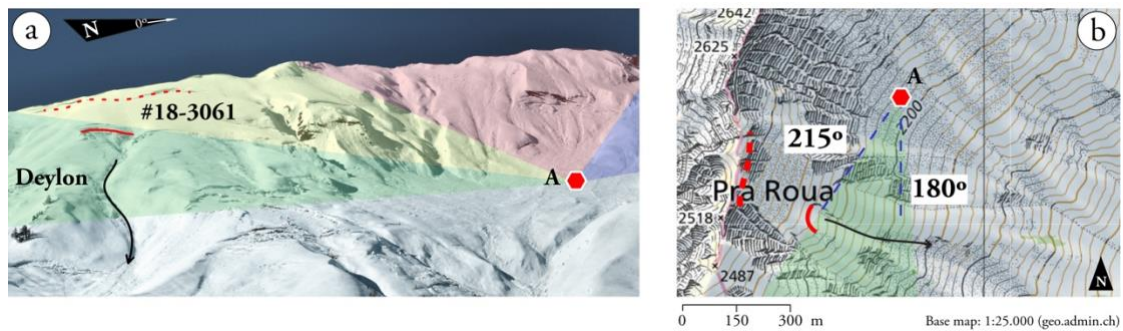
Figure 4.6 - a) Picture of the VDLS Pra Roua region on 19/02/2018 (by Dr. P. Huguenin, SLF-Sion) with the colour shades (green, yellow, red and blue) indicating the back-azimuth ranges of the main release areas (PR2, PR1, CB1 and CB2) from Cavern A (hexagon) (see Subsection 3.d.i for a detailed explanation of the back-azimuth data plot representation). The solid red line delimits the recognized release scar that can be related to snow avalanche #18-3061. The dotted red line indicates a possible scar in an upper position. The black line indicates the snow avalanche path downslope the Deylon channel. b) Map of the VDLS site [Swisstopo - geo.admin.ch] with the position of the seismic station at Cavern A (hexagon) and the possible release area scar (red lines) with the downslope path along the Deylon channel (black arrow). The blue dashed lines indicate the reference back-azimuth directions from Cavern A: 215° and 180°.

- **#18-3062**

The VDLS triggering system was activated from Cavern A at 19:02 UTC on 31/01/2018, 17 hours after trigger #18-3061. The maximum Total Envelope (*At*) is -96.3 dB, lower than -81 dB, the threshold value considered as a criterion for identifying whether or not a snow avalanche flows over the sensor position (Figure 4.7). The snow avalanche was recorded at Cavern B, but no notable high amplitude vibrations were recorded at Cavern C or at Bunker (Cavern D). The amplitude of the seismic signal at Cavern B was even lower than that recorded at Cavern A, suggesting that it was a small/medium size avalanche.

With the STA/LTA algorithm and the *At* values we were able to detect the start of the mass movement properly, which enabled us to establish the limits of the SON section between -53.94 s and -13.93 s (Figure 4.7a, Figure 4.7b and Figure 4.7c). The *BAZ* direction obtained from Cavern A is 317.5° ±5.1°, which corresponds to the CB2 area, in the limit with CB1 (Figure 4.7d).
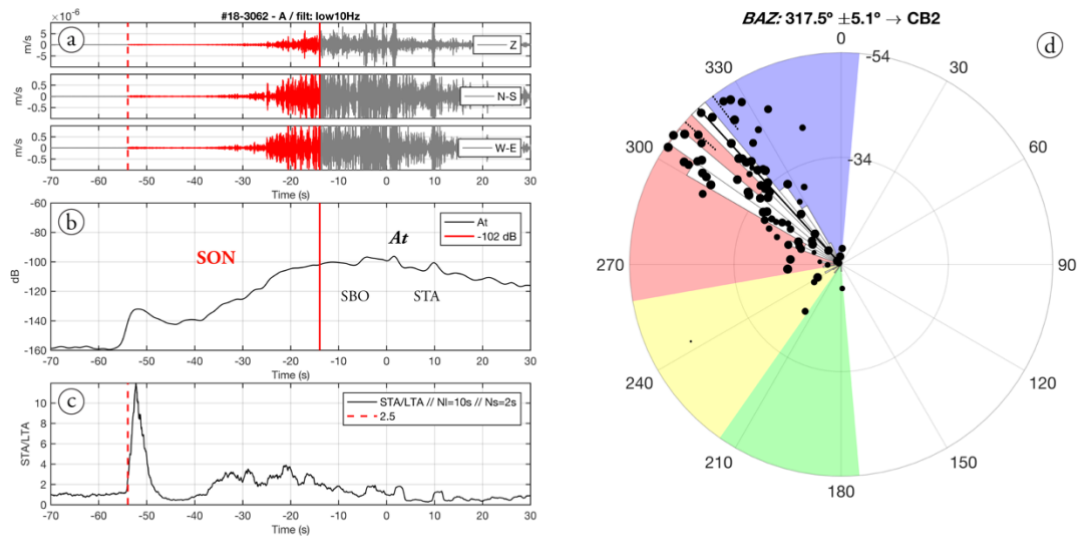
Figure 4.7 - Release area identification for snow avalanche #18-3062. Analysis of the seismic data recorded at Cavern A. a) Time series of the three components [ZNE] of the seismic ground motion (m/s), 10 Hz lowpass filtered, highlighting the SON section in red. b) Total Envelope of the seismic signal (At [dB]) indicating the end of the SON section (red line), the maximum At (<81dB) and the following SBO and STA sections of the seismic signal. c) The STA/LTA ratio plot used to delimit the start of the SON section (red dashed line). d) Polar coordinates plot with the BAZ (black line), standard deviation (short black dashed lines) of the back-azimuth values (black dots) and histogram of the back-azimuth value accumulation (white). The radius values in the circles correspond to the time scale. The background colours correspond to the different snow avalanche release regions at VDLS (see Subsection 3.d.i for a detailed explanation of the back-azimuth data plot representation).

The interpretation of the back-azimuth values plotted in polar coordinates can help us to understand the snow avalanche behaviour and its path down-slope (Figure 4.8). We are able to identify two main groups of back-azimuth values: one around 305° and the other aligned from 320° to 300° as it approaches the end of the SON section (Figure 4.8b). The back-azimuth dots on the topographic map indicate that the first group distribution is in agreement with the release area located close to the axis of the mountain ridge and the second group with the channelized path downslope (Figure 4.8a).

We deduce from the analysis that the release area is at CB1 and that the snow avalanche front descends by the channelled path with a free fall between both areas (slope higher than 45°, see slope map in Figure 3.2, Chapter 3). All data and interpretations fit with one of the snow avalanche release scars recognized in the pictures at CB1 near the mountain ridge, close to CB2 (Figure 4.8a).
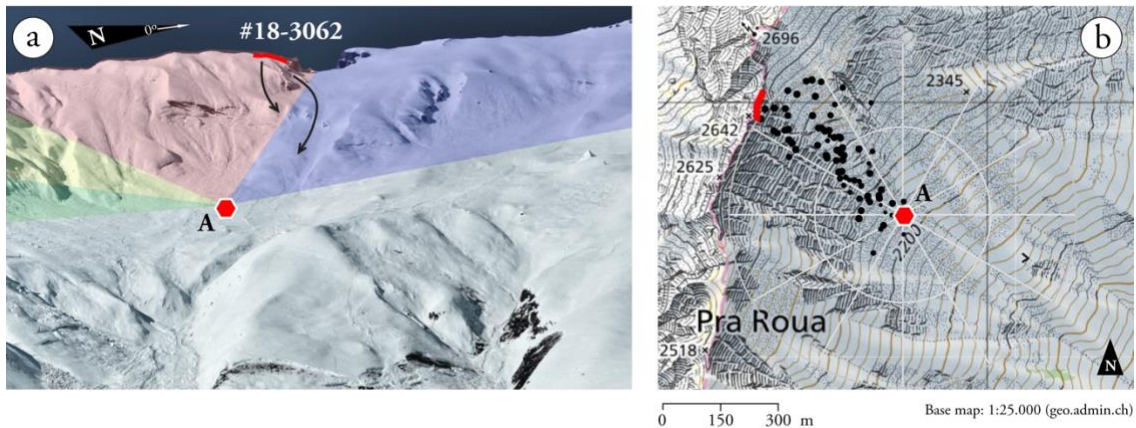
Figure 4.8 - a) Picture of the VDLS central region on 19/02/2018 (by Dr. P. Huguenin) with the colour shades (green, yellow, red and blue) indicating the back-azimuth ranges of the main release areas (PR2, PR1, CB1 and CB2) from Cavern A (hexagon) (see Subsection 3.d.i for a detailed explanation of the back-azimuth data plot representation). The solid red line delimits the recognized release scar of snow avalanche #18-3062. The black arrows indicate the main slope directions and paths deduced from back-azimuth values. b) Map of the VDLS site [Swisstopo - geo.admin.ch] with the position of Cavern A(hexagon) and the back-azimuth values in a polar coordinates plot above it. Note the back-azimuth values following the topography indicating an approximated downslope path for the snow avalanche front.

- **#18-3063**

The VDLS triggering system was activated from Cavern A at 22:36 UTC on 31/01/2018, the same day as triggers #18-3061 and only three hours after trigger #18-3062. The seismic data recorded from this snow avalanche are very similar to those recorded from the previous one (#18-3062, Figure 4.7 and Figure 4.8). From the point of view of the seismic data, this avalanche did not seem larger than the previous one, since the maximum values of the Total Envelope (At) are similar. However, the seismic station at Cavern C recorded this avalanche, which means that it could be slightly larger or that the avalanche rheology allowed a larger runout distance.

The maximum At values at Cavern A are -96.82 dB, which do not exceed the -81 dB value, and therefore the snow avalanche did not pass over the seismic sensor (Figure 4.9b). The STA/LTA algorithm and At thresholds for the SON section isolation functioned correctly, thereby identifying the SON section between -52.61 s and -21.38 s (Figure 4.9a, Figure 4.9b and Figure 4.9c). The BAZ direction obtained for the SON section is 302.5° ±3.2° corresponding to the CB1 region (Figure 4.9d).

A huge top scar on the snow cover mantle can be recognized from the pictures (Figure 4.10a). It is reasonable to affirm that the northernmost section was released during the first trigger (#18-3062), as indicated in Figure 4.10a, and the second avalanche released three hours later (#18-3063) was due to the loss of support from the remaining snow cover (Figure 4.10a). The constant values of the back-azimuth directions around 304° suggest that the topography channelled the snow avalanche that descended directly towards Channel 1 (Figure 4.10).
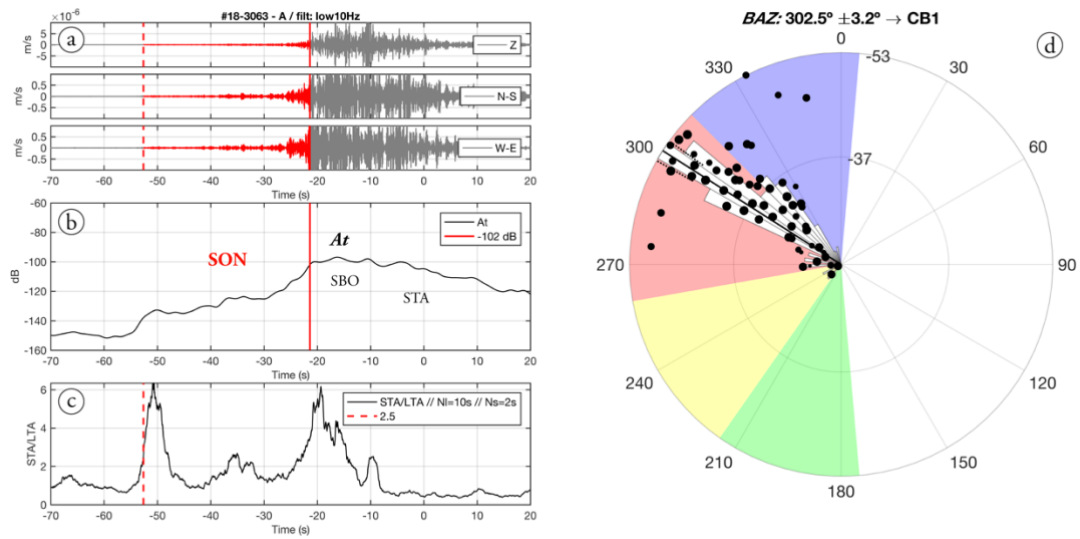
Figure 4.9 - Release area identification for snow avalanche #18-3063. Analysis of the seismic data recorded at Cavern A. a) Time series of the three components [ZNE] of the seismic ground motion (m/s), 10 Hz lowpass filtered, highlighting the SON section in red. b) Total Envelope of the seismic signal (At [dB]) indicating the end of the SON section (red line), the maximum At (<81dB) and the following SBO and STA sections of the seismic signal. c) The STA/LTA ratio plot used to delimit the start of the SON section (dashed red line). d) Polar coordinate plot with the BAZ (black line), standard deviation (short black dashed lines) of the back-azimuth values (black dots) and histogram of the back-azimuth values accumulation (white). The radius values in the circles correspond to the time scale. The background colours correspond to the different snow avalanche release regions at VDLS (see Subsection 3.d.i for detailed explanation of the back-azimuth data plot representation).

Figure 4.10 - a) Picture of the VDLS central region on 19/02/2018 (by Dr. P. Huguenin, SLF-Sion) with the colour shades (green, yellow, red and blue) indicating the back-azimuth ranges of the main release areas (PR2, PR1, CB1 and CB2) from Cavern A (hexagon)(see Subsection 3.d.i for a detailed explanation of the back-azimuth data plot representation). The solid red line delimits the recognized release scar related to snow avalanche #18-3063. The black arrow indicates the path deduced from back-azimuth values. b) Map of the VDLS site [Swisstopo - geo.admin.ch] with the position of the seismic station at Cavern A (hexagon) and the back-azimuth values in a polar coordinates plot above it.

- **#18-3064**

This trigger was on February 12th. 2018, at 07:01 UTC from Cavern A, thirteen days after those previously presented (#18-3061, #18-3062 and #18-3063). The seismic data recorded at Cavern A shows lower amplitude than in the previous triggers (note the 10^{-6} factor in the amplitude seismograms axis in Figure 4.11a). The maximum value of the Total Envelope At is -110.3 dB, lower than -102 dB, the threshold for the SON section isolation criterion. In this case, we considered the maximum At peak as being a good approximation to determine the boundary between the SON and SBO sections (Figure 4.11b). The STA/LTA algorithm functioned correctly (Figure 4.11c). The SON section was isolated between -48.34 s and -28.63 s (Figure 4.11a, Figure 4.11b and Figure 4.11c).

This snow avalanche seems to be much smaller than the avalanches normally studied at VDLS. It was also recorded in Cavern B, but with a lower amplitude and shorter duration than other snow avalanches (not relevant for the release area identification). Small avalanches like this are usually ignored because they do not reach the instrumentation located at Cavern C, and little information is acquired from them. Nevertheless, the seismic data recorded at Cavern A are valid enough to study their origin and to test our method.
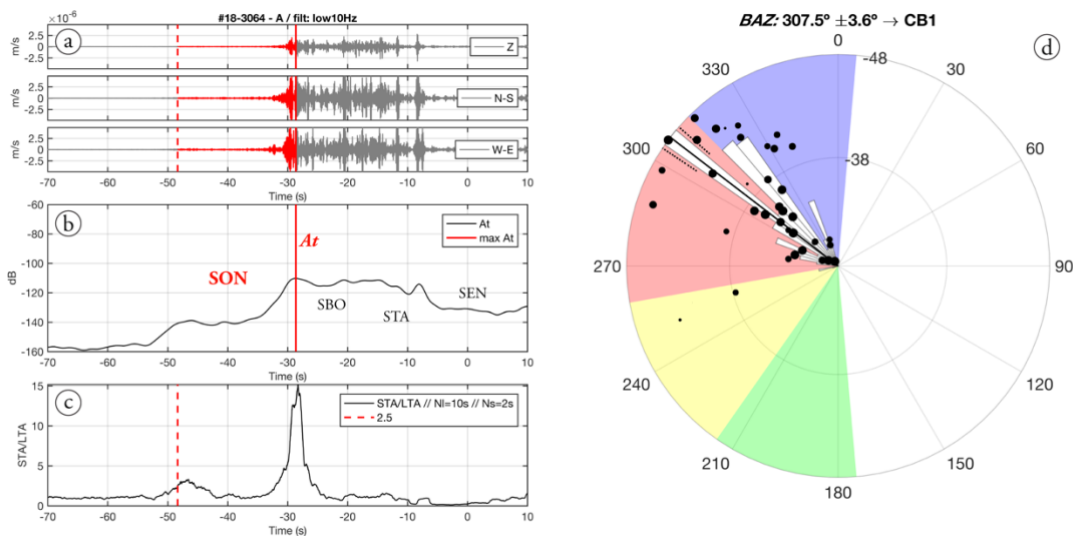
Figure 4.11 - Release area identification for snow avalanche #18-3064. Analysis of the seismic data recorded at Cavern A. a) Time series of the three components [ZNE] of the seismic ground motion (m/s), 10 Hz lowpass filtered, highlighting the SON section in red. b) Total Envelope of the seismic signal (At [dB]) indicating the end of the SON section at the maximum At values -because of the low amplitude seismic signal- (red line) and followed by the SBO, STA and SEN sections. c) The STA/LTA ratio plot used to delimit the start of the SON section (dashed red line). d) Polar coordinate plot with the BAZ (black line), standard deviation (short black dashed lines) of the back-azimuth values (black dots) and histogram of the back-azimuth values accumulation (white). The radius values in the circles correspond to the time scale. The background colours correspond to the different snow avalanche release regions at VDLS (see Subsection 3.d.i for a detailed explanation of the back-azimuth data plot representation).

The *BAZ* direction obtained from the analysis of the SON section is 307.5º ±3.6º, corresponding to the CB1 region (Figure 4.11d). A detailed inspection of the back-azimuth values indicates that they fall into three main groups. The first one with values between 300º and 310º and with a high linearity (big dots). It corresponds to the time windows of the start of the SON section and its values fit with the *BAZ* direction. The second group, in a direction closer to 330º for the windows in the middle position (before -38 s) and with lower linearity (small dots). The third group corresponds to windows closer to the end of the SON section with a larger linearity and back-azimuth values closer to the *BAZ* direction, around 300º (Figure 4.11d).

The back-azimuth values of the first group coincide with the position of the area where the wind conditions tend to accumulate snow, and some release scars were detected by pictures (Figure 4.12a). The back-azimuth values of the second group agree with the direction of the channelled topography, the same back-azimuth direction for the channelled topography found in snow avalanches #18-3062 and #18-3066, from where the avalanche probably descended (Figure 4.12b). The third group of back-azimuth values coincides with those of the closer position of the front to Cavern A. As mentioned before, this snow avalanche is really small and probably stopped close to Cavern A, only a small tail descending to Cavern B. Note that, since it was such a small avalanche, it was recognized because it passed close to the Cavern A position and the VDLS triggering system was activated. If it had occurred farther away, the recording system would not have been triggered nor would it have been studied.
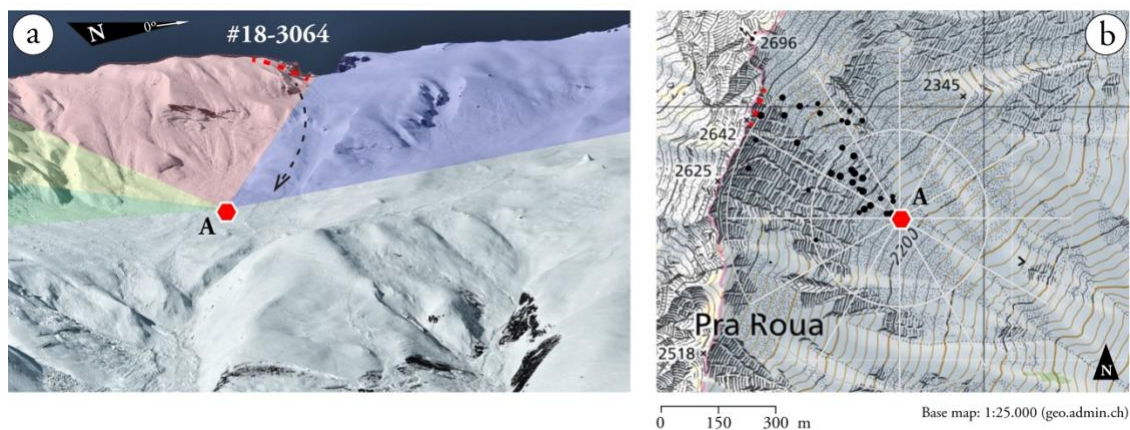
Figure 4.12 - a) Picture of the VDLS central region on 19/02/2018 (by Dr. P. Huguenin, SLF-Sion) with the colour shades (green, yellow, red and blue) indicating the back-azimuth ranges of the main release areas (PR2, PR1, CB1 and CB2) from Cavern A (hexagon) (see Subsection 3.d.i for a detailed explanation of the back-azimuth data plot representation). The dashed red line delimits the possible scar related to snow avalanche #18-3064. The identification of the release area from pictures is not clear enough for a straightforward validation. The dashed arrow indicates the possible path downhill, deduced from the back-azimuth values. b) Map of the VDLS site [Swisstopo - geo.admin.ch] with the position of the seismic station at Cavern A (hexagon) and the back-azimuth values in a polar coordinates plot above it.

- **#18-3065**

On February 12th, 2018, at 12:01 UTC (midday), the triggering system of VDLS was activated at Cavern B. It was on the same day as the previous trigger (#18-3064), but five hours later. We can assess from the spectrograms that this snow avalanche is larger than the other avalanches presented in this section (#18-3061 to #18-3064) from Cavern B and Cavern C seismic data. The seismic sensor at Cavern D also recorded this snow avalanche with low frequencies and low amplitudes. The data recorded in Cavern A suggest that the avalanche did not pass over this sensor, since the maximum Total Envelope value is -96.79 dB. The Total Envelope values (At) are higher enough to be able to find the SON-SBO limit (Figure 4.13b). In addition, the STA/LTA algorithm recognized the start of the seismic vibrations coming from the start of the mass movement (Figure 4.13c), allowing us to isolate the SON section between -83.62 s and -47.43 s (Figure 4.13a, Figure 4.13b and Figure 4.13c). In this case, since the start of the mass movement exceeds the 60 s of pre-trigger, we use the data of the continuous stream from the Cavern A seismic station. This is one of the advantages of the UB-RISKNAT seismic station deployment at VDLS.
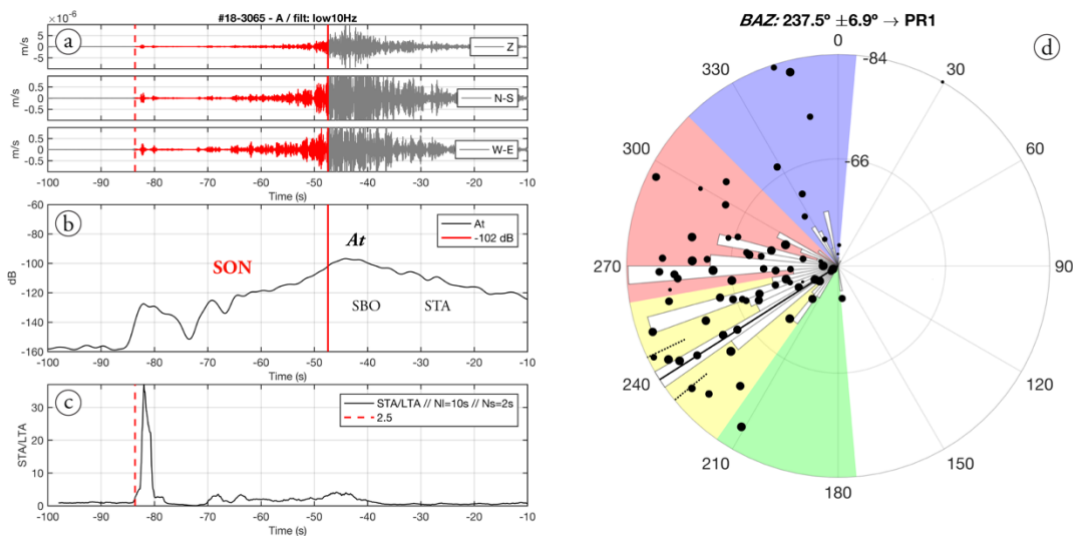
Figure 4.13 - Release area identification for snow avalanche #18-3065. Analysis of the seismic data recorded at Cavern A. a) Time series of the three components [ZNE] of the seismic ground motion (m/s), 10 Hz lowpass filtered, highlighting the SON section in red. b) Total Envelope of the seismic signal (At [dB]) indicating the end of the SON section (red line), the maximum At (<81dB) and the following SBO and STA sections of the seismic signal. c) The STA/LTA ratio plot used to delimit the start of the SON section (dashed red line). d) Polar coordinates plot with the BAZ (black line), standard deviation (short black dashed lines) of the back-azimuth values (black dots) and histogram of the back-azimuth values accumulation (white). The radius values in the circles correspond to the time scale. The background colours correspond to the different snow avalanche release regions at VDLS (see Subsection 3.d.i for a detailed explanation of the back-azimuth data plot representation).

The BAZ direction obtained from Cavern A is 237.5° ±6.9°, pointing to the Pra Roua (PR1) release area (Figure 4.13d). The back-azimuth values are more disperse than in the snow avalanche examples presented in this Chapter, but the representation in polar coordinates using weighted dots shows some tendencies that allow us to deduce the main track of the snow avalanche development in the downslope direction (Figure 4.14b). A

possible situation obtained from the analysis of the values and the picture observation
(Figure 4.14a) is that this snow avalanche was released from PR1 and flowed down along a
channelled area leading to the lower part of the CB1 region before entering Channel 1 (Ch.1
in Figure 4.14a). The back-azimuth values around 270º are in agreement with a simultaneous
activation (or with a few seconds delay) of a second front in a higher position, where a release
scar is also recognized (dashed red lines in Figure 4.14a and Figure 4.14b, respectively).
Moreover, the back-azimuth values around 240º are in agreement with the activation of the
main avalanche front from the scar recognized in this direction (red lines in Figure 4.14a and
Figure 4.14b, respectively) and descend following the topography to Channel 1 (arrows in
Figure 4.14). The trajectories deduced from the back-azimuth directions and the topographic
observations agree with the fact that the mass did not pass over Cavern A, deduced from the
low Total Envelope values (At) obtained.
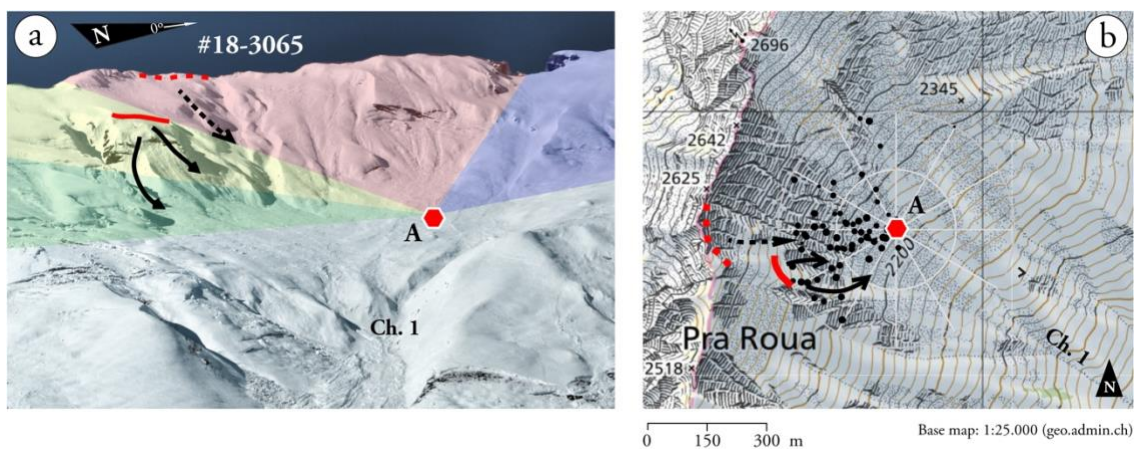
Figure 4.14 - a) Picture of the VDLS central region on 19/02/2018 (by Dr. P. Huguenin, SLF-Sion) with the
colour shades (green, yellow, red and blue) indicating the back-azimuth ranges of the main release areas (PR2,
PR1, CB1 and CB2) from Cavern A (hexagon) (see Subsection 3.d.i for a detailed explanation of the back-
azimuth data plot representation). The solid red line indicates the main scar that fits with the snow avalanche
#18-3065 and the dashed red line delimits a possible scar also related with the same snow avalanche. The
black arrows indicate the downslope path of the snow avalanche. b) Map of the VDLS site [Swisstopo -
geo.admin.ch] with the position of the seismic station at Cavern A (hexagon) and the back-azimuth values
representation in a polar coordinates plot above it. The red lines indicate the recognized scars and the black
arrows the snow avalanche front paths recognized from the back-azimuth values.

4.b.iii. Summary

The automatic triggering system at VDLS was activated 6 times between January 30th
and February 19th, 2018, the days with pictures of the VDLS site. Using only the SON
section seismic data from every trigger activation recorded at Cavern A, we deduced the
back-azimuth directions (BAZ) from where the seismic signal produced by the snow
avalanche came from and related it to the scars in the release areas regions at the top of the
VDLS site.

A summary of the avalanches analysed, and descent paths obtained from the seismic
data is shown above a VDLS release area picture in Figure 4.15. The results are presented
from left to right, according to the release area distribution seen from a bunker position
(from where the picture was taken). The processing of trigger #18-3061 data suggests that

the trigger was activated by a snow avalanche with the release area placed to the south of Cavern A. The seismic signals show the lowest amplitude of all the triggers considered in this chapter. This is in agreement with the fact that this avalanche is the furthest from Cavern A. Due to that low amplitude, the *At* values are also low, close to the *At* threshold values used as a criterion for the isolation of the snow avalanche seismic signal sections. The SON section is shorter than expected, but long enough to obtain two back-azimuth values, both pointing to the PR2 region. The two scars were probably activated during avalanche #18-3061 descending by the Deylon channel, outside the VDLS experimental site (left in Figure 4.15).

The second avalanche from the left in Figure 4.15 corresponds to trigger #18-3065. This trigger activation corresponds to a medium-size avalanche deduced from the seismic signal amplitudes and recordings from all seismic stations at VDLS. The obtained *BAZ* direction points to the PR1 region. The back-azimuth values are more disperse than in other avalanches, enabling us to link different groups of back-azimuth values to different snow mass releases. We detected two scars, one in PR1, just above a cliff heading to Channel 1, and the other on the left of the CB1 region but guiding the avalanche mass to the PR1 region as well as to the Channel 1 entrance (left/centre of Figure 4.15). Both scars where probably activated simultaneously and met each other at the entrance to Channel 1. This could be the cause of the mix of the back-azimuth values, because both avalanche fronts generated ground vibrations simultaneously.

The CB1 region is the most active one in this study, with release areas associated to three different avalanches. Top scars have been recognized in the ridge of the CB1 area, enabling us to link all the avalanches (triggers #18-3062, #18-3063 and #18-3064) to probable release areas. All three trigger activations can be identified as snow avalanches. Avalanche #18-3063 presents the southernmost *BAZ* direction of all three, with good accumulation of back-azimuth values and low dispersion, suggesting a clear release area identification and a single front release. Avalanche #18-3062 also presents a good accumulation of back-azimuth values clearly divided into two groups that can be linked to the effect of the topography. From the interpretation of the back-azimuth values, we deduced that the *BAZ* value points more to the north than the release area, since the avalanche flow adjusts its trajectory to a channelled part (between CB1 and CB2 approx.). The scar on the right of the #18-3063 avalanche can be linked to avalanche #18-3062, both of which are medium-size (centre of Figure 4.15).

Trigger #18-3064 corresponds to the smallest snow avalanche studied in this section, showing the lowest amplitude of ground motion (we do not consider #18-3061 because the avalanche is far from the sensor)-. From this lower amplitude we can deduce that it is a small avalanche, and therefore that the release area is not as large as the others. The back-azimuth values point to a similar direction to that of avalanche #18-3062, with a closer *BAZ* direction and with accumulation of back-azimuth values following the channelled part between CB1 and CB2. The linearity values of the particle motion are low in the first part of the SON seismic signal (smaller dots for back-azimuth values, Figure 4.11d), which is consistent with the observation that it is a small avalanche. The signal to noise ratio is low, making it more

difficult to perform the particle motion studies. We deduced that it is a small purge/sluff in the crest of the CB1 area, where release scars in the snow cover are detected (centre of Figure 4.15). This small avalanche may have been produced by the snow accumulation in the channelled part of the ridge due to wind drift.

The northernmost release scars are linked to the snow avalanches recognized in the trigger #18-3066 analysis (presented in Subsection 4.b.i) and consist of two different fronts with three detected release areas (right of Figure 4.15).

Although all the avalanches considered are of different sizes and types, the release areas can be clearly recognized and well correlated with the areas identified in the pictures. The *BAZ* directions obtained do not always point to the exact position of the release scar identified, although they are always close. The dispersion errors (standard deviation) of the *BAZ* directions give us margins that are generally enough to link them to the release area. The *BAZ* direction is an indicative value that can be used as an approximation or as a quick output value for the snow avalanche release area estimation. For a detailed description of the descent of a snow avalanche along the path from the release area until reaching the Cavern A position, the representation of the back-azimuth values in dots provides a good tool for identification, being able to link it with the topography.
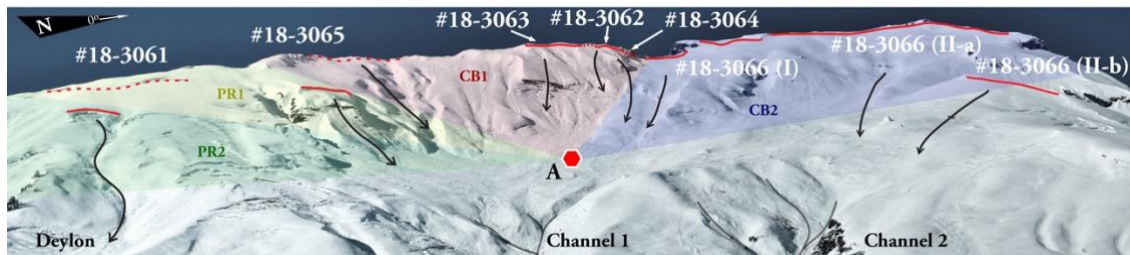
Figure 4.15 - Summary of the avalanches analysed in this chapter (white) on a VDLS picture taken on 19/02/2018 (by Dr. P. Huguenin, SLF-Sion). The colour shades (green, yellow, red and blue) indicate the back-azimuth ranges of the main release areas (PR2, PR1, CB1 and CB2) from Cavern A (hexagon) (see Subsection 3.d.i for a detailed explanation of the back-azimuth data plot representation). In red lines, the scars recognized and the deduced main avalanche tracks and slope directions in black arrows. Channels 1 and 2 of VDLS site are indicated. The picture is oriented from south (left margin) to north (right margin).

4.c. Automatization of the snow avalanche release identification: post-season data processing

The designed for the identification of the release area of a snow avalanche is able to run with a real-time data stream The characteristics of the data acquisition system at VDLS do not currently allow us to process the seismic data in real-time, since it is necessary to transfer the data from the seismic station to the VDLS-Allaus-Server, and from there to the server at the UB-Allaus-Server before processing the seismic data (see Subsection 2.b.i for a detailed description of the data Archive protocol).

To test the ability to identify the release area and the feasibility of the method, all VDLS trigger data available from season 2015-2016 until 2019-2020 were processed. The VDLS trigger system is activated by snow avalanches, and also by other ground vibrations produced by earthquakes, explosions (there is a ski resort close to the site), wind, animals, etc. In the automatic data processing, all the VDLS trigger activations are considered. In consequence, we need to check whether or not the seismic vibrations that activated the trigger system are generated by a snow avalanche before the application of the release area identification algorithm (Figure 4.16a). This part of the data processing algorithm is detailed in the next Subsection 4.c.i.

Once the trigger activation is identified as being produced by a snow avalanche, the seismic data at the Cavern A seismic station are processed following the method for the identification of the release area detailed in Subsection 4.c.ii of this chapter. We designed a three-step algorithm to summarize the whole process for the release area identification (I, II and III in Figure 4.16b).

4.c.i. Seismic data trigger classification

Each activation of the VDLS trigger system is verified daily by the SLF team using the available pictures to identify whether a spontaneous snow avalanche has been released. If the pictures are clear enough, the main deposit of the avalanche can be identified, and the avalanche time release can be approximated, since it is possible to link the trigger activation to the snow avalanche. The SLF-Sion team also obtains on-site field information when the snow avalanche is large enough or when the trigger system activations become more frequent. In most cases, the confirmation of the snow avalanche occurrence is made a few days after the trigger activation rather than on the same day. In this situation, the seismic data provide a good indicator for identifying whether or not the trigger has been activated by a spontaneous snow avalanche.
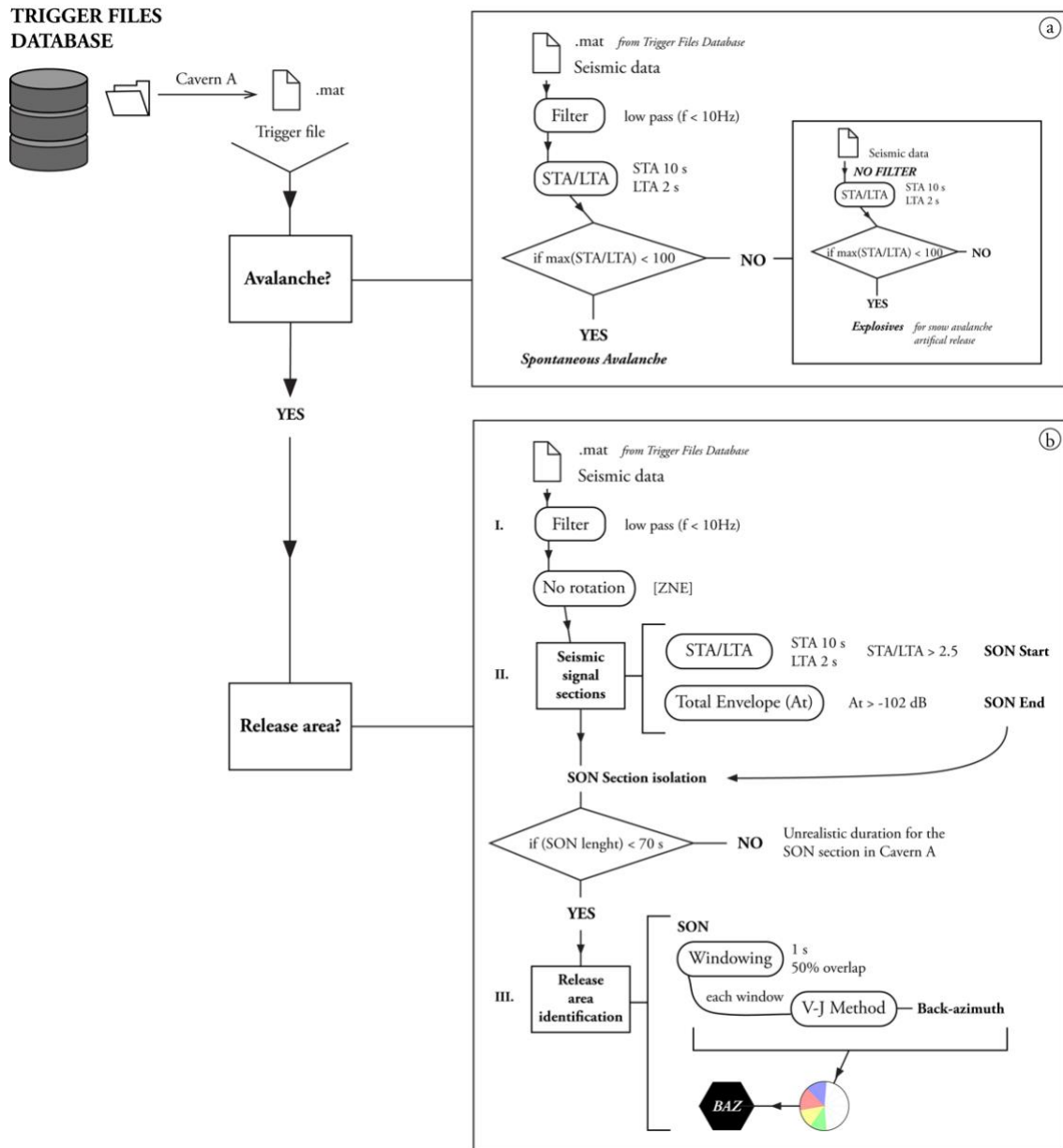
Figure 4.16 - Block diagram of the seismic data processing algorithm (a) identification of the trigger
activations produced by spontaneous snow avalanches, and (b) identification of the snow avalanche release
area. This algorithm is designed to be applied to seismic data at the Cavern A seismic station, for post-season
data processing including all trigger activations.

Differentiation of the seismic signals produced by snow avalanches, earthquakes, explosions or other anthropic seismic noise has been reported in the past (Suriñach et al., 2000; Biescas et al., 2003; Pérez-Guillén et al., 2014). Automatic recognition systems have been applied in other experimental sites with specific configurations of seismometers and the use of machine learning algorithms (Hammer et al., 2017; Heck et al., 2018). However, these are not useful for continuous 3D seismic data stream we have at VDLS. In consequence, as yet there is no automatic recognition system configured for the spatial distribution and seismometer configuration at VDLS. To remedy this situation, at least for the post-season data processing, we created an algorithm based on the STA/LTA ratio

(Figure 4.16a), achieving good results in the identification of seismic vibrations produced by snow avalanches detected by trigger activations.

Given that the STA/LTA is the ratio between a short-time average of the amplitude of the seismic signal and a long-time average of the amplitude if the amplitude values increase gradually, the STA/LTA values remain small. On the other hand, when the amplitude values undergo a rapid increase, the STA/LTA ratio value variation will be greater. In the case of the seismic signals generated by a snow avalanche, the STA and LTA values increase gradually in the SON section. Consequently, the STA/LTA values remain small. Should the VDLS triggering system be activated by an earthquake, an explosion or other single seismic sources, the amplitude of the seismic signal suddenly increases. Note that only local earthquakes generate vibrations strong enough to activate the VDLS triggering system, and the teleseisms are not considered because they do not activate the VDLS trigger system. In these cases, the STA values undergo a sudden increase in comparison to the LTA values. After training, a threshold was determined for the STA/LTA values that separates the two types of events. STA/LTA values less than 100 correspond to snow avalanches, whereas the higher values correspond to other types of events (Figure 4.16a).

The seismic signals corresponding to snow avalanches triggered using explosives during experiment days will be identified as explosions (point source) because of the large seismic signal amplitude generated by the detonation of the explosives. For the automatic execution of the algorithm, we focus only on spontaneous avalanches. Excluding the snow avalanches generated on the experimentation days from the process entails no problems, because the release area of the snow avalanches triggered by explosives is already known. Moreover, the number of these avalanches triggered using explosives on experiment days is small (four in season 2015-2016 and two in 2016-2017).

The trigger system at VDLS was activated 420 times (included 6 explosion triggers) between seasons 2015-2016 and 2019-2020 (Figure 4.17). In this lapse of time, 59 trigger activations can be linked to snow avalanches identified from pictures and field information. The presented algorithm applied to the seismic data of these avalanches recorded at Cavern A identified 56 as snow avalanches, which represents a 95% success rate. Applying the presented algorithm to all the trigger activations between the 2015-2016 and 2019-2020 winter seasons, 232 triggers are identified as spontaneous snow avalanches (Figure 4.17).

When processing the trigger activations data files, the seismic data are filtered with a low pass filter at 10 Hz (Butterworth, 4th order; See Section 3.a.iv for details about seismic data filter). The STA/LTA ratio is calculated with the vertical component [Z] of the filtered seismic signal. The same configuration used for the identification of the start of the SON section (see Subsection 3.a.ii and 3.a.iii) is used (STA=2s and LTA = 10s). In this case we do not focus on a threshold value, but rather check the maximum STA/LTA value.

4.c.ii. Automatic release area identification

When the VDLS trigger system is activated and we are able to confirm that a snow avalanche is the seismic signal source, we proceed to identify from where the snow avalanche is released, considering the major release areas previously identified (PR2, PR1, CB1 and CB2).

The algorithm is simplified in three main steps (I, II and III) that include all the seismic data processing steps already presented (Figure 4.16b).

I. – Seismic data preparation: the seismic data from Cavern A are filtered using a low pass filter at 10 Hz (Butterworth, 4th order) in order to considering only the low frequency band. The 3D seismic signal is not rotated, the ZNE directions being valid for the release area identification.

II. – Seismic signal sections determination: the release area identification is performed on the SON section. With the use of the STA/LTA ratio and the Total Envelope (At), the SON section seismic signal is isolated. The threshold values used in the isolation for both parameters are defined in Section 3.b. Should the snow avalanche present more than one front (multiple SON sections), the automatic algorithm can only identify the first SON section.

The length of the SON section becomes a criterion for checking the validity of the data, providing that the snow avalanche seismic data identification is correct. A SON section duration larger than 70 s is considered to be unrealistic for the SON section at Cavern A. Given the short distance between the release area and the Cavern A position, this will imply unrealistically low avalanche speeds. Of the 232 trigger activations recognized as spontaneous snow avalanches, 157 triggers were recognized from the seismic signal as spontaneous snow avalanches, with a realistic SON length (Figure 4.17). The remaining 75 have a SON section greater than 70 s and cannot be regarded as snow avalanches for the snow avalanche release identification.

III. – Release area identification: the SON section seismic signal is processed in time windows. The V-J method to obtain the back-azimuth direction from the ground particle motion polarization is applied in each window. The mean value from the all the back-azimuth values (BAZ), determines the release area of the snow avalanche identified (method described in detail in Subsection 3.d.i).

The release area identification algorithm is applied over each of the 157 selected seismic data files corresponding to snow avalanches identified as spontaneous. Only 4 of the 157 show an output release area direction (BAZ) outside the previously identified release

areas (PR2, PR1, CB1 and CB2). These high values of success confirm the ability to programmatically estimate the release area of the snow avalanche (Figure 4.17).

Of the 157 triggers identified from the seismic signal as spontaneous snow avalanches, we know from pictures or filed information the release area of 37 of them. The automatic application of the release area identification algorithm to all triggers correctly identifies the release area of 29 out of the 37, representing a 78% success rate (Figure 4.17).
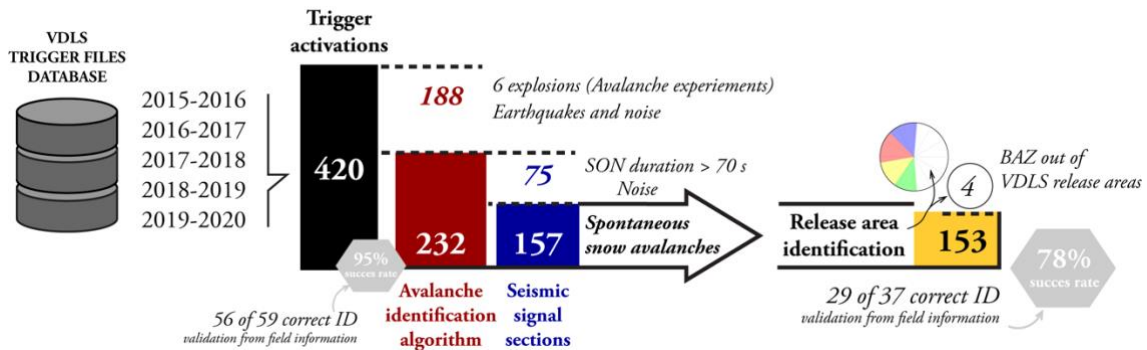
Figure 4.17 - Scheme of the results obtained from the application of the snow avalanche release area identification algorithm for its automatic execution. Data from all trigger activations at the VDLS site for seasons from 2015-2016 to 2019-2020. The red box indicates the avalanche seismic data identification algorithm (see Figure 4.16a). The blue box indicates the seismic signal sections identification from the release area identification algorithm (see Figure 4.16b). The orange box indicates the results obtained from the release area identification algorithm application. All these data are treated using the same data processing steps, executed programmatically using a MATLAB® script.

These results could be improved by a manual revision of the SON section seismic signal and selection of the isolation criterion used for the determination of the start and the end of the SON section. Moreover, when processing the data using the automatic algorithm, we only detect the first avalanche front, the first SON section where to apply the release area identification method.

4.d. Limitations and decisive factors in the snow avalanche release area identification method and SON section isolation criteria

Although the basis of the method works and is functional, some limitations were found. The method can be split into two main data processing steps: a) the SON section isolation, and b) the back-azimuth values calculation (*BAZ* method, release area identification method).

One of our findings is that the *BAZ* method must be applied as it is designed, on the SON section, clearly linked to the first steps of the snow avalanche mass movement. The isolation of this section therefore needs to be as precise as possible. The STA/LTA algorithm is a valid method for detecting the start of the snow avalanche seismic signal and for isolating the SON section. However, if the signal-to-noise-ratio (SNR) is low, the STA/LTA values are affected and the threshold invalid. This may be due to a) the background noise level is

higher than usual, b) the amplitude of the avalanche seismic signal is too low or c) when there are too many amplitude variations, among other causes (i.e., wind, explosions or other close snow avalanches). These situations may result in a poor detection of the start of the snow avalanche.

The determination of the end of the SON section is carried out using the Total Envelope values (At). The selected threshold values of At for the SON isolation are valid if the snow avalanche is large and/or if it is close enough to the Cavern A seismic station. However, for small avalanches, and if they are not close enough to the sensor, the At values are probably not as high as those needed to satisfy the defined threshold criteria (higher than -102 dB for the end of the SON). In these cases, we decided to use the maximum At value as a good approximation to determine the end of the SON section. These changes in the SON isolation criterion could cause part of the SBO to be included in the end of the SON section, leading to some incorrect back-azimuth values that could cause a deviation in the BAZ value. This situation only occurs in small snow avalanches and far from the sensor position, at the boundaries of the usability of this method.

The seismic signal amplitude constitutes a key factor. It is controlled by the distance of the snow avalanche front from the sensor and by the size of the snow avalanche itself. The furthest release areas studied at the VDLS experimental site were around 600 m (furthest points from the CB2 and PR2 areas). With the current sensor configuration at VDLS, we consider this distance to be the limit for the snow avalanche detection and for the usability of seismic data for the release recognition.

As detailed in Section 3.b, each SON section belongs to a snow avalanche front. However, not all snow avalanches have only one front, and normally the same release area can generate different snow avalanche fronts. The use of the back-azimuth values treated as a weighted average is intended to provide a solution in cases when all these mixed ground vibrations reach the seismic sensor in the same SON section seismic signal. The particle motion can be confusing and the clear extraction of a single back-azimuth very difficult because of the overlapping of the seismic waves. In these situations, the linearity (R value) constitutes a key factor for highlighting the clearest and most consistent back-azimuth values.

The mean standard deviation of the back-azimuth values around the BAZ direction is approximately ±7° (mean value of all those of the 150 avalanches processed automatically). It may be lower in a perfectly isolated SON section, but not lower than ±2.5°, a limitation due to the width of the histogram bin from the calculation of the back-azimuth accumulation. The standard deviation values are calculated according to the weight of every back-azimuth value related to their linearity (R). The origin of the dispersion of the back-azimuth values may be due to different factors: a) seismic wave type, b) more than one snow avalanche front, and c) interaction of the snow avalanche front with the topography. We exclude the effect of the length of the time windows and overlapping because both were tested and selected to obtain the best results.

As for the causes of the dispersion, the first case concerns the type of seismic waves recorded. Even when regarding the avalanche as a moving single source, as a first

approximation, we are not only recording direct P-waves as the first arrivals of the seismic vibrations. As the avalanche progresses along its path, seismic waves are generated, and different wave-conversions may also be generated in the ground heterogeneities. The short difference in travel time of these waves and the S-waves makes their identification difficult. The difficulty increases when considering the front as a line of sources. Despite the dispersion in the back-azimuths due to all this mixing of seismic waves, we consider that if statistically treated the mean back-azimuth direction (*BAZ*) will be related to the direction of propagation, and thus closely related to the point from where the seismic waves arise.

The second cause of the dispersion is the existence of different snow avalanche fronts descending from different release areas at the same time. In this case, the situation described above becomes more complex, because the wave propagation direction is not from the same origin. In these cases, the *BAZ* direction is more difficult to evaluate, and the back-azimuth representation in polar coordinates over the topographic map help us to understand the behaviour of the avalanche. Generally, if two fronts are released at the same time (or close in time) the release areas will be close, and the back-azimuth values will be mixed, but pointing to close directions. In an automatic calculation, we will only obtain one *BAZ* direction, although the interpretation of the back-azimuth values may lead us to the identification of both fronts. In other cases, one avalanche could trigger another avalanche downslope or from another release area. In this situation the interpretation of the data becomes more difficult. Although the automatic identification of the release area can be performed, it should be reviewed for a better identification and interpretation. The snow avalanches recorded in triggers #18-3065 and #18-3066 are good examples of that.

The third factor in the back-azimuth values dispersion corresponds to the interaction of the avalanche front with the topographic discontinuities such as rocks, slope changes, free falls, etc. Descending along the snow avalanche path, the snow avalanche front may encounter some of these topographic changes that produce collisions in different ways. These collisions are transferred to the ground as seismic vibrations that are recorded by the seismic sensor. These collisions normally produce higher amplitudes on the seismic signal and the particle motion may become more polarized. In some cases, these seismic vibrations can result in good back-azimuth values in the direction from where the avalanche is coming. In other cases, the collisions can generate vibrations polarized in totally different directions to the propagation path and become incorrect back-azimuth values that do not point to the release area. These back-azimuth values in wrong directions are not usually decisive but may cause variations in the *BAZ* direction value used for the release area identification, because its linearity is high and its weight in the calculation of the *BAZ* direction noticeable.

Considering all these factors, the dispersion obtained in the back-azimuth values is reasonable and acceptable, although for its automatization it needs to be taken into account. The projection of the back-azimuth values on the topographic map help us to recognize clearly the values outside the main trends and whether or not to take them into account for the identification of the release area.

The snow avalanche type and the rheology of the mass descending along the slope do not seem to be key factors in the back-azimuth calculations for the release area identification.

In the initial phases of snow avalanches, the development of the flow regime is still not complete and has no clear effect on the release area identification when using the *BAZ* method. In low amplitude seismic signals, it is more difficult to identify the SON section, and by extension more difficult to apply the release identification method. In this case, the release area of pure powder snow avalanches (with no dense basal layer) could be more difficult to identify, but only due to the low amplitude seismic signal in the initial steps of the snow avalanche flow.

4.d.i. Ability to export the snow avalanche release identification method to other snow avalanche occurrence sites

The release identification method presented herein was developed for the VDLS experimental site and only data from this site were processed. The identification of the location of the release areas was possible thanks to the deep knowledge of the site topography and the current location in the field of seismic sensor at Cavern A. We consider the mountain ridge at the top of VDLS site as a limit for identification and location of the snow avalanche release areas. Moreover, we only processed the seismic data recorded when the VDLS triggering system was activated.

We believe that the developed to identify the release area of snow avalanches can be exported to other areas and regions. However, some considerations and recommendations are necessary. A very good knowledge of the topography of the site and a previous identification of the main release areas of the region are essential. It is also very important to obtain information about the possible and more common paths for the snow avalanche descent, and also to obtain the back-azimuth ranges of the release areas and descent paths. The avalanche hazard maps, the residents in the area and the experts in hazard management for each mountain region are usually already familiar with the most common snow avalanche paths. Furthermore, from slope criteria and historical information, the snow avalanche most common release areas can be easily identified.

The use of only one 3D seismic sensor close to the release area is technically very helpful in mountain areas for an early recognition of the snow avalanche release and can also be very useful in snow avalanche characterization. The sensor must be located and buried in a quiet place to avoid false triggers and to ensure a higher signal-to-noise-ratio (SNR). In cases where more than one seismic sensor is installed in the area, their complementarity can be used to reduce false triggers by comparison. The configuration of the data acquisition system plays a very important in the procedure. In the absence of an external triggering system, a trigger algorithm must be configured, either with amplitude threshold criterion or by running the STA/LTA ratio algorithm for the continuous seismic data stream in real time (depending on the data acquisition system manufacturer). Note that the parameters for the snow avalanche release area identification method must be set correctly for each specific area. The STA/LTA algorithm settings used at VDLS experimental site may be useful as a guideline, but they cannot be applied straightforward without a specific setup test at each new site.

If the continuous data stream can be transferred to a computer in real time, both triggering algorithms can be calculated; that is, the *At* threshold algorithm for the isolation of the SON section and the *BAZ* method applied in real time for a more efficient snow avalanche release identification, such as complementary information for an early warning system. If the seismic data cannot be transferred to a computer in real time, the method can also be applied as a near-real-time method for the snow avalanche release identification.

Moreover, the method is useful for a database construction and for statistical studies of the snow avalanche occurrence in a mountain area, thereby enabling the seismic data to be processed for an entire winter season. This is the approach we adopted for seasons between 2015 and 2020 at VDLS. For these purposes, it is not necessary to compute the data in real time.

4.e. Conclusion

The application of the *BAZ* method in combination with the seismic SON section isolation enabled us to identify the snow avalanche main release areas and deduce the path along which the snow avalanche mass descends in its initial steps. This solves the main problem in the case of spontaneous snow avalanches, which is pinpointing the spot from where the mass is being released. In particular, we have applied the method to the VDLS experimental site. The success of the method is based on the following factors, which can be applied as a whole or individually to the recorded seismic data.

1. The use of *At* values. This constitutes a very useful criterion and works perfectly for the SON section isolation. The calculation of the Total Envelope (*At*) and the definition of the threshold levels allowed us to identify whether or not the snow avalanche flows over the sensor, and to establish the boundary between the SON and the SBO/SOV sections. However, it is very important to consider only the seismic signals generated at the beginning of the snow avalanche and not include the seismic signals from the moment when the snow avalanche is over the seismic sensor, or at the equivalent altitude position-.

2. Application of the STA/LTA algorithm. It enables the first seismic vibrations arising from the beginning of the snow avalanche mass movement to be identified and is therefore the perfect method for determining the start of the SON section. Setting 10s/2s for the STA/LTA length produces very good results. This method is more accurate than simply using the *At* values for the start of the SON section identification. It also provides us with greater accuracy than the automatic triggering system in VDLS and allows us to obtain a greater seismic signal from the initial part of the SON section as well as to identify smaller snow avalanches.

3. Application of the *BAZ* method (based on the polarization method) to a perfectly isolated SON section. It excels at identifying the snow avalanche release area. The application of the V-J method to a seismic signal in shifted time widows allows us to obtain a representation of the origin (source) of the seismic signal along the whole SON section. Linearity values (*R*) are very useful for highlighting the most relevant back-azimuth values. The accumulation of back-azimuth values and the statistical treatment of these values provides us with a *BAZ* value that is clear enough to point to the origin of the seismic signal and, by extension, to the avalanche release area. Likewise, the accumulation of back-azimuth values and the identification of certain trends, in combination with the topography of the site, makes it possible to deduce the snow avalanche path downslope for the SON section and the presence of secondary fronts released in the same SON section.

The good results obtained from applying these methods could be subject to some limitations if a) the signal-to-noise ratio (SNR) is low, b) multiple avalanche fronts are released at the same time, and/or c) the snow avalanche release area is really small or too far from the seismic station.

All the foregoing shows the importance of having seismic data from a 3-component seismic station deployed near the release area for the recognition and description of the snow avalanche. The study of the seismic signal in shifted time windows constitutes a very useful methodology for the detailed interpretation of the avalanche evolution.

The application of the method is easy to export and is easily deployed with little infrastructure. The use of an automatic algorithm for the snow avalanche release identification, using all the seismic data available from the whole season, is a good example of the potential of the methodology, which is capable of being applied in real time seismic data as well as to other sites with the appropriate settings. Moreover, it can be very useful as complementary information for early warning systems and in statistics of snow avalanche occurrence for management of the territory.

Chapter 5

Snow avalanche flow description

Snow avalanche behaviour may differ widely, depending on the amount of snow mobilized, the internal and external temperature (water content), wind, weather, snow cover along the avalanche path (snow incorporation and erosion), etc. (see Chapter 1). The rheology of snow avalanches and their evolution along the path are mandatory factors needed for protection purposes and are very important for snow avalanche model validation. All the classifications are based on different criteria depending on the data available.

From the seismic point of view, the main characteristic used for the snow avalanche flow regime classification is the frequency content (Suriñach et al., 2000; Biescas et al., 2003; Pérez-Guillén et al., 2016). Studies on the seismic frequency content evolution using spectrogram representations become very useful in the recognition and description of snow avalanche seismic signal sections, but it has limitations with respect to a quantified characterization of the flow regime and for the detailed description of the presence of the parts of the snow avalanche and their evolution.

Snow avalanches exhibit different evolutions along their path and over the ground surface composed of different parts (e.g., dense basal layers vs. powder layers, in large Powder Snow avalanches (PSA)). Using seismic data, we aim to identify all these parts and their presence, as well as to determine their interaction with the basal layer and/or with the ground. In this chapter, we present the results obtained with the application of the *DF* calculation, the *Cmean median* and *GRD* values in the SOV section of the seismic signal (see Subsection 3.a.ii for a detailed description of the methods) in order to identify and quantify the characterization of the different flow regimes present in a snow avalanche.

5.a. Snow avalanche reference information

Nowadays, the flow regime identification and the different snow avalanche part information relays on visual confirmation from the avalanche deposits, GEODAR data based on MTI plot signatures (Köhler & McElwaine et al., 2018) and single measurements from the VDLS Mast sensors (flow velocity, flow height and high-speed cameras facing the snow avalanche surface) (Kyburz et al., 2018; Kyburz et al., 2020). In this chapter, as reference information from snow avalanche behaviour we use the GEODAR MTI plots from the VDLS database stored at the Zenodo open-access repository (McElwaine & Köhler et al., 2017). The GEODAR MTI plots interpretations are performed using the method defined by Köhler et al. (2018).

The GEODAR data acquisition and MTI plots are not the object of this PhD thesis. For the interpretation of the GEODAR data, it is important to ensure that the MTI plots are space-time plots that show the changes in radar signal reflectivity and are able to identify the moving objects on the RADAR coverage range. The GEODAR antennas are placed at the Bunker facing the VDLS snow avalanche path and provide a complete coverage of all the snow avalanche path from the release area to the *La Sionne* river (Figure 5.1). Multiple antennas are placed to cover the entire VDLS slope. Data from all the antennas producing the wide coverage of the site (arched blue lines in Figure 5.1). From the trace of the snow avalanche surges on the MTI plot, the approximate velocity can be identified (top-right of the MTI plots), which is very useful for the snow avalanche flow regime identification (see the MTI plot of the #15-0017 snow avalanche, Figure 5.4a).

The position of the Cavern B and Cavern C seismic stations must be identified at the MTI plot for a detailed comparison of the data. The Cavern B position is at 1271 m range from the GEODAR (1897 m.a.s.l.), and the Cavern C seismic station position is at 600 m range from the GEODAR (1637 m.a.s.l.) These positions are indicated with a discontinuous line in all GEODAT MTI plots (see Figure 5.4a as example), providing a reference for the comparison with the seismic data.

For the time synchronization between seismic data and GEODAR MTI plots, we consider the VDLS trigger activation as being the start of the snow avalanche ($t0 = 0$ s). The VDLS trigger system activates at the same time the recordings of the seismic stations (Cavern B, C and Bunker) and the GEODAR data acquisition. This synchronization between instrumentation is precise enough for our purposes. When the snow avalanches are triggered using explosives on the experimental days, the trigger activation is manual in order to obtain data from the whole snow avalanche (GEODAR do not have pre-trigger data acquisition). In these cases, the explosion becomes helpful for double checking the time synchronization between instrumentation data and for performing corrections, if necessary. In spontaneous snow avalanches, the GEODAR data starts when the VDLS trigger is activated, normally losing some of the initial steps of the snow avalanche. This is not a big issue for the study of the flow regimes at Cavern B and Cavern C positions. For the seismic data initial approach, we represent the spectrogram of the Q component (more related to vertical changes on the

snow avalanche flow), which acts as a reference representation for the identification of the surges and snow avalanche sections.

In addition, we extract the snow avalanche description from published papers, cited at every snow avalanche presentation, if available. Complementary information is extracted from the snow avalanche description performed by the SLF Avalanche Dynamics team (included on data reports, unpublished) and the available pictures or videos from SLF, to achieve a global description of the snow avalanche before the interpretation of the seismic data.
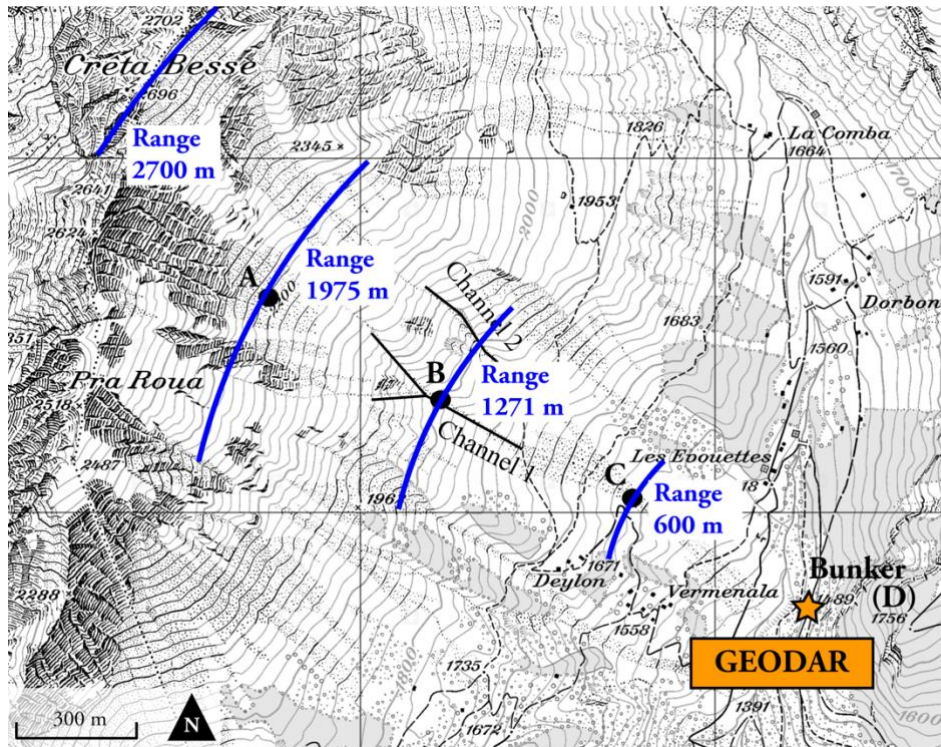
Figure 5.1 - Map of the VDLS site with the position of the Caverns and the Bunker (in black), the GEODAR position at the Bunker (orange) and the GEODAR coverage range at the Cavern positions (in blue).being the start of the snow avalanche (*t0* = 0 s).When the snow avalanches are triggered using explosives on the experimental days, the trigger activation is manual in order to obtain data from the whole snow avalanche (GEODAR do not have pre-trigger data acquisition). In these cases, the explosion becomes helpful for double checking the time synchronization between instrumentation data and for performing corrections, if necessary. In spontaneous snow avalanches, the GEODAR data starts when the VDLS trigger is activated, normally losing some of the initial steps of the snow avalanche. This is not a big issue for the study of the flow regimes at Cavern B and Cavern C positions. For the seismic data initial approach, we represent the spectrogram of the Q component (more related to vertical changes on the snow avalanche flow), which acts as a reference representation for the identification of the surges and snow avalanche sections.

In the following three snow avalanches, the interpretation of the spectrogram plots of the seismic data from Caverns B and C (Q component) in combination with the MTI plot of the GEODAR data from McElwaine & Köhler et al., (2017) are presented. With that reference information for flow regime identification, we present the use of the frequency content values in combination with the seismic particle motion values (*DF*, *Cmean median* and *GRD*) to identify the snow avalanche flow regime regions flowing over the seismic stations (SOV) at Caverns B and C.

5.b. Time evolution of the seismic data frequency content and particle motion

Seismic sensors are able to record vibrations generated by a snow avalanche far from the sensor. These seismic vibrations are modified by the effect of the ground from where they are transmitted. To avoid this effect when looking for information on the flow regime, we use the recorded seismic data of snow avalanches flowing over the seismic station. Moreover, only the seismic data section corresponding to the body of the snow avalanche, the Signal Over sensor (SOV), is considered. This section is isolated using the criterion tool already defined (Section 3.b).

We only used seismic data recorded at Cavern B and Cavern C, located at the track and runout area of the VDLS test site where the snow avalanche is more developed, and where the amount of mass involved is greater than at Cavern A (see Chapter 2 for a detailed description of the site and the cavern positions). Close to the release area, at Cavern A, the snow avalanches are not yet fully developed, and the seismic station is not on the snow avalanche path. The Cavern D (Bunker) seismic sensor is placed outside the avalanche path and no avalanches flow over it. Moreover, the seismic data recorded at Bunker are not interesting for the information we are seeking.

The seismic signal of the SOV section was processed in 1 s time windows (see Subsections 3.a.v and 3.b.ii) to detect the evolution of the frequency content and to obtain information on the angle of incidence of the avalanche with the ground surface. Working on the seismic signal in time windows allows us to be more precise and detailed in its analysis. The parameter studies from the seismic signal (frequency content and particle motion) are linked with the snow avalanche behaviour and constitute key factors for the snow avalanche flow regime identification.

5.b.i. Criteria for the identification of the snow avalanche flow regime in different snow avalanche regions

For the snow avalanche flow classification, we mainly focus on the identification of dense and powder snow avalanche parts. The snow density can be related to the water content (wet/dry snow) and the snow temperature (warm/cold snow). Although the link is not straightforward, but an approximation shows that powder/cold/dry snow types have a similar seismic signature between them, as do dense/warm/wet snow types (see Chapter 1 for a detailed snow avalanche structure description). We focus on the identification of the Frontal region, the Energetic and Turbulent region (hereinafter E/T), and in the Tail region, when they are flowing over the seismic station (SOV section). Note that the E/T can only be present in Powder Snow Avalanches (PSA) (see Chapter 1 for a complete description of the internal structure of PSA).

As already mentioned, the frequency content of the seismic signals generated by an avalanche may be related to its behaviour and flow regime. The *DF-Q*, *DF-L* and *Cmean median* values (defined in Section 3.c) enable us to quantify the frequency content in each time window of the seismic signal. According to their definition, the *DF-Q* values correspond to the ground vibrations in the normal direction to the ground surface (using the "vertical" component [Q]) and the *DF-L* values for the vibrations in parallel to the ground surface direction (using the "horizontal" component in the main slope direction [L]).

In the following we present the criterion used for the interpretation of the frequency content data using the *DF-Q*, *DF-L* and *Cmean median* values (Table 5.1). All are employed to study the seismic data of the SOV section in order to identify snow avalanche flow regimes and the different avalanche regions. The frequency content values can be interpreted with the use of previous information from Pérez-Guillén (2016), applied in detail and improved with the experience acquired from the data processed in this PhD thesis.

> **DF-Q:** This parameter is mostly related to vertical changes in the snow avalanche flow. The E/T regions are characterized by vertical mass fluctuations, flow density stratifications and a considerable height of the snow avalanche flow (Sovilla et al., 2015; Pérez-Guillén et al., 2016; Sovilla et al., 2018), and can be linked to *DF-Q* values below 10Hz (purple in Figure 5.2). In the frontal regions, when only the powder fraction of the snow avalanche is flowing over the sensor, the *DF-Q* may be below 10 Hz, and tends to be between 10 and 20 Hz when the dense core of the avalanche is present. This is due to the mixture of the seismic signals generated by the powder snow and the dense snow flow (green in Figure 5.2). In the dense tails, the *DF-Q* values are mainly above 20Hz (brown in Figure 5.2).

DF-L: This parameter is mainly related to the horizontal vibrations produced by a snow avalanche, probably linked to the friction forces or lateral changes (acceleration, deceleration, etc.). Its values tend to be less consistent and difficult to link with the snow avalanche behaviour. However, the accumulation of *DF-L* values in the high frequency bands can be linked to the presence of a dense base layer in the frontal regions (green in Figure 5.2).

Cmean median: Note that the process to obtain *Cmean median* values includes information from the Q and L components, smoothed in a moving median. It provides an easy-to-calculate quality criterion tool that allows a comparison between avalanches and also between sensors (see Section 5.c for a detailed comparison). The *Cmean median* values allows the frequency content evolution for the snow avalanche classification to be identified, as a mix and reference output from *DF* values.

The *GRD* values (defined in Section 3.d) are a representation of the seismic signal particle motion in the Q-L plane, considering the direction of the ground particle motion and the linearity as a quality factor of the polarization. The *GRD* values are between $-\pi/2$ (against the ground surface) and $\pi/2$ (outside the ground surface). The zero values indicate a ground particle motion parallel to the ground surface and parallel to the flow direction of the snow avalanche. Because the *GRD* values may have a high variability, we decided to calculate the *GRD median*, regarding it as a guideline for the evolution of the *GRD* values and a criterion tool for the interpretation. In the following, we present the criterion used for the interpretation of the *GRD* and *GRD median* values (Table 5.1). All are used in the study of the SOV section seismic data and for the purpose of identifying snow avalanche flow regimes and the behaviour of different avalanche regions. The following criterion for the *GRD* value interpretation is defined by the interpretation of all the data processed in this PhD thesis and based on the experience acquired therefrom.

GRD: The positive *GRD* values (close to $+\pi/4$) are considered to be mainly related to flow dynamics from the ground surface, entrainment and accelerations in the flow velocity. The negative *GRD* values (close to $-\pi/4$) are mainly related to deposition and deceleration processes of the flow. The *GRD* values close to zero (between $+\pi/4$ and $-\pi/4$) are considered to be related to snow flowing in the main slope direction, parallel to the ground surface. The ground particle motion values with low linearity polarization values also correspond to *GRD* values close to zero (due the *GRD* calculation, see Section 3.d), being related to snow flow with constant velocity and low internal dynamics.

GRD median: The use of the moving median of the *GRD* values allows us to detect the most dominant trends. The interpretation of the *GRD median* values can be made in a similar way to the *GRD* values, except when the variability of the *GRD* values is high. With oscillations from the positive to the negative, the *GRD median* will show a main trend around zero.

The accumulation of *GRD* values on the same side of the space are more valuable than random *GRD* values on all the different sides. The continuity of the *GRD* values with persistent values as the snow avalanche advances are very useful for the flow regime interpretations.

With the use of the *DF-Q* and *GRD* values, different flow regimes of the snow avalanche when flowing over the sensor can be identified (Table 5.1). The *DF-L*, *Cmean median* and *GRD median* are valuable in a joint interpretation with *DF-Q* and *GRD* values. The identified flow regimes may be present on different parts of the snow avalanche flowing at the same time over the seismic sensor (e.g.: dense core with powder snow avalanche part on top), identified from the seismic signal using the *DF-Q* and *GRD* values. The combination of flow regimes can be linked to different snow avalanche regions: Front, E/T and Tail (see Chapter 1 for a detailed snow avalanche structure description) (Table 5.1).

Table 5.1 - The values used for the interpretation of the frequency content evolution (*DF-Q*), and particle motion evolution (*GRD*) at the SOV section, used as a tool for flow regime identification and avalanche region classification. The *DF-L*, *Cmean median* and *GRD median* values can be interpreted using the same criterion for *DF-Q* and *GRD* values.

Criterion		Flow regime		Avalanche region	
DF-Q *DF-L* *Cmean median*	> 10 Hz	Dense		Tail	Front
	< 10 Hz	Powder		Front	E/T

GRD *GRD median*	+	Acceleration	Entrainment	Front	E/T
	0	Constant Velocity	No entrainment	E/T	Tail
	-	Deceleration	Deposition	Tail	

The different limits on *DF*, *Cmean median* and *GRD* values are not strict and have some margins on their values (Figure 5.2). On the data interpretation for the flow regime and snow avalanche region identification, the accumulation of values along contiguous time windows is more valuable than individual values. The SOV section frequency content and particle motion values are represented in time series to perform the interpretations and correlation between them and to identify correlated tendencies in all values.
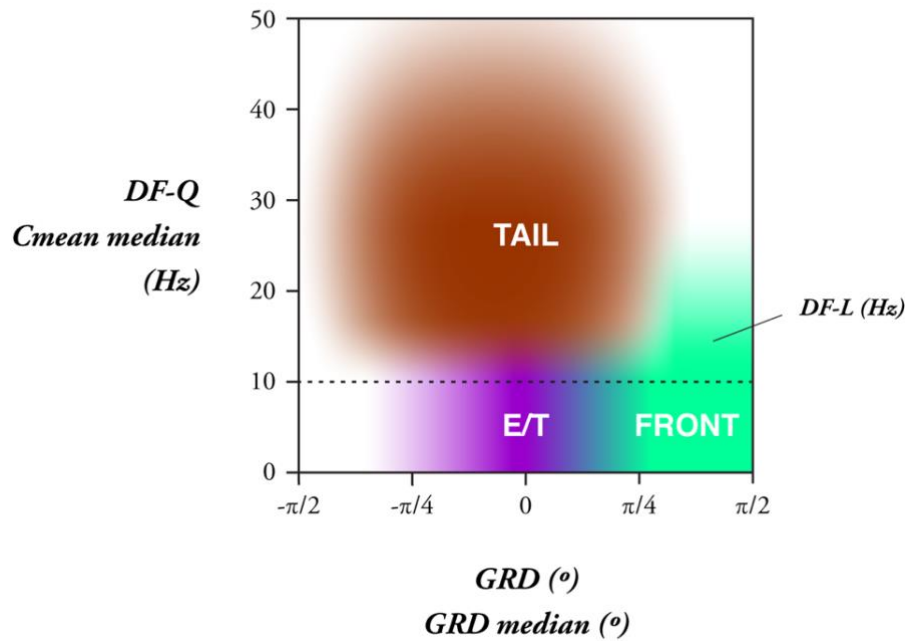
Figure 5.2 - Snow avalanche region classification with the use of the frequency content information (*DF-Q*, *Cmean median*) in Hz on the vertical axis, and the particle motion information (*GRD* and *GRD median*) on the horizontal axis. The brown colours indicate the Tail region, the green colour indicates the Frontal region, and the purple colour indicates the Energetic and Turbulent region (E/T). The *DF-L* values are mostly valuable on frontal regions, high frequency content (>10Hz), related with the presence of a dense basal layer.

Moreover, values outside the main tendencies can also be identified, and are probably related to other seismic generators (e.g., secondary fronts, collisions between snow avalanche parts or abrupt topographic changes). These detailed interpretations are not considered in the general flow regime classification, being less relevant for the flow regime identification and snow avalanche part classification.

Working on seismic data recorded on Cavern B and Cavern C seismic stations, the processing steps are as follows: a) identify if the snow avalanche flows over the seismic sensor -criterion based on *At* threshold values (Figure 5.3a); b) isolate the seismic section corresponding to the SOV section -criterion based on *At* values (Figure 5.3b); c) process the SOV section seismic signal in 1 s time windows -10% overlap. For every time window seismic signal, we perform the calculation of the *DF*, *Cmean* and *GRD* values, and when all the SOV section is computed we calculate the *Cmean median* and the *GRD median* using 5 samples (n) moving median (Figure 5.3c). In Subsection 3.d.ii the detailed methodology with all the necessary calculations of the frequency content and ground particle motion is presented.

After processing all the SOV section seismic signal, the parameters obtained can be studied using the criterion defined in this chapter and considering its evolution in time. By extension, the *DF-Q* and *GRD* values evaluation becomes a good tool to identify the flow behaviour and the snow avalanche regions flowing over the seismic sensor (SOV section).
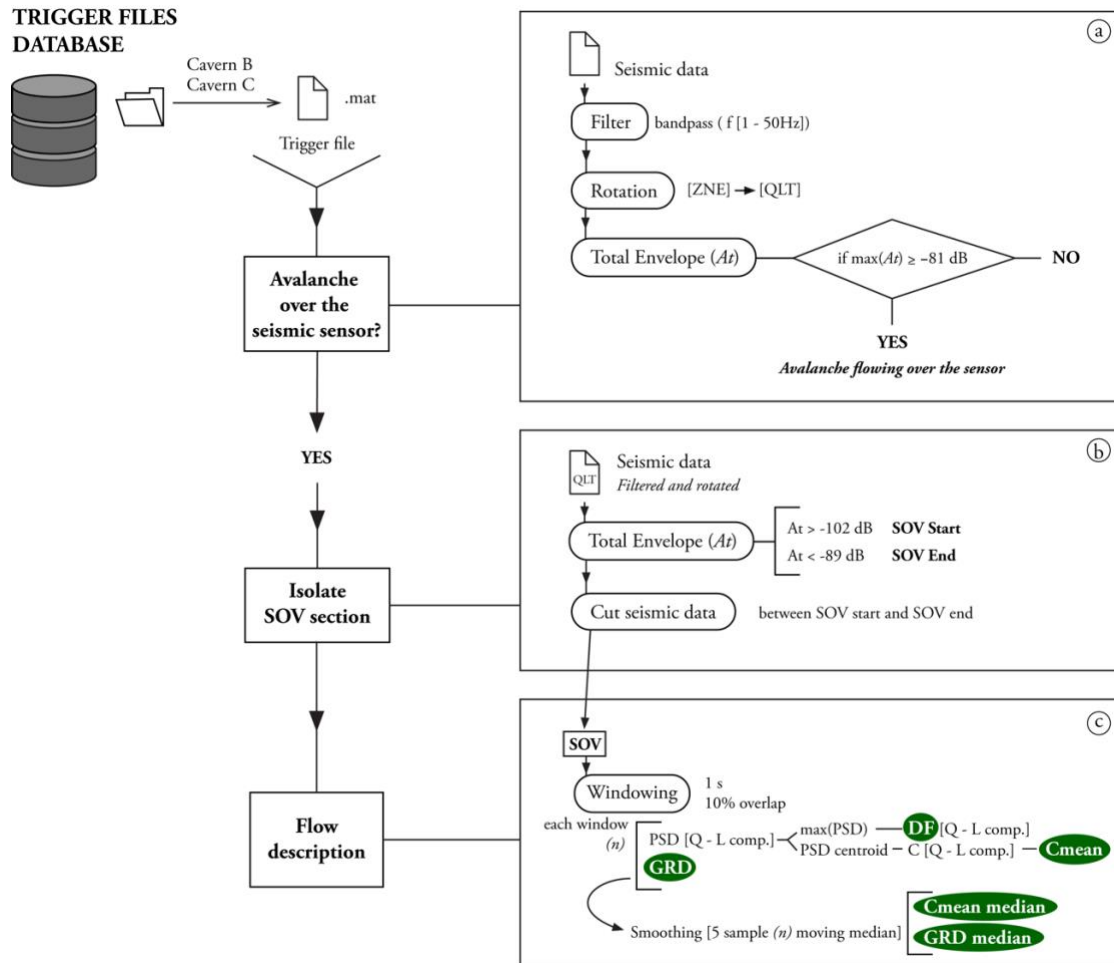
Figure 5.3 - Seismic data process algorithm to perform the snow avalanche flow description with the use of seismic data from Cavern B and Cavern C seismic stations. The steps of the seismic data process are: (a) identification of whether the snow avalanche flows over the seismic sensor or not. If so, (b) isolation of the SOV section (Signal Over the seismic sensor) and (c) application on the SOV section of the method designed for the description of the flow based on the frequency content and the evaluation of the movement of particles. The main outputs are indicated in green. Find a detailed explanation of every step in Chapter 3.

5.b.ii. Flow regimes and avalanche region characterization of a powder snow avalanche (PSA)

Snow avalanche #15-0017 was released on February 3rd, 2015, at 10:45 UTC, from the CB1 area in VDLS (see Figure 2.2 in Section 2.a for a VDLS map) (Köhler et al., 2016). The snow avalanche was triggered using explosives, the second avalanche being released during the experiment day. Avalanche #15-0017 descended along Channel 1 and stopped close to the bottom of the valley flowing over Cavern B and Cavern C. The initial mass released was not especially large, but the snow entrainment along the avalanche path increased the size of the avalanche, which became a large Powder Snow Avalanche (PSA) and fully developed (SLF classification and Köhler et al., 2016). The avalanche flowed over the deposits of a previous avalanche (#15-0016) that was released the same day from the Pra Roua region (Pérez-Guillén et al., 2016, Sovilla et al., 2018).

The GEODAR MTI plot (McElwaine & Köhler et al., 2017) indicates that the avalanche had fully developed structures in the major surge, with the powder cloud in the front followed by the energetic and turbulent region and the dense core (Köhler et al., 2016). Figure 5.4 shows the GEODAR MTI (McElwaine & Köhler et al., 2017) in (a) and in (b) and (c) the spectrograms of the Q component seismic data recorded at Caverns B and C during snow avalanche #15-0017. In the MTI plot we can mainly identify two surges, labelled as Main surge and Last surge in Figure 5.4a. The main surge had a velocity between 35 to 40 m/s for all the descending path (in blue), which can be linked to the existence of a constant flow regime along the path with no transition. It can be identified as a large Powder Snow Avalanche (PSA) because of the high velocity. Furthermore, this snow avalanche had a large tail and reached the *La Sionne* river (MTI range 100 m). We focus on the two snow avalanche surges at the Cavern B and C positions for the correlation with the seismic data. The arrival times of the main surge (36.5s at Cavern B and 56s at Cavern C) (Figure 5.4a, #1 and #2), and the last surge (58s at Cavern B and 82s at Cavern C) (Figure 5.4a, #3 and #4) are also observed at the same times in the seismic data spectrograms (Figure 5.4b and Figure 5.4c). The main surge reached the *La Sionne* river (range 100 m) at 72 s. At 80 s on the MTI plot, we can identify the abrupt stopping shock of the avalanche and some backward stopping shock close to the Cavern C position (Figure 5.4a, #5).

The seismic section identification is performed on the basis of the seismic data, which are identified using the *At* values criterion. The SOV sections deduced from the seismic signal are also indicated on the MTI plot (Figure 5.4). At Cavern B, the SOV section begins at the same time that the main surge reaches the seismic station position and ends at the same time that the more intense red colours on the MTI plot fade out (Figure 5.4b). At Cavern C, the SOV section begins before the main surge reaches the seismic station position (Figure 5.4c). This is because the powder front generates seismic vibrations (included in the SOV section) that the GEODAR data are unable to detect (Köhler et al., 2016).

The different snow avalanche regions of this large PSA avalanche were developed at successive times and can be recognized in the seismic time series using the frequency content and the particle motion information. Moreover, the different velocities of the different snow avalanche regions cause a greater separation between them as the snow avalanche progresses down the slope.

The parameters obtained from the analysis of the SOV section of Cavern B are presented in Figure 5.5. The maximum *At* value observed is -67.4 dB at 41 s (Figure 5.5a). The *DF* and *Cmean median* values are between 20 to 30 Hz from the start of the SOV section until 42s. (Figure 5.5b). This time window is the same where the *GRD median* values are positive, between zero and $\pi/4$, and the *GRD* values are disperse (Figure 5.5c). All these values can be interpreted in the sense that this part of the signal corresponds to the frontal region of the main surge (FRONT1 in Figure 5.5d). The dispersion in the *GRD* values can be interpreted as the result of a collision process between the snow avalanche front and the snow cover. In relation to the MTI plot (Figure 5.4a), the main surge arrives at Cavern B at 36.5s, at the start of the frontal region recognized with the seismic signal. From these we can deduce that the maximum *At* values are linked to the passage of the maximum flow height

and/or the more energetic parts (more seismic amplitude), described as the start of the E/T region (E/T1 in Figure 5.5d).

Figure 5.4 - Data from snow avalanche #15-0017. a) The GEODAR MTI plot from McElwaine & Köhler et al. (2017). b) & c) The spectrogram of the seismic data (Q component) recorded at Cavern B and C. On the GEODAR MTI plot are indicated the relative position of the seismic stations, the arrival time of the main surge (#1, #2) and the last surge (#3, #4) at the Cavern positions, and the stop at the Cavern C position (#5). Also, the SON section duration deduced from seismic signal indicated on the MTI plot and on the seismic signal spectrograms.

Frequencies below 10 Hz can be recognized in the seismic signal after 42 s and until 52 s (Figure 5.5b). The *DF-Q* values are stable close to 4 Hz. On the other hand, the *DF-L* values remain above 40 Hz. This may be due to the presence of a dense basal body that generates a high frequency, producing resonances in the terrain because of the presence of changes in the topography in this gully part (Cavern B position, see Chapter 2). In this interval (42-52 s) the *Cmean median* values remain close to 20 Hz. The *GRD median* values

remain between zero and $+\pi/4$, and the *GRD* values are stable, close to the *GRD median* values (Figure 5.5c). These values can be interpreted in the sense that part of the signal corresponds to the passage of the energetic and turbulent region (E/T1 in Figure 5.5d) with the exception of the 46-47 s time window where the frequency content of Q component suddenly increases. This increase in frequency can be interpreted as being caused by the arrival of an internal surge and/or the presence of a large dense body (INT. in Figure 5.5d).

A sudden change in the *DF-Q* is observed after 52 s. The values become higher than 30 Hz and the *DF-L* values around 20 Hz (Figure 5.5b), with the result that the *Cmean median* values remain close to 30 Hz, which is a slightly higher value than in the previous snow avalanche region. The *GRD* values tend to be closer to zero than in the previous snow avalanche regions (Figure 5.5c). We link these values to the existence of a constant velocity flow, parallel to the ground surface without entrainment or deposition of snow. This part of the signal can be interpreted as corresponding to a Tail region (TAIL1 in Figure 5.5d). However, few *GRD* values at approx. 55s are close to $-\pi/4$, which is not reflected in the *GRD median* values. At this time no special changes are recognized in the *DF* and *Cmean median* values. These characteristics could correspond to the seismic signal generated by the frontal region of the last surge of the snow avalanche arriving at Cavern B (FRONT2 in Figure 5.5d) that overlaps the signal of the first Tail region. The same frequency content as the first frontal region (above 10 Hz) and the *GRD* values outside the *GRD median* tends support this assertion. At 58.5s, after the frontal region, a one-time window with *DF-Q* value below 10 Hz (Figure 5.5b) coinciding with a maximum peak of *At* values (*At* = -84.2 dB) can be recognized (Figure 5.5a). These values can be interpreted in the sense that this part of the signal corresponds to the pass of a short energetic and turbulent region (E/T2 in Figure 5.5d). This sequence is similar to that observed in the previous surge. However, the E/T2 region is shorter in this surge than in the first one. This may be due to the last surge arriving at the Cavern B position when the tail of the main surge is still flowing over Cavern B. The E/T2 region of the second surge is followed by a signal with a high frequency content and *GRD* values close to zero, which can be identified as the tail of the last surge (TAIL2 in Figure 5.5d). The negative *GRD* values can be linked to the collision between the last surge and the main surge tail. The comparative low amplitude of the signal indicates that the second tail could be close to Cavern B, but not strictly over it.

Figure 5.5 - Synthesis of the parameters obtained from the SOV section seismic data recorded at the Cavern B seismic station. Snow avalanche #15-0017. a) Total Envelope, indicating the Main surge and Last surge *At* values; b) *DF* values (red) for the Q (squares) and L (asterisk) components and *Cmean median* values (blue); c) *GRD* values (black dots) and *GRD median* values (pink). d) Interpretation of the snow avalanche regions from the combination of all output parameters: light green for the frontal regions, purple for the energetic and turbulent regions and brown for the tail regions. The INT corresponds to the arrival of an internal surge or the presence of a large dense body

At Cavern C, the situation is different than at Cavern B, because this cavern is placed in the runout area. At that point, the snow avalanche is more developed, and the different regions are more separated in time because of the relative velocity between them. Moreover, it is important to notice that the main obstacles for the snow avalanche measurements managed by the SLF Avalanche Dynamic team are placed at Cavern C area. The Mast is placed 60 m in up-slope direction from Cavern C seismic station (see Chapter 2 for a detailed description of the VDLS site instrumentation location). The interaction of the avalanche front with the Mast produces ground vibrations (not strictly linked to the snow avalanche dynamics) that can be recorded by the seismic station. Part of these vibrations have frequencies lower than 1 Hz due to the mast oscillation transferred to the ground (recorded

in Lennartz Broadband sensor, see Chapter 2). To eliminate this effect, frequencies lower than 1 Hz are filtered from the seismic data (see Chapter 3 for a detailed filtering routine).

The frequency content of the signal (*DF* and *Cmean median* values) and the particle motion values (*GRD*) can be used with the same criterion for the identification of the different snow avalanche parts. The maximum *At* value (-80.9 dB) is at 59 s (Figure 5.6a). The SOV section at Cavern C begins at 48.5 s, before the passage of the main surge recognized from the MTI plot (Figure 5.4a). The *DF-Q* and *DF-L* have similar values and the component parallel to the ground surface (L) is not affected by the resonances due to the topography (as in Cavern B). The frequency content varies from below 10 Hz between 48.5 and 56 s to over 20 Hz between 56 and 60 s (Figure 5.6b). The *Cmean median* values also follow this tendency. The Cavern C site has a topography with an open and constant slope with no potential lateral topographic collisions (see Chapter 2 for a detailed site description). In brief, the *DF-Q* and *DF-L* values are similar and the *Cmean median* values follow the same evolution. The *GRD* values, before the maximum *At* values, from 48.5 to 60 s are more variable, ranging from values below $-\pi/4$ to values above $+\pi/4$. However, the *GRD median* values are positive (Figure 5.6c). All these observations can be interpreted as the seismic signature generated by the frontal region of the snow avalanche (FRONT1 in Figure 5.6d).

The *DF-Q* values between 61 and 63 s, and between 66 and 70 s, are close to 4 Hz (Figure 5.6b) and the *GRD* values become more stable with positive values close to zero like the *GRD median* (Figure 5.6c). These values agree with those of the seismic signal of an E/T region flowing over the seismic station (E/T1 in Figure 5.6d). The *DF-L* values remain high, around 20Hz. The difference in values between the component parallel to the ground surface (L) and the component orthogonal to the ground surface (Q) can be explained by the existence of more vertical fluctuations produced by an energetic and turbulent region (E/T1 in Figure 5.6d). Between 63-66 s, the frequency content of Q component increases and remains over 10 Hz, close to *DF-L* and *Cmean median* values. This increase in frequency corresponds to the same internal and/or the presence of a large dense body identified at Cavern B (INT. in Figure 5.6d).

The *DF* values between 70 and 76 s are higher than 10 Hz, and the *Cmean median* values are between 20 and 30 Hz (Figure 5.4b and Figure 5.4c). These values agree with those of a seismic signal generated by a dense flow behaviour. The *GRD* values remain stable around zero, indicating a constant flow velocity. The values obtained in this part agree with those of a seismic signal generated by a tail region, prior to the second surge arrival at Cavern C (TAIL2 in Figure 5.6d). This interpretation agrees with that of the MTI plot (Figure 5.4a).

After 80 s, the *DF* and *Cmean median* values stay at a relatively high frequency (closer to 10 Hz), and the *GRD* values become less stable (Figure 5.6b and Figure 5.6c). This time corresponds to the snow avalanche front reaching the bottom of the *La Sionne* river valley and the main front stopping suddenly at 80s, as deduced from the MTI plot (Figure 5.4a). Although these changes in the main avalanche front did not occur above the seismic station, since the vibration produced is more energetic than the vibration of the tail flowing over the sensor, the seismic information may overlap, being mixed and confusing. The arrival of the last surge can be recognized in the *At* values at 82.5 s (*At* = -93.4 dB) approximately,

although this surge cannot be clearly described (FRONT2 and TAIL2 in Figure 5.6d, dashed lines).

Figure 5.6 - Synthesis of the parameters obtained from the SOV section seismic data recorded at the Cavern C seismic station. Snow avalanche #15-0017. a) Total Envelope, indicating the Main surge and Last surge *At* values; b) *DF* values (red) for the Q (squares) and L (stars) components and *Cmean median* values (blue); c) *GRD* and *GRD median* value *GRD* values (black dots) and *GRD median* values (pink). d) Interpretation of the snow avalanche regions from the combination of all output parameters: light green for the frontal regions, purple for the energetic and turbulent regions and brown for the tail regions. The INT corresponds to the arrival of an internal surge or the presence of a large dense body.

It is important to note that the *DF* values throughout the SOV section remained mainly below the *Cmean median* values. This could be interpreted as an indication of a high presence of a powder fraction. Although a dense basal layer exists that generates a high frequency content, the presence of the powder region generates a lower frequency content that makes the *DF* values lower. This is interesting to compare with the signal in the runout area (Cavern C) in the following snow avalanche examples (Subsections 5.b.iii and 5.b.iv).

5.b.iii. Flow regime and avalanche region characterization of a transitional avalanche

Snow avalanche #13-3019 was released on February 1st, 2013, at 16:15 UTC from the CB1 area (find a VDLS map in Figure 2.2 in Section 2.a). It was a spontaneous avalanche recorded by the automatic activation of the trigger system at VDLS. The avalanche was recognized as a fully transitional snow avalanche, starting as a cold-dry Powder Snow Avalanche (PSA) until reaching 1720 m.a.s.l. (GEODAR range 900 m) between Cavern B and Cavern C (Figure 5.7a, McElwaine & Köhler et al., 2017). At this altitude the snow cover became wet because of the rain, and the snow avalanche changed to full warm-wet in all the runout area (Wet Snow Avalanche - WSA) (Köhler & Fischer et al., 2018). Two main surges were recognized at the beginning of the snow avalanche. Both surges had high frontal velocities related to a cold-dry behaviour, 30-35 m/s measured with GEODAR. However, Doppler Radar measurements give velocities of 50-60 m/s (Köhler & Fischer et al., 2018) (blue and green lines, Figure 5.7a). After leaving the gully part (GEODAR range 900 m), the avalanche was warm-dense with slower velocities and more cohesion in the snow, ending with snow debris deposits (Köhler & Fischer et al., 2018) (blue line, Figure 5.7a).

Figure 5.5 shows in (a) the GEODAR MTI plot (McElwaine & Köhler et al., 2017) and in (b) and (c) the spectrograms of the Q component seismic data of this snow avalanche (#13-3019) recorded at Caverns B and C. Since it was a spontaneous avalanche, the automatic triggering system at VDLS activated the recording systems (*t0*, t=0 s) when the snow avalanche had already started. On the MTI plot we can observe the two fronts released during this snow avalanche: in green the first surge and in blue the main surge (Figure 5.7a #1 and #2). We assume that the second surge is the main and largest one because it presents the largest runout. Both surges had a very similar velocity, close to 37 m/s at Cavern B, at the beginning of the snow avalanche flow (0-50 s), as deduced from MTI plot (Figure 5.7a #1 and #2). At 940 m range, after the transition of the flow to a more warm-wet snow, the main front velocity drastically reduced to 2.5 m/s (Figure 5.7a, #3). At Cavern C small surges inside the main surge can be recognized (dotted blue line, Figure 5.7a #4). The intensity of the GEODAR signal is also more powerful at the Cavern C position (more intense red colours), indicating a higher response of the GEODAR from the dense avalanche parts. In the spectrogram of the seismic signal at Cavern B, two surges (#1 and #2) are identified in the region with greater amplitude (Figure 5.7b). The start of the SOV section at Cavern B, at 21.5 s, agrees with the arrival of the first surge detected on the MTI plot, considering that it has a powder behaviour. The end of the SOV is at 86 s, although it is not identified on the MTI plot. These values were obtained from the *At* values (shown later in this chapter). Note that the end of the flow at the Cavern B position on the MTI plot (#5 in Figure 5.7a) agrees with the end of the high frequency content of the seismic signal in the spectrogram (#5 in Figure 5.7b). In the spectrogram of the Cavern C seismic signal, only the main surge (#3 in Figure 5.7c) is identified. The small surges inside the main surge, identified as #4 on the MTI plot, are not visible in the spectrogram (Figure 5.7a and Figure 5.7c). The SOV section at the Cavern C spectrogram starts at 118 s, before the arrival of the main surge identified on the MTI plot. The end of the SOV section, at 278 s, coincides with the stopping phase identified on the MTI plot (#6), just at the Cavern C position. Other stopping phases closer to the Cavern C position are identified in the spectrogram (#7 in Figure 5.7a and Figure 5.7c).
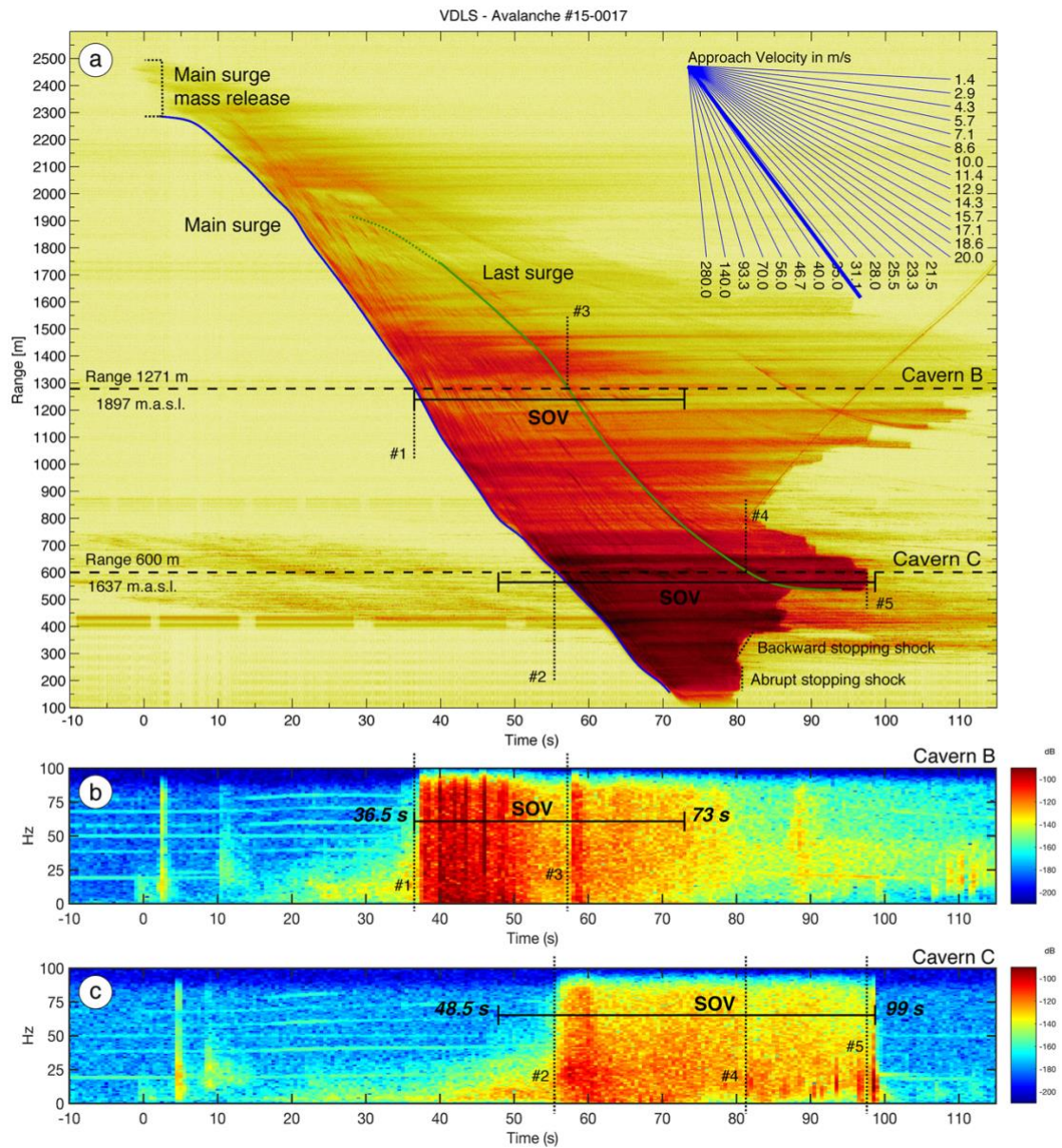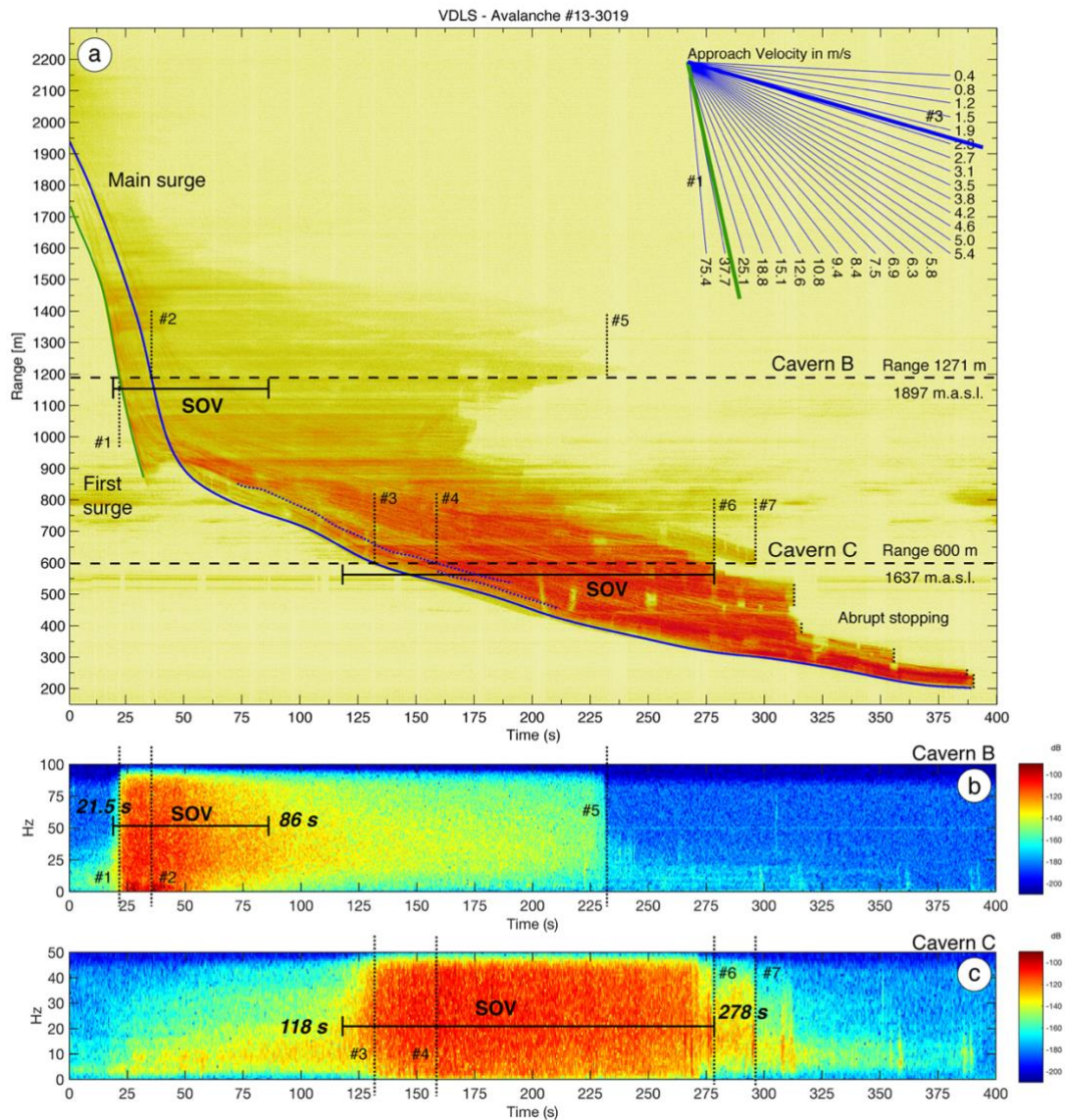
Figure 5.7 - Data from snow avalanche #13-3019. a) The GEODAR MTI plot from McElwaine & Köhler et al. (2017). b) & c) The spectrogram of the seismic data (Q component) recorded at Caverns B and C. At the GEODAR MTI and seismic spectrogram plots, the relative position of the seismic stations, the arrival time of the first surge (#1) and the main surge (#2, #3) at the Caverns position are indicated. The internal surge (#4), the endo of the flow at Cavern B (#5) and the stopping at Cavern C position (#6 and #7) are also indicated. The duration of the SON section deduced from seismic signal is indicated on the MTI plot and also in the seismic signal spectrograms.

Using the *At* values, the two previously mentioned surges observed in the spectrogram SOV section of Cavern B can be clearly recognized. They present very similar maximum *At* values: -80.6 dB the first surge at 27 s and -79.3 dB the main surge at 37 s (Figure 5.8a).

The frequency content information allows us to identify the snow avalanche frontal region and the energetic and turbulent flow region for both surges (Figure 5.8b). The *DF-Q* values remain close to 20 Hz for the first 3s (21-24 s; first surge frontal region; FRONT1 in Figure 5.8d) falling to values below 10 Hz between 24 and 30 s (energetic and turbulent region of the first surge; E/T1 in Figure 5.8d). The *DF-Q* values rise above 20Hz between 30 and 34 s (main surge frontal region; FRONT2 in Figure 5.8d) and drop to values below

10 Hz between 34 and 43 s (energetic and turbulent region of the second surge; ET/2 in Figure 5.8d). The *DF-L* values are not as high as in the previous avalanche (#15-0017) but are above the *Cmean median* values with some exceptions close to *DF-Q* in the energetic and turbulent regions (Figure 5.8b). These values suggest a lack of a dense layer in the frontal and turbulent (E/T) regions of this snow avalanche. In this interval, the *GRD* values remain stable positive and close to zero (around $+\pi/18$), suggesting a dynamic of passing over the snow cover with some entrainment (Figure 5.8c). From 43 s up to the end of the SOV section, the *DF-Q* and *DF-L* values are above 20 Hz (with some specific exceptions) and the *Cmean median* values remain stable around 30 Hz. The *GRD* values are positive, close to zero, although with more fluctuations (Figure 5.8c). The values obtained indicate that this part of the seismic signal was generated by a tail region (TAIL in Figure 5.8d). Only two *GRD* values are negative (at 48s and at 51s), coincident with the moment when the front of the avalanche reaches 1720 m.a.s.l. (range 940m) and starts the transition from cold-dry to warm-wet flow regime, with the implicit decrease in the front snow avalanche velocity (GEODAR MTI plot in Figure 5.7a).

The snow avalanche structure recognized at Cavern B agrees perfectly with a Powder Snow Avalanche behaviour (PSA), with the front followed by the E/T region and ending with the dense tail. In this case, two fronts can be recognized, with an identical seismic signature in the frequency content and seismic particle motion. Moreover, the description of all the snow avalanche flow regime behaviour is very clear. All these observations agree with the description of a total PSA behaviour at the Cavern B position, which transitions to a Wet Snow Avalanche (WSA) behaviour in the runout area, as obtained from the MTI plot.

At the runout area, when the snow avalanche reached Cavern C, the flow regime had already totally changed to a warm-wet behaviour. The SOV section at Cavern C seismic data starts at 118 s and is longer (160 s) than at Cavern B (64.5 s). The spectrograms in Figure 5.7b and Figure 5.7c show that the snow avalanche front reaches Cavern C (at 118 s, Figure 5.7 #3) notably later than Cavern B (at 21.5 s, Figure 5.7 #1), indicating a loss of velocity of the snow avalanche between both positions. This agrees with the existence of a warm-wet snow avalanche flow regime. The SOV section ends at 278 s (Figure 5.9a). The *At* values rise from the start of the SOV section until reaching their maximum (-80.9 dB) at 160 s. After the maximum, the *At* values remain high, slightly decreasing until the end of the SOV section (Figure 5.9a).
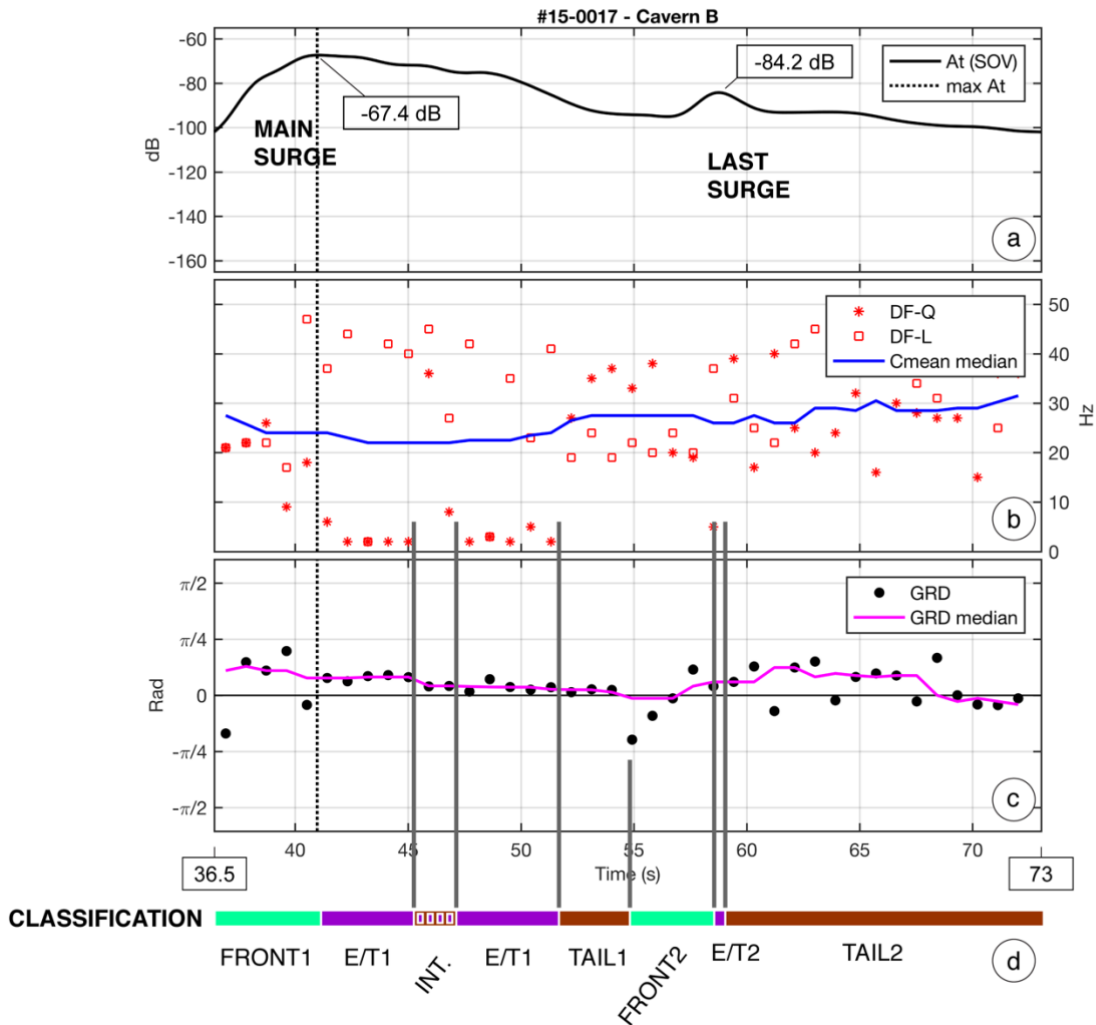
Figure 5.8 - Synthesis of the parameters obtained from the SOV section seismic data recorded at the Cavern B seismic station. Snow avalanche #13-3019. a) Total Envelope, indicating the First surge and Main surge *At* values; b) *DF* values (red) for the Q (squares) and L (asterisk) components and *Cmean median* values (blue); c) *GRD* values (black dots) and *GRD median* values (pink). d) Interpretation of the snow avalanche regions from the combination of all output parameters: light green for the frontal regions, purple for the energetic and turbulent regions and brown for the tail regions.

Of the two snow avalanche surges recognized at Cavern B, only the main surge reaches Cavern C, recognized in the SOV section seismic data. The frequency content has also a clear tendency toward high values, being between 10 to 20 Hz at the start of the SOV section and rising to more than 30 Hz (Figure 5.9b) until 138 s. These initial parts of the SOV can be identified as the frontal part of a dense snow avalanche (FRONT in Figure 5.9d), although more difficult to classify than a powder snow front. However, the remainder of the SOV section assists in the frontal region identification. After 138 s until the end of the SOV section, the *DF-Q* and *DF-L* values show a large variability, but not below 10 Hz. The *Cmean median* values remain constant in the high frequency values. All these observations are consistent with the description of the seismic signal generated by a warm-dense snow avalanche with a slow velocity (Figure 5.9d).

The *GRD* values at the beginning of the SOV section show a great variability, ranging from $-\pi/4$ to more than $+\pi/4$, with a clear dominance of positive values and a tendency to zero until 138 s. The *GRD* values in the remainder of the SOV section are more variable with no clear tendencies, but the *GRD median* remains oscillating close to zero (Figure 5.9c). These values of the particle motion describe a constant velocity flow and agree with the presence of a dense flow over the seismic station with a granular flow (due to the increase in water content, as in a warm-wet avalanche flow) and rough deposits. The observed values correspond to those of a seismic signal generated by the tail of the snow avalanche (TAIL in Figure 5.9d).
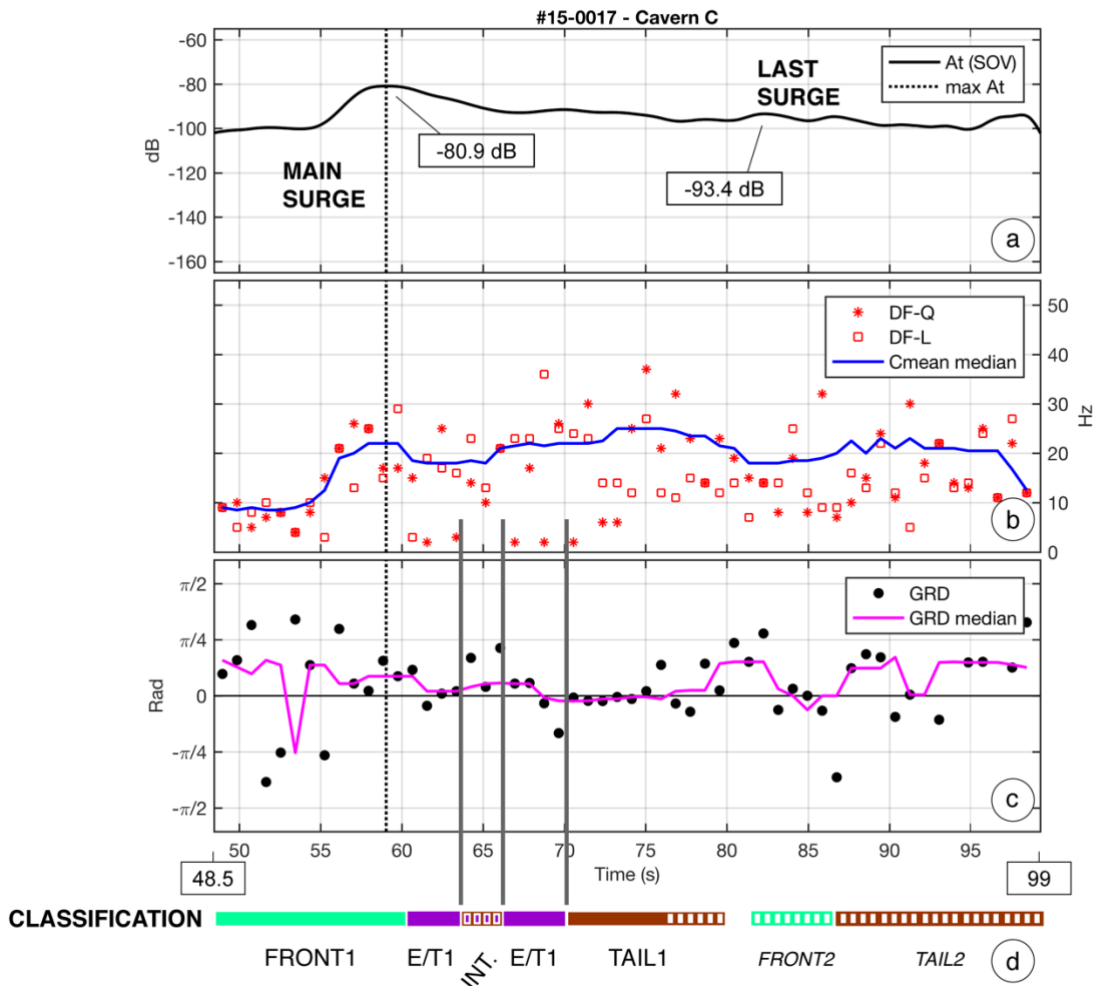

Figure 5.9 - Synthesis of the parameters obtained from the SOV section seismic data recorded at the Cavern C seismic station. Snow avalanche #13-3019. a) Total Envelope indicating the Main surge *At* values; b) *DF* values (red) for the Q (squares) and L (asterisk) components and *Cmean median* values (blue); c) *GRD* values (black dots) and *GRD median* values (pink). d) Interpretation of the snow avalanche regions from the combination of all output parameters: light green for the frontal region and brown for the tail region. Intermittent white bands because of low consistency of the data at the frontal region and to indicate stopping phase at the end of the SOV.

A change in the behaviour of all the parameters starts after 268 s. The *DF-Q*, *DF-L* and *Cmean median* values tend to decrease to values between 10 and 20 Hz and the *GRD* values increase clearly to values close to +π/4. These values agree more with the characteristics of a stopping phase seismic signal and the existence of an abrupt stopping of the mass flowing. This is very common in dense avalanches and more remarkable in the seismic data, when it occurs just above the seismic station. In Figures 5.7a and 5.7c, the stopping phase is clearly identified in the spectrograms of the seismic data and on the GEODAR MTI plot (#6 and #7 in Figure 5.7). The first stopping phase identified (#6) is at the end of the SOV section and just above the Cavern C seismic station. Other stopping phase (#7 and others not labelled) can be recognised on the GEODAR MTI plot close to Cavern C but not above it. These other abrupt stoppings can also be recognized in the spectrogram (Figure 5.7c), but with lower intensity. These are outside the SOV section and not studied herein.

Note that during the whole SOV section at the runout area (Cavern C), the *DF* values remained around the *Cmean median* values trend, in an approximate ±15 Hz range. This can be interpreted as an indication of a complete dense snow behaviour, with a total lack of powder fraction. The presence of the powder region would generate a lower frequency content that would make the *DF* values remain lower than the *Cmean median*. It is interesting to compare this SOV section in Figure 5.9b with the parameters obtained in the previous avalanche #15-0017 (Subsection 5.b.ii, Figure 5.6b), in order to detect the difference in the *DF* and *Cmean median* values caused by the presence of the powder fraction.

5.b.iv. Flow regime and avalanche region characterization of a large Mixed/PSA

Snow avalanche #17-3032 was artificially released at 08:42 UTC from the Pra Roua release area on March 8th, 2017, in the field experiment carried out in VDLS (find a VDLS map in Figure 2.2, Section 2.a). Although different measurements of physical parameters of this avalanche were obtained, unfortunately GEODAR data were not acquired due to technical issues. The avalanche was described by the SLF as one of the largest and biggest recorded at VDLS. It is classified as a mixed PSA with a large powder section followed by a huge dense tail. The avalanche descended by three main paths from the release area, but only one corresponds to Channel 1 and only two reached the Cavern C position (Figure 5.10a). The pictures in Figure 5.10a and Figure 5.10b are extracted from a video of the experiment time synched with the seismic data recorded by the SLF. The different paths can be identified in Figure 5.10a, showing the snow avalanche fronts descending by all channelled paths from the Pra Roua area, in black arrows. The snow avalanche fronts descending by Deylon channel (at the left side of VDLS Channel 1) are outside those instrumented and are not included in the study.

In the absence of GEODAR data, we relied only on the visual description and the seismic data to describe the snow avalanche behaviour and flow regime identification. Figure 5.10 corresponds to a picture of the avalanche 41 s after the VDLS trigger activation. We

can recognize the powder cloud of the snow avalanche descending by the slope between Cavern B and Cavern C. The front position is indicated with a dashed black line. It is not possible to see the flow regime of the internal parts of the snow avalanche. The picture in Figure 5.10b corresponds to t=185 s and shows the position of a dense flow at the Cavern C position (dashed line). It corresponds to a secondary front with a dense snow flow regime behaviour.
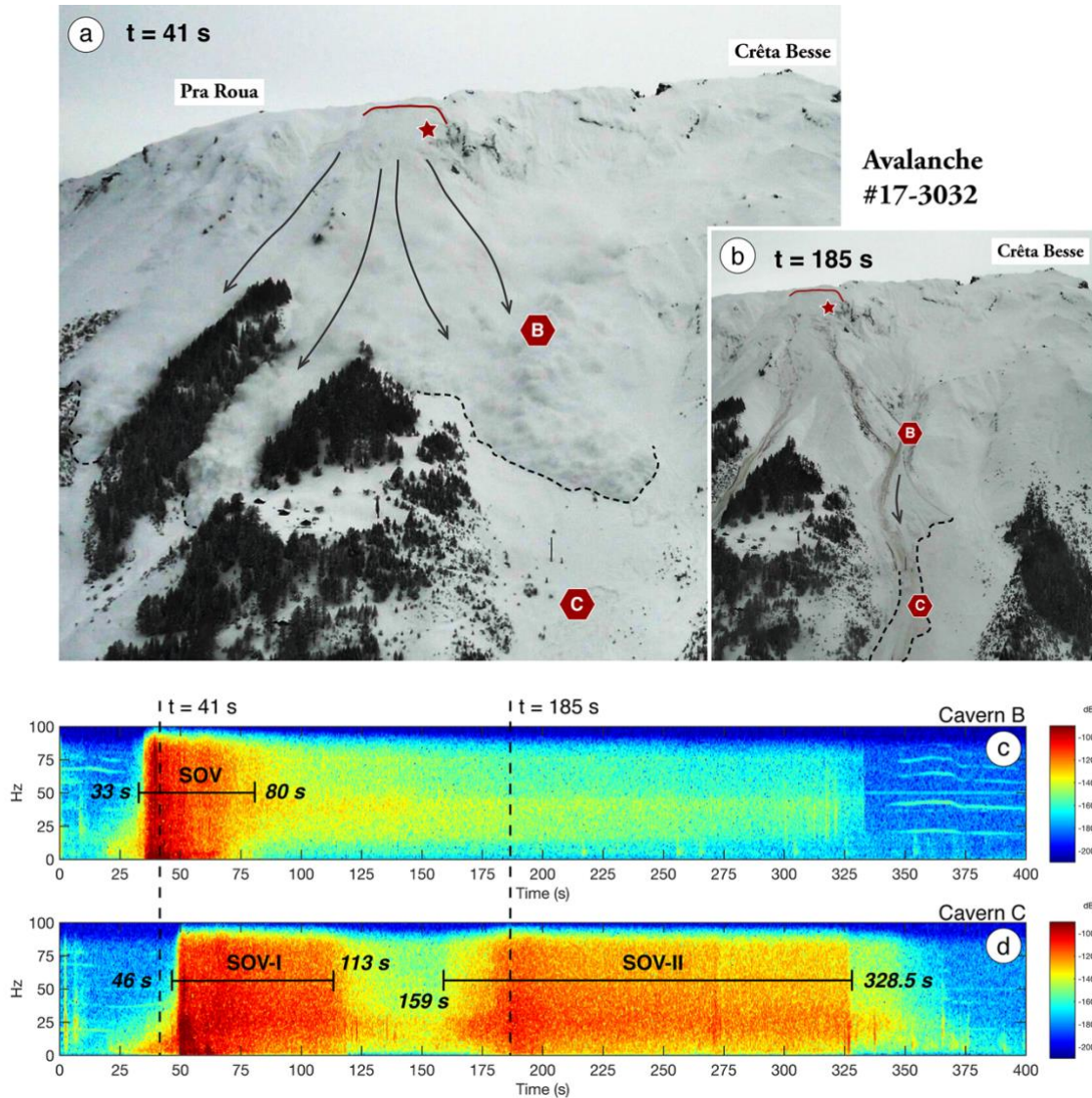
Figure 5.10 - Pictures and data of snow avalanche #17-3032. The pictures correspond to video-frames extracted from a recording of the avalanche performed by the SLF. Picture a) corresponds to the snow avalanche at 41 s from the trigger activation and picture b) at 185 s. In both pictures, the red star indicates the detonation position, the red line the release scar, the grey arrows the snow avalanche descending directions and the red hexagons the Cavern B and Cavern C positions. c) and d) are the spectrograms of the seismic data (Q component) recorded at Cavern B and Cavern C seismic stations. Indicated the pictures are a) and b) time stamps, the duration of the SOV section at Cavern B and SOV-I & SOV-II at Cavern C.

The spectrograms show that at both caverns the amplitude values are really high at the beginning of the SOV section (intense reddish colours) (Figure 5.10b and Figure 5.10c). Notice that the arrival time of the main front at the different cavern positions is short and the duration of the seismic signal produced by the snow avalanche is long. All these

perceptions agree with the description of the spectrogram of a large mixed PSA (SLF classification). On seismic data from Cavern B, only one snow avalanche front can be identified, with the SOV section starting at 33 s (identified using the *At* values, shown in further steps in this data process). Is interesting how the seismic signal recorded at Cavern B produced by the snow avalanche lasts longer than 325 s (Figure 5.10c). On the seismic data from Cavern C can be clearly identified, which can be studied as two different SOV sections: SOV-I starting at 46 s and the SOV-II starting at 159 s (Figure 5.10d).

At Cavern B, the SOV section is 47 s long [33-80 s] and the maximum *At* value (-64.9 dB) is reached at 38s, increasing from the start of the SOV section (Figure 5.11a). Between 33 s and 38 s, the frequency content replicates the observed pattern of the frontal region in a PSA: the *DF-Q* values at the beginning of the SOV section close to 10 Hz decrease to values close to 4 Hz between 33 and 38 s. This trend is also followed by the *DF-L* values and the *Cmean median* values (Figure 5.11b). The high frequency content is related to the presence of a dense basal layer and the low frequency content to the presence of a powder fraction. In the same span of time, the *GRD* values are positive close to $+\pi/4$ with a descendent tendency to zero until 38 s, which can be interpreted as being produced by an acceleration and entrainment process (Figure 5.11c). All these observations agree with the description of a frontal region starting at 38 s (FRONT in Figure 5.11d). Between 38 and 45 s, the frequency content (*DF* and *Cmean median* values) is the lowest for the whole SOV section. The *DF-Q* and *DF-L* values are constant close to 4 Hz and the *Cmean median* values close to 10 Hz (Figure 5.11b). The *GRD* values for the same time interval are positive between zero and $+\pi/4$, close to the *GRD median* (Figure 5.11c). All these observations agree with the description of the seismic signal generated by an E/T flow region (E/T in Figure 5.11d).

From 45 to 65 s, the *DF-L* values rise to above 30 Hz, while the *DF-Q* values remain in values below 10 Hz. The *Cmean median* rise to values between 20 and 30 Hz. The high frequency content of the *DF-L* indicates the presence of a dense base layer. However, the low frequency in *DF-Q* values suggests that a turbulent flow regime is still present (Figure 5.11c). The *GRD* values remain between zero and $+\pi/4$, close to the *GRD median*, with some exceptions at 51 s (*GRD* > $+\pi/4$) and 55 s (*GRD* = 0) (Figure 5.11c). Positive *GRD* values can be interpreted as acceleration in the flow and entrainment process. At 51 s, the *DF-Q* is over 10 Hz and *DF-L* over 30 Hz. This information agrees with the arrival of a minor surge at the seismic station position, also visible in the *At* values (Figure 5.11a, Figure 5.11b and Figure 5.11c). At 55 s, the *DF-Q* is above 10 Hz, but the *DF-L* is below 10 Hz, probably linked to a sudden velocity reduction of the base layer or to entrainment (Figure 5.11a, Figure 5.11b and Figure 5.11c). This part of the SOV section corresponds to a mix of an E/T flow region, with the presence of a dense basal body and internal dynamics (minor surge, acceleration and entrainment) causing variability on the *DF* and *GRD* values (E/T + DENSE BASE in Figure 5.11d).

From 65 s until the end of the SOV section at 80 s, the frequency content rises to values above 20 Hz for *DF-Q, DF-L* and the *Cmean median* (Figure 5.11b). The *GRD* values become more disperse between -$\pi/4$ and $+\pi/4$, but the *GRD median* remains oscillating

around zero, enabling it to be linked with a constant flow velocity (Figure 5.11c). All this information from the seismic signal parameters agrees with the description of a dense tail flowing over the seismic station (TAIL in Figure 5.11d).
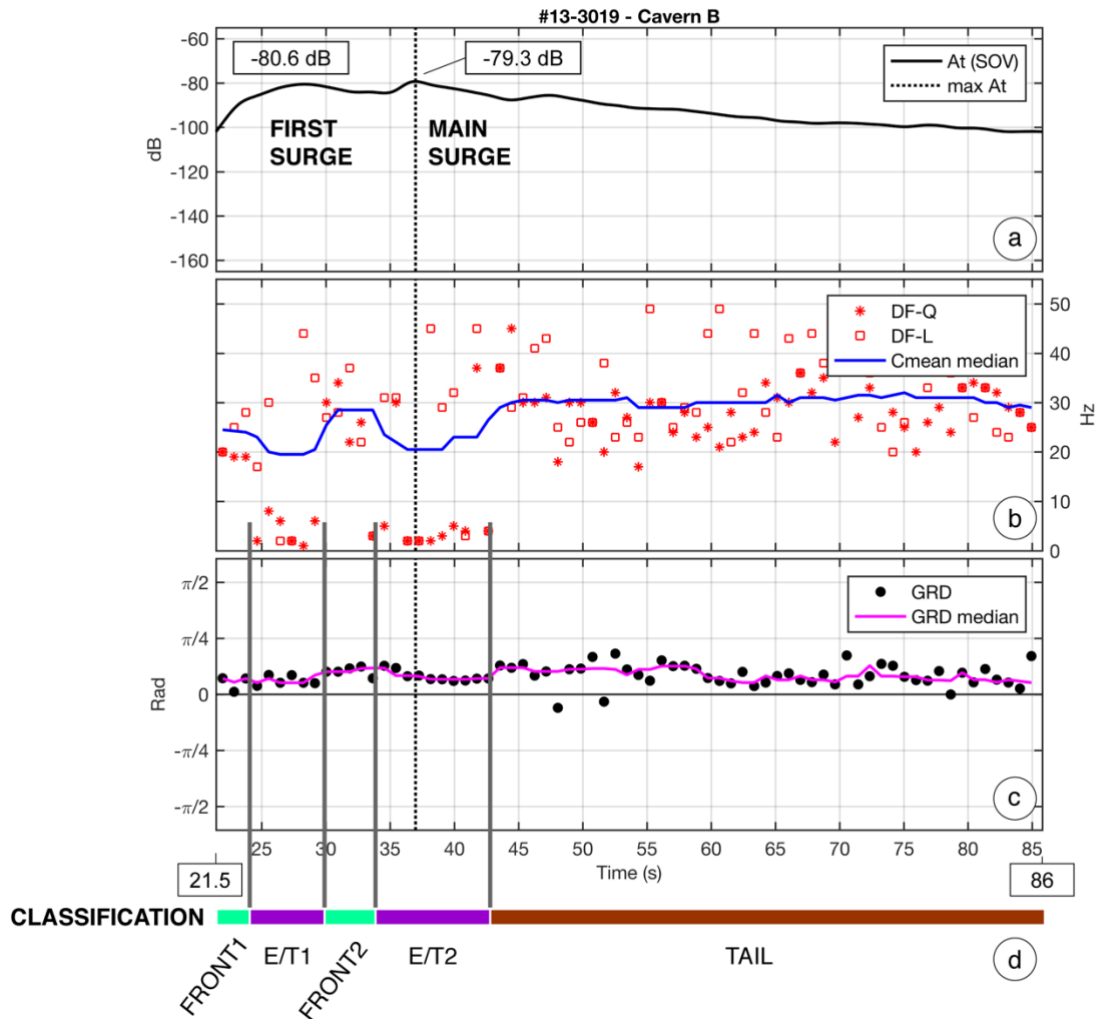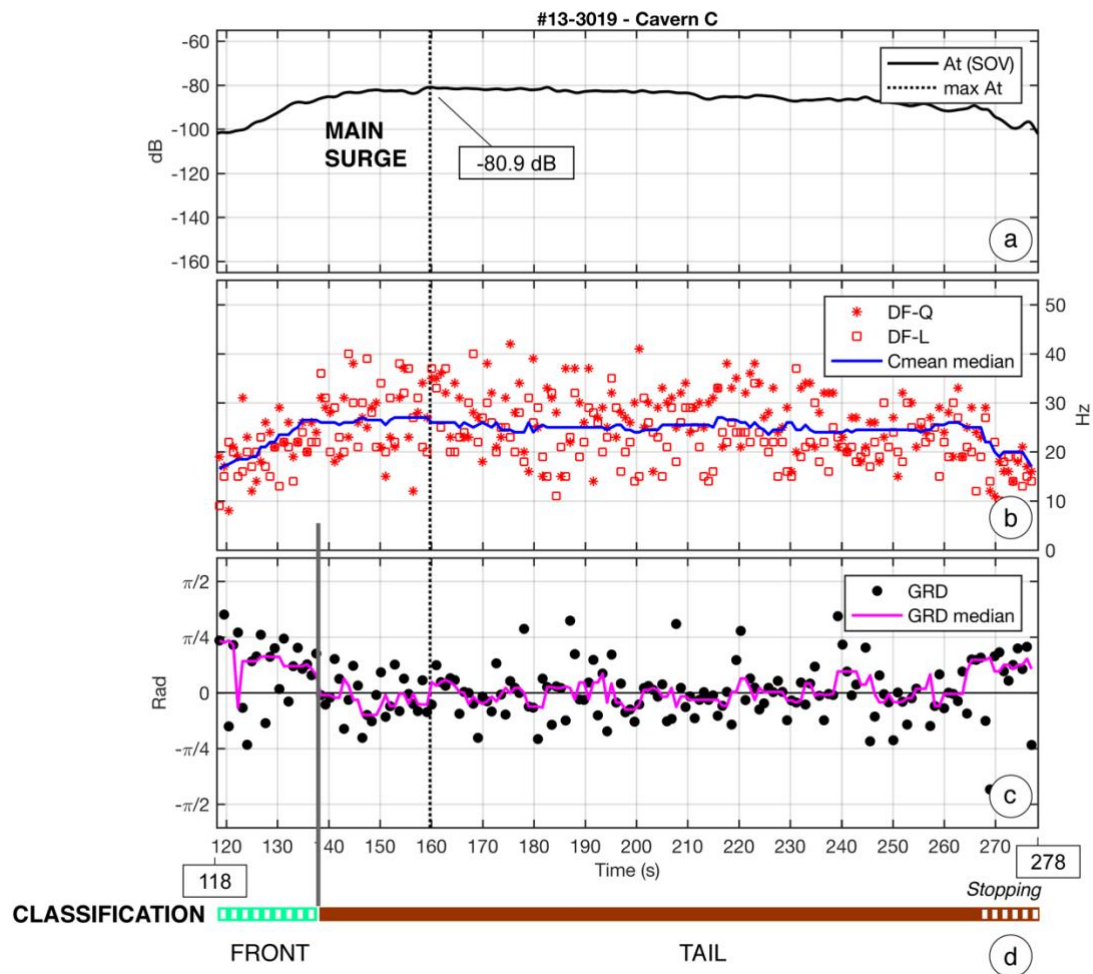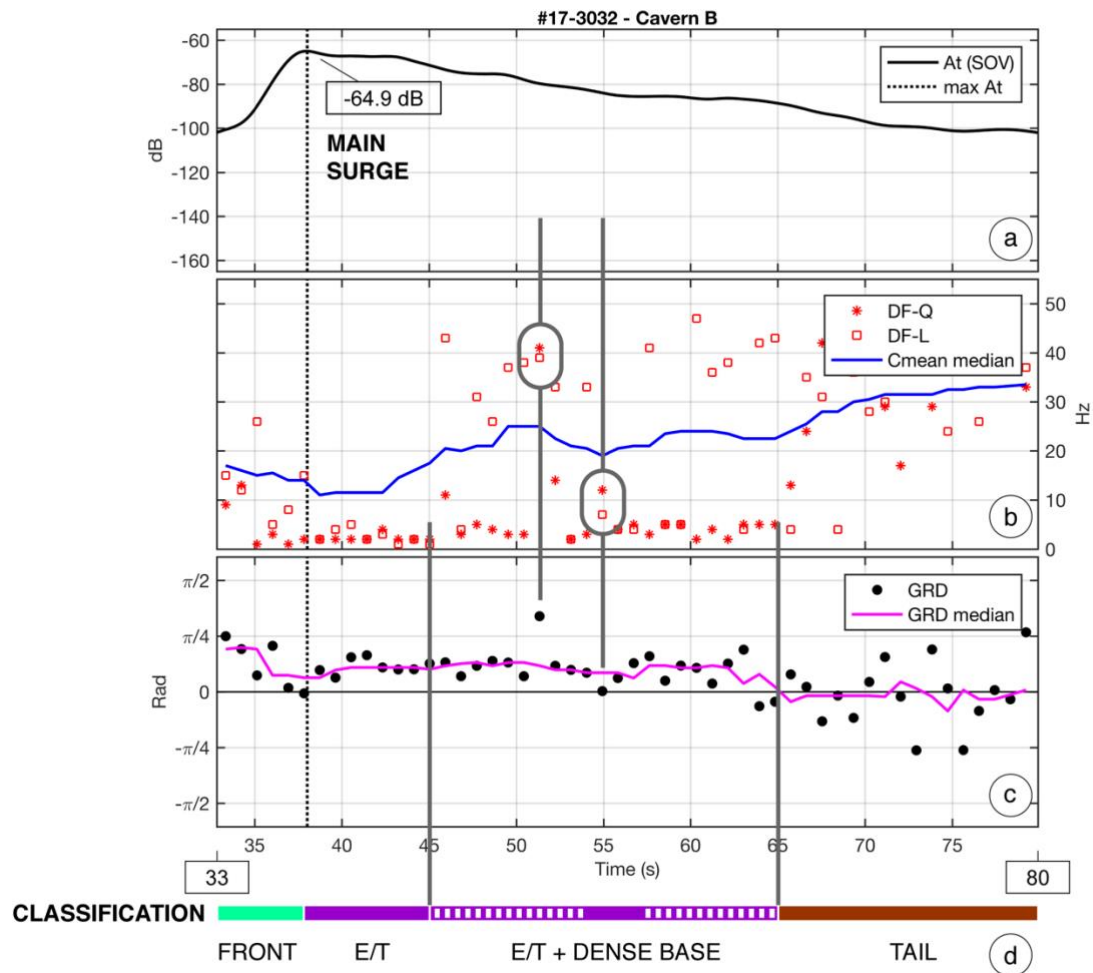

Figure 5.11 - Synthesis of the parameters obtained from the SOV section seismic data recorded at the Cavern B seismic station. Snow avalanche #17-3032. a) Total Envelope, indicating the Main surge *At* values; b) *DF* values (red) for the Q (squares) and L (asterisk) components and *Cmean median* values (blue); c) *GRD* values (black dots) and *GRD median* values (pink). d) Interpretation of the snow avalanche regions from the combination of all output parameters: light green for the frontal regions, purple for the energetic and turbulent regions and brown for the tail regions. Intermittent white bands on E/T when the dense basal layer is identified.

In the spectrogram of the Cavern C seismic data, two fronts can be clearly identified and studied as two different SOV sections (Figure 5.10d). The first avalanche front (SOV-I) corresponds to the main surge. We isolated it to the SOV-I section between 46 and 113 s, using the *At* values isolation criterion. The maximum *At* value is -58.8 dB at 51 s and is the largest *At* value obtained from all the avalanches studied in this work. It corresponds to the seismic recording starting after the picture at 41 s in Figure 5.10a. Due to the dimensions of the snow avalanche, the *At* values considered are higher than expected and the isolation criterion tool (Table 3.1 in Subsection 3.b.ii) was adjusted to perform a correct snow avalanche section identification. In this case we considered the start of the SOV-I when the

At values are higher than -87.5 dB. The end of the SOV-I is identified when the *At* values become lower than -87.5 dB. These values are evaluated from the comparison with other snow avalanches (*DF*, *Cmean median* and *GRD* values). This modification in the *At* value thresholds is exceptional, but also it is a good example to show that the thresholds are not unique and that for extreme snow avalanche sizes some adjustments must be incorporated.

From 46 to 56 s, the *DF-Q*, *DF-L* and the *Cmean median* values remain over 10 Hz (Figure 5.12b), and the *GRD* values are positive between zero and $+\pi/4$ (Figure 5.12c). All these values agree with the description of the seismic signal of a PSA frontal region (FRONT in Figure 5.12d). After that, between 56 and 63 s, the *DF-Q* and *DF-L* values decrease to frequencies close to 4 Hz and the *Cmean median* values are around 16 Hz (Figure 5.12b), describing the main presence of a powder region. The *GRD* values remain around zero and decrease to negative values between zero and $-\pi/4$. The *GRD median* follows these values (Figure 5.12c). All these observations agree with the classification of this part as the E/T region (E/T in Figure 5.12d). The negative values of *GRD* can be related to a more persistent entrainment, deacceleration processes, or to energetic collisions with the ground (or with the mast), more evident because of the dimensions of the avalanche.

From 63 s until 113 s, the *DF-Q*, *DF-L* and *Cmean median* values remain above 20 Hz (Figure 5.12b). The *GRD* values are negative, between zero and $-\pi/4$, but the *GRD median* remains around zero (Figure 5.12c). The frequency content describes the seismic signal generated by a dense flow behaviour, and the *GRD* values a constant velocity flow with some deacceleration and deposition processes. These parameters agree with those of a dense tail snow avalanche region (TAIL in Figure 5.12d).

The second surge of the snow avalanche reached the Cavern C position 46 s after the end of the SOV-I. The SOV-II started at 159 s and lasted until 328.5 s (Figure 5.13a); isolated using the *At* criterion defined in Table 3.1. The *DF-Q*, *DF-L* and *Cmean median* values remain above 10 Hz for the whole SOV-II section, and mainly above 20 Hz (Figure 5.13b), indicating that it is a signal mainly generated by a dense snow flow. The *GRD* values at the beginning of the SOV-II are close to zero oscillating from the positive to the negative, but the *GRD median* remains close to zero (Figure 5.13c), values which agree with those of a seismic signal generated by a constant velocity snow avalanche flow. The maximum *At* value is -80.7 dB at 188 s, but no difference in the frequency content and particle motion value is identified before and after the *At* maximum (only a slight frequency shift and more positive *GRD* values before the *At* max). This behaviour agrees with that of a seismic signal generated by a complete dense flow regime, with no powder fraction (DENSE TAIL in Figure 5.13d). Note that the frontal region flows over the tail of the first snow avalanche surge, deduced from the sequential occurrence of the snow avalanche descending by the same path, and indicated by no major changes on the *DF*, *Cmean median* and *GRD* values in the initial part of the SOV-II section, before the maximum *At* value (DENSE FRONT in Figure 5.13d).
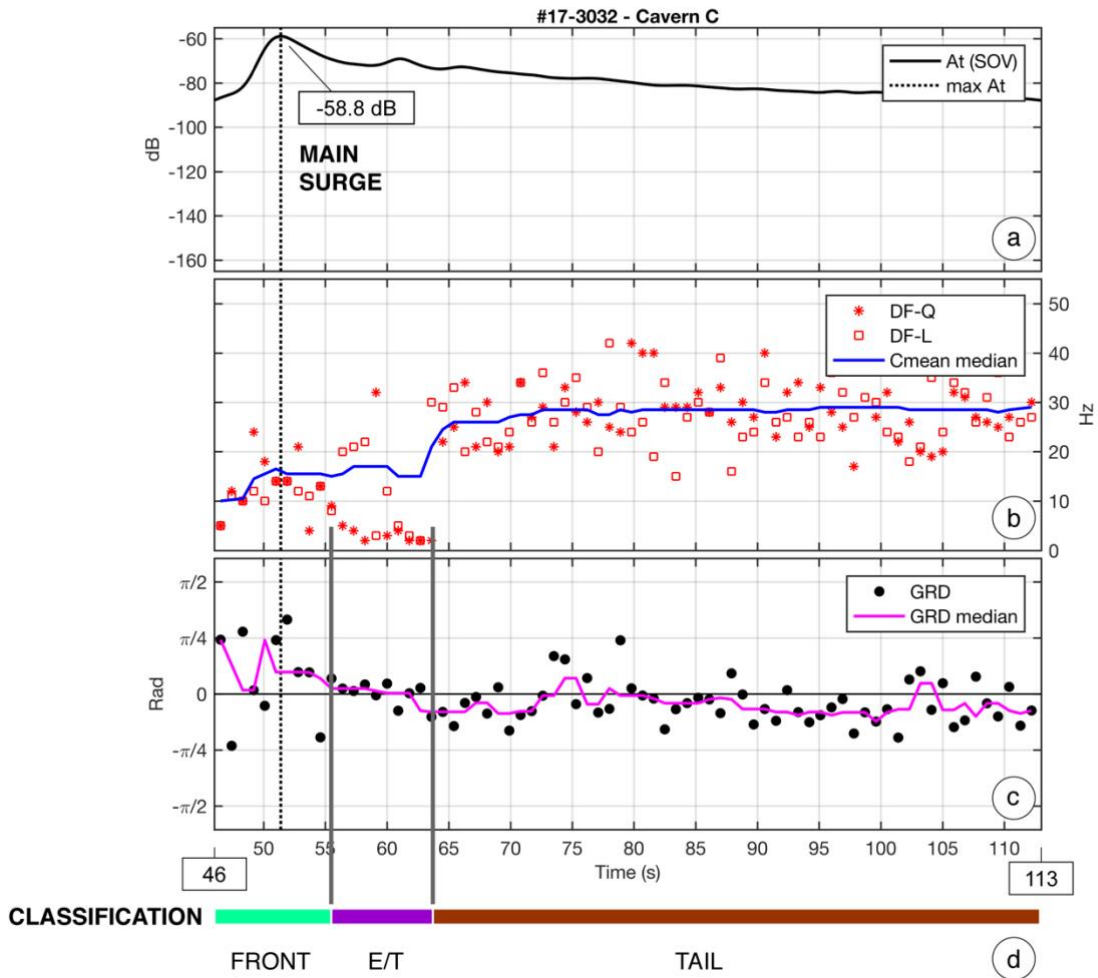
Figure 5.12 - Synthesis of the parameters obtained from the SOV-I section seismic data recorded at the Cavern C seismic station. Snow avalanche #17-3032. The isolation criterion for the SOV-I section is adapted to *At* values higher to -87.5 dB, due the extreme dimension of the snow avalanche. a) Total Envelope, indicating the Main surge *At* values; b) *DF* values (red) for the Q (squares) and L (asterisk) components and *Cmean median* values (blue); c) *GRD* values (black dots) and *GRD median* values (pink). d) Interpretation of the snow avalanche regions from the combination of all output parameters: light green for the frontal regions, purple for the energetic and turbulent regions and brown for the tail regions.

All these observations agree with the existence of a second snow avalanche surge characterized by a dense behaviour, with no powder front or turbulent region (Figure 5.13d). The changes in the *GRD* values can accommodate a deceleration process in the dense tail, with more deposition and remobilizations in the deposit (see the picture of the flow in Figure 5.10b).

136
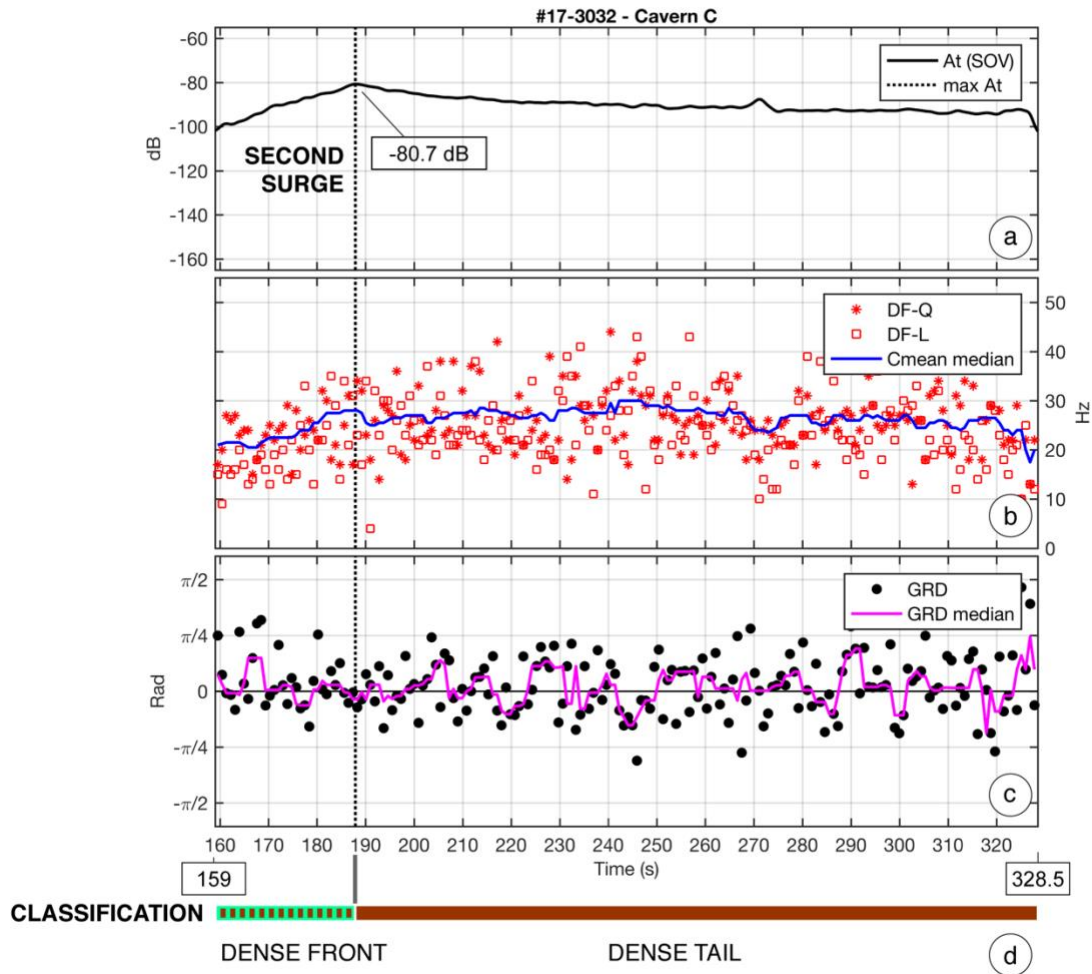
Figure 5.13 - Synthesis of the parameters obtained from the SOV-II section seismic data recorded at the Cavern C seismic station. Snow avalanche #17-3032. a) Total Envelope, indicating the Second surge maximum *At* values; b) *DF* values (red) for the Q (squares) and L (asterisk) components and *Cmean median* values (blue); c) *GRD* values (black dots) and *GRD median* values (pink). d) Interpretation of the snow avalanche regions from the combination of all output parameters: light green with brown bands for the dense frontal region and brown for the dense tail region.

5.c. Differences between seismic data information from track and runout zones for snow avalanche classification

The instrument setting and the snow avalanche path area must be considered when interpreting seismic data. The snow avalanche flow regime evolves and changes along the path. The most extreme case is the transitional avalanche, in which the flow regime changes from a totally cold snow behaviour (faster and with low density) to a totally warm snow behaviour (slower and denser) (Köhler & Fischer et al., 2018), as seen in snow avalanche #13-3019 (Subsection 5.b.iii).

The different location of the seismic stations along the avalanche path enable us to obtain data from different areas and to interpret the seismic data according to the snow

avalanche position in relation to the whole snow avalanche path. The seismic data information recorded at Cavern B and Cavern C are different because the seismic stations are located in the track area and in the runout area, respectively.

Information such as the duration of the SOV section, the *Cmean median* and *GRD median* values and its evolution along the SOV section can help us to understand the general behaviour of the avalanches and find the differences between cold/light/dry and warm/dense/wet snow avalanche behaviour. We decided to compare most of the avalanche data available and combine all the *Cmean median* and *GRD median* values of all the snow avalanches recorded at VDLS between the winter seasons 2013 and 2020.

Below we separate data from the Cavern B (Track zone) and Cavern C (Runout zone) seismic stations (find a VDLS map in Figure 2.2, Section 2.a). We take all the snow avalanche seismic data SOV sections and represent all the *Cmean median* and *GRD median* values in the same plot, for each seismic station. We are seeking a way to define a detailed classification of the snow avalanche behaviour and to identify the most common values in every snow avalanche path zone.

- **Track zone**

A total of 18 snow avalanches flowed over Cavern B, located in the Track Zone, providing enough energy to be studied. These avalanches include all flow regimes possible in the Cavern B position at VDLS.

The *Cmean median* values of the signals of all these snow avalanches for the SOV section are shown in Figure 5.14a. Note that all values are above 10 Hz. The *Cmean median* values in the initial part of the SOV section (0-15s) are in the range [10 - 35] Hz (#1 in Figure 5.14a). According to the frequency content interpretation criterion defined in Subsection 5.b.i, the *Cmean median* values closer to 10 Hz correspond to powder frontal regions, whereas the *Cmean median* values above 20 Hz are for dense frontal regions. This indicates that there are no specific predominant avalanche flow regimes in that first part of the SOV section. To help in the interpretation, we bear in mind that the presence of a dense basal layer enhances the high frequency content vibration in the L component at Cavern B. For this reason, the *Cmean median* values become higher with the presence of a dense basal layer in comparison with a pure powder snow front, which produces low frequency vibrations and lower *Cmean median* values.

After the frontal region, between 15 and 60 s, there are few avalanches with *Cmean median* values closer to 10 Hz (#2), but a large group with *Cmean median* values up to 30-35 Hz (#3) are observed (Figure 5.14a). The first group can be related to an energetic and turbulent region (E/T), more prone to producing low frequency content, whereas the second group can be related to a dense tail flow regime, more likely to produce high frequency content. In this second group, the snow avalanches with the longest SOV, lasting more than 60 s until 147 s and with *Cmean median* values around 30 Hz or higher, are observed (#4 in Figure 5.14a).

The duration of the SOV section is also an important factor to take into account, because it is related to the velocity of the avalanche front, and therefore to its flow regime. The shorter the SOV section the faster is the snow avalanche front and tail. Ideally, an avalanche with a pure powder behaviour (dry snow) without a dense basal layer or dense tail would be the fastest, with the shortest SOV section and lowest *Cmean median* values. On the other hand, a pure dense snow avalanche (wet snow) would have the longest SOV section with higher *Cmean median* values. In addition, compared to the rest of the body and the tail of the avalanche, produces a separation between the snow avalanche regions, which may increase as the snow avalanche progresses along the avalanche path.

The large snow avalanches reach the Cavern B position while still accelerating, developing all the avalanche regions and with large snow avalanche tails flowing away from Cavern B. Small avalanches can produce deposits at Cavern B, and since the frontal and body regions are short in time, the SOV section is also short. The maximum length of the SOV section measured at Cavern B is 147 s. However, most of the avalanche SOV sections at Cavern B are not longer than 60 s.

Regarding the particle motion at Cavern B, the *GRD median* values are shown in Figure 5.14b. The greatest accumulation is on the positive values, between zero and $+\pi/4$. The values at the beginning of the SOV section can be linked to the snow avalanche front flowing over the seismic station at high velocity with low interaction with the ground and/or with entrainment and incorporation of snow to the flow (#1). The major accumulation of positive *GRD median* values (#2) is between 15 and 60 s, coinciding with some negative *GRD median* values between zero and $-\pi/4$ (#3). The positive *GRD median* values can be linked to acceleration and entrainment. The negative *GRD median* values can be interpreted as snow avalanches producing deposition in this time interval. The end of the SOV sections in the same interval supports this interpretation (Figure 5.14b).

For SOV sections larger than 60 s, the *GRD median* values are always positive but with lower values than the frontal region (not over $+\pi/8$) (#4). These values can be related to the large avalanche tail still in acceleration and/or with entrainment produced by the dense basal layer (Figure 5.14b). Values closer to zero are related to seismic particle motion parallel to the slope direction and can be related to snow avalanche flowing over the seismic station in constant velocity (no acceleration, no entrainment and no deposition) (Figure 5.14b).
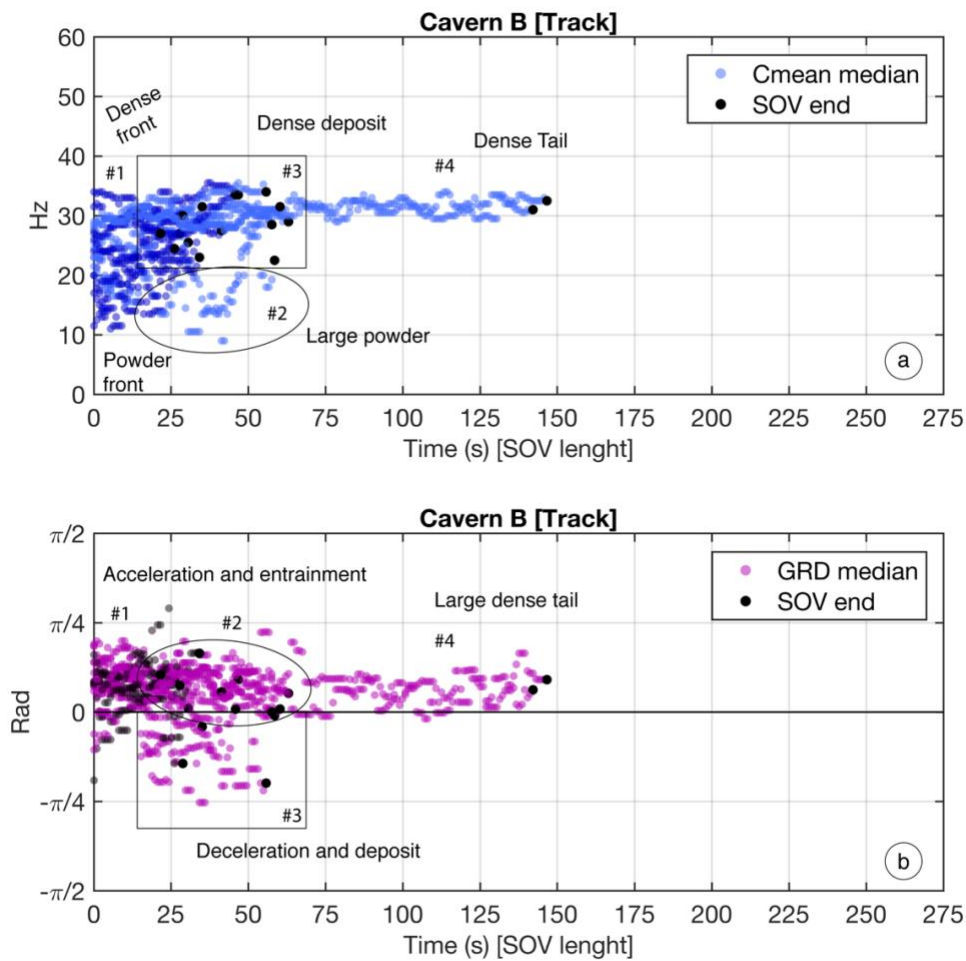
Figure 5.14 - Data from 18 snow avalanches SOV section at Cavern B (Track Zone). a) *Cmean median* values in blue (in Hz) and b) *GRD median* values in purple (in Rad). Colour intensity related to value accumulation. The black dots indicate the end of the SOV sections, related to their maximum duration (time axis corresponding to SOV length). Numeration indicates the interpretation of the snow avalanche regions and flow behaviour.

- **Runout zone**

A total of 17 snow avalanches flowed over Cavern C with enough energy to be studied. In Figure 5.15a, the calculated *Cmean median* values are shown. In the first 4 s of the SOV section, all the snow avalanches have *Cmean median* values lower than 10 Hz, except two, which have *Cmean median* values above 15 Hz (#1 in Figure 5.15a). These low frequency *Cmean median* values can be interpreted as the presence of a powder front separated from its basal layer. The high frequency *Cmean median* values (>15 Hz) can be related to a frontal region with the presence of a dense basal layer. In a few other cases it could be also related to an incorrect SOV section isolation;, for example, in extra-large avalanches like the #17-3032 (Subsection 5.b.iii).

Four main tendencies in the 4-50 s interval of the SOV section are detected when observing the *Cmean median* values in detail: a) remaining at low frequencies (<10 Hz) (#2),

b) rising and remaining around 10Hz for more than 50 s (#3), c) rising close to 20 Hz and falling to 10Hz (#4) and d) rising to more than 20 Hz (#4) (Figure 5.15a). The four different main tendencies in 4-50 s interval are detailed below:

a) Only two snow avalanche *Cmean median* values remain at low frequencies throughout the SOV section. These can be related to full PSAs with a low-density basal layer or to avalanches with a complete dry-cold behaviour (with no dense tail) (#2 in Figure 5.15a). It is not frequent that this type of snow avalanches reaches the runout area. These low frequency values may also be due to the effect of the collision of the snow avalanche with the Mast, resulting in ground deformation recorded on the lowest frequency range of the seismic signal.

 b) The *Cmean median* values remain in the low frequency region, but close to 10 Hz, and after 50 s tend to rise to 15-20 Hz (#3 in Figure 5.15a). We interpret these *Cmean median* values as corresponding to Large wet avalanches with a long SON duration (WSA), generating signals with a transition in low-to-high frequency content, meaning that the snow avalanche flow velocity is low.

c) The *Cmean median* values rise to more than 20 Hz and remain constant in high frequency values (#4 in Figure 5.15a). Between 25 and 50 s, some *Cmean median* values drop from close to 20 Hz to 10 Hz when the SOV section ends. We interpret these observations as corresponding to Large PSAs with the presence of a dense basal layer (high frequency content), but with a short tail.

d) Linked to SOV sections larger than 50 s, the *Cmean median* values rise to more than 20 Hz at the beginning of the SOV section. Some SOV sections stop before 50 s, which agrees with the description of PSA with a dense tail (#5 in Figure 5.15a).

After 50 s, all the *Cmean median* values are over 20 Hz (with the exception of the second group #3 with low frequency content, already mentioned) with a tendency to increase or with constant *Cmean median* values close to 30 Hz. We interpret the long duration and the *Cmean median* values (#6) linked to the presence of a dense tail flowing slowly over the seismic station. In these cases, the avalanche must be large and have enough mass for the snow flow to last more than 4 minutes (Figure 5.15a). At the end of the SOV section the *Cmean median* values tend to decrease, which is probably related to the stopping phases, as seen in the examples in this Chapter 5 (Figure 5.15a).
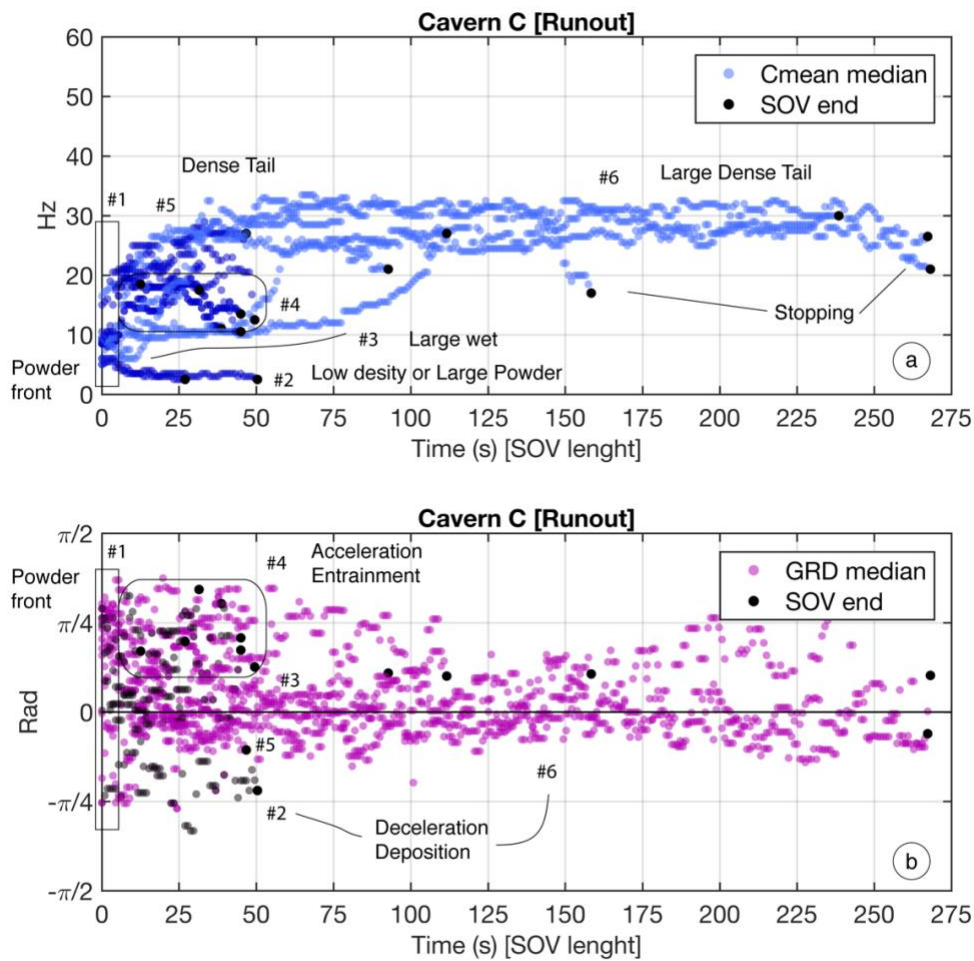
Figure 5.15 - Data from 17 snow avalanches SOV section at Cavern C (Runout Zone). a) *Cmean median* values in blue (in Hz) and b) *GRD median* values in purple (in Rad). Colour intensity related to values accumulation. The black dots indicate the end of the SOV sections, related to their maximum duration (time axis corresponding to SOV length). Numeration indicates the interpretation of the snow avalanche regions and flow behaviour.

Regarding the *GRD median* values, most of them are positive (Figure 5.15b), although there are more negative values than in Cavern B (Figure 5.15b). The dispersion of the *GRD median* values at the beginning of the SOV section is larger than in Cavern B. The *GRD median* values larger than $+\pi/4$ at the beginning of the SOV section can be interpreted as being caused by large Powder Snow Avalanches fully developed with more vertical changes in the snow avalanche front when reaching Cavern C (#1). However, they can also generate negative values due to the high velocities in the frontal region. After the frontal region, from 4 to 55 s, the negative *GRD median* values would be related to deacceleration and deposition processes (#2), and the positive *GRD median* values to acceleration and entrainment processes (#4). The accumulation of *GRD median* values around 0 is a clear sign of snow avalanche flow with constant velocity and low entrainment (#3 and #5 in Figure 5.15b).

After 55 s, the large accumulation of negative *GRD median* values, close to zero, indicates the flowing of a dense tail over the sensor, generating a noisy particle motion

142

and/or a parallel to the flow direction particle motion, related to more deposition than entrainment and to deceleration processes (#6 in Figure 5.15b).

At Cavern C, the snow avalanches with longer tails may have a more internal dynamic, including deposition and collisions between the different snow layers, arrivals of secondary snow avalanche surges, other fronts, etc. The *GRD median* values of the last part of the longest SOV sections (175-250 s) show *GRD median* values around $+\pi/4$, probably related to the aforementioned dynamical snow avalanche phenomena. We interpret the negative *GRD median* values, still present and dominant, to the presence of a dense tail and a velocity loss (Figure 5.15b). This corresponds to the most common behaviour at the end of the SOV sections in the runout area.

The same criterion for the SOV section duration, and for the *Cmean median* and *GRD median* values used at Cavern B, can also be used at Cavern C for the snow avalanche identification and the deduction of the flow regime. Moreover, the combination of the information obtained from the Cavern B and Cavern C signals for the same avalanche is a key factor for obtaining an in-depth description of snow avalanche evolution (e.g., transitional avalanches).

5.d. Conclusion

A valid method is presented for the characterization of snow avalanches based on the information extracted from seismic vibrations produced by snow avalanches. We are able to identify the snow avalanche regions (front, E/T and tail) and perform detailed descriptions of the snow avalanche flow regimes when the snow avalanche flows over the seismic sensor. All these characterizations are based on the interpretation of the snow avalanche flow collisions with the ground surface, with the snow cover and/or between the snow layers. Constitute a novel approach to snow avalanche flow description.

To accomplish this objective, the seismic signal processing steps are crucial. All the methods designed make their own special contribution to the results obtained.

1. Seismic data rotation. The rotation to the QLT coordinates system allows us to better link the seismic signal to the snow avalanche flow direction. Working with the QLT components of the seismic data enables us to arrive at deeper interpretations, more closely linked to the flow position over the seismic sensor and the direction of the snow mass interactions.

2. Identification of the SOV section. The method designed for the identification of the seismic signal sections, based on the *At* values threshold, is outstanding for its simplicity and reliability.

3. Seismic signal processing in time windows. It enables us to identify changes inside the SOV section seismic signal, becoming essential for the

identification of the snow avalanche regions. It allows us to discretize the SOV section seismic signal and identify changes in its evolution.

With the frequency content information (*DF* and *Cmean*) we were able to identify in detail the evolution of the frequency content along the SOV section. We validate the previous observations on the link of the frequency content to snow avalanche density and extend its application. The fluctuation of the frequency content in the Q component shows how the Energetic and Turbulent regions (E/T) produce low frequency vibrations related to vertical flow fluctuations (only present on powder snow avalanches). Moreover, the dense Tail regions stand out with a clear dominance of the high frequency content. Differences between the seismic signal components (Q and L) show that the vertical changes in the flow (Q component) are more linked to the flow regime behaviour.

The ground particle motion information (*GRD* values) is more related to flow velocity changes and snow avalanche entrainment. It is more outstanding in the comparisons between track zone (B) and runout zone (C). Likewise, with the identification of the internal dynamic of the snow avalanche flow, an idea of the flow behaviour is given for its classification. The *GRD* values alone are usually insufficient for the snow avalanche flow description, but the correlation with the frequency content completes the possible interpretations and becomes a powerful tool for snow avalanche flow regime characterization.

Thanks to the spatial distribution of the seismic sensors at the VDLS test site, we were able to perform the same studies at different stages of the snow avalanche along its path. Differences in the parameters extracted from the seismic signal between Cavern B and Cavern C allowed us to identify the snow avalanche behaviour in the snow avalanche track zone (B) and runout zone (C) and link them to its flow regime.

The presented herein requires a detailed supervision in order to provide better descriptions of snow avalanche flow. But despite its limitations, the utility of all the proposed methods is proved. They can be used for the snow avalanche description throughout its passage over the seismic station position (seismic data SOV section). We consider that further steps in this direction can provide information on the friction coefficients, snow cohesion and snow avalanche entrainment.

Chapter 6

Discussion

The results presented in this PhD thesis are aimed at solving two different approaches to snow avalanche characterization with the use of the seismic data: the release area identification and the flow regime characterization. The homogenization of the seismic data generated by snow avalanches and the database created become an indispensable step for the seismic data interpretation. All parts of the seismic data process are designed to obviate the need for assistance in processing, seeking the ability to automate the procedures. Part of the methods designed are common in seismic signal data treatment (e.g., seismic sections isolation, windowing) and in ground particle motions studies, but adapted here to the information we find in each part of the snow avalanche (e.g., back-azimuth values in the SON section, incidence values in the SOV section).

This chapter is dedicated to discussing the application of all the seismic data processing methodologies used in this PhD thesis and to show its strengths and weaknesses for snow avalanche seismic studies.

6.a. Benefits and limitations of homogenizing seismic data for snow avalanche studies

The main seismic data representations used by the UB-RISKNAT Avalanche research Group are the seismograms, the spectrograms and the envelopes of the seismic signal transformed to ground velocity (m/s). These are used as reference plots for further analysis and a means of checking the information available on the seismic signal. Since they began in the early 90's, these data representations have become common in all seismic snow avalanche studies, but the values of the representation scales, filtering and spectrogram configuration are not all the same; for example, the window length and amplitude scale values are not the same (Biescas et al., 2003; Vilajosana et al., 2007b; Pérez-Guillén et al., 2016; Suriñach et al., 2020). Although the values were chosen for a detailed representation of each study, this does not help when comparing between data of different seasons and seismic stations, and it is not easy to perform visual interpretations -snow avalanche descriptions- from the seismic data.

Seeking to establish a standard representation of the seismic data, I defined a common criterion to homogenize the data processing, from its acquisition until its representation and classification, for the creation of the database. Everything is carried out with the expertise of the UB-RISKNAT Avalanche Research Group. As a result, all the data are stored in an easy-to-access database with common representation parameters. The raw seismic data files (in counts) are transformed into ground motion (m/s), corrected for offset and detrend (usual steps in seismic signal processing), and time synchronized between the different seismic stations (to obtain a common base time). The time zero ($t0$) corresponds to the time of the VDLS trigger activation. However, the records contain 60 s before $t0$, as the pre-trigger signal which is very useful for the release area identification procedure. We decided not to alter the seismic signal with filtering in the trigger files database in order to preserve all the information available.

The seismic data are stored in ground motion units (m/s) and together with all contextual information for its analysis (sampling rate, pre-trigger duration seismic situation and geophone transformation function). Moreover, the data from every seismic station are stored together with their representation in seismograms and spectrograms for every component [ZNE]. The seismograms of the vertical components [Z] are joined in a common data plot for the comparison between seismic stations in order to achieve a complete data visualization in a single image. The spectrogram representations are in a logarithmic colour scale, and their amplitude representation is locked between [-210 -90] dB. With these values, the colour scale for all spectrograms is the same, and the comparison between seismic stations and between snow avalanches data becomes easier. In this way, the first data visualization allows us to perform straightforward interpretations as well as helping us to decide if the data are suitable for the studies we plan to perform. Furthermore, considering the amplitude values in dB, it enables us to visually identify the approximate snow avalanche runout distance (if it reached the Cavern B or Cavern C position), the approximated snow avalanche size and if the snow avalanche flowed over the seismic stations or not.

The seismic data homogenization method is applied automatically over all the seismic data trigger files at VDLS (winter seasons 2012-2013 until 2019-2020). When the seismic data processing is conducted manually, only the largest snow avalanches are normally processed, as fully described by the SLF. The automatization of the steps for the seismic data transformation and its homogenization allowed us to build a complete seismic database in which all seismic data from VDLS trigger activations (Trigger files database) were processed. With this automatization we are able to visualize all seismic data and to identify small snow avalanches, spontaneous snow avalanches and also other seismic sources that activate the trigger system. As result of the database automatization, more snow avalanches can be recognized, thus providing more data and consequently the tests of the release area identification method and flow regime identification can be performed over a larger number of cases.

The seismic data process and its automatization must be revised and adapted to the seismic sensor configuration (sampling rate, seismic sensor used, seismic DAS used, trigger file duration, pre-trigger duration, etc.) for each new winter season at the VDLS site (or at any other site) to avoid wrong ground motion values.

6.b. Contribution to seismic data processing methods for snow avalanche studies

Different seismological techniques were adopted in the seismic data processing to obtain information that can lead us to the identification of the release and the identification of the flow regime. These techniques are not new, but their application enabled us to extract deeper information from the seismic signal.

6.b.i. The use of 1 s seismic signal windowing

The application of time windows to the seismic signal (windowing) gave us greater precision in the studies of seismic signals. The application of windowing to the seismic signal is usual in the calculation of the spectrogram representations. However, it should be taken into account that the information contained in the seismic signal frequency content and ground particle motion polarization values is conditioned by the duration of the seismic signal time window and by the overlap between time windows. Longer time windows give more low-frequency range (due to the Nyquist-Shannon theorem, see Subsection 3.a.v) but the precision is lost in the evolution of the seismic signal. With shorter time windows the low frequency range is lost, and artifacts can appear in the high frequency content, but more precision is gained in the information of the seismic signal evolution. That is why it is necessary to establish a compromise between the durations.

Given the frequency range of the seismic signal produced by a snow avalanche, time windows 1 s long are the perfect duration to prevent loss of information and to gain time resolution on the seismic signal evolution. For the back-azimuth calculations, we decided to

use a 50% of overlap of the time windows, considering it a good compromise to maintain the continuity between back-azimuth values without over-sampling it. If the overlap were greater, the particle motion would have too many parts in common between contiguous time windows, resulting in too similar polarization values. The accumulation of back-azimuth values will determine the weighted mean of all the back-azimuth values for the whole SON section (*BAZ* value, see Subsection 3.d.i). If the overlap were less than 50%, or no overlap is considered, part of the information of the particle motion would be lost. As an extreme example, ground vibrations related to the start of the snow avalanche could be spread in contiguous time windows, resulting in two consecutive time windows with back-azimuth information, although incomplete, pointing to wrong directions not related to the release area.

We decided to use an 80% overlap of the 1 s time windows for the flow characterization. We have considered a greater overlap than in the back-azimuth calculation in order to achieve better continuity between the values of the contiguous time windows. For the flow characterization the following parameters are obtained for each time window: frequency content values (Dominant Frequency (*DF*) and Spectral Centroid (C), see Subsection 3.d.ii) and ground particle motion polarization values (*GRD*, obtained from incidence values [*in*] by linearity values [R], see Subsection 3.d.ii). Regarding the values of the particle motion polarization, in this case a shorter overlap causes large changes in the ground motion incidence angle (*in*) and *GRD* values, due to the large number of seismic sources acting at the same time over the seismic sensor. The overlap considered gives a good balance to achieve a good representation of the evolution of the *GRD* values throughout the SOV section without oversampling.

All the calculations performed on the seismic signal sections are conditioned by the precision in their identification. The seismic signal sections are related to the relative position of the snow avalanche and the seismic sensor. The definition of these sections in a snow avalanche is not new, already defined by the UB-RISKNAT for snow avalanche studies (Pérez-Guillen et al., 2016; Roig et al., 2018; Suriñach et al., 2020). However, its parametrization and identification constitute a novel approach and the basis for more in-depth studies for the identification of snow avalanches from their seismic signal.

───────

6.b.ii. The use of STA/LTA and Total Envelope (*At*) of the seismic signal

It was possible to detect the start of spontaneous avalanches from Infrasound data (Kogelnig et al., 2011), but it was not identified from the seismic signal acquired near the release area (Cavern A). In this PhD thesis, the use of data from the Cavern A seismic station is an important contribution and an advantageous approach to snow avalanche release identification. The STA/LTA triggering algorithm applied to the Cavern A seismic data appears to be the perfect option for detecting snow avalanches in near-field seismic data. The STA/LTA algorithm in combination with the automatic triggering system of VDLS (based on the amplitude threshold) enabled the precise detection of the start of the snow avalanche mass movement and highlighting it from the background noise. In addition, a finer calibration of the STA/LTA threshold allowed us to infer the source of the trigger activation and to be able to identify snow avalanches (in a near-field) from other seismic sources such as explosions or earthquakes.

The STA/LTA algorithm is a common technique in seismology, widely tested and also included as a triggering system in most of the current Data Acquisition Systems (DAS). For snow avalanche detection, it could be an interesting technique to apply it to a continuous data stream, in combination with amplitude thresholds. With an appropriate configuration it could form the basis for identifying the snow avalanche release in its very first movement, when generating the first seismic vibrations. Instead, the STA/LTA configuration is not straightforward and leads to more false positive triggers or overlooking the interesting ones if is not configured correctly. The durations of the mean amplitude that we stablished for the detection of snow avalanches is 2 s for the short average (STA) and 10 s for the large average (LTA). The ratio threshold that we consider for a trigger activation is 2.5 (STA/LTA) (see Subsection 3.a.iii). These values work well for seismic data already isolated by the activation of the VDLS trigger system. The algorithm needs adjustments and detailed testing in these values (duration of the short and long average, and threshold values) for snow avalanche detection with continuous data stream. Likewise, if it is used in other snow avalanche release sites, where an appropriate characterization of the site should be carried out.

The start of the SON section is identified using the STA/LTA algorithm, whereas the other seismic sections are identified using the Total Envelope values (*At*). The use of logarithmic values (dB) for the amplitude values of the seismic is perfect for exporting the UB-RISKNAT expertise in identifying snow avalanche seismic data based on spectrogram colour scale interpretation. The *At* values thresholds defined for the identification of the seismic signal section become unequivocal in medium to large snow avalanches. This is a key feature for the release area identification and flow characterization. The incorrect isolation of the seismic sections leads to misinterpretations on the particle motion and frequency content evolution. For this reason, it is very important to ensure the correct isolation of the seismic sections. The *At* thresholds do not work in extreme large snow avalanches, identifying the start of the SOV section before the snow avalanche is over the seismic sensor (see Subsection 5.b.iv). In avalanches that are too small, it fails to identify whether or not the flow is over the seismic sensor. These snow avalanche size limitations for the use of the *At*

thresholds are strongly related to the ground velocity vibrations. The proximity of the snow avalanche to the seismic sensors is also a limitation, due to the ground attenuation that could reduce the amplitude values. However, the method is valid for the seismic signal section isolation at the VDSL site. With a specific configuration and a testing period, this method capable of being exported to other sites.

6.b.iii. The use of 3D seismic signal rotation

The rotation of the 3D seismic data was already used in VDLS data, with the same purpose as in this PhD thesis, achieving good results in snow avalanche flow regime studies (Pérez-Guillén et al., 2016). This rotation is not necessary for the identification of the snow avalanche release area (SON section), because we prefer to have this information in the ZNE coordinate system to better link the angles obtained from the seismic signal to the topographic description of the site and the position of the seismic station. However, the rotation of the seismic data to the QLT coordinate system is very useful for the flow regime characterization on the SOV section, since it allows us to obtain a better link between the seismic data and the flow behaviour, aligning the seismic data with the main flow direction.

The direction of the +L component is chosen based on the main slope direction, assuming that this is the main direction of descent of the snow avalanche. However, not all snow avalanches take exactly the +L direction and may differ by a few degrees if the trajectory of the snow avalanche front is considered (e.g., if the snow avalanche descends Channel 2, the snow avalanche will enter the runout area facing more to the south of the VDLS test site (find a VDLS map in Figure 2.2). This is not a big issue, but it can cause some errors in seismic data studies based on the SOV section, and it is important to take them into account when performing data interpretations after the rotation to QLT coordinates (in Cavern B and Cavern C seismic data).

All the methods detailed should always be used in accordance with the position of the seismic sensors and their spatial relationship to the snow avalanche front. Likewise, for the capability of exporting these methodologies to other snow avalanche sites (experimental or not) for the detection and study of snow avalanche based on seismic data, the spatial distribution of the seismic stations in relation to the snow avalanche flow is an important decision and could determine its usability.

6.b.iv. The use of frequency content and ground particle motion time evolution

As previously pointed out, each time window of the seismic signal studies of the frequency content and ground particle motion is applied to obtain information about the source of the seismic signal (corresponding to SON or SOV section).

The frequency content information is acquired with the use of the Power Spectral Density (PSD) function, which is performed in every time window. It is only applicable for

the flow regime studies in the SOV section. The parameters for flow characterization are the following: Dominant Frequency values (*DF*) (frequency band with the largest PSD value) and Spectral Centroid (*C*) (weighted average of the spectral frequency content) acquired for every time window and for components Q and L. The *DF* values for the Q and L components (*DF-Q* and *DF-L*) for every time window are obtained, and the mean between the *C* values on the Q and L components (*Cmean*) are calculated. The evolution of these values throughout the whole SOV section is what provides more information in the interpretation.

With the identification of powder snow in movement as a source of low frequency content, and the dense snow as a source of high frequency content as reference information, we can identify trends in the *DF* and *Cmean* values, linked to the snow avalanche behaviour and its evolution. Comparison of these parameters between the different seismic signals from sensors placed at different positions along the snow avalanche path enables us to identify the avalanche characteristics and define a common criterion for their interpretation. These values become perfect for exporting in numerical information the expertise in qualitative interpretation of spectrogram data for the snow avalanche description of the UB-RISKNAT Avalanche Research Group.

The methodology for the study of the ground particle motion in 3D seismic data (V-J method, see Subsection 3.a.vi) is used for the snow avalanche flow identification and in the release area identification. The back-azimuth values (*ba*), obtained from the ground particle motion polarization over the SON section (ZNE coordinates), are used for the identification of the release area and the calculation of the *BAZ* direction. For the flow characterization, the incidence values (*in*) over the SOV section (QLT coordinates) are used for the calculation of the *GRD*. The *BAZ* value is obtained from the weighted average of all the back-azimuth values (*ba*) using their linearity (*R*) as a weight for the calculation of the mean (see Subsection 3.d.i). The *GRD* values are calculated with the multiplying the incidence angle and the linearity values (*R*) (*GRD=in·R*) for every time window, (see Subsection 3.d.ii).

The degree of linearity of the particle motion (*R*) is highly relevant, adding a numerical criterion to evaluate the polarization of the ground particle motion and weighting the *ba* or *in* values in the *BAZ* and *GRD* calculations. It is proven that the polarized ground particle motions that have a greater linearity are more relevant for describing the type of snow avalanche flow and for identifying the release area. Furthermore, the absence of a clear polarization direction is valuable information for identifying more chaotic seismic sources (e.g., dense basal layer flow).

In the calculation of *GRD* values, the information from the T component (orthogonal to the plane Q-L) is not considered. Assuming that the +L direction is in the direction of the snow avalanche flow (with some variation margin, as mentioned above), we consider that the vibrations recorded in the T component will be linked to those recorded in the other two components, and the information that can be identified from the T component is already included in the Q-L plane. Regarding the vibrations contained in the plane parallel to the slope (Q-L plane), those that are mostly in the +L component will be more related to snow avalanche velocity changes (high frequency), and the vibrations that are mostly in the Q

component, showing lower amplitudes in the L-T plane, will be more related to entrainment and deposition (see Subsection 5.b.i). The use of information from T component could be interesting when looking for lateral dynamics and changes in the snow avalanche front direction. This information is neither studied nor considered for snow avalanche flow identification.

With all the information obtained, we consider that the high utility and usability of the ground particle motion information on snow avalanche seismic data has been verified, also enhancing the usefulness of the 3D seismic stations for the study of mass movements. The goodness of the use of windowing methods is also verified, which allows us to apply the V-J method in small portions of the seismic signal and is a key piece of the seismic data processing in this PhD thesis. The use of windowing techniques opens up the opportunity to define novel approaches for the use of seismic signals for snow avalanche studies. Other mass movements and moving seismic sources can also be used in the study.

6.c. Benefits and limitations in automating the release area and flow characterization process

One of the strengths of the seismic data is the non-invasive position of the seismic stations and the ability to process the data in real time. For these reasons, all the methods presented in this PhD thesis are designed with the capability of being automated, with a view to their application to an autonomous snow avalanche identification system and/or to provide information for snow avalanche risk assessment.

With the automatic execution of the release area identification, we are able to achieve a 78% success rate (see Section 4.c). We regard it as a good starting point for its use in post-season seismic data processing. Currently, we are still testing the *BAZ* method on VDLS seismic data with the aim of obtaining information about all trigger activations and release areas of the snow avalanches (from all sizes and with multiple fronts). In the automatic execution, we found a significant limitation regarding the identification of the release areas of snow avalanches with multiple release areas. By conducting detailed studies of the seismic signal to find the SON section corresponding to the different fronts released, we can identify different fronts with the use of the *BAZ* method (as shown in avalanche #18-3066, Subsection 4.b.i). However, this detailed identification cannot be applied straightforwardly without review. The method may result in a correct value (within the region of the recognized release areas) without being linked to the snow avalanche release area, or it may only be related to one of the multiple releases. The same could happen if the background noise levels are too high (e.g., explosions, strong winds, bad weather).

The obtention of the parameters for the flow characterization *DF-Q*, *DF-L*, *Cmean* and *GRD* has been calculated automatically for all the VDLS snow avalanche data available between 2013 and 2020 (see Section 5.c). Furthermore, we performed different tests to automate the flow classification based on the presented criteria, but the classification and identification are not clear enough to be applied without supervision. The boundary

conditions and contextual information for their interpretation remain an important part of the snow avalanche flow identification and flow regime classification.

While the flow characterization method presented in this PhD thesis is not self-sufficient in the current stage of development, it can work very well as complementary data for carrying out the snow avalanche flow description (e.g., identification of the presence of a powder cloud, identification of the dense basal layer, identification of the flow transition). The flow characterization from seismic data is more valuable in detailed studies of snow avalanche behaviour than as an automatic snow avalanche classification method. As a tool for the identification of the snow avalanche parts (with different behaviours), it would constitute the basis for the quantification of the snow avalanche basal stress and friction, with further effort in the ground particle motion studies and frequency content evolution.

Given the automatization conducted, the ability to process a large amount of data, allows more in-depth studies of seismic snow avalanche data, with more results available from different seasons and different sizes and types of snow avalanches. The basis of the method is clear and simple enough to be automated using other coding languages that are easier to implement in low-power machines (e.g., Python). In addition, it can be exported to the study of other mass movements and other moving seismic sources.

- **Application to a real case**

Experiences like the Rigopiano avalanche, modelled with RAMMS and validated with the use of seismic data from regional seismic network (Braun et al., 2020) and mentioned in Chapter 1, reinforces the need to locate seismic sensors in positions close to snow avalanche sites (complementary to other snow avalanche protection systems) for snow avalanche hazard monitoring. The Rigopiano avalanche slope is a well-known avalanche trigger site, where an avalanche as large as the one that destroyed the Hotel at the end of the path was never expected. In this case, the Rigopiano avalanche was only detected a posteriori at a seismic station belonging to an earthquake monitoring system, located 17 km away. The dangerous situation of the Hotel at the bottom of the valley justifies the deployment of a seismic station in a near field for avalanche detection and monitoring as a warning system. In comparison to other geophysical measurements, the 3D seismic sensors are easy to deploy and with a low maintenance. Moreover, the information thereby acquired can be crucial in hazardous situations.

The *BAZ* method presented in this PhD thesis would provide a very good means for the detection of smaller avalanches on the site as well as a comprehensive monitoring of the occurrence of avalanches throughout the winter season. The description of the flow is not useful as an early warning system, but in future studies the complementary information from the seismic data could improve the validation of the numerical snow avalanche modelling necessary to reduce the risk of avalanches.

Furthermore, experiences such as the study of the Mt. Fuji avalanches modelled with Titan2D and recorded in seismic stations to monitor volcanic activity (Pérez-Guillén et al., 2019) reinforce and demonstrate the high interest of seismic sensors dedicated to the monitoring of snow avalanches, where the presented methods could be applied.

Chapter 7

Conclusion

This PhD thesis explores the use of seismic data for snow avalanche monitoring purposes, focusing on a full description of them from the seismic data point of view. With the novel creation of two complementary methodologies (release area identification and flow regime characterization), we are able to provide a full description of snow avalanche behaviour from its starting area until the identification of the flow regime progression along the snow avalanche path. Likewise, it constitutes a step forward in the seismic data treatment protocols for snow avalanche studies, applicable to the study of seismic data generated by other gravitational mass movements.

First of all, we have established a homogeneous protocol for the seismic data treatment of the VDLS site, thereby arriving at a standard transformation of the data to ground velocity and its representation. The processing steps are not new. The unification of all the protocols in a single automatic script, and the homogenization of the snow avalanche data representation, constitute a novelty in the management of the whole UB-RISKNAT data base and an indispensable step for the development of the rest of the investigation in this PhD thesis. Maintaining a unified classification for all seismic data with easily available access is an important step forward in the verification of snow avalanche information in the seismic data. This ensures that none of the information is lost and enables identification of the source of the trigger activations, based solely on the visualization of the seismic data (from homogeneous representations). We successfully applied the database classification to all trigger activations between seasons 2012-2013 and 2019-2020 VDLS seismic data (and still ongoing for season 2020-2021). It includes all the data files generated by trigger activation from all the seismic stations. While this protocol was specifically designed for the VDLS

seismic data collection, the scheme is also valid for application to all other seismic station deployments for gravitational mass movements studies.

As already defined, the recorded seismic signal of snow avalanches (moving sources) can be divided into different sections regarding the relative position of the source from the seismic station. While not being entirely new, we nevertheless establish a new basis for its classification by combining multiple interpretations performed by the UB-RISKNAT team. The most notable contribution concerns the identification of the total envelope (At) amplitude thresholds as a criterion for the isolation of the seismic signal sections. The method has limitations that depend on the snow avalanche size and is overly conditioned by the proximity of the sources to the seismic sensor (near field). However, it allows us to describe the results of our expertise in the interpretation of spectrograms with numerical values. Furthermore, the identification of whether or not the snow avalanche flows over the seismic sensor is a key feature for the subsequent analysis of the snow avalanche seismic signal. The seismic signal sections become the fundamental element in the rest of this PhD thesis and provide a novel criterion for snow avalanche identification.

In this sense, the determination of the start of the snow avalanche (first vibrations produced by the snow avalanche mass) is mandatory for the isolation of the first section of the seismic signal. We identify the start of the snow avalanche in the seismic signal recorded at Cavern A station by using a detailed configuration of the STA/LTA trigger algorithm. The use of common techniques employed in the study of single sources adapted for use in moving sources (such as the STA/LTA, windowing methods, PSD and particle motion polarization with the V-J method), simplifies the seismic signal processing steps and strengthens the results. All the methods have been widely tested.

The main drawbacks in the monitoring and description of snow avalanches lie in the determination of their release areas and the identification of their flow behaviour. Both are the main focus of this PhD thesis, which seeks to provide a cost-effective solution with non-invasive methods for tackling these problems and finding a solution. At the very least, our purpose is to provide information that is reliable enough to validate other measurements and contribute to the complete description of the snow avalanches from the seismic point of view.

For the identification of the snow avalanche release areas, we designed a novel method that yielded very good results in controlled interpretations. The *BAZ* method is suitable for snow avalanche release area identification and other moving seismic sources in the near field. The results of its automatic application are not as reliable as might be expected in an early warning system. Its accuracy can be improved with a supervision of the seismic signal SON section isolation process (seismic signal produced at the start of the snow avalanche movement). The use of the seismic data from Cavern A is also an important milestone, as they are 3D seismic data acquired at the seismic station closest to release areas.

On the snow avalanche flow regime and snow avalanche regions extracted from the generated seismic signal, the general information refers to frequency content studies (Biescas et al., 2003; Pérez-Guillén et al., 2016). We seek to provide more detailed information of the

frequency content evolution using windowing methods on the seismic signal to find a numerical output for the spectrogram representations. The study of the ground particle motion in the same time windows led us to identify the main mass movements as sources of the seismic signal, linked to the flow behaviour. We conclude with a classification of the flow regime based on the combination of the frequency content information and that of the ground particle motion. These outcomes respond to the main problem that we face and can be considered as the first step to quantify a) the interaction of the base of the snow avalanche with the ground, and b) the collisions of the snow avalanche front with the snow mantle. For the flow regime studies, the rotation of the 3D seismic signal in the direction of the slope is mandatory.

All results reinforce the VDLS seismic station distribution (placed on the snow avalanche path) and the high benefit of having 3D seismic data with a frequency range down to 1 Hz. Although broadband seismic data for the study of snow avalanche also seem to provide interesting information, they are not studied in this PhD thesis.

7.a. Outlook

I consider this PhD thesis as part of a project that is coming to an end, and part of a point of departure for fresh studies of snow avalanche seismic data with a newer approach. Building the database for the VDLS data constitutes an effective means of collecting all the information as a history of the work performed at the site. Furthermore, the homogenization of the seismic data represents the culmination of all the expertise acquired by the UB-RISKNAT Avalanche Research Group in the use of seismic signals for snow avalanche monitoring purposes (detection and characterization).

On the other hand, the use of the trigger system STA/LTA at Cavern A, the windowing methods, the ground particle motion polarization and detailed descriptions of the snow avalanche flow over the seismic sensor provide as a novel approach to the treatment of the seismic data for the study of the gravitational mass movements.

The STA/LTA and seismic amplitude thresholds can be configured in a continuous seismic data stream for the automatic selection of snow avalanche events. To date, the trigger activations have not differentiated the seismic sources. I believe that further work on the seismic data acquired in a position close to the snow avalanche release area (e.g., Cavern A in VDLS) will lead to the automatic identification of snow avalanche release, distinguishing between earthquakes, explosions and other sources. The methods presented in this PhD thesis are valid for their application, but further tests and detailed configuration are needed for their automation in the continuous seismic data stream.

The seismic data detected by an automatic trigger system identification as a snow avalanche release can be treated with the use of the *BAZ* method. This guarantees the identification of the release area and automatically identifies the snow avalanche occurrence. However, it is necessary to improve the system to enable multiple fronts. to be identified. Testing of the *BAZ* method at other snow avalanche sites is indispensable, with the

deployment of a seismic station close to the release area. In addition, the use of a seismic sensor with a lower frequency range may also be of interest. The sensor used at Cavern A is a short period with a 2 Hz eigenfrequency. The difference of the information of the seismic data obtained with a 1 Hz eigenfrequency sensor will probably not be noticeable, but it might be interesting to test the use of a broadband seismic sensor to search for information at lower frequencies. However, we consider that the first vibrations of the snow avalanche are above 2 Hz, and there should be little low frequency information related to the snow avalanche first mass movements.

Regarding the characterization of the flow regime, I consider there is still much work to be done. The evolution of the flow is already very well described using physical measurements by invasive methods (e.g., pressure sensors, velocity sensors, …) and non-invasive methods (e.g., GEODAR, thermography videos, …). However, the internal dynamics of the snow avalanche has not been measured but has only been deduced from other observations (such as velocity changes or density fluctuations). Furthermore, the interaction of the snow avalanche body with the snow cover can be identified but not quantified from direct measurements. The seismic signal generated by the snow avalanche when it flows over the seismic sensor and measured therein, is one of the measurements most closely linked to the internal dynamics of the snow avalanche and the interaction of the snow avalanche body with the snow mantle. Moreover, the measurement is non-intrusive and does not alter the flow. The parameters $DF\text{-}Q$, $DF\text{-}L$, $Cmean$ and GRD are a valuable information for identifying snow avalanche behaviour. More detailed analysis and comparisons with other measurements will lead us to a better understanding of the internal dynamics of snow avalanches.

All the presented methods are robust enough to be exported to other snow avalanche sites. It may be of interest to deploy seismic stations in other mountain areas to detect snow avalanches in different conditions, with the application of the methods presented in this PhD thesis. Increasing the database of snow avalanche seismic data is mandatory for validating the methods presented, testing it in different conditions and, by extension, achieving greater precision in snow avalanche monitoring.

In addition, the release identification and flow identification methods are also easy to apply when studying other moving seismic sources, such as landslides or lahars. Detailed configurations of these seismic methods could also lead to a better understanding of other gravitational mass movements, and to a creation of more precise early warning systems. A deeper understanding of all the hazardous phenomena is the key to a better risk assessment. The seismic signal is our main tool and I trust in its utility for tackling these problems.

REFERENCES

Aki, K. & Richards, P. G. (1980). *Quantitative Seismology. Theory and Methods.* 2nd ed. J. Ellis. University Science Books. Mill Valley, California. 742p.
ISBN: 978-1-891389-63-4

Ammann, W. J. (1999). *A new Swiss test-site for avalanche experiments in the Vallée de la Sionne/Valais.* Cold Regions Science and Technology, 30, 3–11.
https://doi.org/10.1016/S0165-232X(99)00010-5

Ash, M., Brennan, P. V., Keylock, C. J., Vriend, N. M., McElwaine, J. N., & Sovilla, B. (2014). *Two-dimensional radar imaging of flowing avalanches.* Cold Regions Science and Technology, 102, 41–51.
https://doi.org/10.1016/j.coldregions.2014.02.004

Ash, M., Chetty, K., Brennan, P., McElwaine, J., & Keylock, C. (2010). *FMCW radar imaging of avalanche-like snow movements.* IEEE National Radar Conference - Proceedings, 102–107. https://doi.org/10.1109/RADAR.2010.5494643

Biescas, B. (2003). *Aplicación de la sismología al estudio y detección de aludes de nieve. PhD Thesis.* Universitat de Barcelona.

Biescas, B., Dufour, F., Furdada, G., Khazaradze, G., & Suriñach, E. (2003). *Frequency content evolution of snow avalanche seismic signals.* Surveys in Geophysics, 24(5–6), 447–464. https://doi.org/10.1023/B:GEOP.0000006076.38174.31

Bouchut, F., Mangeney-Castelnau, A., Perthame, B., & Vilotte, J. P. (2003). *A new model of Saint Venant and Savage–Hutter type for gravity driven shallow water flow.* Comptes Rendus Mathematique, 336(6), 531–536.
https://doi.org/10.1016/S1631-073X(03)00117-1

Braun, T., Frigo, B., Chiaia, B., Bartelt, P., Famiani, D., & Wassermann, J. (2020). *Seismic signature of the deadly snow avalanche of January 18, 2017, at Rigopiano (Italy).* Scientific Reports, 10(1), 1–10.
https://doi.org/10.1038/s41598-020-75368-z

Brennan, P. V, Ash, M., Isa, F. M., Keylock, C. & Mcelwaine, J. (2009). *Advanced Radar Imaging of Geophysical Flows.* In Procedings of the 3rd IASME/WSEAS International Conference GES'09, 147p.

Brigham, E. O. (1974). *The Fast Fourier Transform.* New Jersey: Prentice-Hall, Inc.

Christen, M., Kowalski, J., & Bartelt, P. (2010). *RAMMS: Numerical simulation of dense snow avalanches in three-dimensional terrain.* Cold Regions Science and Technology, 63(1–2), 1–14.
https://doi.org/10.1016/j.coldregions.2010.04.005

Earle, P. S., & Shearer, P. M. (1994). *Characterization of global seismograms using an automatic-picking algorithm.* Bulletin - Seismological Society of America, 84(2), 366–376.

Firstov, P., Sukhanov, L., Pergement, V., & Rodionovskiy, M. (1992). *Acoustic and seismic signal from snow avalanches.* Transactions (Doklady) of the U.S.S.R. Academy of Sciences: Earth Science Sections, 312, 67–71.

Gauer, P., & Issler, D. (2004). *Possible erosion mechanisms in snow avalanches.* Annals of Glaciology, 38(1979), 384–392.
https://doi.org/10.3189/172756404781815068

Guinau, M., Tapia, M., Pérez-Guillén, C., Suriñach, E., Roig, P., Khazaradze, G., Torné, M., Royán, M. J., Echeverria, A. (2019). *Remote sensing and seismic data integration for the characterization of a rockslide and an artificially triggered rock fall.* Engineering Geology, 257 (December 2017).
https://doi.org/10.1016/j.enggeo.2019.04.010

Hammer, C., Fäh, D., & Ohrnberger, M. (2017). *Automatic detection of wet-snow avalanche seismic signals.* Natural Hazards, 86(2), 601–618. https://doi.org/10.1007/s11069-016-2707-0

Heck, M., Hammer, C., Herwijnen, A. van, Schweizer, J., & Fäh, D. (2017). *Automatic detection of snow avalanches in continuous seismic data using hidden Markov models,.* Natural Hazards and Earth System Science, 18, 383–396.
https://doi.org/10.5194/nhess-18-383-2018

Heck, M., Herwijnen, A. van, Hammer, C., Hobiger, M., Schweizer, J., & Fäh, D. (2018). *Automatic detection of avalanches combining array classification and localization,* Earth Surf. Dynam., 7, 491–503.
https://doi.org/10.5194/esurf-7-491-2019

Herwijnen, A. van, Heck, M., & Schweizer, J. (2016). *Forecasting snow avalanches using avalanche activity data obtained through seismic monitoring.* Cold Regions Science and Technology, 132, 68–80. https://doi.org/10.1016/j.coldregions.2016.09.014

Incorporated Research Institutions for Seismology (IRIS). *Data services on-line information.* https://ds.iris.edu/ [January 2020].

Jóhannesson, T., Hakonardottir, M. Lied, K. Issler, D., Gauer, P., Naaim, M., Faug, T. Natale, L., Barbolini, M., Cappabianca, F., Pagliardi, M., Rammer, L., Sovilla, B., Platzer, K., Surinach, E., Villajosana, I. (2006) *Avalanche test sites and research equipment in Europe: an updated overview.* M. Barbolini, D. Issler (Eds.), Deliverable No. 8 of the EU Project SATSIE (Avalanche studies and model validation in Europe), contract EVG1-CT2002-00059. 172 pp.

Jurkevics, A. (1988). *Polarization Analysis of Three-Component Array Data.* Bulletin of the Seismological Society of America, 78(5), 1725–1743.

Kogelnig, A., Hübl, J., Suriñach, E., Vilajosana, I., & McArdell, B. W. (2014). *Infrasound produced by debris flow: Propagation and frequency content evolution.* Natural Hazards, 70(3), 1713–1733. https://doi.org/10.1007/s11069-011-9741-8

Kogelnig, A., Suriñach, E., Vilajosana, I., Hübl, J., Sovilla, B., Hiller, M., & Dufour, F. (2011). *On the complementariness of infrasound and seismic sensors for monitoring snow avalanches.* Natural Hazards and Earth System Science, 11, 2355–2370. https://doi.org/10.5194/nhess-11-2355-2011

Köhler, A., Fischer, J. T., Scandroglio, R., Bavay, M., McElwaine, J., & Sovilla, B. (2018). *Cold-to-warm flow regime transition in snow avalanches.* Cryosphere, 12(12), 3759–3774. https://doi.org/10.5194/tc-12-3759-2018

Köhler, A., Lok, L. B., Felbermayr, S., Peters, N., Brennan, P. V., & Fischer, J. T. (2020). *mGEODAR—A mobile radar system for detection and monitoring of gravitational mass-movements.* Sensors (Switzerland), 20(21), 1–15. https://doi.org/10.3390/s20216373

Köhler, A., McElwaine, J. N., & Sovilla, B. (2018). *GEODAR Data and the Flow Regimes of Snow Avalanches.* Journal of Geophysical Research, 123, 23. https://doi.org/10.1002/2017JF004375

Köhler, A., McElwaine, J. N., Sovilla, B., Ash, M., & Brennan, P. (2016). *The dynamics of surges in the 3 February 2015 avalanches in Vallée de la Sionne.* Journal of

Geophysical Research: Earth Surface, (February 2015).
https://doi.org/10.1002/2016JF003887

Köhler, A., Sovilla, B., & Mcelwaine, J. (2018). *7 years of avalanche measurements with the GEODAR radar system.* In ISSW18 proceedings, International Snow Science Workshop, Innsbruck, Austria, 2018 (pp. 665–669).

Kyburz, M., Sovilla, B., Gaume, J., & Ancey, C. (2018). *Avalanche pressures at the Vallée de la Sionne Test site: Interaction of Avalanches and narrow structures studied with DEM.* In ISSW18 proceedings, International Snow Science Workshop, Innsbruck, Austria, 2018 (pp. 40–42).

Kyburz, M., Sovilla, B., Gaume, J., & Ancey, C. (2020). *Decoupling the role of inertia, friction and cohesion in dense granular avalanche pressure build-up on obstacles.* JGR: Earth Surface, 1–37.
https://doi.org/10.1029/2019JF005192

Levy, C., Mangeney, A., Bonilla, F., Hibert, C., Calder, E. S., & Smith, P. J. (2015). *Friction weakening in granular flows deduced from seismic records at the Soufrière Hills Volcano, Montserrat.* Journal of Geophysical Research B: Solid Earth, 120(11), 7536–7557.
https://doi.org/10.1002/2015JB012151

Lucas, A., Mangeney, A., & Ampuero, J. P. (2014). *Frictional velocity-weakening in landslides on Earth and on other planetary bodies.* Nature Com. 5, 3417.
https://doi.org/10.1038/ncomms4417

Mangeney, A., Bouchut, F., Thomas, N., Vilotte, J. P., & Bristeau, M. O. (2007). *Numerical modeling of self-channeling granular flows and of their levee-channel deposits.* Journal of Geophysical Research: Earth Surface, 112(2), 1–21.
https://doi.org/10.1029/2006JF000469

Mangeney-Castelnau, A., Bouchut, F., Vilotte, J. P., Lajeunesse, E., Aubertin, A., & Pirulli, M. (2005). *On the use of Saint Venant equations to simulate the spreading of a granular mass.* Journal of Geophysical Research, 110, 1–17.
https://doi.org/10.1029/2004JB003161

Marchetti, E., Ripepe, M., Ulivieri, G., & Kogelnig, A. (2015). *Infrasound array criteria for automatic detection and front velocity estimation of snow avalanches: Towards a real-time early-warning system.* Natural Hazards and Earth System Sciences, 15(11), 2545–2555.
https://doi.org/10.5194/nhess-15-2545-2015

Marshall, H. P., Schneebeli, M., & Koh, G. (2007). *Snow stratigraphy measurements with high-frequency FMCW radar: Comparison with snow micro-penetrometer.* Cold Regions Science and Technology, 47(1-2 SPEC. ISS.), 108–117.
https://doi.org/10.1016/j.coldregions.2006.08.008

McClung, D., & Schaerer, P. A. (1993). *The Avalanche Handbook.* The Mountaineers Books Ed. (USA).

McElwaine, J. N., Köhler, A., Sovilla, B., Ash, M., & Brennan, P. (2017). *GEODAR data of snow avalanches at Vallée de la Sionne: Seasons 2010/11, 2011/12, 2012/13 & 2014/15* [Data set]. Zenodo.
https://doi.org/http://doi.org/10.5281/zenodo.1042108

Moog, B. (1964). *Voltage-controlled electronic music modules.* In Audio Engineering Society, 16th annual meeting (p. 19). New York: Audio Engineering Society.

Nyquist, H. (1928). *Certain Topics in Telegraph Transmission Theory.* Transactions of the American Institute of Electrical Engineers, 47(2), 617–644.
https://doi.org/10.1109/T-AIEE.1928.5055024

Pérez-Guillén, C. (2016). *Advanced seismic methods applied to the study of snow avalanche dynamics and avalanche formation.* PhD Thesis. Universitat de Barcelona.

Pérez-Guillén, C., Sovilla, B., Suriñach, E., Tapia, M., & Köhler, A. (2016). *Deducing avalanche size and flow regimes from seismic measurements.* Cold Regions Science and Technology, 121, 25–41.
https://doi.org/10.1016/j.coldregions.2015.10.004

Pérez-Guillén, C., Tapia, M., Furdada, G., Suriñach, E., McElwaine, J. N., Steinkogler, W., & Hiller, M. (2014). *Evaluation of a snow avalanche possibly triggered by a local earthquake at Vallée de la Sionne, Switzerland.* Cold Regions Science and Technology, 108, 149–162.
https://doi.org/10.1016/j.coldregions.2014.07.007

Pérez-Guillén, C., Tsunematsu, K., Nishimura, K., & Issler, D. (2019). *Seismic detection and tracking of avalanches and slush flows on Mt. Fuji, Japan.* Earth Surface Dynamics Discussions, 1–29.
https://doi.org/10.5194/esurf-2019-25

Peterson, J. (1993). *Observations and modeling of seismic background noise.* Report. US Geological Survey.
https://doi.org/10.3133/ofr93322

Plešinger, A., Hellweg, M., & Seidl, D. (1986). *Interactive high-resolution polarization analysis of broad-band seismograms.* Journal of Geophysics, 59, 129–139.
https://geophysicsjournal.com/article/203

Roig, P., Pérez-Guillén, P., Sovilla, B., Suriñach, E., Köhler, A., Tapia, M., & Furdada, G. (2018). *Comparative analysis of avalanche seismic signals and GEODAR data at Vallée de la Sionne test site (2018).* In ISSW18 proceedings, International Snow Science Workshop, Innsbruck, Austria, 2018 (pp. 1–5).

Roig-Lafon, P., Levy, C., Suriñach, E., Mangeney, A., & Durand, V. (2018). *SHALTOP as a snow avalanche modeling software: seismic and radar data validations.* Geophysical Research Abstracts. EGU General Assembly 2018.

Roig-Lafon, P., Suriñach, E., Bartelt, P., Pérez-guillén, C., & Tapia, M. (2017). *First approximations in avalanche model validations using seismic information* (Vol. 19, p. 8048). Geophysical Research Abstracts. EGU General Assembly 2017.

Sabot, F., Naaim, M., Granada, F., Suriñach, E., Planet, P., & Furdada, G. (1998). *Study of avalanches dynamics by seismic methods, image-processing techniques and numerical models.* Annals of Glaciology, 26, 319–323.
https://doi.org/10.3189/1998AoG26-1-319-323

Salm, B. (1993). *Flow transition and runout distances of flowing avalanches.* Annals of Glaciology, 18, 221–226.
https://doi.org/10.3189/s0260305500011551

Saló, L., Corominas, J., Lantada, N., Matas, G., Prades, A., & Ruiz-Carulla, R. (2018). *Seismic Energy Analysis as Generated by Impact and Fragmentation of Single-Block.* Journal of Geophysical Research: Earth Surface, 1–29.
https://doi.org/10.1029/2017JF004374

Shannon, C. E., & Weaver, W. (1964). *The Mathematical theory of communication.* The University of Illinois press (Vol. 8). Board of Trustees of the University of Illinois.
https://doi.org/10.1145/584091.584093

Smith, S. W. (2011). *The Scientist and Engineer's Guide to Digital Signal Processing.* California Technical Publishing.

Sovilla, B., & Bartelt, P. (2002). *Observations and modelling of snow avalanche entrainment.* Natural Hazards and Earth System Sciences, 2(3–4), 169–179. https://doi.org/10.5194/nhess-2-169-2002

Sovilla, B., Faug, T., Köhler, A., Baroudi, D., Fischer, J. T., & Thibert, E. (2016). *Gravitational wet avalanche pressure on pylon-like structures.* Cold Regions Science and Technology, 126, 66–75. https://doi.org/10.1016/j.coldregions.2016.03.002

Sovilla, B., McElwaine, J. N., & Louge, M. Y. (2015). *The structure of powder snow avalanches.* Comptes Rendus Physique, 16(1), 97–104. https://doi.org/10.1016/j.crhy.2014.11.005

Sovilla, B., McElwaine, J. N., & Köhler, A. (2018). *The Intermittency Regions of Powder Snow Avalanches.* Journal of Geophysical Research: Earth Surface. https://doi.org/10.1029/2018JF004678

Sovilla, B., McElwaine, J. N., Steinkogler, W., Hiller, M., & Dufour, F. (2013). *The full-scale avalanche dynamics test site Vallée de la Sionne.* In ISSW13 proceedings, International Snow Science Workshop, Grenoble – Chamonix Mont-Blanc, 2013 (pp. 3–10).

Sovilla, B., Schaer, M., Kern, M., & Bartelt, P. (2008). *Impact Pressures and flow regimes in dense snow avalanches observed at the Vallée de la Sionne test site.* Journal of Geophysical Research: Earth Surface, 113(1), 1–14. https://doi.org/10.1029/2006JF000688

Suriñach, E., Flores-Márquez, E. L., Roig-Lafon, P., Furdada, G., & Tapia, M. (2020). *Estimation of Avalanche Development and Frontal Velocities Based on the Spectrogram of the Seismic Signals Generated at the Vallée de la Sionne Test Site.* Geosciences, 10(3), 113, 15–22. https://doi.org/10.3390/geosciences10030113

Suriñach, E., Furdada, G., Sabot, F., Biescas, B., & Vilaplana, J. M. (2001). *On the characterization of seismic signals generated by snow avalanches for monitoring purposes.* Annals of Glaciology, 32, 268–274. https://doi.org/10.3189/172756401781819634

Suriñach, E., Sabot, F., Furdada, G., & Vilaplana, J. M. (2000). *Study of seismic signals of artificially released snow avalanches for monitoring purposes.* Physics and Chemistry of the Earth, Part B, 25(9), 721–727. https://doi.org/10.1016/S1464-1909(00)00092-7

Suriñach, E., Tapia, M., Pérez-Guillén, C., Khazaradze, G., & Roig, P. (2016). *Comparison of seismic and infrasound wave fields generated by snow avalanches.* Geophysical Research Abstracts. EGU General Assembly 2016 (18, 9515).

Suriñach, E., Vilajosana, I., Khazaradze, G., Biescas, B., Furdada, G., & Vilaplana, J. M. (2005). *Seismic detection and characterization of landslides and other mass movements.* Natural Hazards and Earth System Science, 5(6), 791–798. https://doi.org/10.5194/nhess-5-791-2005

Suriñach, E., Vilajosana, I., Kleemayr, K., & Rammer, L. (2011). *Study of the wavefield generated by a gas exploder used for artificial avalanche release.* Cold Regions Science and Technology, 66(1), 17–29. https://doi.org/10.1016/j.coldregions.2011.01.002

Swiss Geological Survey. *Geological Atlas of Switzerland (GA25), Saint Léonard, no. 35.* http://map.geo.admin.ch/. [December 2019].

Tapia, M., Guinau, M., Roig, P., Pérez-Guillén, C., Suriñach, E., & Khazaradze, G. (2020). *Data in brief Seismic data of a rockslide: Evaluation of noise levels, site effects, frequency content and identification of seismic phases.* Data in Brief, 1–9. https://doi.org/10.1016/j.dib.2020.105250

Trnkoczy, A., & Bormann, P. (2012). *Understanding and parameter setting of STA/LTA trigger algorithm.* In New Manual of Seismological Observatory Practice 2 (NMSOP-2) (p. 20 pp.). https://doi.org/10.2312/GFZ.NMSOP-2_IS_8.1

Vail, M. (2014). *The Synthesizer.* Oxford University Press.

Veitinger, J., & Sovilla, B. (2016). *Linking snow depth to avalanche release area size: Measurements from the Vallée de la Sionne field site.* Natural Hazards and Earth System Sciences, 16(8), 1953–1965.
https://doi.org/10.5194/nhess-16-1953-2016

Vidale, J. E. (1986). *Complex polarization analysis of particle motion.* Bulletin of the Seismological Society of America, 76(5), 1393–1405.

Vilajosana, I. (2008). *Seismic detection and characterization of snow avalanches and other mass movements.* PhD Thesis. Universitat de Barcelona.

Vilajosana, I., Khazaradze, G., Suriñach, E., Lied, E., & Kristensen, K. (2007a). *Snow avalanche speed determination using seismic methods.* Cold Regions Science and Technology, 49, 2–10. https://doi.org/10.1016/j.coldregions.2006.09.007

Vilajosana, I., Suriñach, E., Abellán, A., Khazaradze, G., Garcia, D., & Llosa, J. (2008). *Rockfall induced seismic signals: case study in Montserrat, Catalonia.* Natural Hazards and Earth System Science, 8(4), 805–812.
https://doi.org/10.5194/nhess-8-805-2008

Vilajosana, I., Suriñach, E., Khazaradze, G., & Gauer, P. (2007b). *Snow avalanche energy estimation from seismic signal analysis.* Cold Regions Science and Technology, 50, 72–85.
https://doi.org/10.1016/j.coldregions.2007.03.007

Vriend, N. M., McElwaine, J. N., Sovilla, B., Keylock, C. J., Ash, M., & Brennan, P. V. (2013). *High-resolution radar measurements of snow avalanches.* Geophysical Research Letters, 40(4), 727–731.
https://doi.org/10.1002/grl.50134

Withers, M., Aster, R., Young, C., Beiriger, J., Harris, M., Moore, S., & Trujillo, J. (1998). *A comparison of select trigger algorithms for automated global seismic phase and event detection.* Bulletin of the Seismological Society of America, 88(1), 95–106.